3 1293 00577 0023

2273570 6

Michigan State University

This is to certify that the

dissertation entitled

AN ANALYTICAL AND EXPERIMENTAL STUDY OF THE ELASTODYNAMIC RESPONSE CHARACTERISTICS OF PLANAR LINKAGE MECHANISM WITH BEARING CLEARANCES

presented by

KUEIMING SOONG

has been accepted towards fulfillment
of the requirements for

PH.D degree in M.E.

Brian S. Thompson
Major professor

Date SEP. 13, 1988

MSU is an Affirmative Action/Equal Opportunity Institution

O-12771

RETURNING MATERIALS:
Place in book drop to remove this checkout from your record. *FINES* will be charged if book is returned after the date stamped below.

AN ANALYTICAL AND EXPERIMENTAL STUDY OF THE ELASTODYNAMIC RESPONSE CHARACTERISTICS OF PLANAR LINKAGE MECHANISM WITH BEARING CLEARANCES

By

Kueiming Soong

A DISSERTATION

Submitted to

Michigan State University

in partial fulfillment of the requirements

for the degree of

DOCTOR OF PHILOSOPHY

Department of Mechanical Engineering

1988

2 0 7 3 6 1 6

ABSTRACT

AN ANALYTICAL AND EXPERIMENTAL STUDY OF THE ELASTODYNAMIC RESPONSE CHARACTERISTICS OF PLANAR LINKAGE MECHANISM WITH BEARING CLEARANCES

By

Kueiming Soong

A comprehensive investigation of the dynamic response characteristics of a general planar linkage mechanism featuring both rigid and flexible links with and without radial clearance in the revolute joints is presented. In the coherent combination of analytical, computational, and experimental work undertaken herein, the equations governing the dynamical behavior of this general mechanical system are established by incorporating a four-mode model of the phenomenological behavior of the principal elements of each revolute joint into the generalized form of Lagrange's equations. A displacement finite element formulation is developed for undertaking the nonlinear vibrational analysis of general flexible linkage mechanisms. This formulation incorporates elastic geometrical nonlinearities and also terms coupling the rigid-body kinematics of the linkage mechanism and the elastic deformations. The equations of motion for this class of mechanical

system are composed of a mixed set of ordinary differential equations and algebraic constraint equations. These governing equations are solved by employing a quasi-static procedure, Adams numerical integration scheme and the mode superposition approach of vibrational analysis. Four different illustrative examples are considered and the analytical and experimental results show impressive correlation.

To my parents

and

to my wife

Jui-Mei

ACKNOWLEDGMENTS

I would like to express my deepest gratitude to my advisor, Professor Brian S. Thompson for his help and support during all stages of this research program. Grateful thanks are extended to the other members of the guidance committee, Professors M.V. Gandhi, D.H. Yen and C.Y. Wang. Also I would like to thank all the students in Machinery Elastodynamics Laboratory for their valuable suggestions and assistance.

The author wishes to gratefully acknowledge the four-year financial support of the Chung-Cheng Institute of Technology, Taiwan, which has enabled him to undertaken this research.

A debt of thankfulness is owed to my lovely wife, parents, parents-in-law and my two children for their encouragements and supports, without which my research could have not been finished.

TABLE OF CONTENTS

		Page
LIST OF FIGURES		viii
NOMENCLATURE		xvi
CHAPTER		
I.	INTRODUCTION	1
1.1	Motivation	1
1.2	Literature review	5
1.2.1	Mechanisms with rigid-links and featuring bearings without clearances	6
1.2.2	Mechanisms with rigid-links and featuring bearing clearances	7
1.2.3	Flexible-links in mechanical systems without bearing clearances	14
1.2.4	Flexible-links in mechanical systems with bearing clearances	19
1.3	Thesis outline	22
1.4	Principal contributions	25
II.	GENERAL PLANAR MECHANISMS FEATURING RIGID-LINKS WITH RADIAL CLEARANCES IN THE REVOLUTE JOINTS	27
2.1	Introduction	27

2.2 Model of a general planar rigid-linked mechanism with bearing clearances 28
(i) Contact-mode 32
(ii) Free-flight-mode 32
(iii)Impact-mode 33
(iv) Transient-mode 33
2.3 Governing equations for the contact-mode 34
2.4 Governing equations for the free-flight-mode 40
2.5 Governing equations for the impact-mode 42
2.6 Strategy for a numerical solution 45
2.7 Illustrative Example - Dynamical response model of a slider-crank mechanism with clearance in the gudgeon-pin joint 49
2.7.1 Equations of motion for the contact-mode 49
2.7.2 Equations of motion for the free-flight-mode 51
2.7.3 Equations of motion for the impact-mode 52
2.7.4 Equations of motion for the transient-mode 54
2.7.5 Simulation protocols 54
(i) Contact loss 54
(ii) Termination of the Free-flight-mode 56
(iii)Restoration of the contact-mode 57
(iv) Solution procedure 57
2.7.6 Experimental slider-crank mechanism, associated instrumentation, and experimental procedure 60
2.7.7 Comparison of experimental and numerical results 67
2.8 Conclusions of the chapter 76

III. GENERAL PLANAR MECHANISMS FEATURING FLEXIBLE-LINKS AND BEARINGS WITHOUT RADIAL CLEARANCE 77
3.1 Introduction 77
3.2 Equations of motion of a flexible body describing a general planar motion 78
3.3 Solution procedure 89
3.4 Illustrative Example - Elastodynamic response of a slider-crank mechanism with a flexible connecting rod 93
3.4.1 Equations of motion 97
3.4.2 Some remarks on the elastodynamic behavior of a flexible connecting rod 101
3.4.3 Comparison of experimental and numerical results 109
3.5 Conclusions of the chapter 110
IV. ELASTODYNAMIC ANALYSIS OF A GENERAL PLANAR MECHANISMS FEATURING FLEXIBLE-LINKS WITH RADIAL CLEARANCES IN THE REVOLUTE JOINTS 117
4.1 Introduction 117
4.2 Model of a general planar mechanism with flexible-links and featuring radial clearances in the revolute joints .. 118
(i) Contact-mode 118
(ii) Free-flight-mode 119
(iii) Impact-mode 119
(iv) Transient-mode 120
4.3 Equations of motion 120
4.3.1 Equations of motion for the contact-mode 129
4.3.2 Equations of motion for the free-flight-mode 132
4.3.3 Equations of motion for the impact-mode 133

4.4 Illustrative Example 1 - Dynamical behavior of a compound pendulum subjected to impact 138
4.4.1 Equations of motion for the free-flight-mode 139
4.4.2 Equations of motion for the contact-mode 142
4.4.3 Equations of motion for the impact-mode 142
4.4.4 Solution procedures 143
4.4.5 Comparison of experimental and theoretical results 147
4.5 Illustrative Example 2 - A slider-crank mechanism with a flexible connecting-rod featuring radial clearance in the gudgeon-pin joint 152
4.5.1 Equations of motion for the contact-mode 154
4.5.2 Equations of motion for the free-flight-mode 156
4.5.3 Equations of motion for the impact-mode 158
4.5.4 Equations of motion for the transient-mode 161
4.5.5 Simulation protocols 161
4.5.6 Comparison of experimental and theoretical results 167
4.6 Conclusions of the chapter 174
V. CONCLUSIONS AND RECOMMENDATIONS 175
APPENDIX 181
List of publications 181
BIBLIOGRAPHY 239

LIST OF FIGURES

Figures		Page
Chapter I		
Figure 1.1	Classical design of linkage mechanism	11
Figure 1.2	First generation of analysis techniques for elastodynamic design of flexible mechanisms. Two-pass method	12
Figure 1.3	New analysis techniques for elastodynamic design of flexible mechanisms. One-pass method	13
Figure 1.4	Modeling strategy	25
Chapter II		
Figure 2.1	Radial clearance in the revolute joint in a planar mechanism system	29
Figure 2.2	Definition of the position vectors and reference frames modeling a planar mechanism system with bearing clearances	29

Figure 2.3 Schematic diagram presenting the four-mode describing the phenomenological behavior of a revolute joint with clearance 31

Figure 2.4 (a) The slider-crank mechanism showing dominant clearance at the gudgeon-pin bearing
(b) Vector-loop model of the mechanism 48

Figure 2.5 Free-body diagram of the slider-crank mechanism in the impact-mode 53

Figure 2.6 Flow chart for the computer protocol 59

Figure 2.7 Photograph of experimental planar slider-crank mechanism 62

Figure 2.8 Schematic of experimental apparatus and associated instrumentation 63

Figure 2.9 Photograph of accelerometer configuration at the gudgeon-pin bearing of the experimental slider-crank mechanism 64

Figure 2.10 Photograph of experimental apparatus for measuring the impactive force in the gudgeon-pin bearing and determining the associated coefficient of restitution between the pin and the journal of the bearing ... 66

Figure 2.11 Schematic diagram of the experimental apparatus and instrumentation for determining the coefficient of restitution of the gudgeon-pin bearing 68

Figure 2.12 Gudgeon-pin bearing characteristics: Velocity characteristics of the impactive behavior between pin and journal at a pin excitation frequency of 20 Hz 69

Figure 2.13 Gudgeon-pin bearing characteristics: Excitation force characteristics and associated velocity characteristics of the pin impacting the journal at a frequency of 20 Hz 69
Figure 2.14 Connecting-rod tangential acceleration. Mechanism operating speed 200 rpm 70
Figure 2.15 Connecting-rod tangential acceleration. Mechanism operating speed 300 rpm 70
Figure 2.16 Slider acceleration. Mechanism operating speed 200 rpm 71
Figure 2.17 Slider acceleration. Mechanism operating speed 300 rpm 71
Figure 2.18 Connecting-rod longitudinal acceleration. Mechanism operating speed 200 rpm 72
Figure 2.19 The theoretical prediction of the longitudinal acceleration of the connecting-rod. Mechanism operating 300 rpm 72
Figure 2.20 The maximum impactive force between the pin and journal. The radial clearance was 0.000127 meters. 73
Figure 2.21 The maximum impactive force between the pin and journal. Mechanism operating speed 300 rpm 73

Chapter III

Figure 3.1 Generalized coordinate of two adjacent links 80
Figure 3.2 The nodal displacement of each element 80
Figure 3.3 Axial force is represented as a linear function .. 85

Figure 3.4 Quasi-static solution procedures 93

Figure 3.5 (a)The slider-crank mechanism with flexible connecting rod

(b)Vector-loop model of the mechanism 95

Figure 3.6 The six finite elements of the connecting rod 96

Figure 3.7 Photograph of the flexible connecting rod with strain gauges 96

Figure 3.8 The relationship between the natural frequency and the axial force 104

Figure 3.9 The relationship between the damping factor and the axial force 105

Figure 3.10 Simulation of a simply-supported beam by applying an external tensile force 105

Figure 3.11 Simulation of a simply-supported beam by applying an external compressive force 106

Figure 3.12 The mode shape of the first three modes 106

Figure 3.13 The variation of the natural frequency: the first mode 107

Figure 3.14 The variation of the natural frequency: the second mode 107

Figure 3.15 The variation of the natural frequency: the third mode 108

Figure 3.16 The mode shape of the first-mode at 0, 45, 180, and 225 degree of crank angle. Mechanism operating speed 185 rpm 108

Figure 3.17 The mid-span deflection of the connecting rod. Mechanism operating speed 185 rpm 111

Figure 3.18 The mid-span deflection of the connecting rod. Mechanism operating speed 225 rpm 111
Figure 3.19 The mid-span deflection of the connecting rod. Mechanism operating speed 258 rpm 112
Figure 3.20 The acceleration of the slider. Mechanism operating speed 258 rpm 112
Figure 3.21 The acceleration of the slider. Mechanism operating speed 185 rpm 113
Figure 3.22 The variation of the acceleration of the slider between the rigid-link and flexible-link of a slider -crank mechanism. Mechanism operating speed 185 rpm 113
Figure 3.23 The variation of the acceleration of the slider between the rigid-link and flexible-link of a slider -crank mechanism. Mechanism operating speed 225 rpm 114
Figure 3.24 The variation of the acceleration of the slider between the rigid-link and flexible-link of a slider -crank mechanism. Mechanism operating speed 258 rpm 114
Figure 3.25 The magnitude of the pin force in gudgeon-pin bearing. Mechanism operating speed 185 rpm 115
Figure 3.26 The force angle of the pin force in gudgeon-pin bearing. Mechanism operating speed 185 rpm 115
Figure 3.27 The variation of the pin force in the gudgeon-pin bearing between the rigid-link and flexible-link of a slider-crank mechanism. Mechanism operating speed 185 rpm 116

Figure 3.28 The variation of the force angle in the gudgeon-pin bearing between the rigid-link and flexible-link of a slider-crank mechanism. Mechanism operating speed 185 rpm 116

Chapter IV

Figure 4.1 Generalized coordinate of two adjacent links 122
Figure 4.2 A schematic diagram of a compound articulating under gravitational loading prior to impating with a fixed mechanical stop 139
Figure 4.3 Photograph of the compound pendulum and stationary mechanical stop 146
Figure 4.4 Photograph of experimental compound pendulum showing the pin and the bearing 146
Figure 4.5 The experimental mid-span deformation of the compound pendulum. The initial angular position 60 degrees 148
Figure 4.6 The theoretical mid-span deformation of the compound pendulum. The initial angular position 60 degrees 149
Figure 4.7 The theoretical angular velocity of the compound pendulum. The initial angular position 60 degrees 149
Figure 4.8 The theoretical angular position of the compound pendulum. The initial angular position 60 degrees 150
Figure 4.9 The experimental mid-span deformation of the compound pendulum. The initial angular position 30 degrees 150

Figure 4.10 The theoretical mid-span deformation of the compound pendulum. The initial angular position 30 degrees 151

Figure 4.11 The theoretical angular velocity of the compound pendulum. The initial angular position 30 degrees 151

Figure 4.12 The theoretical angular position of the compound pendulum. The initial angular position 30 degrees 152

Figure 4.13 (a)The slider-crank mechanism with flexible connecting rod showing dominant clearance at the gudgeon-pin bearing

(b)Vector-loop model of the mechanism 153

Figure 4.14 Flow-chart for the computer simulation 166

Figure 4.15 Slider acceleration. Mechanism operating speed 185 rpm 169

Figure 4.16 Slider acceleration. Mechanism operating speed 199 rpm 169

Figure 4.17 Slider acceleration. Mechanism operating speed 225 rpm 170

Figure 4.18 Slider acceleration. Mechanism operating speed 258 rpm 170

Figure 4.19 Connecting-rod tangential acceleration. Mechanism operating speed 185 rpm 171

Figure 4.20 Connecting-rod tangential acceleration. Mechanism operating speed 199 rpm 171

Figure 4.21 Connecting-rod tangential acceleration. Mechanism operating speed 225 rpm 172

Figure 4.22 Connecting-rod tangential acceleration. Mechanism operating speed 258 rpm 172

Figure 4.23 The mid-span deflection of the connecting rod. Mechanism operating speed 185 rpm 173
Figure 4.24 The mid-span deflection of the connecting rod. Mechanism operating speed 199 rpm 173
Figure 4.25 The mid-span deflection of the connecting rod. Mechanism operating speed 258 rpm 174

NOMENCLATURE

Chapter II

General Formulation

F_i External force imposed upon the system

F_e^j External force imposed on the j-th link

F_{ij} Force imposed by link i on link j

$\hat{F}$ Impulsive force

ℓ_i Length of the i-th link

m_i Mass of the i-th link

m_{ij} Generalized mass

n The normal direction of the contact surface

q_k Generalized coordinates

Q_k Generalized force associated with coordinate q_k, including both conservative and nonconservative effects

$\tilde{Q}_k$ Generalized external impact force associated with the generalized coordinate q_k

$\hat{Q}_k$ Generalized impulse associated with coordinate q_k

r_k^p Position vector defining any point p of the kth link relative to the origin of the inertial reference frame OXY

$r_{Q\alpha}$ Position vector of any contact point Q of the link α relative to the origin of the inertial reference frame OXY

$r_{\alpha/\beta}^{\ell}$ Position vector defining the relative location of point α and point β on link ℓ

T Total kinetic energy of the system

α_j Angular acceleration of link j

ϕ_p Holonomic or nonholonomic constraint equations

λ_p p-th Lagrange multiplier

$(\cdot)$ Time derivative

ρ_k Position vector defining the center of mass of the kth link relative to the origin of the inertial reference frame

$*$ Denotes post-collision parameter or characteristic

ϵ Coefficient of restitution

ω_j Angular velocity of link j

Illustrative Example

F_{12} Resultant force at crankshaft bearing

I_{G2} Mass moment of inertia of the crank about the gravitational center

I_{G3} Mass moment of inertia of the connecting rod about the gravitational center

m_2 Mass of the crank

m_3 Mass of the connecting rod (including the mass of the bearings and the mass of the accelerometers)

m_s Mass of the slider

r_2 Length of the crank

r_3 Length of the connecting rod

r_4 Radial clearance at the Gudgeon-pin joint

r_{G2} Length between the axis of rotation of the crank shaft and the mass center of the crank

r_{G3} Length between the crank-pin and the mass center of the connecting rod

$\hat{T}_{or}$ Impulsive torque imposed on the crank during the impact-mode

θ_2 Argument of the crank

θ_3 Argument of the connecting rod

θ_4 Argument of the vector representing the bearing clearance

μ Frictional coefficient between the slider and the guide

Chapter III

General Formulation

$F(x)$ The axial force at any point of the link

ℓ The length of an element

$M_{\eta\eta}$ The mass matrix related to the inertia coordinate

$M_{\eta u}$ The mass matrix related to the inertia and elastic coordinate

M_{uu} The mass matrix related to the elastic coordinate

n_i The direction of impactive force

Q_k Generalized force associated with cooedinate q_k, including both conservative and nonconservative effects

r_i The posotion vector of any point p in the deformed body

r_{oi} The components measured in the moving frame of the position vector of the origin of the body axes relative to the origin of the inertial frame

r_{Ri} The position vector of point p in the reference state relative to the origin of the body axes

T_e The kinetic energy of any element

u_k The generalized elastic coordinates

u_x The axial deformation in the ox direction

u_y The transverse deformation in the oy direction

(U) The nodal displacement of a element

V_e The potential energy of any element

X_A The component in OX direction of point A relative to the inertia frame

Y_A The component in OY direction of point A relative to the inertia

$[\check{R}]$ External forces on the elastic link

T_e The kinetic energy of any element

u_i The deformation displacement vector

u_i The generalized elastic coordinates

u_x The axial deformation in the ox direction

u_y The transverse deformation in the oy direction

$\{U\}$ The nodal displacement of a element

V_e The potential energy of any element

ξ x/ℓ

ρ_e The mass density of any element

$(')$ The spatial derivative with respect to x

$(")$ The second spatial derivative with respect to x

ϕ_i The ith generalized constraint equations

$(\dot{})$ The first time derivative

$(\ddot{})$ The second time derivative

λ_i The Lagrange multipliers

conservative and nonconservative effects

ω_n The natural frequencies of the link

η_i The generalized coordinates in modal transformation

Illustrative Example

E The modulus of elasticity of the connecting rod

ρ The mass density of the connecting rod

n	N-1
r_2	The length of the crank shaft
r_3	The length of the connecting rod
$\ddot{s}$	The acceleration of the slider
u_i	The nodal displacements
θ	The angular position of the compound pendulum in inertia frame
$\dot{\theta}$	The angular velocity of the compound pendulum in inertia frame
$(_)$	Denotes a row matrix or a column matrix
θ_2	The crank angle
θ_3	The argument of the connecting rod
$\dot{\theta}_2$	The crank angular velocity
$\dot{\theta}_3$	The angular velocity of the connecting rod
$\ddot{\theta}_2$	The crank angular acceleration
$\ddot{\theta}_3$	The angular acceleration of the connecting rod
ρ	The mass density of the connecting rod

Chapter I

INTRODUCTION

1.1 MOTIVATION

Mechanisms and mechanical systems with discontinuities in their kinematic chains have made significant contributions to many diverse fields of engineering, ranging from the military and aerospace environments to computer-integrated-manufacturing environments. Typically these machine systems incorporate gears, geneva mechanisms, linkages, articulating levers, ratchets, and bearings with radial clearances. While these systems are frequently incorporated in many products in these diverse marketplaces, the dynamic phenomena associated with the discontinuities in these kinematic chains cannot be predicted using classical design methodologies. This observation, coupled with the dearth of design guidelines of this field, and also the importance of these mechanical systems have motivated the research program reported in this thesis.

Upon reviewing the frequency with which these mechanical systems and kinematic pairs with discontinuities are featured in a broad range of mechanical systems in the diverse military, advanced manufacturing, automotive and industrial products, it is clearly evident

that articulating systems with bearing clearances are the most frequently encountered class of mechanical system. Bearing clearances are attributed to wear in the elements of anti-friction rolling contact multi-element precision bearings, or due to the prescribed functional clearance in bushings and journal bearings. The magnitude of this radial clearance is typically of the order of a few thousandth of inches. Hence, in general, the displacement characteristics of a mechanism system with bearing clearances differ from those developed by the same mechanism system without clearances by only a small percentage of the total path generated by a specific trace point on a link. Of course this may render the output totally unacceptable in the case of a precision mechanism, and mandate the deployment of expensive precision preloaded bearings which do not featuring clearance. However, the associated velocity and acceleration characteristics, and also the associated dynamical effects created by the presence of bearing clearances, are generally dramatically different from the zero-clearance case, consequently the performance of the machine is generally drastically modified by the presence of clearance in the joints of the system. The most important phenomena are generally those associated with impact forces in the joints and also dynamical stresses in the structural members, which are generally of a much greater magnitude than those of a system without clearances. The large impulsive forces developed in these systems with discontinuities result in the accelerated wear of the bearings and also the development of a significant vibrational response of the mechanism which can result in high levels of noise radiation and the link members are exposed to a more severe fatigue environment. Moreover, these vibratory motions of the links generally contaminates

the kinematic output-characteristics of the mechanism which is especially undesirable when these characteristics are the principal output of the system.

Recent reports from NSF-sponsored studies on the state-of-the-art of U.S. research on mechanical systems have clearly identified the significant void in the field of mechanical systems with bearing clearances for coherent analytical, computational, and experimental investigations on the dynamic response of these systems [3,6]. The comprehensive work presented herein is directed towards partially filling this void in the literature, by proposing a phenomenological model of a revolute joint with radial clearance which captures the four principal behavioral modes of the dynamical response of these systems prior to evaluating the predictive capabilities of this model by comparing the theoretical results with experimental results from a complementary laboratory study. These modes are classified, herein, as the contact-mode, the free-flight-mode, the impact-mode, and the transient-mode. By capturing these behavioral modes in a mathematical framework, the dynamical response of generally mechanical systems with bearing clearances can be accurately predicted.

Traditionally, mechanism design has been based on rigid-body analyses in which all mechanism members are treated as rigid bodies [66,74]. Stresses in the mechanism members due to inertia forces and external loading are then calculated in a sequential manners using quasi-static analyses. In the past two decades, mechanisms have been designed to operate at higher and higher speeds in order to increase industrial productivity. A consequence of this trend is that the members of these systems can no longer be treated as rigid bodies since initial

loads are dominant at high speeds [26,52,53,89]. In order to reduce the inertial loading imposed on the machine, the weight of mechanism members need to be made as light as possible without sacrificing structural integrity. However the lighter members are more likely to deform and vibrate due to the inertial and external forces. The inaccuracy of the position, velocity, etc. due to the large elastic deformation and occasionally due to the resonant condition will cause the design unacceptable. Hence the elastodynamic analysis of a mechanical system becomes necessary and important. On the other hand, if the links were fabricated with lightweight and high-stiffness materials, the vibrational motion of links can be reduced. Some pioneering research [82,90,91] has been undertaken on fabricating mechanism links in composite materials.

Furthermore, if clearances are presented in the bearings of the mechanism, then the impact forces in the joints will increase thereby increasing the acoustical radiation from the machine and also reduce the life of parts which are subjected to a more severe fatigue environment [20,87].

The dearth of experimental investigations in the field of mechanism systems incorporating joints with radial clearance, and also the significant void in the literature for publications presenting coherent combinations of theoretical and experimental work in the field, have motivated the comprehensive investigation reported herein. This investigation presents a methodology for analyzing the elastodynamical response of planar linkage systems with bearing clearances in the joints. A four-mode model is employed to model the dynamic behavior in each joint with clearance and a multi-step Gear algorithm is employed in

the computer simulations. A complementary experimental investigation of a slider-crank mechanism with prescribed radial clearances in the gudgeon-pin bearing is undertaken in order to furnish viable laboratory data with which to evaluate the predictive capability of the proposed approach.

1.2 LITERATURE REVIEW

The branch of scientific analysis which deals with motions, time, and forces is called mechanics and is made up of two parts, statics and dynamics. Statics deals with the analysis of stationary systems, i.e., those in which time is not a factor, and dynamics deals with systems which change with time. Dynamics is also made up of two major disciplines, kinematics and kinetics. Kinematics is the study of the relative motion of machine parts in which the displacement, velocity, and acceleration are considered while kinetics deals with the forces acting on the parts of a machine and the motions resulting from these forces.

A kinematic chain is a system of links, which are either joined together or are in contact with one another in a manner that permits them to move relative to one another. If one of the links is fixed and the movement of any other link to a new position will cause each of the other links to move to definite predictable positions, which generate a desired function, the system is a constrained kinematic chain. A linkage mechanism is a constrained kinematic chain. A linkage mechanism is called planar linkage if all the intended motions are parallel to a single plane.

The following literature review can be divided into four distinct sections in which different model classifications are proposed to analyze this class of mechanical system. These classifications are dependent upon whether the link members are assumed to be either rigid or flexible bodies, and whether or not the joints are assumed to contain clearance at the pin-journal interface.

1.2.1 Mechanisms with rigid-links and featuring bearings without clearances

Traditionally [55,66,74,100] the kinematic analysis of linkage mechanisms was undertaken by assuming that the links of linkage mechanisms were treated as rigid-bodies and without considering the effects of bearing clearances. The kinematic solutions were obtained by using the graphical method, and then analytical method for simple cases. The forces, torques on links were then obtained based upon the kinematic data.

Since the traditional graphical and analytical methods are only available for simple cases of linkage mechanisms and because of the broad usage of computers, numerical solutions for linkage mechanisms were then developed. Chace, et.al. [6,7,8] made significant contributions to the development of viable methodologies for predicting the dynamic response of mechanical systems by employing Lagrange's equations to simulate the dynamical behavior of highly constrained, multi-degree-of-freedom mechanical systems without considering bearing clearances. This pioneering research resulted in the development of a commercially-available simulation software tool, DRAM which is used

extensively throughout U.S. industry and to a less extent Europe [11]. Uicker, et al. [73] developed a general purpose program, IMP, which gained wide acceptance in the academic community, but failed to be marketed commercially. Haug, et al. [63] developed a package similar to DRAM entitled DADS, which is beginning to emerge in the commercial marketplace. Paul [64] presented an overview of the various principles and techniques proposed for formulating the equations of motion of mechanical systems, prior to seeking the appropriate numerical schemes for solving this class of dynamical problems. Kane and Levinson [44] addressed the complexity of multibody dynamics problems, in which the equations of motion were formulated by both Lagrange's equations and the principle of virtual work. The results of these two methods were then compared. They concluded that the latter formulation was more laborious than the former formulation, and also lead to equations having a superior form for purposes of numerical integration. In fact, to choose a viable method for the formulation and rapid solution of the equations of motion of mechanical systems is not an easy undertaking since is is determined by seeking minimal computing time, complexity of the equations of motion, desired characteristics,..., etc..

1.2.2 Mechanisms with rigid-links and featuring bearing clearances

The serious undesirable effects of bearing clearances on the dynamic behavior of high-speed mechanical systems, have motivated numerous theoretical investigations on the different dynamical phenomena associated with the behavior of revolute joints [37]. However. in sharp contrast to the large number of analytical and computational studies in

this area, the academic community has not developed experimental programs to further motivate these purely theoretical studies, and only in a limited number of cases have combined theoretical and experimental studies been undertaken. The field is, therefore, somewhat, immature and not well developed.

Garrett and Hall [30] investigated the effect of tolerance and clearance in linkage design, in which the effects of these tolerances and clearances are presented in the form of mobility bands for the linkages. Kolhatkar and Yajnik [50] analyzed the errors caused by play in the revolute joints of a precision function generating linkage, in which the error occurring in the output angular displacement of a four-bar linkage is shown to be maximum for a given angular input when the vectors representing the clearances are parallel to the coupler. Earles and Wu [23] who employed a modified Lagrange's equation approach in which constraints were incorporated using Lagrange multipliers in order to predict the behavior of rigid-link mechanism with clearance in a bearing. The clearance in the bearing was modeled by a massless imaginary link, but the simulation was restricted to only predicting when contact between the pin and the journal was terminated. Later Earles and Wu investigated the prediction of contact-loss in a bearing of a linkage mechanism [24,25,105] in which they proposed that contact-loss would not occur if $\dot{\gamma}/R < 1$, where R is the magnitude of minimum bearing reaction force and $\dot{\gamma}$ is the rate of change of R which were obtained from a zero-clearance analysis of the mechanism. Wilson and Fawcett [102] assumed clearance exist in the sliding bearing in a slider-crank mechanism in which a theoretical investigation into the

effects of parameters, such as the geometry, speed and mass distribution of the mechanism, upon the transverse motion of the slider was reported. In their simulation, the theoretical trajectories of slider corners were evaluated. Eventhough the experimental results were not shown in the paper, they reported that 0.4 of the coefficient of restitution was chosen for the simulation, since the theoretical results agreed best with the experimental results on this choice.

The dynamic effects of bearing clearances in mechanisms can cause increased bearing load and noise [13,37,80,87]. These undesirable effects occur when contact is remade in a bearing after relative motion of the two parts of the bearing within the clearance space. Thus if loss of contact could be prevented, the impulsive loading which would normally occur would be eliminated. Under this concept, Grant and Fawcett proposed a method to prevent contact loss between the pin and journal of a revolute joint with clearance [35]. Their experimental results verified the approach for a limited class of systems [36], but the method is not universal [37]. Mansour and Townsend [54,92] modeled a four-bar crank-rocker mechanism with clearance as two sets of compound pendulums in a theoretical study. They ignored the motion in contact-mode entirely, a close succession of small pseudo-impacts were assumed for the simulation. Subsequently, Miedema and Mansour [59] extended their previous two-mode model, for the free flight and impact modes, to a three-mode model in which a following mode was proposed. In their numerical simulations the following-mode was always assumed to occur immediately after the impact-mode, however, this is frequently not observed in practice [37]. Dubowsky and Freudenstein , instead of the use of coefficient of restitution, formulated an impact pair model to

predict the dynamic response of an elastic mechanical joint with clearances [12,13]. In their model, springs and dashpots were arranged as Kelvin-Voigt model [33]. This work was subsequently extended and presented in references [14-16,21]. Recent work by Haines [38-40] and Bengisu, et al.[3] has emphasized the prediction of contact-loss in mechanisms with clearances. Haines constructed a design chart from the numerical solutions of the equations of motion with the assumption that during the noncontact phase the locus of the contact force is a straight line, but this assumption is not universally viable as shown by Bengisu, et al. [3]. Bengisu, et al. developed a separation parameter for a four-bar linkage mechanism which was based on a zero-clearance analysis. The theoretical results are compared with the experimental results and showed qualitatively agreement. However, the generality of their formulation is currently unknown.

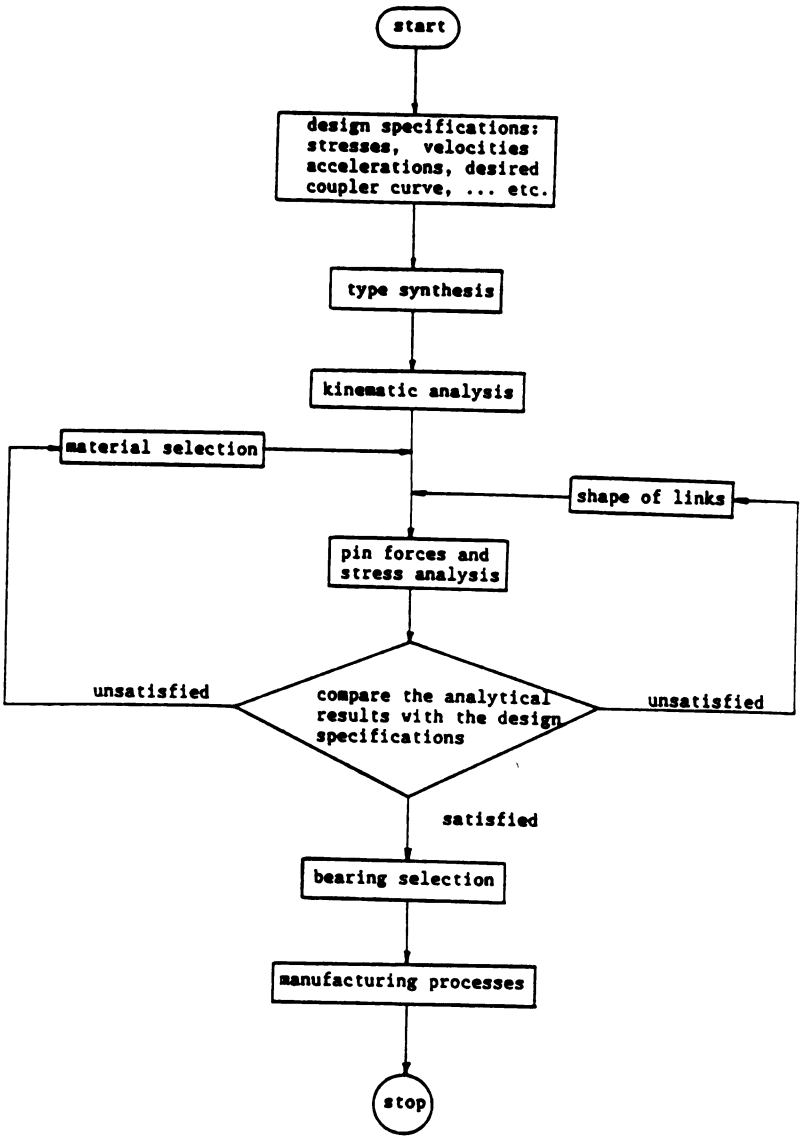

Figure 1.1 Classical design of linkage mechanisms

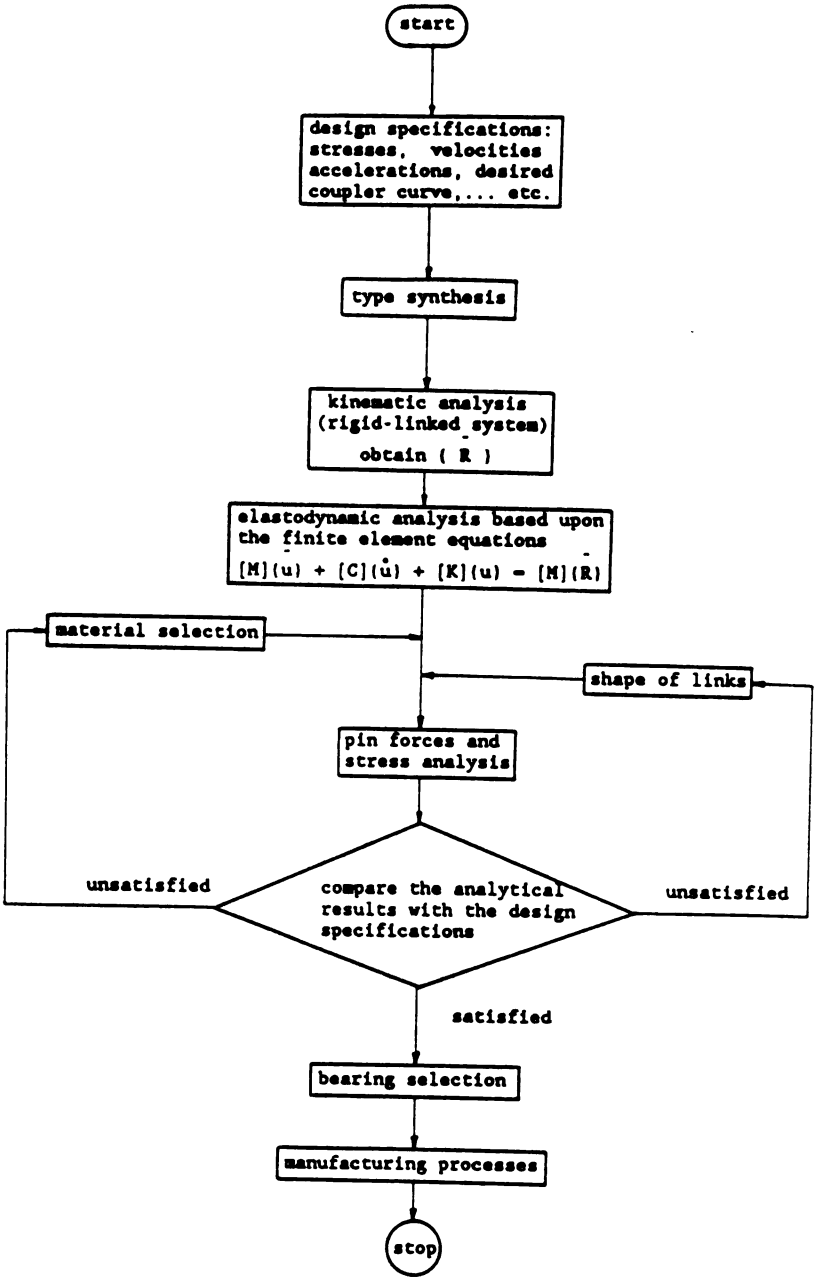

Figure 1.2 First generation of analysis techniques for elastodynamic design of flexible mechanisms. Two-pass method

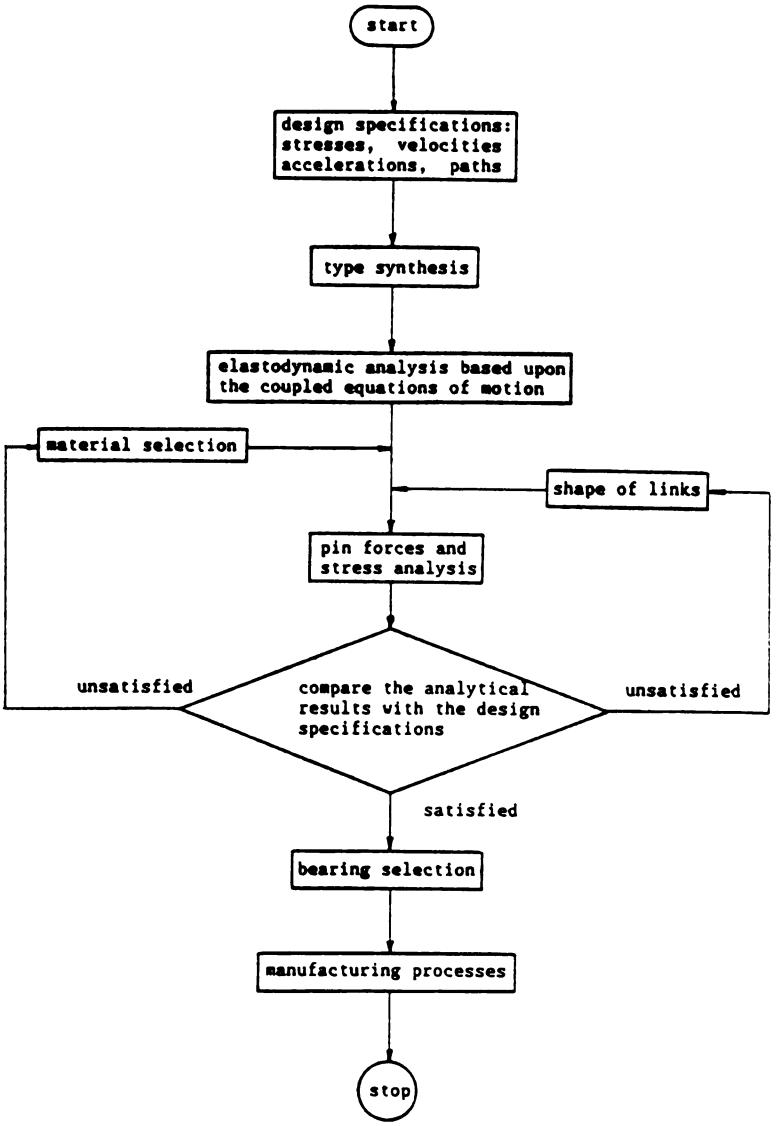

Figure 1.3 New analysis techniques for elastodynamic design of flexible mechanisms. One-pass method

1.2.3 Flexible-links in mechanical systems without bearing clearances

Traditionally, mechanisms have been designed on the basis of the assumption that the members in mechanism are rigid-bodies. Thus, only a geometrical relationship between the input and the output is required and, therefore, once the input is specified the output is completely determined. However the linkages may undergo severe elastic deformations due to its own inertia when operating at a high-speed condition and due to the external loads. In order to achieve higher degree of accuracy of the performance, the elastic deformation of the members in a mechanism have to be taken into consideration.

The methodologies proposed for analyzing flexible-linkage mechanisms may be classified into two major groups: the one-pass and two-pass methods. The one-pass method models the inertia motions, which is relative to the inertial frame, and the elastic motion, which is relative to the moving frame, of the link simultaneously. Based on this method, a system of coupled differential equations are obtained. The two-pass method needs two sets of analytical systems. Before analyzing the vibrational response of flexible links, the mechanism system is analyzed as if it were rigid and thus yielding the inertial characteristics. These inertial characteristics are then become the external and inertia forces of the flexible links, upon which the responses of the flexible links are estimated.

The design procedures of linkage mechanisms can be clearly shown by the following three schematic figures. Figure 1.1 presents the classical design procedures of linkage mechanisms. Design

specifications, such as maximum working stresses, velocities, accelerations, desired paths,.., etc., are requested. Accordingly, a designer has to synthesis the proper linkage mechanism, and then rigid-body analysis is executed to find the kinematic properties. Upon selecting the proper material and shape of links, the pin forces in joints and stresses in the link can be analyzed. By comparing the analytical results with the expected specifications, the material and shape of links may be modified to improve the design. Finally, the design procedures are fulfilled by choosing an economic and efficient manufacturing processes. Figure 1.2 presents the first generation of analysis techniques for elastodynamic design of flexible mechanisms, i.e., the two-pass method. According to the design specifications, the designer has to synthesis a linkage mechanism to generate the desired paths and functions. Kinematic analysis of this linkage mechanism is done as if it were rigid. Upon selecting the proper material and shape of links, the elastodynamic analysis of the links is accomplished by incorporating the kinematic properties which already known in the previous procedure. The global characteristics of the linkage mechanism are obtained by superposing the elastic characteristics on the inertial characteristics. Based on the global characteristics, the pin forces and stresses of links are calculated. By comparing the designed characteristics with the design specifications, the design is completed by choosing a proper manufacturing processes. Figure 1.3 presents the procedures of one-pass method. Again, according to the design specifications, the designer has to synthesis a linkage mechanism to generate the desired paths and functions. A system of coupled differential equations is formulated. The global characteristics of the

linkage mechanism are obtained by solving the coupled governing equations. The pin forces and stresses of links are calculated. The design problem ending with a proper choice of manufacturing processes.

The following literature review can be divided into two categories according to two different approaches, two-pass method and one-pass method.

Two-pass method

Neubauer, Cohen and Hall [62] investigated the transverse vibrational characteristics of the connecting rod in a slider-crank mechanism by neglecting the axial vibrations and friction, the Coriolis component of acceleration, the additional tangential acceleration and normal acceleration due to the transverse deflection of the connecting rod but external loading on the piston was considered. Winfrey [103] investigated the elastic behavior of flexible link in a mechanism by using the assumption of superposition of gross rigid-body motion and a small elastic deformation. An investigation of the vibratory bending responses of the elastic connecting rod of a slider-crank mechanism was studied by Viscomi and Ayre [97], in which the longitudinal vibration of the link was neglected and the nonlinear equations of motion was solved analytically. In his study, he concluded that within the frequency range of interest, the second mode is relatively unimportant and the response is closely approximated by the first mode; At low frequency ratios, where the response is small, the linear and nonlinear equations gave closely similar results. However, in regions of large response, the solution are quite different. Erdman, Sandor and Oakberg [26] employed

kineto-elastodynamic method for the analysis and synthesis of mechanisms, in which the effects of elastic deformation upon the inertia forces are included. Sadler and Sandor [68,69] developed a method of kineto-elastodynamic analysis by employing lumped parameter model for simulating moving mechanism components subject to elastic bending vibration. In their studies, the higher order acceleration terms, such as the Coriolis, normal and tangential accelerations, were taken into consideration but buckling effect of the rigid-body axial forces. Chu and Pan [9] studied the transient dynamic response of an elastic connecting rod in the slider-crank mechanism in both the transverse and longitudial direction on the basis of the ratio of the length of the crank and length of the connecting rod, crank speeds, viscous damping and natural frequencies. In their results, the solutions were compared by using a Runge-Kutta method and a Piecewise Polynomial method.

Midha , Erdman and Frohrib [56] employed displacement finite element method to develop the mass and stiffness properties of an elastic link. They derived the nodal displacements and accelerations by including the terms coupling the elastic and rigid-body motions. However they ignored the Coriolis, normal and tangential acceleration terms when formulating kinetic energy and no buckling effect was considered. In their another study [57], a numerical procedure based on an iterative scheme was employed for obtaining an approximate particular solution from equations of motion of an elastic link with small damping and at subresonant speeds. Nath and Ghosh [60] employed finite element method to analyze general flexible mechanisms in which the Coriolis, tangential and normal components of elastic acceleration had been derived for a moving link and also included the geometric effects of axial forces.

Turcic and Midha [93] developed a generalized equations of motion for an elastic mechanism system by employing displacement finite element method, in which none of the higher order acceleration terms were neglected. By improving their equations of motion, a geometric stiffness matrix was added to the stiffness matrix of the equations of motion by assuming a constant axial force [94]. By comparing the theoretical results and experimental results, the improved equations of motion showed better results [95].

Thompson and Barr [84] employed a variational principle to systematically develop equations of motion of members of elastic mechanisms. Thompson and Ashworth investigated the resonance in planar mechanisms mounted on vibrating foundations [83,85], in which an average perturbation method was employed. Gandhi and Thompson [29] formulated the finite element equations of motion by using a mixed-variational principle, prior to solving the equations of motion by employing the Newmark method. Based on a previous variational principle [81], a nonlinear finite element analysis of flexible linkages was derived by Thompson and Sung [88].

Having reviewed the literature on two-pass method, the attention now focuses upon reviewing the one-pass method.

One-pass method

The one-pass method accounts for the coupling of elastic and inertial characteristics, which is analytically precise and, of course, the equations of motion are more complicated than the two-pass method. Song and Haug [78] treated each member in a mechanical system as being

flexible and combined the kinematic constraint equations and also the equations of motion to obtain a coupled system of equations prior to solving the problem using an implicit numerical integration method. The effect of the geometrical nonlinearity was not included in their formulation, neither was the material damping. The authors analyzed a slider-crank mechanism with a flexible connecting rod. All the members were assumed rigid. This single flexible link was treated by modeling it using one, two and three finite elements using a displacement model. Their results were not verified by experimental data. Indeed, a principal void in this area is the shortage of experimental work to evaluate the predictive capabilities of the analytical and numerical formulations developed. Only the following reports have been found comparing their numerical results with the experimental data : Alexander and Lawrence [1], Thompson-Gandhi group [86,88] and Midha, et al. [95].

1.2.4 Flexible-links in mechanical systems with bearing clearances

Intermittent motion occurs in many practical mechanisms, in which jump discontinuities manifest themselves in the kinematic chains. Some mechanisms are for manufacturing equipment in what the primary function is for punching, cutting, milling, ..., etc.. Under these conditions intermittent motion, or impact, will routinely occur during their normal usage. Some examples such as rachets, geneva mechanisms, the touch down of airplanes, the gap between two matched gears, and clearances in joints will cause intermittent motion. A typical change for the mechanism in the intermittent motion occurs in the mathematical

model of these systems when there is a change in the constraints and impulsive forces may occur as well.

Dubowsky and Gardner [17] investigated the effects of clearances and link flexibility on the stresses in joints of high-speed mechanisms. They extended their former impact pair [15] to impact beam model (IBM) and solved the problem by employing displacement functions which is the normal mode shape of vibration. Latter on, they studied the dynamic behavior of general planar mechanism with elastic links and multiple clearance connections by using a perturbation coordinate approach [18]. The bearing forces in a scotch yoke mechanism was studied. Dubowsky and Moening [19] experimentally verified the usefulness of their impact beam model. Deck and Costello joined Dubowsky's work and extended his model from planar mechanism to spatial mechanical system [22], in which finite element technique was incorporated.

In recent years, the intermittent motion has been studied by several researchers. Wehage and Haug [99] studied the dynamic analysis of systems with impulsive forces, impact, discontinuous constraints, and discontinuous velocities, in which momentum-impulse relations were obtained by integrated the Lagrange's equations with Lagrange multipliers [33], and the coefficient of restitution was incorporated in the equations of motion. A weapon mechanism and a trip-plow were simulated while assuming all links were rigid. They also presented a computer-based method for formulation and efficient solution of nonlinear, constrained differential equations of motion for mechanical systems [98]. The dynamic analysis of spatial substructures with large angular rotations has been studied by Shabana and Wehage [71]. The mode

superposition method was employed for the solution and the eigenvalue problem was solved only once even though the resulting set of differential equations is highly nonlinear. In their studies [71, 98, 99], the geometrical nonlinearity has never been considered, thus, the natural frequency is constant during the simulation, which is a contradiction to the author's experimental results presented in Chapter Three. By using the same formulation, Shabana and Wehage [70,72] studied the dynamic response of inertia-variant flexible mechanical systems. The same technique was applied on the transient dynamic analysis of a vehicle system which was composed of interconnected rigid and flexible bodies in a paper by Kim, Shabana and Haug [48]. Khulief and Shabana [46,47] investigated the impactive responses of constrained systems of rigid and flexible bodies by employing the Rayleigh-Ritz method, in which a planar slider-crank mechanism and a crank-rocker mechanism are studied. None of the material damping and the effect of the geometric nonlinearity were considered. The effect of geometric nonlinearity is first incorporated into the equations of motion by Bakr and Shabana in 1987 [2], in which its effect on the impact response of flexible multi-body systems was studied. However, they treated the axial force as a constant. Haug, Wu and Yang presented a uniformed formulation of the equations of motion for constrained multi-body system with Coulomb friction, stiction, impact and constraint addition-deletion [41,106,107]. None of the theoretical results prescribed in publications by Haug or Shabana are verified by experimental data. Hence a question of credibility exists when modeling such complex phenomenological systems.

The field of research on mechanical systems with flexible links and incorporating bearings with radial clearances has been reviewed, it is clear that in order to predict the elastodynamic behavior of linkage mechanisms, the higher-order coupling terms like Coriolis acceleration, normal and tangential accelerations due to the transverse deflection of the link, cannot be ignored. Furthermore, it is hypothesized that the geometric nonlinearity, or buckling effect, must be considered in the formulation. Numerous research studies have been done on the field of mechanical systems with clearances using analytical methods, finite element methods, variational principles, or perturbation method. Moreover, it is clearly evident from this literature review that none of the current techniques are able to model all of the phenomena while manifest themselves in the behavior of mechanism systems featuring bearings with radial clearances. In addition, with the emphasis on purely theoretical studies in the literature, it is clearly evident that a coherent combination of analytical, computational, and experimental work be undertaken in order to establish a viable design guidelines and direction for subsequent studies in this important field.

1.3 THESIS OUTLINE

The modeling strategy, which is an iterative process [33,76], presented in this thesis can be represented in the block diagram of Figure 1.4. The start is the recognition of the problem and the reviewing of the existing researches on this problem, a new mathematical model for this problem is then proposed. By evaluating the existing and expecting equipments, the test problem is defined. The numerical results

of the proposed mathematical model are then compared with the experimental data. The mathematical model is adjusted by adding more assumptions until the comparison is satisfied.

One-pass method and the finite element method are employed to formulate the highly coupled nonlinear equations of motion by incorporating the Lagrange's equations and Lagrange multipliers. All of the higher-order coupling terms are included in the equations of motion, the axial force for the geometric matrix is linearly assumed, which is different from other reports, thus generates two geometric matrices. During intermittent motion in a mechanical system the mathematical formulation mandates the incorporation of different constraints to model the complex phenomenal behavior of the elements. The link being treated as pin-free beam during free-flight-mode and as simply-supported beam during contact-mode.

In Chapter Two, model of a general planar rigid-linked mechanism with bearing clearances are derived. A four-mode model is proposed to describe the dynamical response of the mechanism. The criteria for the contact loss, termination of the free-flight-mode and restoration of the contact-mode are also defined. Finally, a slider-crank mechanism with clearance in the gudgeon-pin joint is considered as an illustrative example. The theoretical and experimental results are then compared. Correlation is demonstrated very favorable between the two sets of results

In Chapter Three, the governing equations for moving links are derived by using a displacement finite element method which combines the kinematic constraint equations and the equations of motion to obtain a coupled system of equations including both the rigid-body motion and the

elastodynamic responses of flexible links. The higher-order coupling acceleration terms such as the Coriolis acceleration, normal and tangential accelerations due to the transverse deflection of the link are included. The buckling effect of the axial force is included in the geometrically-nonlinear stiffness matrix. The eigen values, or natural frequencies, are found to vary with time and this is verified experimentally. Finally, a slider-crank mechanism with a flexible connecting rod without bearing clearances is considered. The theoretical responses of the link are compared with the experimental results. The variation of the dynamical characteristics between rigid link and flexible link are also calculated.

In Chapter Four, mechanical systems with flexible links and joints featuring bearing clearances are studied. The mathematical model combines the modelling techniques which presented in Chapter Two and in Chapter Three, and therefore a modified governing equation is obtained. The criteria and the equations of motion for four-mode model are dependent upon the deformation of the links.

Two examples are studied. The first example features a compound pendulum, which incorporates a flexible link, whose tip impacts against a stationary mechanical stop during its motion. The theoretical elastodynamic responses of the mid-span of the link and the angular position are compared with the experimental results. The second example features a slider-crank mechanism with flexible connecting rod incorporating clearance in the gudgeon-pin joint. The experimental and theeretical results are also compared.

1.4

1.

of

ipli

2.

bach

Zero

Fie

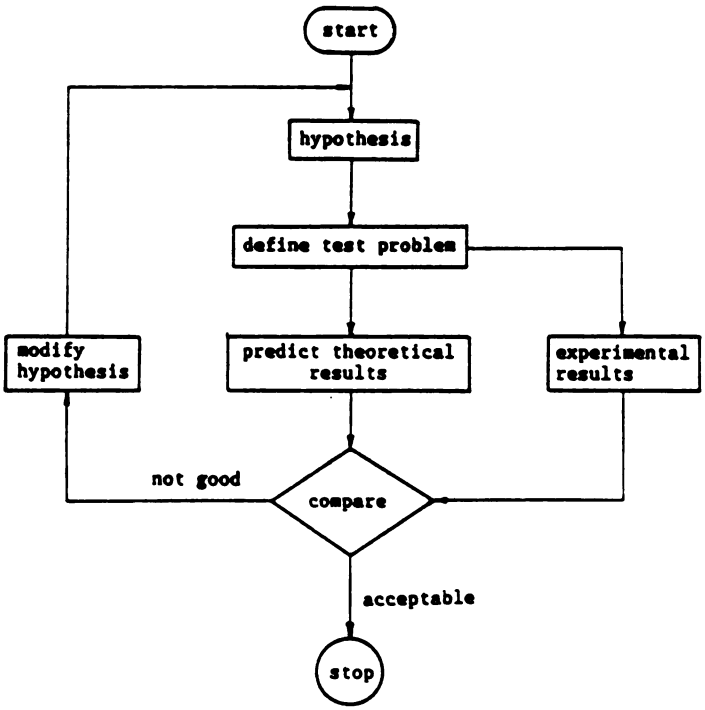

Figure 1.4 Modeling strategy

1.4 PRINCIPAL CONTRIBUTIONS

1. An analytical model was dynamic developed for predict the response of mechanical systems featuring both rigid and flexible links with joints incorporating clearances.

2. Experimental works have been done on a mechanical system featuring both rigid and flexible links with and without radial clearance in the revolute joint. These works not only partially fill the void of the field, but motivate and guide the development of theoretical models of

with prescribed radial clearance in the joints of the systems, but these results provide motivation and guidance in the future development of theoretical models of mechanical systems featuring flexible links with radial clearances.

3. A criterion has been established to predict the restoration of the contact-mode. This has not been addressed before in the literature. A four-mode model was developed in order to predict the behavior of a joint with radial clearance.

4. The experimental investigation indicates that the damping ratio in a link is dependent not only on the material, but also on the axial forces imposed on the link.

5. A quasi-static procedure to solve the coupled system of equations is proposed.

6. When the geometrical effect was added, the axial force was modelled as a linear function of displacement. This generated an extra geometrical matrix, K_{G2} in equation (3.48), which differs from the traditional constant axial force assumption.

7. The initial values for simulating a moving flexible link are determined by the first mode of the link, and the coefficients for the displacement, velocity and acceleration are found from experimental results. This procedure is quite different from previous theoretical publications where $u_0 = \dot{u}_0 = \ddot{u}_0 = 0$ were given.

Chapter II

GENERAL PLANAR MECHANISMS FEATURING RIGID-LINKS WITH RADIAL CLEARANCES IN THE REVOLUTE JOINTS

2.1 INTRODUCTION

Bearing clearances cannot be avoided in mechanical systems unless extremely stringent, and hence expensive, criteria are imposed upon the design, engineering and manufacture of the joints of these systems tolerances and also upon the wear in these kinematic pairs. Bearing clearances are, therefore, a common feature in a very large percentage of articulating mechanical systems developed for the industrial and commercial marketplaces. Even though the displacement characteristics of these mechanism systems with bearing clearances frequently differ from the displacement characteristics of the zero clearance system by only a small percentage of the overall characteristic, some other kinematic characteristics, such as the velocity, acceleration and jerk profiles, are often dramatically different from the zero-clearance case and these characteristics frequently results in the development of unacceptable products. In this chapter, the equations of motion for a general planar mechanical system

with bearing clearances are developed and a four-mode model is proposed and developed to describe the dynamic response of bearings with radial clearance. A slider-crank mechanism with radial clearance in the gudgeon-pin joint is employed as an illustrative example to demonstrate the proposed methodology.

2.2 MODEL OF A GENERAL PLANAR MECHANISM WITH BEARING CLEARANCES

The dynamical response of a general planar mechanism system incorporating revolute joints which feature a distinct radial clearance, as shown in Figure 2.1, is considered herein by modeling the system as an assemblage of interconnected rigid bodies by employing the mathematical model presented in Figure 2.2. The position vectors shown in Figure 2.2 not only define the position and orientation of the bodies but they are also employed to describe the behavior of the joints in the system. The pin and journal is assumed well-arranged in the same plane, and thus no out-of-plane motion is concerned. Collectively, these vectors impose kinematic, or geometrical, constraints on the motion of the bodies. Utilizing the classical notation for generalized constraint equations between system coordinates, such as those presented in references [42] and [51] for example, then a set of i generalized constraint equations ϕ_i may be written

$$\phi_i = \phi(q_1, q_2, \cdots\cdots, q_N) = 0 \qquad (2.1)$$

where there are N generalized coordinates q_N.

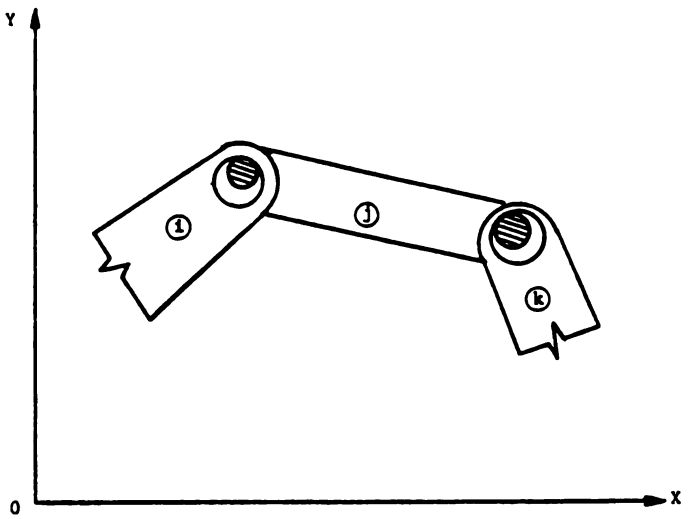

Figure 2.1 Radial clearances in the revolute joint in a planar mechanism system

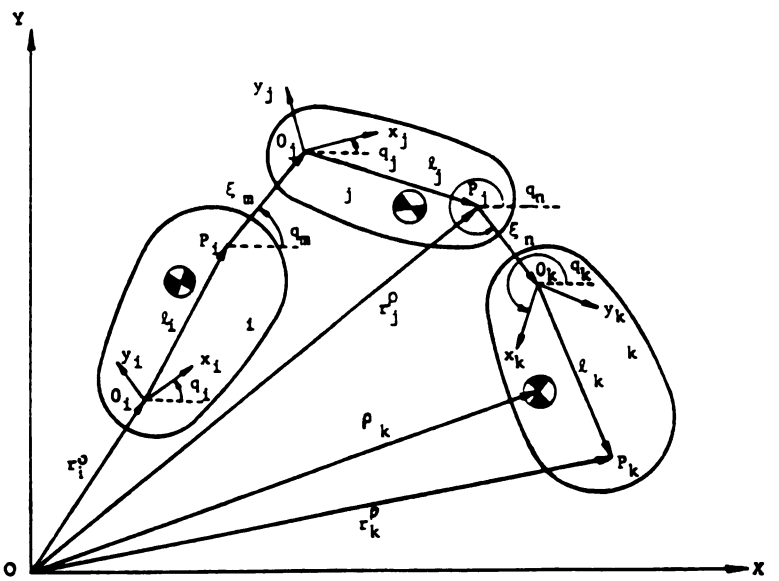

Figure 2.2 Definition of the position vectors and reference frames modeling a planar mechanism system with bearing clearances

In general, the minimization of functionals with constraint equations can be achieved by employing the Lagrange multiplier method and the penalty function method [65]. The penalty function method involves the reduction of conditional extremum problems to extremum problems without constraints by the introduction of a penalty function associated with the constraints, while the method of Lagrange multipliers offers a viable approach to developing the equations governing the response of a general mechanical system when the i constraint equations cannot be conveniently manipulated to express i of the generalized coordinates in terms of the (N-i) remaining generalized coordinates. This classical method [43,52] involves modifying the Lagrangian equations of motion for an unconstrained system of bodies, by introducing additional terms which are the product of a Lagrange multiplier and the derivative of the associated constraint equation. By incorporating the second time derivative of equation (2.1), the Lagrange multiplier approach yields a set of algebraic and differential equations governing the dynamical response of the system. These equations are generally cast in a matrix format prior to solving for the Lagrange multipliers and the acceleration terms which are subsequently integrated to obtain the velocities and displacements of the system.

The Lagrange multiplier method readily enable the joint forces of the system to be calculated and which is an essential ingredient of any methodology for predicting the dynamical behavior of mechanical systems with bearing clearances.

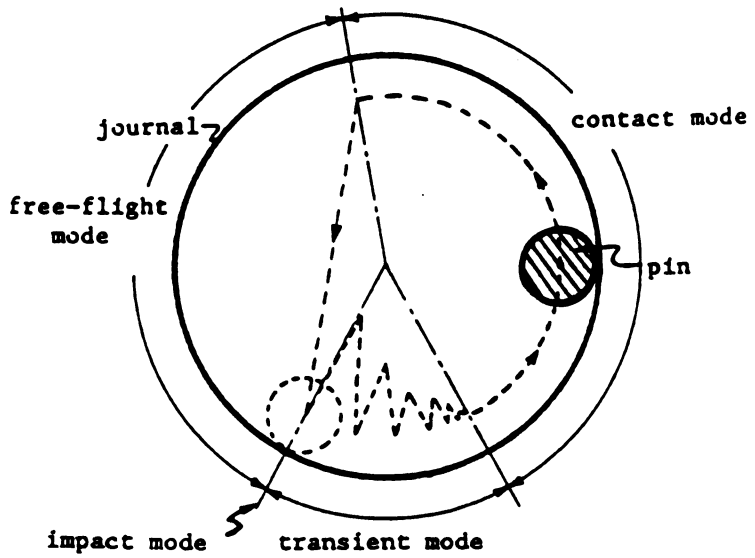

Figure 2.3 Schematic diagram presenting the four-modes describing the phenomenological behavior of a revolute joint with clearance

A four-mode model is proposed herein for predicting the dynamical response of planar articulating mechanical systems with bearing clearances. The form of this model is motivated by experimental dynamical response-data presented herein in a subsequent section. Upon reviewing these experimental results, it is clearly evident that four distinct phenomena manifest themselves in the planar motion of these dynamical systems. These four modes can be conveniently classified as the contact mode, the free-flight-mode, the impact-mode and the transient-mode. These modes are schematically presented in Figure 2.3 which illustrates the typical dynamical behavior exhibited by a revolute joint with clearance.

(i) Contact-Mode:

In the contact-mode, the pin and the journal are in contact and the relative motion between these members of the joint is assumed to described by a sliding motion. Experimental evidence suggests that rolling does not occur and hence it is not considered in the modeling process. Furthermore, the contact surface is assumed to be smooth and frictionless, thus there is no energy loss in this mode. Since the principal members of the revolute joint, the pin and the journal, cannot transmit a tensile force across the pin-journal interface in the contact-mode, this mode is assumed to terminate when the contact force between the pin and the journal becomes tensile in the computer simulation. Clearly in practice this mode is terminated at the instant when the pin and journal separate, however the computer simulation is based on a time-step philosophy, where the state of the system is only known at discrete times, therefore, in order to determine the precise configuration in which the contact force is zero, this time instant must be known prior to initiating the simulation. As a compromise, in order to avoid utilizing even smaller step sizes, the simulation software package was formulated to trigger the change from the contact-mode to the free-flight- mode when the contact force in a joint reached a small fictitious tensile state.

(ii) Free-Flight-Mode:

In the free-flight-mode, the pin and the journal in a specific joint are not in contact, hence there are no reaction forces between these two members. Under these conditions, a complex multi-element system can be treated as several compound subsystems of articulating

bodies which do not interact with each other and whose initial dynamical state is obtained from the simulation results at the termination of the previous mode. Thus for example, if a slider-crank mechanism is assumed to feature significant clearance in the gudgeon-pin bearing, the system would be treated as two independent dynamical systems during the free-flight-mode. One system would comprise two compound pendulums and the other system would comprise a translating block. This mode would be terminated when a geometric constraint mandated the triggering of a different mode.

(iii) Impact-Mode:

The sudden contact of the pin and the journal which generally occurs at the termination of the free-flight-mode triggers significant impactive behavior. This behavior is the basis for the impact-mode. This contact, which occurs in an extremely short time interval, is characterized by a discontinuity in the kinematic and kinetic characteristics, and a significant exchange of momentum occurs between the two members. Herein, this phenomenon is modeled by invoking a momentum-exchange approach which incorporates the coefficient of restitution. This coefficient, which captures the material properties of the impacting bodies, is dependent upon the stiffness of the contacting materials, the roughness of the contact surfaces, the geometrical shape of the impacting bodies, and also the velocities of the bodies prior to impact. The value of the coefficient of restitution is generally determined experimentally.

(iv) Transient-Mode:

The transient-mode begins at the first impact between the pin and the journal in a specific joint, and ends with the restoration of

contact between these members. Thus this mode generally comprises a sequence of several free-flight-modes of progressively smaller time duration and also several impact-modes. Herein the simulation software requires the pin and journal to always separate and enter the free-flight-mode after completing the impact-mode unless the time duration of the free-flight-mode is less than a prescribed extremely small time-interval and also the original point of contact differs from the subsequent point of contact by a very small prescribed quantity. Upon satisfying these criteria, control in the algorithm then transfers to the contact-mode. Although the duration of this mode is relatively small compared with the overall cycle of the pin-journal interactions, this intermittent motion behavior is clearly evident from the experimental results presented herein.

Having described the phenomenological aspects of the problem, attention now focuses upon capturing this behavior in a mathematical framework prior solving the governing equations. The subsequent sections present the mathematical apparatus for modeling each mode.

2.3 GOVERNING EQUATIONS FOR CONTACT-MODE

The equations of motion of mechanical systems with constraints and bearing clearances are formulated herein by employing the generalized Lagrange's equations in which the Lagrangian multipliers are utilized in order to incorporate the system constraints into the equations of motion. In this case the radial clearances in the revolute joints are represented by position vectors, and only compressive forces

are permitted to develop at the pin and journal interfaces in these joints.

If a dynamical system is characterized by s holonomic constraint equations, then these constraints can be incorporated within the generalized Lagrange's equations and written as

$$\frac{d}{dt}\left(\frac{\partial T}{\partial \dot{q}_k}\right) - \frac{\partial T}{\partial q_k} = Q_k + \sum_{p=1}^{s} \lambda_p \frac{\partial \phi_p}{\partial q_k} \tag{2.2}$$

where ϕ_p represents the p-th holonomic constraint equation. The term $\lambda_j \frac{\partial \phi_j}{\partial q_k}$ in equation (2.2) is a generalized force which imposes the j-th constraint which is associated with the k-th coordinate. Each constraint thus contributes an additional generalized force to each of the equations of motion.

If r clearances are present in a general dynamical system with ℓ links, then at any time instant, t, the position vector of the mass center of the arbitrary k-th link can be represented by the position vector ρ_k

$$\rho_k = \rho_k(q_1, q_2, \cdots, q_N), \text{ where } N = \ell + r. \tag{2.3}$$

Thus, the velocity of the mass center of the k-th link may be written

$$\dot{\rho}_k = \sum_{i=1}^{N} \frac{\partial \rho_k}{\partial q_i} \dot{q}_i . \tag{2.4}$$

The kinetic energy of the mechanical system may, therefore, be written

$$T = \frac{1}{2} \sum_{i=1}^{\ell} m_i \dot{\rho}_i \cdot \dot{\rho}_i = \frac{1}{2} \sum_{i=1}^{N} \sum_{j=1}^{N} m_{ij} \dot{q}_i \dot{q}_j \tag{2.5}$$

where the generalized mass m_{ij} is defined

$$m_{ij} = \sum_{i=1}^{\ell} m_i \frac{\partial \rho_i}{\partial q_i} \cdot \frac{\partial \rho_i}{\partial q_j} . \tag{2.6}$$

Since the vectors defined representing the joint clearances in Figure 2.2 are massless quantities, the generalized mass can be rewritten as

$$m_{ij} = \sum_{i=1}^{N} m_i \frac{\partial \rho_i}{\partial q_i} \cdot \frac{\partial \rho_i}{\partial q_j} . \tag{2.7}$$

Furthermore, the corresponding first and second time-derivatives of the constraint equations, equation (2.1), are respectively

$$\dot{\phi}_p = \sum_{i=1}^{N} \frac{\partial \phi_p}{\partial q_i} \dot{q}_i \tag{2.8}$$

and

$$\ddot{\phi}_p = -\sum_{i=1}^{N}\sum_{j=1}^{N} \frac{\partial^2 \phi_p}{\partial q_i \partial q_j} \dot{q}_j \dot{q}_i + \sum_{i=1}^{N} \frac{\partial \phi_p}{\partial q_i} \ddot{q}_i . \tag{2.9}$$

Utilizing equation (2.2), the dynamical equations of motion of the k-th link of the general kinematic chain can be written

$$\sum_{i=1}^{N} m_{ki} \ddot{q}_i + \sum_{i=1}^{N}\sum_{j=1}^{N} \frac{\partial}{\partial q_j}\left(m_{ki}\right) \dot{q}_j \dot{q}_i - \frac{1}{2}\sum_{j=1}^{N}\sum_{i=1}^{N} \frac{\partial}{\partial q_k}\left(m_{ij}\right) \dot{q}_j \dot{q}_i$$

$$- \sum_{i=1}^{p} F_i \cdot \frac{\partial r_i}{\partial q_k} + \sum_{i=1}^{s} \lambda_i \frac{\partial \phi_i}{\partial q_k} \tag{2.10}$$

Equations (2.9) and (2.10) constitute the equations of motion governing the behavior of a general constrained planar mechanical system with bearing clearances in the contact mode. These equations can be reformulated in a matrix format and can be compactly written as

$$\begin{bmatrix} M & \dfrac{\partial \Phi}{\partial q} \\ \left(\dfrac{\partial \Phi}{\partial q}\right)^T & 0 \end{bmatrix} \begin{bmatrix} \ddot{q} \\ -\lambda \end{bmatrix} = \begin{bmatrix} g \\ f \end{bmatrix} \tag{2.11}$$

where

$$\left[\ \bar{q}\ \right] = \left[\ \bar{q}_1 \cdots\cdots \bar{q}_N\right]^T$$

$$\left[\ \lambda\ \right] = \left[\lambda_1 \cdots\cdots \lambda_s\right]^T$$

$$\left[\ g\ \right] = \left[g_1 \cdots\cdots g_N\right]^T \tag{2.12}$$

$$\left[\ f\ \right] = \left[f_1 \cdots\cdots f_s\right]^T$$

$$g_k = \sum_{i=1}^{p} F_i \cdot \frac{\partial r_i}{\partial q_k} - \sum_{i=1}^{N}\sum_{j=1}^{N} \frac{\partial}{\partial q_j}\left(m_{ki}\right)\dot{q}_j\dot{q}_i + \frac{1}{2}\sum_{j=1}^{N}\sum_{i=1}^{N} \frac{\partial}{\partial q_k}\left(m_{ij}\right)\dot{q}_j\dot{q}_i$$

$$k=1,\ 2,\ \cdots,\ N \tag{2.13}$$

$$f_p = -\sum_{i=1}^{N}\sum_{j=1}^{N} \frac{\partial^2 \phi_p}{\partial q_i \partial q_j}\dot{q}_j\dot{q}_i\ ,\ p = 1,\ 2,\ \cdots,\ s \tag{2.14}$$

$$\left[\ M\ \right] = \begin{pmatrix} m_{11} & m_{12} & \cdots\cdots & m_{1N} \\ m_{21} & m_{22} & \cdots\cdots & m_{2N} \\ \cdots & \cdots & \cdots & \cdots \\ m_{N1} & m_{N2} & \cdots\cdots & m_{NN} \end{pmatrix} \tag{2.15}$$

$$\left[\frac{\partial \Phi}{\partial q}\right] = \begin{bmatrix} \frac{\partial \phi_1}{\partial q_1} & \frac{\partial \phi_2}{\partial q_1} & \cdots\cdots & \frac{\partial \phi_s}{\partial q_1} \\ \frac{\partial \phi_1}{\partial q_2} & \frac{\partial \phi_2}{\partial q_2} & \cdots\cdots & \frac{\partial \phi_s}{\partial q_2} \\ \cdots\cdots & \cdots\cdots & \cdots\cdots & \cdots\cdots \\ \frac{\partial \phi_1}{\partial q_N} & \frac{\partial \phi_2}{\partial q_N} & \cdots\cdots & \frac{\partial \phi_s}{\partial q_N} \end{bmatrix} \tag{2.16}$$

In equation (2.11) the differential equations are represented as a set of simultaneous, linear algebraic equations in the variables $\ddot{q}_i$ and λ_p, and the coefficient matrix can be conveniently partitioned into four submatrices. The upper-left submatrix is symmetric and contains the generalized mass coefficients m_{ij}, which are the coefficients of the second-order acceleration terms in the Lagrange's equations. The main diagonal coefficients of this matrix are constants. The upper-right submatrix, which is the system Jacobian, is the transpose of the lower-left submatrix. The lower-left submatrix is formed directly from the second-order terms of the constraint equations, while the upper-right submatrix is composed of the Lagrange multiplier coefficients.

The column vector of dependent variables includes the second-order derivatives $\ddot{q}$ in the upper sub-vector, while the lower sub-vector, $-\lambda$, includes the Lagrange multiplier terms, which originated in the generalized Lagrange's equations. On the right-hand side of equation (2.11) the column vector contains displacement and velocity-dependent forces, $g(q,\dot{q})$, pertaining to the particular Lagrange's equation, or the constraint equation associated with the row in which they appear. The terms g_k include the effect of all external forces, as well as the

centripetal and Coriolis components, while the terms f_p contain the centripetal and Coriolis terms from the loop-closure equation for the mechanical system.

2.4 GOVERNING EQUATIONS FOR FREE-FLIGHT-MODE

During the free-flight-mode, in a specific revolute joint with clearance, the constraints imposed at the joint during the contact mode are not enforced during the short time duration in which relative motion between the pin and the journal occurs as the pin moves across the bearing clearance. Consequently the Lagrangian multipliers imposing the constraints at these joints disappear for those joints in which contact has been lost and the free-flight-mode initiated. The equations of motion for the free-flight-mode assume the same general format as equation (2.11). Thus they may be obtained by deleting the columns and rows associated with those Lagrangian multipliers which are zero in order to relax the associated constraints. If there are "a" joints in the phase of free-flight-mode, the equations of motion become

$$\begin{bmatrix} M^f & \dfrac{\partial \Phi^f}{\partial q^f} \\ \left(\dfrac{\partial \Phi^f}{\partial q^f}\right)^T & 0 \end{bmatrix} \begin{bmatrix} \ddot{q}^f \\ -\lambda^f \end{bmatrix} - \begin{bmatrix} g^f \\ f^f \end{bmatrix} \tag{2.17}$$

where

$$\left(\ddot{q}^f\right) = \left(\ddot{q}_1^f \cdots\cdots \ddot{q}_{N-a}^f\right)^T$$

$$\left[\lambda^f\right] = \left[\lambda_1^f \cdots\cdots\cdots \lambda_{s-2a}^f\right]^T \tag{2.18}$$

$$\left[g^f\right] = \left[g_1^f \cdots\cdots\cdots g_{N-a}^f\right]^T$$

$$\left[f^f\right] = \left[f_1^f \cdots\cdots\cdots f_{s-2a}^f\right]^T$$

$$g_k^f = \sum_{i=1}^{p} F_i \cdot \frac{\partial r_i}{\partial q_k^f} - \sum_{i=1}^{N-a}\sum_{j=1}^{N-a} \frac{\partial}{\partial q_j^f}\left(m_{ki}\right) \dot{q}_j^f \dot{q}_i^f + \frac{1}{2}\sum_{j=1}^{N-a}\sum_{i=1}^{N-a} \frac{\partial}{\partial q_k^f}\left(m_{ij}\right) \dot{q}_j^f \dot{q}_i^f$$

$$k=1,\ 2,\ \cdots,\ N-a \tag{2.19}$$

$$f_p^f = -\sum_{i=1}^{N-a}\sum_{j=1}^{N-a} \frac{\partial^2 \phi_p^f}{\partial q_i^f \partial q_j^f} \dot{q}_j \dot{q}_i \ ,\ p = 1,\ 2,\ \cdots,\ s-2a \tag{2.20}$$

$$\left[M^f\right] = \begin{bmatrix} m_{11} & m_{12} & \cdots\cdots\cdots & m_{1d} \\ m_{21} & m_{22} & \cdots\cdots\cdots & m_{2d} \\ \cdots & \cdots & \cdots & \cdots \\ m_{d1} & m_{d2} & \cdots\cdots\cdots & m_{dd} \end{bmatrix} \ ,\ d = N-a \tag{2.21}$$

$$\left[\frac{\partial \Phi^f}{\partial q^f}\right] = \begin{bmatrix} \dfrac{\partial \phi_1^f}{\partial q_1^f} & \dfrac{\partial \phi_2^f}{\partial q_1^f} & \cdots\cdots & \dfrac{\partial \phi_{s-2a}^f}{\partial q_1^f} \\ \dfrac{\partial \phi_1^f}{\partial q_2^f} & \dfrac{\partial \phi_2^f}{\partial q_2^f} & \cdots\cdots & \dfrac{\partial \phi_{s-2a}^f}{\partial q_2^f} \\ \cdots & \cdots & \cdots & \cdots \\ \dfrac{\partial \phi_1^f}{\partial q_d^f} & \dfrac{\partial \phi_2^f}{\partial q_d^f} & \cdots\cdots & \dfrac{\partial \phi_{s-2a}^f}{\partial q_d^f} \end{bmatrix} \ ,\ d = N-a \tag{2.22}$$

2.5 GOVERNING EQUATIONS FOR THE IMPACT-MODE

The discontinuities associated with mechanical systems with bearing clearances, create impulsive phenomena when the two principal members of a revolute joint suddenly contact. This behavior is modeled in the impact-mode of the proposed model by employing a formulation developed in Goldsmith's classical text on impact phenomena [33] which is based on the form of Lagrange's equations presented by equation (2.2).

Integration of equation (2.2) over the interval t to t+τ, if τ is assumed arbitrarily small, yields the equation

$$\left(\frac{\partial T}{\partial \dot{q}_k}\right)^* - \left(\frac{\partial T}{\partial \dot{q}_k}\right) = \hat{Q}_k + \sum_{p=1}^{s} \hat{\lambda}_p \frac{\partial \phi_p}{\partial q_k} \tag{2.23}$$

where

$$\frac{\partial T}{\partial \dot{q}_k} = \sum_{i=1}^{N} m_{ki} \dot{q}_i \tag{2.24}$$

$$\hat{Q}_k = \int_t^{t+\tau} \bar{Q}_k \, dt = \sum_{j=1}^{p} \hat{F}_j \frac{\partial r_j}{\partial q_k} \cdot n_j \tag{2.25}$$

and $\hat{F}$ is defined as the impulse in the n direction.

In order to solve equations (2.23), (2.24) and (2.25) for the unknown quantities ($\dot{q}_i^*$, $\hat{\lambda}_i$, $\hat{F}_i$), a velocity constraint relationship must

be developed and also a relationship for the kinematic behavior before and after the impact must be formulated. The first requirement is satisfied by employing equation (2.8) and the second requirement is satisfied by developing an expression incorporating the coefficient of restitution ϵ at each joint. Equation (2.8) may be applied to model the impact phenomenon by utilizing the expression

$$\dot{\phi}_r^* - \dot{\phi}_r - \sum_{i=1}^{N} \frac{\partial \phi_r}{\partial q_i} (\dot{q}_i^* - \dot{q}_i) = 0. \tag{2.26}$$

The coefficient of restitution is defined as

$$\epsilon = - \frac{(\dot{r}_{Qa}^* - \dot{r}_{Qb}^*)\cdot n}{(\dot{r}_{Qa} - \dot{r}_{Qb})\cdot n} \quad , \text{ where } \dot{r} = \sum_{i=1}^{N} \frac{\partial r}{\partial q_i} \dot{q}_i \tag{2.27}$$

where the relative velocity after impact is $(\dot{r}_{Qa}^* - \dot{r}_{Qb}^*)$ while $(\dot{r}_{Qa} - \dot{r}_{Qb})$ is the relative velocity before impact. Since $\dot{r}_{Qa}$ and $\dot{r}_{Qb}$ are both dependent on $\dot{r}(q_i, \dot{q}_i)$, equation (2.27) can be rewritten as

$$\epsilon = - \frac{\left(\sum_{i=1}^{N} \frac{\partial r_k}{\partial q_i} \dot{q}_i^* \cdot n_k \right)}{\left(\sum_{i=1}^{N} \frac{\partial r_k}{\partial q_i} \dot{q}_i \cdot n_k \right)} \tag{2.28}$$

Equations (2.23), (2.26) and (2.28) are the equations governing the impact-mode. These expressions can be easily expressed in matrix form as

$$\begin{bmatrix} M & \frac{\partial \Phi}{\partial q} & \frac{\partial R}{\partial q} \\ \left(\frac{\partial \Phi}{\partial q}\right)^T & 0 & 0 \\ \left(\frac{\partial R}{\partial q}\right)^T & 0 & 0 \end{bmatrix} \begin{bmatrix} \dot{q}^* \\ -\hat{\lambda} \\ -\hat{F} \end{bmatrix} - \begin{bmatrix} p \\ g \\ f \end{bmatrix} \tag{2.29}$$

where

M - generalized mass matrix

$\left(\frac{\partial \Phi}{\partial q}\right)$ - system Jacobian matrix associated with the Lagrangian multipliers

$\left(\frac{\partial R}{\partial q}\right)$ - system Jacobian matrix associated with the impulse

$$[\dot{q}^*] = [\dot{q}_1^*, \dot{q}_2^*, \cdots\cdots, \dot{q}_N^*]^T$$

$$[\hat{F}] = [\hat{F}_1, \hat{F}_2, \cdots\cdots, \hat{F}_p]^T$$

$$[\hat{\lambda}] = [\hat{\lambda}_1, \hat{\lambda}_2, \cdots\cdots, \hat{\lambda}_s]^T \tag{2.30}$$

$$[p] = [p_1, p_2, \cdots\cdots, p_N]^T$$

$$[\ g\ ] = [g_1,\ g_2,\ \cdots\cdots,\ g_s]^T$$

$$[\ f\ ] = [f_1,\ f_2,\ \cdots\cdots,\ f_N]^T$$

$$p_k = \sum_{k=1}^{N} m_{ki}\dot{q}_i \qquad k = 1,\ 2,\ \cdots\cdots,\ N \tag{2.31}$$

$$g_j = \sum_{i=1}^{N} \frac{\partial \phi_j}{\partial q_i}\ \dot{q}_i\ , \qquad j = 1,\ 2,\ \cdots\cdots,\ s \tag{2.32}$$

$$f_k = -\epsilon \sum_{k=1}^{N} \left(\frac{\partial r_k}{\partial q_j} \cdot n_k\right)\ \dot{q}_j\ , \qquad k = 1,\ 2,\ \cdots\cdots,\ p \tag{2.33}$$

This completes the development of the equations of motion for study the dynamic phenomena in revolute joint with radial clearance. Attention now focuses on establishing a viable numerical algorithm for solving the system of algebraic-differential equations which govern this class of dynamic problems.

2.6 STRATEGY FOR A NUMERICAL SOLUTION

The equations of motion, equations (2.11) and (2.17), governing the dynamical behavior of a planar mechanical system with bearing clearances are written as a mixed set of differential and algebraic equations which can be expressed in the matrix form

$$[\ A\ ]\ \{\ X\ \} = \{\ B\ \} \tag{2.34}$$

where the coefficients in matrix [A] and vector {B} are dependent upon the displacements and velocities of the kinematic chain. Thus upon selecting the initial values for those kinematic parameters, [A] and {B} can be determined using a step-by-step procedure which discretizes the time domain prior to solving equation (2.34) for {X} using PLU-factorization in conjunction with forward and backward substitution [79]. The column vector {X} includes the second-order derivatives, $\ddot{q}_k$, and also the Lagrangian multipliers λ. The displacements and the velocities at the next time step are determined by subsequently integrating the accelerations $\ddot{q}_k$. This integration process was accomplished by employing the subroutine, DGEAR, in the IMSL subroutine library which featured both a fifth-order Gear algorithm for stiff systems, which is referred to as any initial-value problem in which the complete solution consists of fast and slow components [31,32,43,63,81], and also a twelfth-order implicit Adams method. The numerical results presented herein were obtained by invoking the Adams method, since for systems where stiffness is not a problem, the Adams method uses fewer time-steps and is more accurate than the Gear algorithm [31].

In order to initiate the simulation software, a set of initial conditions are required, and the selection of the appropriate conditions is crucial in the prediction of the dynamical behavior of this class of nonlinear mechanism systems. The initial conditions for the methodology proposed herein are based upon the results of kinematic and dynamic analyses of the mechanism system in which all of the joints are assumed to be characterized by zero clearance. The orientations of the position vectors representing the clearance in each revolute joint of a mechanism system with bearing clearances are assumed to coincide with the

direction of the vector representing the resultant force at each respective joint, and the angular velocity of these position vectors are assumed to be equal to the rate of change of the angular orientation of these resultant force vectors. The subsequent initial conditions for each time-step in the simulation are obtained in the usual manner from the final conditions of the previous time-step.

Industrial and commercial kinematic chains featuring revolute joints with bearing clearances exhibit discontinuities in their dynamical response behavior which invariably occur in the transition from one mode to the subsequent mode. A typical example is the distinct change in velocity between the contact-mode and the free-flight-mode. In the simulation of these phenomena, these discontinuities can be amplified to yield erroneous results. In order to minimize these effects, the critical point in switching from one mode to the next is carefully predicted using the bisectional method [81] in which smaller and smaller time-steps are employed in the mode-transfer time-zone.

The mathematical apparatus is now complete for predicting the dynamical response of general planar mechanism systems incorporating radial clearance in the revolute joints. The equations governing this class of nonlinear systems have been described and a four-mode model proposed for predicting the complex phenomenological behavior of these systems. Furthermore, the subtleties of simulating these systems have also been enunciated. Attention now focuses upon applying this proposed approach to a planar slider-crank mechanism with radial clearance at the gudgeon-pin bearing, in order to illustrate the approach, prior to comparing the theoretical results with experimental data from a complementary study.

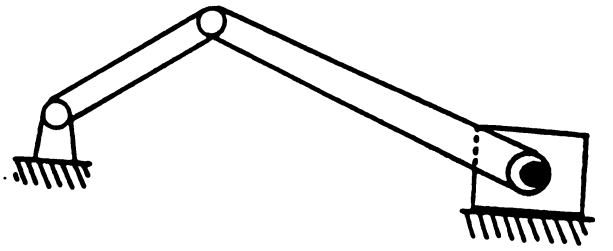

(a)

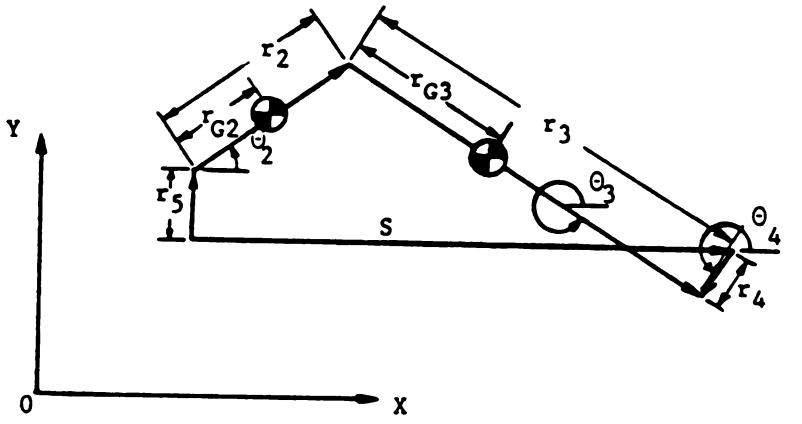

(b)

Figure 2.4 (a) The slider-crank mechanism showing dominant clearance at the gudgeon-pin bearing
(b) Vector-loop model of the mechanism

2.7 THEORETICAL MODEL OF SLIDER-CRANK MECHANISM WITH CLEARANCE IN THE GUDGEON-PIN JOINT

A planar slider-crank mechanism with a prescribed non-zero radial clearance at the gudgeon-pin joint between the connecting-rod and the slider was analyzed using the proposed methodology prior to comparing the theoretical results with experimental response data from an accompanying experimental investigation. The friction between the pin and journal is ignored. A schematic of the mechanism is presented in Figure 2.4(a) and the relevant kinematic parameters are presented in Figure 2.4(b). The subsequent paragraphs systematically describe the equations governing the dynamical response of the linkage when the pin and journal of the gudgeon-pin are in the contact-mode, the free-flight-mode, the impact-mode, and finally the transient-mode prior to describing the complementary experimental program.

2.7.1 Equations of motion for the contact-mode

The dynamical behavior of the slider-crank mechanism in the contact-mode is governed by a set of independent simultaneous second-order differential equations which are established using equations (2.11)-(2.16). The final equations can be expressed in matrix form, as

$$[A_1] \{ X_1 \} = \{ B_1 \} \qquad (2.35)$$

where

$$[A_1] = \begin{bmatrix} -1 & m_3 r_2 r_{G3} \cos(\theta_3-\theta_2) & 0 & 0 & r_2 \sin\theta_2 & -r_2\cos\theta_2 \\ 0 & I_{G3}+ m_3 r_{G3}^2 & 0 & 0 & r_3\sin\theta_3 & -r_3\cos\theta_3 \\ 0 & 0 & 0 & 0 & -r_4\sin\theta_4 & r_4\cos\theta_4 \\ 0 & 0 & 0 & m_s & 1 & 0 \\ 0 & r_3\sin\theta_3 & -r_4\sin\theta_4 & 1 & 0 & 0 \\ 0 & -r_3\cos\theta_3 & r_4\cos\theta_4 & 0 & 0 & 0 \end{bmatrix} \tag{2.36}$$

and,

$$\{X_1\}^T = [\lambda_3 \;\; \ddot{\theta}_3 \;\; \ddot{\theta}_4 \;\; \ddot{s} \;\; \lambda_1 \;\; \lambda_2] \tag{2.37}$$

while,

$$\{B_1\} = \begin{bmatrix} m_3 r_2 r_{G3}\dot{\theta}_3^2 \sin(\theta_3-\theta_2) \\ -m_3 r_2 r_{G3}\dot{\theta}_2^2 \sin(\theta_3-\theta_2) \\ 0 \\ -(sgn)\mu M_s g \\ -r_2\dot{\theta}_2^2\cos\theta_2 - r_3\dot{\theta}_3^2\cos\theta_3 + r_4\dot{\theta}_4^2\cos\theta_4 \\ -r_2\dot{\theta}_2^2\sin\theta_2 - r_3\dot{\theta}_3^2\sin\theta_3 + r_4\dot{\theta}_4^2\sin\theta_4 \end{bmatrix} \tag{2.38}$$

The crank is assumed to operate with a constant angular velocity $\dot{\theta}$ thereby requiring the angular acceleration of the crank-shaft to be zero. This situation mandates the introduction of the Lagrange

multiplier λ_3 which represents the torque required to maintain this constant crank frequency. The Lagrangian multipliers λ_1 and λ_2 in equation (2.37) represent, F_{s3x}, the force imposed on link 3 by the slider in the ox direction, and, F_{s3y}, the force imposed on link 3 by the slider in the oy direction respectively.

2.7.2 Equations of motion for the free-flight-mode

The loss of contact between the connecting rod and the slider in the free-flight-mode mandates that the mechanism to be modeled as two systems. One system is the double-pendulums arrangement of the crank and the connecting rod which moves independently of the second system which comprises the slider. Thus, the pin force at the gudgeon-pin joint is zero, since there is no contact between the pin and journal of this bearing. Utilizing the constrained Lagrange's equation again, only three second-order differential equations govern this mode and they can be written, in matrix form, as

$$[\ A_2\ ]\ \{\ X_2\ \} = \{\ B_2\ \} \tag{2.39}$$

where

$$[\ A_2\ ] = \begin{bmatrix} -1 & m_3 r_2 r_{G3}\cos(\theta_3 - \theta_2) & 0 \\ 0 & I_{G3} + m_3 r_{G3}^2 & 0 \\ 0 & 0 & M_s \end{bmatrix} \tag{2.40}$$

$$\{\ X_2\ \}^T = [\lambda_1\ \ddot{\theta}_3\ \ddot{s}\ ] \tag{2.41}$$

and,

$$\{ B_2 \} = \begin{bmatrix} m_3 r_2 r_{G3} \dot{\theta}_3^2 \sin(\theta_3 - \theta_2) \\ -m_3 r_2 r_{G3} \dot{\theta}_2^2 \sin(\theta_3 - \theta_2) \\ -(sgn)\mu M_s g \end{bmatrix} \tag{2.42}$$

where μ is the coefficient of friction between the slider and the guide.

2.7.3 Equations of motion for the impact-mode

With reference to the free-body diagram presented as Figure 2.5, the equations of motion governing the impact behavior between the pin and the journal in the gudgeon-pin bearing are established using equations (2.29)-(2.33). Upon applying these general equations to the planar slider-crank mechanism, the following equations emerge

$$[A_3] \{ X_3 \} = \{ B_3 \} \tag{2.43}$$

where

$$[A_3] = \begin{bmatrix} -1 & m_3 r_2 r_{G3} \cos(\theta_3 - \theta_2) & 0 & -r_2 \sin(\theta_2 - \theta_4) \\ 0 & m_3 r_{G3}^2 + I_{G3} & 0 & -r_3 \sin(\theta_3 - \theta_4) \\ 0 & 0 & m_s & -\cos\theta_4 \\ 0 & -r_3 \sin(\theta_3 - \theta_4) & -\cos\theta_4 & 0 \end{bmatrix}, \tag{2.44}$$

$$\{ X_3 \}^T = [\hat{T}_{or} \quad \dot{\theta}_3^* \quad \ddot{s}^* \quad \hat{F}] , \tag{2.45}$$

and,

$$[\,B_3\,] = \begin{bmatrix} m_3 r_2 r_{G3} \dot{\theta}_3 \cos(\theta_3 - \theta_2) \\ (m_3 r_{G3} + I_{G3})\,\dot{\theta}_3 \\ m_s \dot{s} \\ \left\{ \epsilon\,(r_2 \dot{\theta}_2 \sin(\theta_2 - \theta_4) + r_3 \dot{\theta}_3 \sin(\theta_3 - \theta_4) + \dot{s}\cos\theta_4) \right. \\ \left. \quad + r_2 \dot{\theta}_2 \sin(\theta_2 - \theta_4) \right\} \end{bmatrix} \qquad (2.46)$$

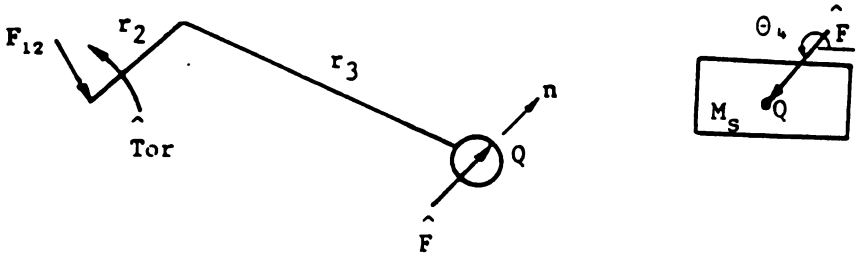

Figure 2.5 Free-body diagram of the slider-crank mechanism in the impact-mode

The coefficient of restitution, ϵ, which is an energy-dissipation parameter was experimentally determined to be 0.46 for the gudgeon-pin bearing by dynamically stimulating the bearing in a carefully controlled environment in order to replicate the impactive dynamical environment imposed on the journal and pin by the articulating mechanism. This experimental procedure is described in section 2.7.6.

2.7.4 Equations of motion for the transient-mode

The transient-mode, which is clearly evident in the experimental response profiles furnished by the transducers from the complementary laboratory investigation, comprises a series of impact and free-flight-modes which are terminated when the contact-mode is initiated. The governing equations have therefore, been documented in the previous sections.

2.7.5 Simulation protocols

This section of the thesis documents the mathematical formulations which define the bounds of the different behavioral modes described previously for revolute joints with radial clearance, and also the subtleties incorporated into the simulation software.

(i) Contact Loss

Two criteria were employed in order to trigger the change from the contact-mode to the free-flight-mode. First, in every time-step of the simulation, the resultant contact force between the pin and journal at the gudgeon-pin joint was calculated using the expression,

$$F_s = \lambda_1 \cos \theta_4 + \lambda_2 \sin \theta_4 \qquad (2.47)$$

The physical system remains in the contact-mode provided that the resultant contact force between the pin and the journal, F_s, is compressive. Thus from a mathematical standpoint, where compressive forces are assumed to be negative, this notation mandates that F_s will

always be less than zero when the pin and journal are in the contact-mode. Experience accrued in the complementary experimental investigation clearly indicates that this criterion is only valid at crank speeds below 100 rpm for the specific slider-crank mechanism under investigation. The generality of this observation is unknown. Other experimental mechanisms with different kinematic and dynamic characteristics would need to be designed, engineered and fabricated in order to investigate this observation.

A second criterion was, therefore, introduced in order to overcome the lack of generality associated with the first criterion. This second criterion states that a loss of contact will occur when F_s assumes a minimum value and, in addition, the rate-of-change of the pressure angle is high relative to other values of this parameter. The pressure angle is defined as the angle of the resultant force vector F_s relative to the inertial reference frame OXY. This criterion is the result of both theoretical and experimental observations. If only the pin force criterion alone is employed to predict the loss of contact, then the simulation software will predict that the pin and journal remain in the contact-mode provided that F_s is negative, no matter how rapidly the pressure angle changes with time. However, experimental results both herein, and also in references [25,37,38], clearly contradict this statement since contact loss is normally characterized by a high rate of change of pressure angle. Consequently, the simulation software package predicts that contact between the pin and the journal of a revolute joint will be lost when the contact force at the joint is small and also the angular rate-of-change of the force vector is high. These criteria capture the instability characteristics

associated with this dynamical state.

(ii) Termination of the Free-Flight-Mode

The pin of a revolute joint is assumed to be in the free-flight-mode relative to the journal until the following geometrical inequality criterion is violated whereupon the impact-mode is initiated,

$$0 < (\Delta x^2 + \Delta y^2)^{1/2} - \xi. \tag{2.48}$$

where ξ denotes the radial clearance. This constraint relates the locations of the geometrical centers of the pin and the journal relative to the radial clearance in the joint. The terms Δx and Δy are obtained from the loop-closure constraint. Namely,

$$\Delta x = r_2\cos\theta_2 + r_3\cos\theta_3 - r_4\cos\theta_4 - s \tag{2.49}$$

$$\Delta y = r_5 + r_2\sin\theta_2 + r_3\sin\theta_3 - r_4\sin\theta_4 \tag{2.50}$$

Ideally, if $(\Delta x^2 + \Delta y^2)^{1/2} = \xi$, then the system will be in the impact-mode, since this mode is assumed to follow the free-flight-mode. However, in all digital simulation work, computational round-off errors accumulate and a tolerance must inevitably be introduced in order to accommodate these small inaccuracies in the numerical results. Thus, the system was assumed to be in the impact-mode if the following inequality was satisfied

$$|1.0 \times 10^{-8}| \leq [\ (\Delta x^2 + \Delta y^2)^{1/2} - \xi\ ] \qquad (2.51)$$

(iii) Restoration of the Contact-Mode

The software was written to incorporate the constraint that the motion of the pin and journal is governed by the free-flight-mode following the impact-mode provided that the duration of the flight-time of the pin and journal between contact-loss and the re-establishment of contact subtends more than a twentieth of a degree of crank rotation. If contact between the pin and journal is re-established within a twentieth of a degree of crank rotation and there is also an insignificant difference between the original contact point and the new contact point, then the simulation control switches to the contact-mode.

(iv) Solution Procedure

A flow chart documenting the logic of the simulation software for predicting the dynamic response of planar mechanisms incorporating bearing clearances is presented in Figure 2.6. The initial conditions for simulating the dynamical behavior of the slider-crank mechanism were based upon the assumption that the position vector representing the clearance in the gudgeon-pin joint had the same direction as the angle of the resultant force in the bearing. The magnitude of this angle was obtained from an analysis of the mechanism incorporating a gudgeon-pin bearing with zero clearance, and in addition, the angular velocity of the clearance-vector was assumed to equal the rate-of-change of the angle of the resultant force. The step-by-step simulation, therefore, began in the contact-mode, and the equations of motion were expressed in matrix form as presented by equation (2.35). Upon determining the appropriate initial values for the system, the coefficients of, $[A_1]$ and

$\{B_1\}$ were then evaluated prior to calculating the vector $\{X_1\}$ which included the terms $\ddot{\theta}_3$, $\ddot{\theta}_4$, $\ddot{s}$, λ_1, λ_2, and λ_3. PLU-factorization was employed in conjunction with forward and backward substitution in order to undertake this task. Subsequently, the second-order variables $\ddot{\theta}_3$, $\ddot{\theta}_4$, and $\ddot{s}$ were transformed into a set of first-order equations, and a subroutine "DGEAR" in the IMSL subroutine library was employed to integrate these second-order derivatives and obtain values of $\dot{\theta}_1$, θ_1, $\dot{s}$, and s. The joint force and the rate-of-change of the angle of the resultant force were also calculated at each time-step. Simulation control switched to the free-flight-mode once the criteria for contact loss were satisfied, and equation (2.39) was then solved. The equation governing the impact-mode, equation (2.43) was solved, once the inequality relationship (2.51) was satisfied. After the first impactive motion, the simulation entered the transient-mode, and following a series of relatively brief free-flight and impactive-mode states, the control returned to the contact-mode again provided the criteria for the restoration of the contact-mode were satisfied. The average CPU-time for one cycle was 2 minutes and 50 seconds on a Vax-11/750 computer.

Having described the equations of motion governing the dynamical response of a planar slider-crank mechanism with radial clearance at the gudgeon-pin joint, and discussed the salient features of the computational scheme for solving these equations, attention now focuses on describing a complementary experimental program which furnished experimental response data for evaluating the predictive capabilities of the proposed methodology.

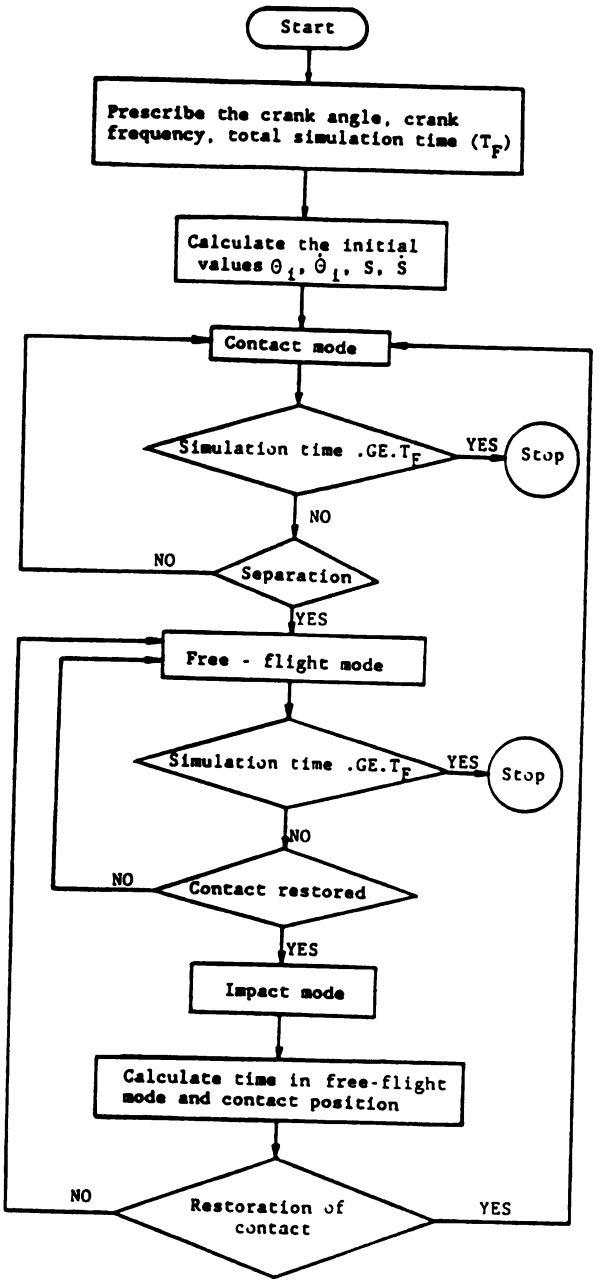

Figure 2.6 Flow chart for the computer protocol

2.7.6 Experimental apparatus and procedures

The comprehensive experimental study presented herein, on the dynamical response of a planar slider-crank mechanism featuring a bearing with a prescribed radial clearance in one joint is motivated by the dearth of experimental studies in the literature on this subject. The literature reporting on experimental studies on planar slider-crank mechanisms with rigid links and bearing clearances is confined to only two publications [28,75]. Funabashi, et al. [28] investigated the input torque and the relative displacement of the pin and journal where the clearance occurred in the crank bearing in a planar slider-crank mechanism. Shimojima, et al. [75] measured the relative displacement of the pin and journal where the clearance presented in the crank bearing in a planar slider-crank mechanism by employing an optical method. Thus there is a dearth of experimental work in this important field of predicting the dynamical behavior of planar mechanisms with radial clearances.

The principal subassembly in this experimental investigation was a planar slider-crank mechanism incorporating substantially rigid links which articulated in a plane perpendicular to the gravitational field. The essential features of the mechanism are presented in Figure 2.7. The crank, which had a length, r_2, of 48 mm, was fabricated as an integral part of a 146 mm diameter flywheel. This heavy circular disc was keyed to a 19.05 mm diameter drive-shaft, which was supported on a matched pair of Timken type TS4A-6 tapered-roller bearings, and was powered by a 0.56kW Dayton variable-speed dc motor, model 2Z846A. The slider of the classical slider-crank mechanism was represented by the

translating table of a Micro Slides,Inc., type 2050-RW-118-5 linear crossed-roller slide assembly, which is a precision preloaded system without clearance. The mass of this sliding element was 0.63607 kg.

The connecting-rod assembly of the classical slider-crank linkage comprised three components: a uniform steel bar with dimensions 267x6x19 mm^3, a crank-pin bearing, and a gudgeon-pin bearing. The total length of this link member was 293 mm between bearing centerlines, the total mass of the link and joints, m_3, was 0.21435 kg, and the moment of inertia I_{G3} was 0.003883 $kg\text{-}m^2$. The crank-pin bearing was designed to incorporate a matched pair of instrument ball bearings, type R4DB12, supplied by FAG Bearings Limited. The spindle diameter was 6.35 mm. This bearing assembly was carefully preloaded using a Dresser Industries torque-limiting screw driver. This procedure enabled bearing clearance to be removed from the assembly, since the vibrational response associated with this clearance at the crank-pin would have contaminated the experimental data from the transducers monitoring the dynamic response of the system at the gudgeon-pin.

The gudgeon-pin bearing was fabricated as a journal bearing with a prescribed radial clearance. This was achieved by employing a steel pin of diameter 6.35 mm which was supported in a threaded hole in the reciprocating portion of the crossed-roller slide assembly. The journal element of the bearing was provided by a brass bushing with an internal diameter of 6.604 mm which when assembled with the pin provided a bearing with a radial clearance of 0.127 mm.

In addition, a second bearing assembly was designed and developed for the gudgeon-pin in order to develop a joint with zero clearance. This action was motivated by the necessity to generate a

reference set of experimental data for comparison with the results from the linkage with the prescribe radial clearance at the gudgeon-pin bearing. This precision bearing assembly without radial clearance incorporated a matched pair of preloaded instrument ball bearings, type R4DB12, supplied by FAG Bearings Limited. The spindle diameter was 6.35 mm.

The experimental apparatus and the associated instrumentation is schematically represented in Figure 2.8. The operating speed of the mechanism was measured by a Hewlett Packard 5314A universal counter which was activated by an Electro Corporation digital-magnetic pickup, model 58423, which sensed a 60-tooth spur gear mounted on the crank shaft. This gear and the associated pickup are clearly evident in Figure 2.7.

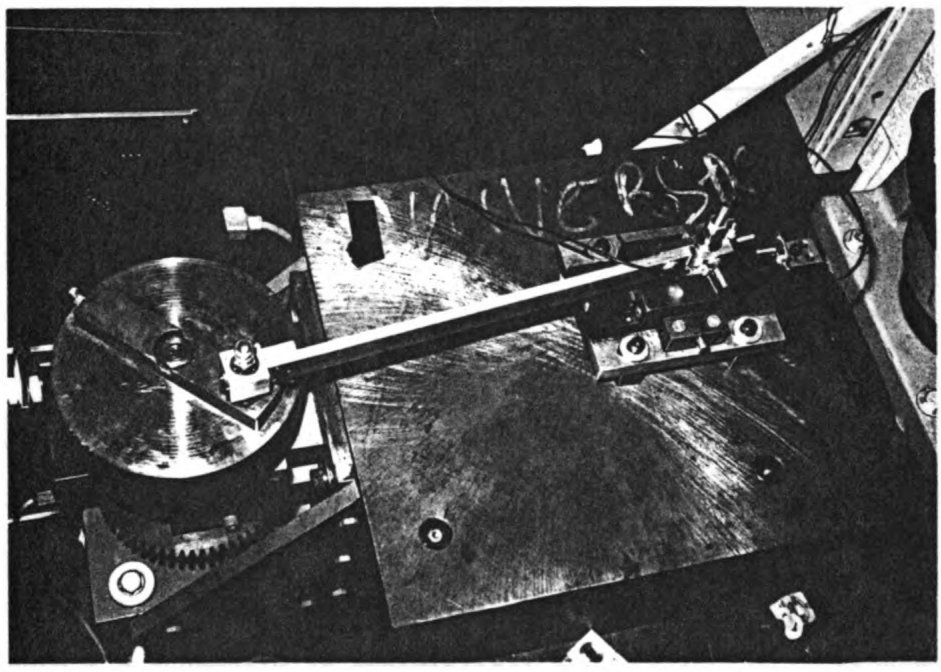

Figure 2.7 Photograph of experimental planar slider-crank mechanism

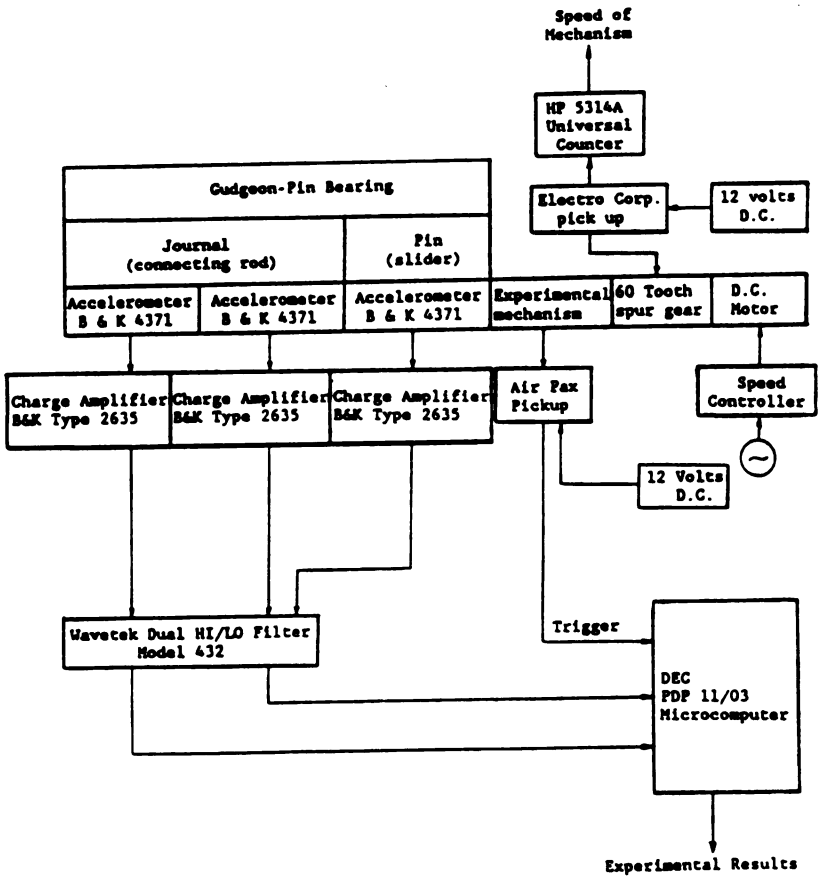

Figure 2.8 Schematic of experimental apparatus and associated instrumentation

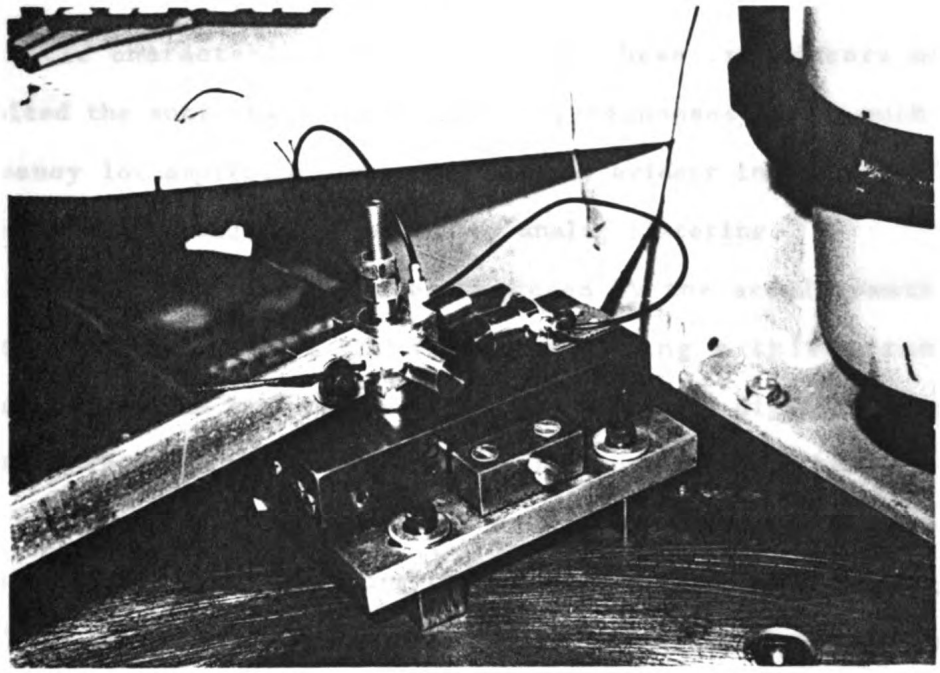

Figure 2.9 Photograph of accelerometer configuration at the gudgeon-pin bearing of the experimental slider-crank mechanism

The dynamic behavior of the slider and the connecting rod of the experimental slider-crank mechanism were monitored using three Bruel and Kjaer piezoelectric accelerometers, type 4371, which were each connected to Bruel and Kjaer charge amplifiers, type 2635. These accelerometers were positioned at the gudgeon-pin bearing in order to measure the dynamic response of the reciprocating slider and also the longitudinal and lateral motions of the connecting rod. This cluster of accelerometers are clearly evident in the right-hand-side of Figure 2.9. The signals from these accelerometers were fed to a Wavetek HI/LO analog filter, model 432, prior to being recorded on a PDP11-based digital-data-acquisition system. In order to clarify the response profiles, frequencies above 60 hz were removed by analog filtering. This cut-off frequency was selected by studying the experimental response-data from the accelerometers clustered at the gudgeon-pin bearing when this bearing featured the zero-clearance FAG instrument ball bearings. The

kinematic characteristics furnished by these transducers not only exhibited the anticipated low-frequency responses but a much higher frequency low amplitude ripple was clearly evident in the signal. This component was subsequently removed by analog filtering.

The response profiles measured by the accelerometers were related to the angle of the crankshaft using a third transducer arrangement, which featured an Airpax zero-velocity digital pickup, type 14-0001. This transducer was employed to sense the bolt head protruding from the flywheel when the crank was in the conventional zero crank-angle position, prior to firing the Schmitt triggers on the input/output panel of the data-acquisition system. The highest sampling rate employed in this study was 2,500 samples per second.

In addition to the apparatus assembled to measure the dynamic response of the laboratory slider-crank mechanism with controlled radial clearance at the gudgeon-pin joint, a second apparatus was designed, engineered and fabricated in order to evaluate the dynamic behavior of the gudgeon-pin joint in a carefully controlled environment similar to the environment experienced by the joint during the articulation of the mechanism. The objective of this investigation was to excite an impactive motion in the gudgeon-pin joint and then measure the velocities of both the pin and the journal before and after impact in order to distill an empirical value for the coefficient of restitution from the experimental response-data. The value of this coefficient would then be employed in the complementary computer simulations for predicting the dynamical response of the experimental system. The experimental procedure involved exciting the Microslides table, and hence the pin of the gudgeon-pin bearing, by a Ling Dynamic Systems vibrator, model 411, which was driven by Wavetek function generator,

model 275, and a Hafler power amplifier, model P500. These tests were performed with the connecting-rod disconnected from the crank in order to isolate the motion between the two impacting machine elements at the revolute joint with prescribed clearance. The connecting rod was configured so that the longitudinal axis of the member was colinear with the axis of translation of the slider as shown in Figure 2.10, and very soft rubber springs were connected to it in order to ensure continual co-axial alignment during the experiments.

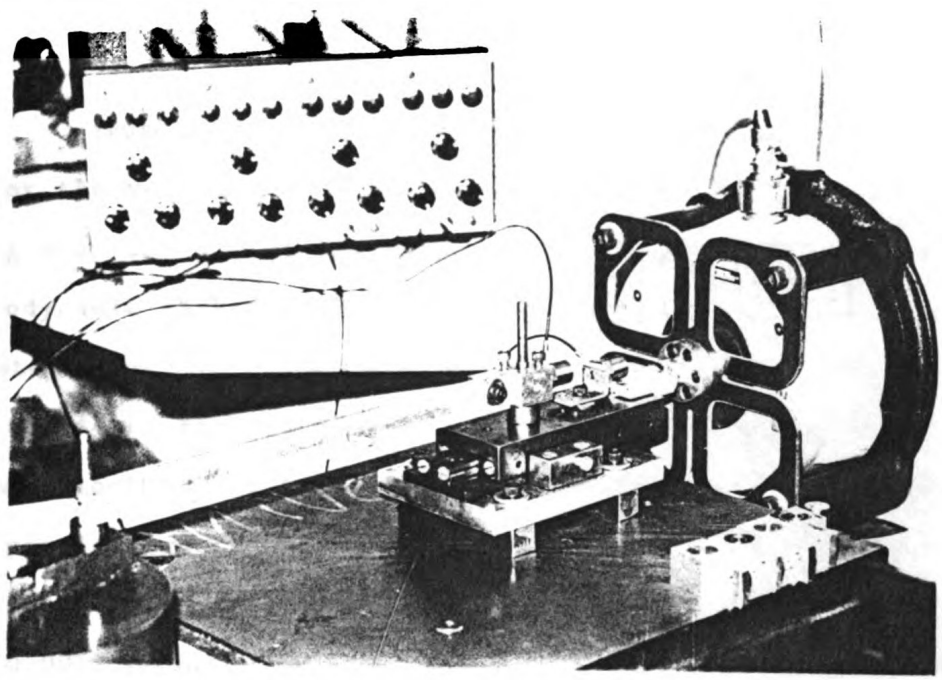

Figure 2.10 Photograph of experimental apparatus for measuring the impactive force in the gudgeon-pin bearing and determining the associated coefficient of restitution between the pin and the journal of the bearing

A Bruel and Kjaer force transducer, model 8200, was incorporated in the fixture between the shaker head and the sliding table in order to continuously monitor the forcing function imposed upon the gudgeon-pin bearing. The dynamical motion of the journal and also the pin were both carefully monitored by strategically locating Bruel

and Kjaer piezoelectric accelerometers, type 4371, on the bearing assembly. These transducers were operated in conjunction with Bruel and Kjaer , charge amplifiers, type 2635, which contain built-in integrators that permit velocity and displacement histories to be measured. Figure 2.10 presents a photograph of the experimental arrangement, and Figure 2.11 presents a schematic diagram of the apparatus and the associated instrumentation.

2.7.7 Experimental and numerical results

Figure 2.12 presents a typical set of experimental response data for the velocities of the pin and the journal of the gudgeon-pin bearing when the pin of the gudgeon-pin bearing was excited by an electrodynamic shaker at 20 Hz. The coefficient of restitution was calculated to be 0.46 using these response data since that the relative velocity of the pin and journal before impact was 5.81 cm/sec and the relative velocity after impact was 2.67 cm/sec. Figure 2.13 shows the corresponding impact force, which was monitored at the head of the shaker by the force transducer. The duration of the impact was measured to be 0.0012 seconds. The frictional coefficient, μ, between the slider and guide was calculated to be 0.0224 by employing $\mu = W_s/F_d$, where W_s is the weight of the slider while F_d is the total countweight which caused the slider began to slide. These data were employed in the model of the slider-crank mechanism in order to predict the dynamical behavior of the system.

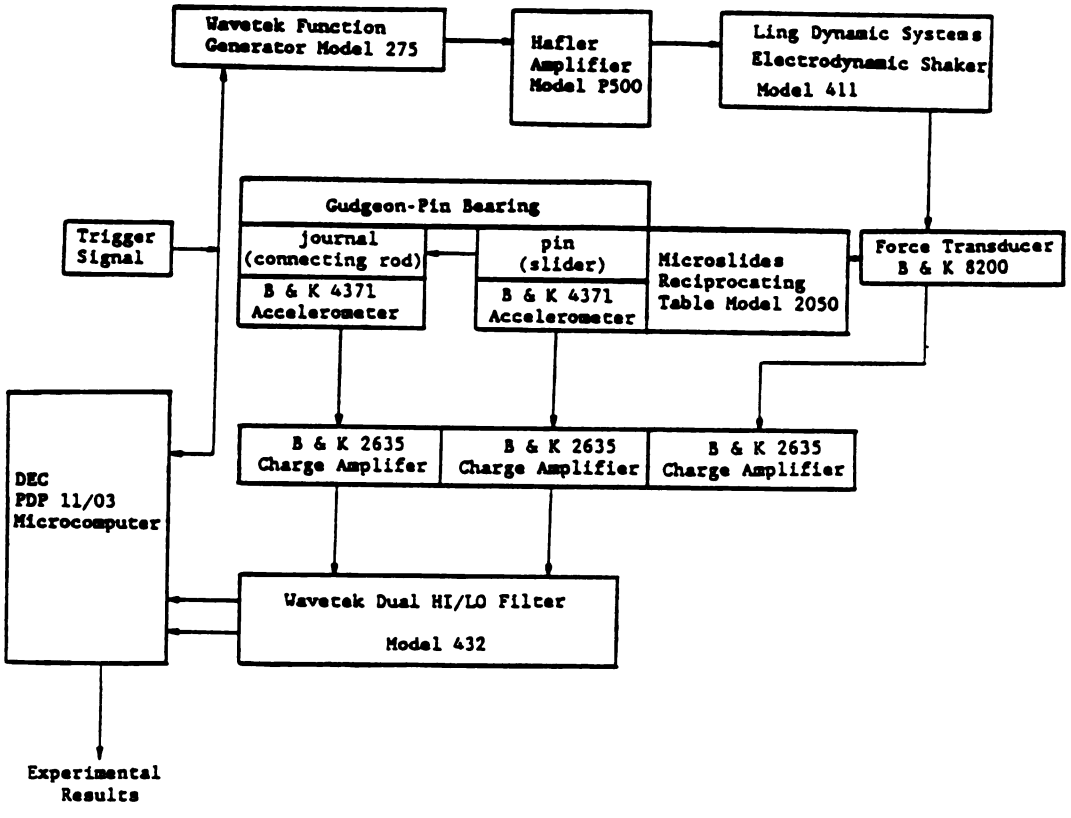

Figure 2.11 Schematic diagram of the experimental apparatus and instrumentation for determining the coefficient of restitution of the gudgeon-pin bearing

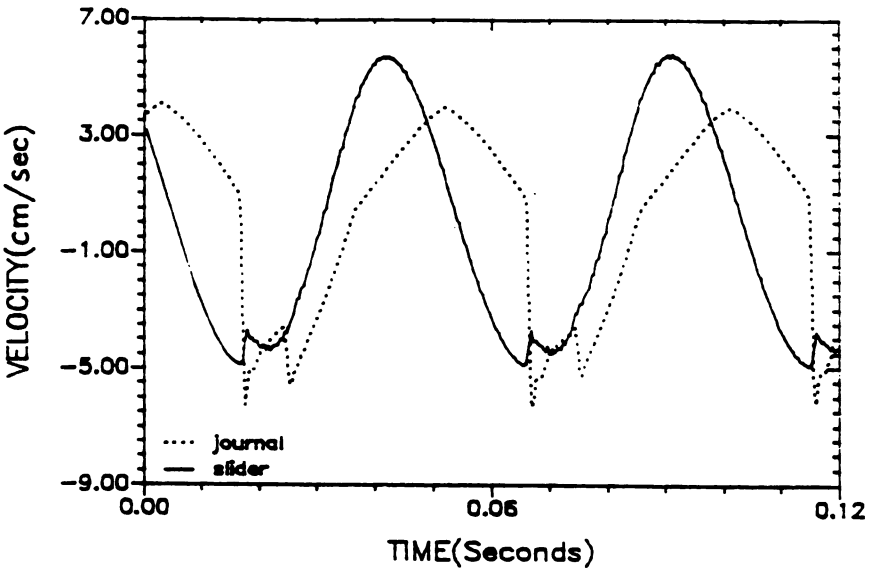

Figure 2.12 Gudgeon-pin bearing characteristics: Velocity characteristics of the impactive behavior between pin and journal at a pin excitation frequency of 20 Hz

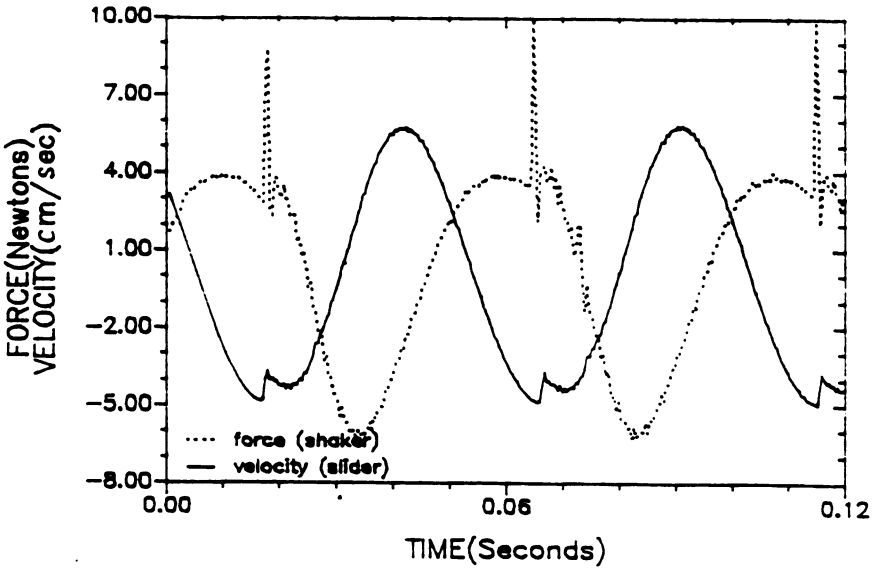

Figure 2.13 Gudgeon-pin bearing characteristics: Excitation force characteristics and associated velocity characteristics of the pin impacting the journal at a frequency of 20 Hz

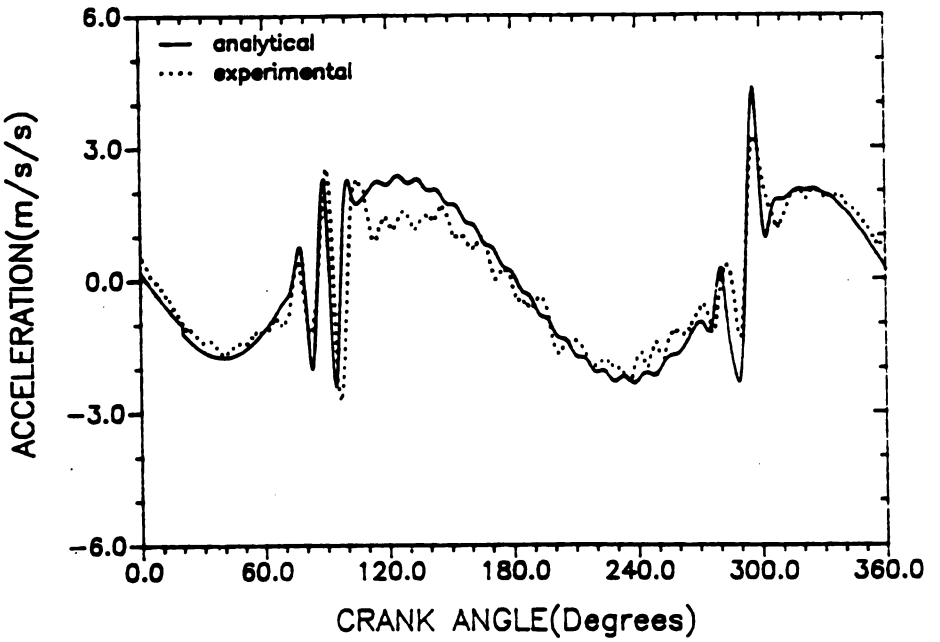

Figure 2.14 Connecting-rod tangential acceleration. Mechanism operating speed 200 rpm

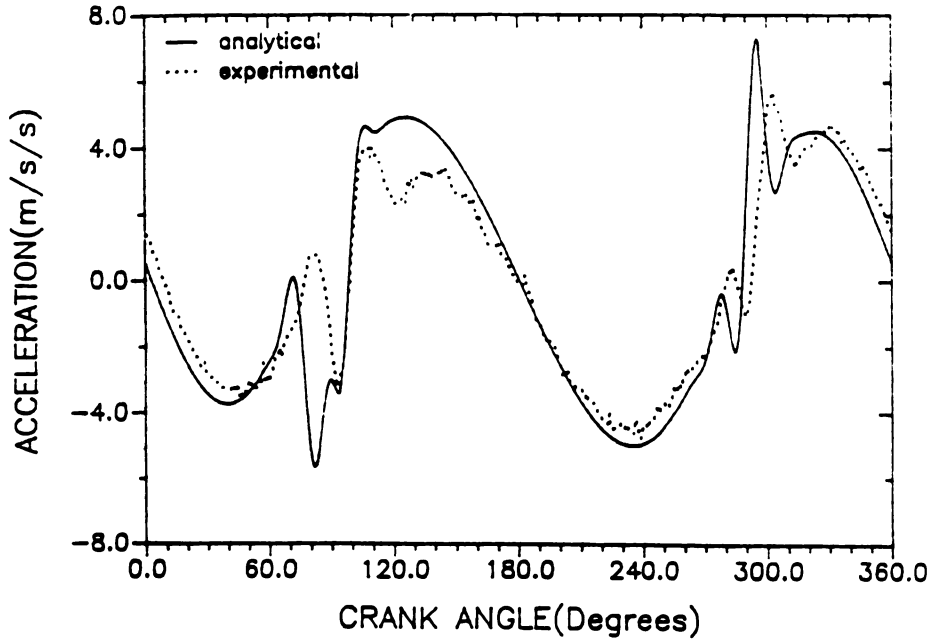

Figure 2.15 Connecting-rod tangential acceleration. Mechanism operating speed 300 rpm

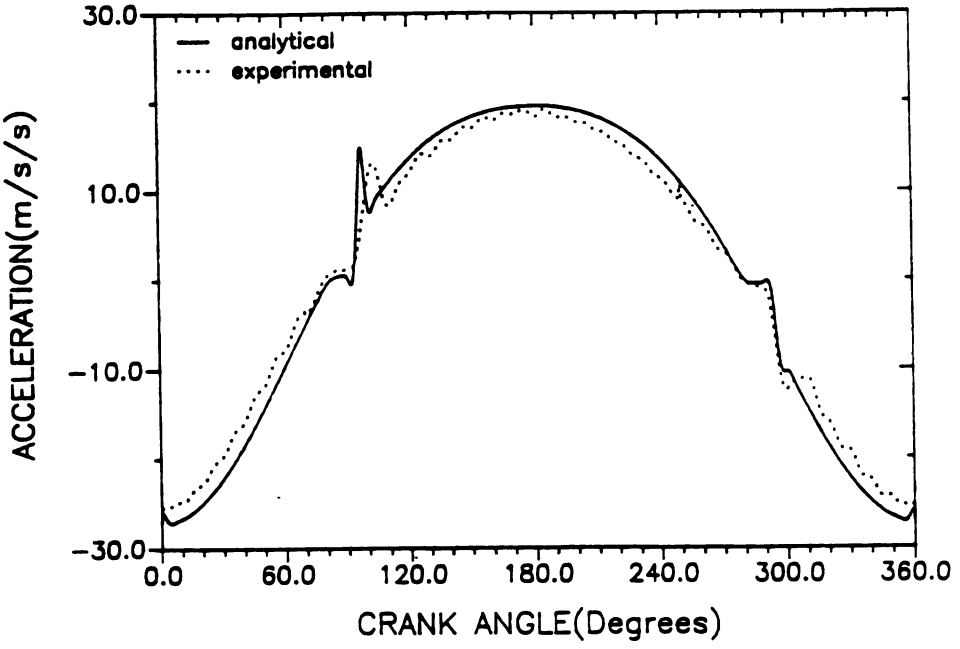

Figure 2.16 Slider acceleration. Mechanism operating speed 200 rpm

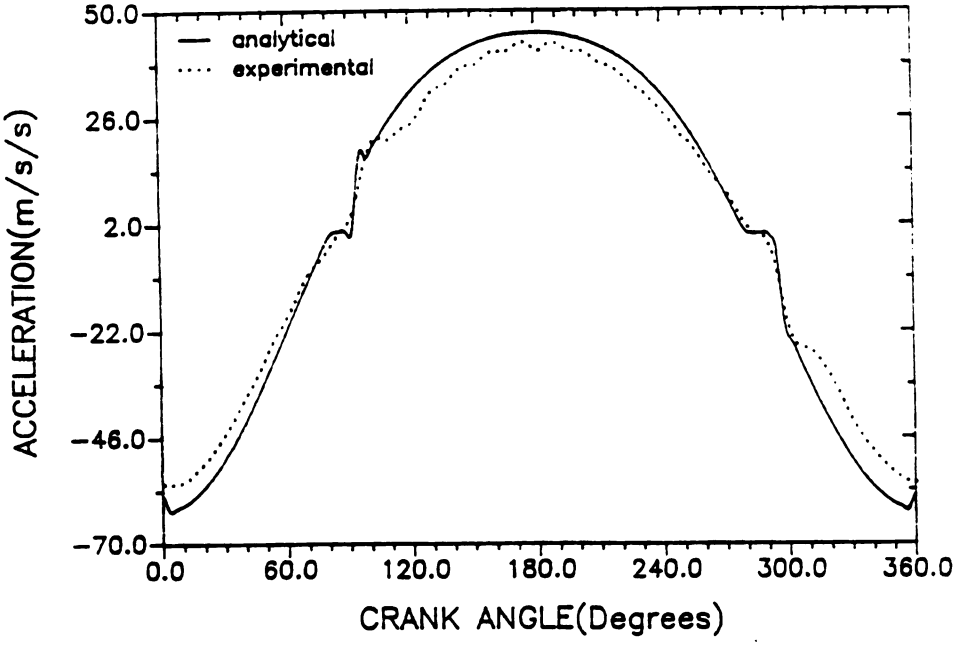

Figure 2.17 Slider acceleration. Mechanism operating speed 300 rpm

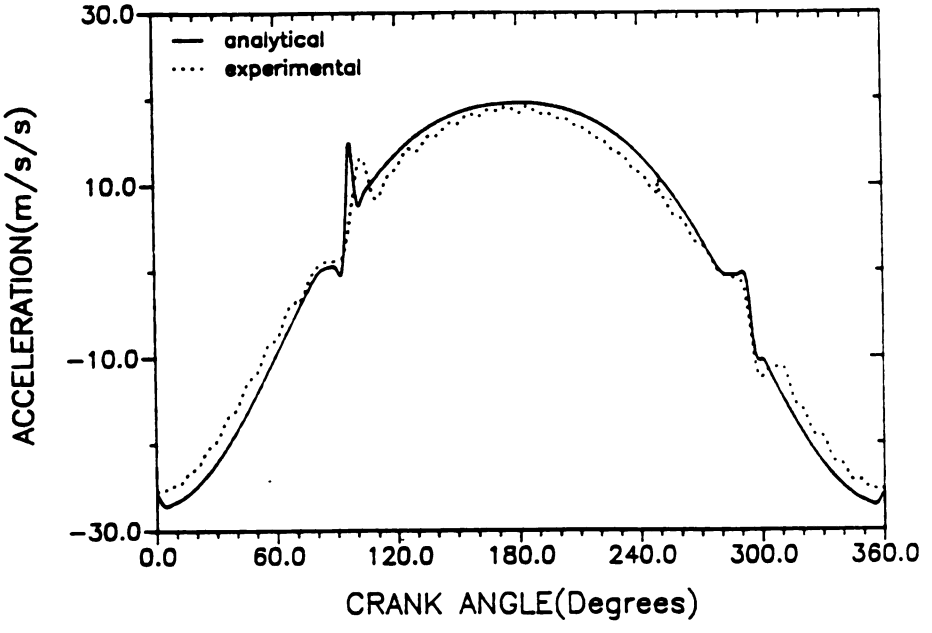

Figure 2.16 Slider acceleration. Mechanism operating speed 200 rpm

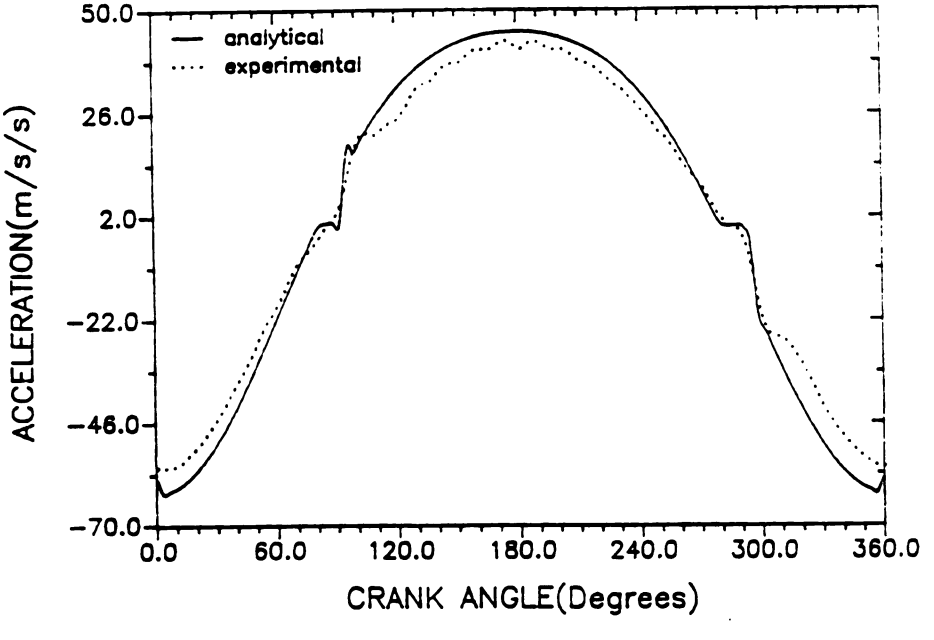

Figure 2.17 Slider acceleration. Mechanism operating speed 300 rpm

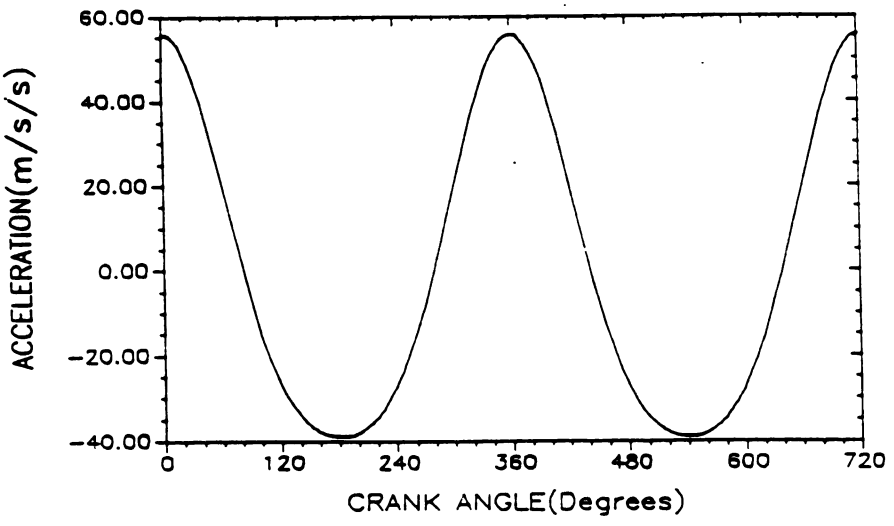

Figure 2.18 Connecting-rod longitudinal acceleration. Mechanism operating speed 200 rpm

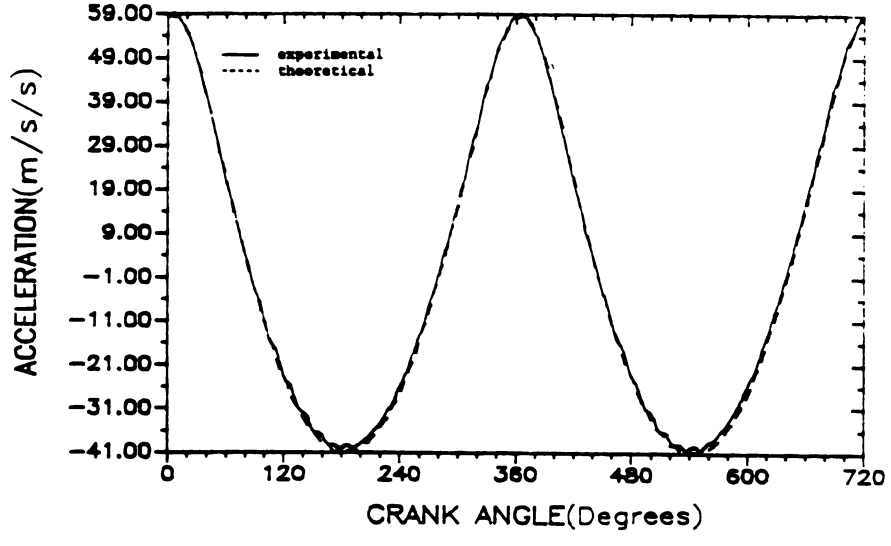

Figure 2.19 The theoretical prediction of the longitudinal acceleration of the connecting-rod. Mechanism operating speed 300 rpm

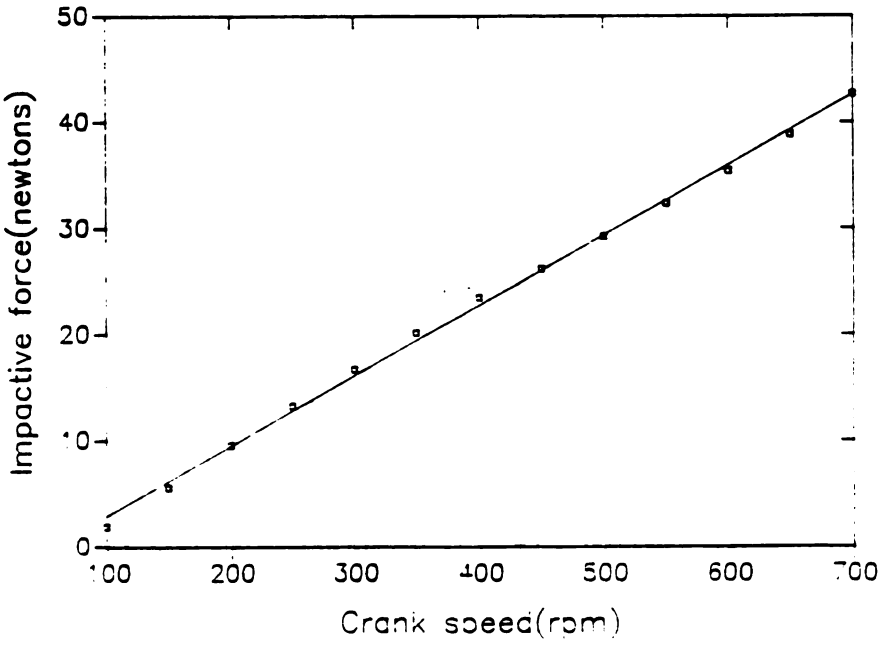

Figure 2.20 The maximum impactive force between the pin and journal. The radial clearance was 0.000127 meters

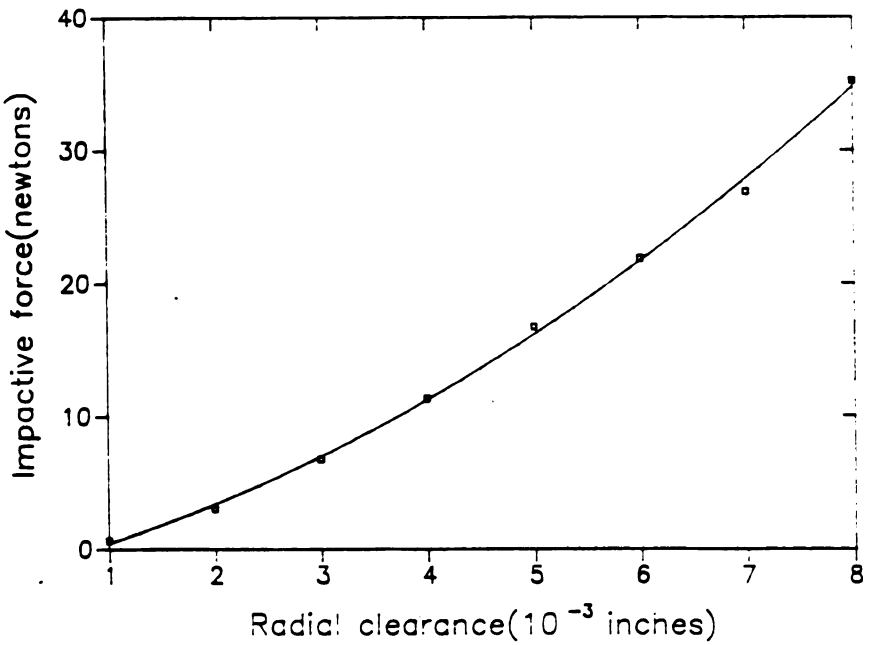

Figure 2.21 The maximum impactive force between the pin and journal. Mechanism operating speed 300 rpm

Figures 2.14 - 2.17 present experimental and theoretical response data for the slider-crank mechanism operating at crank frequencies of 200 and 300 rpm. The radial clearance is 0.127 mm in the gudgeon-pin bearing for all response profiles. Figures 2.14 and 2.15 present the tangential accelerations of the connecting rod at 200 and 300 rpm respectively while Figures 2.16 and 2.17 present the corresponding accelerations of the slider.

In order to develop a viable environment for comparing the analytical and experimental results, the numerical results were subjected to digital filtering, using LSP$FILTER_NONREC, which is a nonrecursive, finite impulse response, filtering software on a DEC MicroVAX II/GPX workstation [96]. This was undertaken in order to remove the fictitious very high frequency components from the theoretical results which were attributed to the very small time-steps employed in the computational algorithm.

Upon reviewing the acceleration profiles presented in Figures 2.14 - 2.19, it is clearly evident that there is excellent correlation between the theoretical and experimental results for a broad range of operating conditions. Thus, the proposed four-mode model for predicting the complex phenomenological behavior of planar mechanism systems incorporating a distinct radial clearance in the revolute joints is able to accurately predict the dynamical response of these systems in the contact-mode, the free-flight-mode, the impact-mode, and the transient-mode which comprise the global response regime. Moreover, it is also clearly evident that the tangential acceleration characteristics of the connecting rod are much more sensitive to clearance in the gudgeon-pin bearing than the longitudinal acceleration characteristic. A consequence in practice of this distinct sensitivity of the lateral

acceleration component to bearing clearance manifests itself as high levels of acoustical radiation in these systems because the vigorous lateral motion excites the adjacent fluid medium [87].

Moreover, upon reviewing Figures 2.14 - 2.17, it is clearly evident that the pin and journal loose contact and undergo major excursions relative to each other twice during each revolution of the crank shaft, and the restoration of contact occurs at the end of the transient-mode. The first separation generally occurred at approximately 80 degrees of crank rotation and the second separation occurred at approximately 280 degrees of crank rotation. Figures 2.16 and 2.17, indicate that the most severe impact conditions occur at 98 degrees and 295 degrees of crank rotation, while the experimental results indicate that the most serious impact occurs at 102 degrees and 295 degrees of crank rotation. This is an impressive predictive capability for such a complex nonlinear mechanical system.

Figures 2.14 and 2.15 indicate that at approximately 80 degrees of crank rotation the first impact creates a more severe vibrational response of the transverse acceleration characteristic of the connecting-rod in the transient-mode than the second impact which occurs at approximately 290 degrees of crank rotation. This phenomenon has not been reported before in the literature.

Figures 2.18 presents the analytical and experimental longitudinal acceleration characteristics of the connecting rod for two revolutions of the crank shaft at 300 rpm for the case where the gudgeon-pin has zero clearance. These profiles present a null check in the evaluation of the software and they also provide a measure of the experimental behavior of the system under these classical operating conditions. Figure 2.19 presents the numerical predictions for the

longitudinal acceleration of the connecting rod at 300 rpm with 0.127 mm clearance in the gudgeon-pin bearing. Upon examining these two curves it is clearly evident that bearing clearance in the gudgeon-pin has very little affect on the longitudinal dynamic behavior of the connecting rod.

The maximum impactive force between the pin and journal in the gudgeon-pin bearing was also calculated during the simulation. Figure 2.20 presents the predict results which shows that the impactive force increases proportionally with the crank speed. The radial clearance was 0.000127 meters. Figure 2.21 shows the relationship between the maximum impactive force and the magnitude of the radial clearance at the gudgeon-pin bearing while the crank speed was 300 rpm. Since the measurement of the impactive force between the pin and the journal is not available, only simulation results are presented.

2.8 CONCLUSIONS OF THE CHAPTER

Analytical and computational models of general planar mechanisms with rigid links and bearing clearances have been developed. A four-mode model of the complex phenomenological behavior of revolute joints with radial clearance has been proposed and incorporated in a methodology for predicting the dynamic response of these mechanical systems. As an illustrative example of the approach, a slider-crank mechanism with radial clearance in the gudgeon-pin bearing was studied in a comprehensive analytical, computational and experimental investigation and the numerical results are in qualitative agreement with the results from a complementary experimental program.

Chapter III

GENERAL PLANAR MECHANISMS FEATURING FLEXIBLE-LINKS AND BEARINGS WITHOUT RADIAL CLEARANCE

3.1 INTRODUCTION

Traditionally, mechanism design has been based on rigid-body analyses in which all mechanism members are treated as rigid bodies in order to study the kinematic and kinetic characteristics of these articulating mechanical systems [55,66,74,100]. The stresses in the mechanism members due to inertia forces and external loading are then calculated in a sequential algorithm in which kinematic, kinetic and elastic considerations are all decoupled. More recently, the operating speeds of mechanisms are being continually increased to increase industrial productivity. In order to reduce the inertia force of the machine and driving torque of the motor, the weight of mechanism members need to be made as light as possible. However the lighter members are more likely to deform and vibrate due to the inertia and external forces. The position inaccuracy and occasionally the resonant condition will cause the design unacceptable. Hence the elastodynamic analysis of a mechanical system becomes necessary and important.

In this chapter, a coupled system of equations is developed by combining the second-order constraint equations and the equations of motion for a general planar linkage mechanism featuring flexible links and bearings without radial clearance. This coupled system of equations are then divided into two sets of equations in the basis of inertial coordinates and elastic coordinates, respectively. The flexible links are assumed homogeneous, isotropic and have a small deflection. Since the thickness-to-length ratio of the links considered in this study is 0.00433, the effects of shear deformation and rotary inertia shall be ignored. Each link is modelled by employing the Euler-Bernoulli beam theory which is incorporated in a geometrically nonlinear formulation for predicting the coupled axial and flexible responses of each link. Finally, a slider-crank mechanism with a flexible connecting rod is analyzed in an illustrative example. The planar linkage system incorporating bearings without clearance is analyzed using the general formulation developed herein prior to evaluating the predictive capabilities of the methodology by comparing the theoretical results with results from a complementary experimental investigation.

3.2 EQUATIONS OF MOTION OF A FLEXIBLE BODY DESCRIBING A GENERAL PLANAR MOTION

Consider the elastodynamic motion of a general planar linkage mechanism moving relative to an inertia reference frame OXY. Each link has a Lagrangian coordinate oxy fixed in it. Figure 3.1 shows two arbitrary adjacent links, i and j of the mechanism. OXY denotes the

inertial reference frame, while $o_i x_i y_i$ denote the Lagrangian coordinates fixed in the body in an undeformed reference state. At any instant t, a general point in the ith-link was denoted as p_i and p'_{ij} before and after deformation. Therefore, the general point p after deformation can be expressed as

$$r_i = r_{oi} + r_{Ri} + u_i \tag{3.1}$$

where r_{oi} are the components measured in the $o_i x_i y_i$ frame of the position vector of the origin of the body axes relative to the origin of the inertial frame. Similarly, r_{Ri} denotes the position vector of point p in the reference state relative to the origin of the body axes and u_i is the deformation displacement vector, may be expressed as $u_x e_1 + u_y e_2$, where u_x is the axial deformation in the ox direction and u_y is the transverse deformation in the oy direction. Terms e_1 and e_2 are the unit vectors in the ox and oy direction measured relative to the moving reference frame, respectively.

Since the finite element method is employed for the derivation of the equations of motion, the link may be divided into many elements. The elastic deformation of each element can be described by six nodal displacements, ul - u6, illustrated in Figure 3.2,

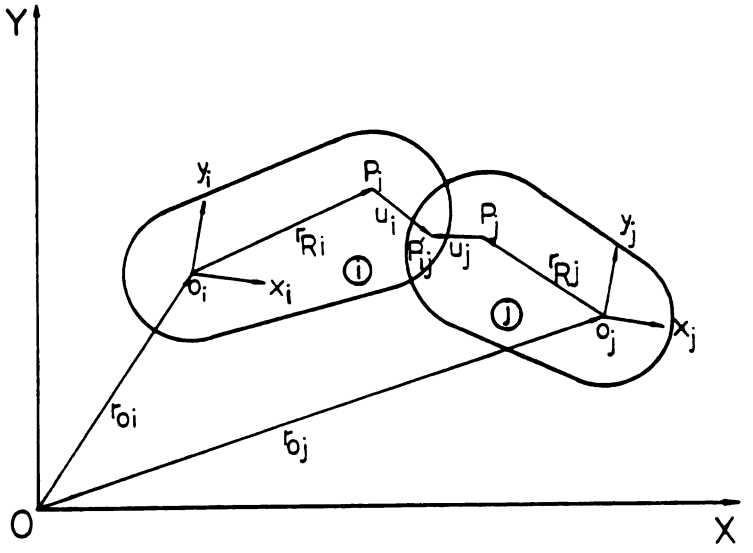

Figure 3.1 Generalized coordinate of two adjacent links

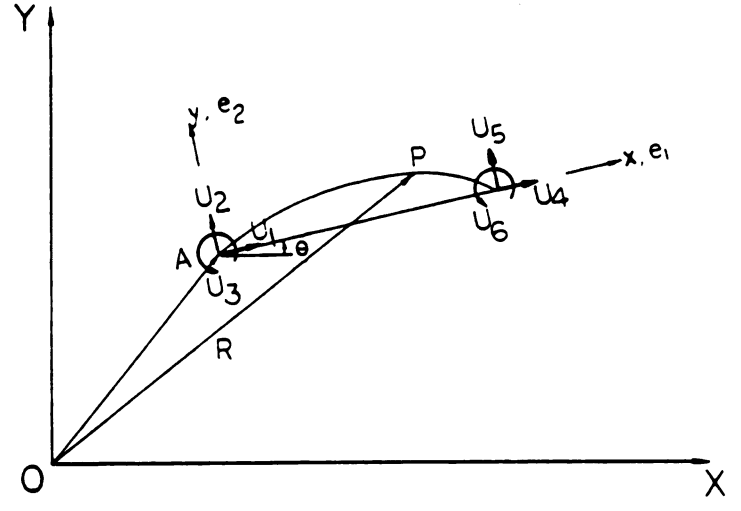

Figure 3.2 The nodal displacement of each element

From Figure 3.2, a general point p in the element can be expressed in the fixed reference frame in the deformed state

$$\mathbf{R}_i = [X_A+(x+u_x)\cos\theta - u_y\sin\theta]\mathbf{i} + [Y_A+(x+u_x)\sin\theta - u_y\cos\theta]\mathbf{j} \tag{3.2}$$

where $X_A\mathbf{i} + Y_A\mathbf{j}$ is the position vector of point A relative to the inertial frame.

Differentiating equation(3.2) with respect to time, yields the velocity

$$\dot{\mathbf{R}}_i = [\dot{X}_A + \dot{u}_x\cos\theta - (x+u_x)\dot{\theta}\sin\theta - \dot{u}_y\sin\theta + u_y\dot{\theta}\cos\theta]\mathbf{i}$$
$$+ [\dot{Y}_A + \dot{u}_x\sin\theta + u_x\dot{\theta}\cos\theta + \dot{u}_y\cos\theta - u_y\dot{\theta}\sin\theta]\mathbf{j} \tag{3.3}$$

Equations (3.2) and (3.3) can be expressed relative to the rotating frame,

$$\mathbf{r}_i = (X_A\cos\theta + Y_A\sin\theta + x + u_x)\mathbf{e}_1 + (-X_A\sin\theta + Y_A\cos\theta + u_y)\mathbf{e}_2 \tag{3.4}$$

$$\dot{\mathbf{r}}_i = (\dot{X}_A\cos\theta + \dot{Y}_A\sin\theta - u_y\dot{\theta} + \dot{u}_x)\mathbf{e}_1$$
$$+ [-\dot{X}_A\sin\theta + \dot{Y}_A\cos\theta + (x+u_x)\dot{\theta} + \dot{u}_y]\mathbf{e}_2 \tag{3.5}$$

The displacement at any point in the element can be expressed in terms of the nodal displacements as

$$u(x,t) = [\ N\ ]\ \{\ U\ \} \tag{3.6}$$

where N is the shape function and is dependent upon the position only, and u is function of time.

The deformation of the flexible link in e_1 and e_2 directions can now be expressed as

$$u_x = [N_x]\{U\} \tag{3.7}$$

and,

$$u_y = [N_y]\{U\} \tag{3.8}$$

where

$$[N_x] = [N_1\ 0\ 0\ N_4\ 0\ 0]$$

$$[N_y] = [0\ N_2\ N_3\ 0\ N_5\ N_6]$$

$$\{U\}^T = \{u_1\ u_2\ u_3\ u_4\ u_5\ u_6\}$$

$$N_1 = 1 - \xi$$

$$N_2 = 1 - 3\xi^2 + 2\xi^3$$

$$N_3 = \ell(\xi - 2\xi^2 + \xi^3)$$

$$N_4 = \xi$$

$$N_5 = 3\xi^2 - 2\xi^3$$

$$N_6 = \ell(-\xi^2 + \xi^3),\ \xi = x/\ell$$

Equation(3.5) can be rewritten in the following form by introducing equation (3.7) and (3.8) into equation(3.5),

$$\dot{r} = (\dot{x}_A - [N_y]\{u\}\dot{\theta} + [N_x]\{\dot{u}\})e_1 + (\dot{y}_A + x\dot{\theta} + [N_x]\{u\}\dot{\theta} + [N_y]\{\dot{u}\})e_2 \tag{3.9}$$

where $\dot{x}_A = \dot{X}_A\cos\theta + \dot{Y}_A\sin\theta$, and $\dot{y}_A = -\dot{X}_A\sin\theta + \dot{Y}_A\cos\theta$

For convenience equation(3.7) can be rewritten in matrix form as

$$\begin{bmatrix} \dot{r}_x \\ \dot{r}_y \end{bmatrix} = [\, I \; A \; B \,] \begin{bmatrix} \dot{p} \\ \dot{\theta} \\ \dot{u} \end{bmatrix} \tag{3.10}$$

where

$$I = \begin{bmatrix} 1 & 0 \\ 0 & 1 \end{bmatrix}, \quad A = \begin{bmatrix} -[N_y] & [u] \\ x+[N_x] & [u] \end{bmatrix}, \quad B = \begin{bmatrix} [N_x] \\ [N_y] \end{bmatrix},$$

and $$\dot{p} = \begin{bmatrix} \dot{x}_A \\ \dot{y}_A \end{bmatrix} \tag{3.11}$$

If the link is assumed to be homogeneous with constant cross sectional area (A_e) and mass density (ρ_e), the kinetic energy of an element can be expressed as

$$T_e = \frac{1}{2} \rho_e A_e \int_0^{\ell} \dot{r}_i \cdot \dot{r}_i \, dx \tag{3.12}$$

By using equation(3.10), the kinetic energy can be rewritten as

$$T_e = \frac{1}{2} \rho_e A_e \int_0^{\ell} [\, \dot{p}^T \dot{\theta} \; \dot{u} \,] \begin{bmatrix} I \\ A^T \\ B^T \end{bmatrix} [I \; A \; B] \begin{bmatrix} \dot{p} \\ \dot{\theta} \\ \dot{u} \end{bmatrix} dx \tag{3.13}$$

$$= \frac{1}{2} \rho_e A_e [\, \dot{p}^T \dot{\theta} \; \dot{u} \,] \left\{ \int_0^{\ell} \begin{bmatrix} I & A & B \\ A^T & A^T A & A^T B \\ B^T & B^T A & B^T B \end{bmatrix} dx \right\} \begin{bmatrix} \dot{p} \\ \dot{\theta} \\ \dot{u} \end{bmatrix} \tag{3.14}$$

The kinetic energy of the link , therefore, is

$$T_i = \sum_{e=1}^{n} T_e \quad , \text{ n is the number of elements in each link} \tag{3.15}$$

In equation(3.14), defining $q = [p\ \theta]$, then $\dot{q} = [\dot{p}\ \dot{\theta}]$, where q denotes the corresponding generalized coordinate. Therefore, equation(3.14) can be expressed as

$$T_e = \frac{1}{2} [\dot{q}\ \dot{u}] \begin{bmatrix} M_{qq} & M_{qu} \\ M_{qu}^T & M_{uu} \end{bmatrix} \begin{bmatrix} \dot{q} \\ \dot{u} \end{bmatrix}$$

$$= \frac{1}{2} [\dot{q}\ \dot{u}]\ [M] \begin{bmatrix} \dot{q} \\ \dot{u} \end{bmatrix} \tag{3.16}$$

where

$$[M] = \begin{bmatrix} M_{qq} & M_{qu} \\ M_{qu}^T & M_{uu} \end{bmatrix} \tag{3.17}$$

$$M_{qq} = \rho_e A_e \int_0^{\ell} \begin{bmatrix} I & A \\ A^T & A^T A \end{bmatrix} dx \tag{3.18}$$

$$M_{qu} = \rho_e A_e \int_0^{\ell} \begin{bmatrix} B \\ A^T B \end{bmatrix} dx \tag{3.19}$$

$$M_{uu} = \rho_e A_e \int_0^{\ell} \left(B^T B \right) dx \tag{3.20}$$

The strain energy of the element can be expressed as

$$V_e = \frac{1}{2} \int_0^{\ell} EI \left(\frac{\partial^2 u_y}{\partial x^2} \right)^2 dx + \frac{1}{2} \int_0^{\ell} EA \left(\frac{\partial u_x}{\partial x} \right)^2 dx$$

$$+ \frac{1}{2} \int_0^{\ell} F(x) \left(\frac{\partial u_y}{\partial x} \right)^2 dx \tag{3.21}$$

The first and the second terms in equation(3.21) are the strain energy due to the transverse and axial deformation of the link while the the third term is the work done by the axial force F(x) due to the change in the horizontal projection of an element.

The introduction of equations (3.7) and (3.8) into equation (3.18) permits the strain energy to be written as

$$V_e = \frac{1}{2}\int_0^{\ell} EI(U)^T[N_y'']^T[N_y''](U)dx + \frac{1}{2}\int_0^{\ell} EA(U)^T[N_x']^T[N_x'](U)dx$$

$$+\frac{1}{2}\int_0^{\ell} F(x)(U)^T[N_y']^T[N_y'](U)dx$$

$$= \frac{1}{2}(U)^T[K](U) + \frac{1}{2}\int_0^{\ell} F(x)(U)^T[N_y']^T[N_y'](U)dx \qquad (3.22)$$

where [K] is known as stiffness matrix which equals

$$\int_0^{\ell} EI[N_y'']^T[N_y'']dx + \int_0^{\ell} EA[N_x']^T[N_x']dx \qquad (3.23)$$

where (") denotes the second spatial derivative with respective to x, while (') denotes the spatial derivative with respective to x.

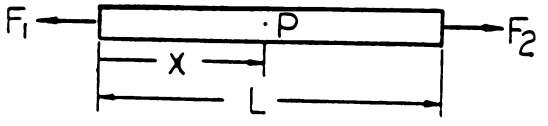

Figure 3.3 Axial force is represented as a linear function

The axial force at any point in the link may be expressed as, refers to Figure 3.3,

$$F(x) = F_1 + (F_2 - F_1)\frac{x}{\ell} = F_1 + \Delta F\frac{x}{\ell} \qquad (3.24)$$

Substituting equation(3.23) into equation(3.21), the strain energy of the link can be rewritten as

$$V_e = \frac{1}{2}(U)^T[K](U) + \frac{1}{2}F_1(U)^T[K_{G1}](U) + \frac{1}{2}\Delta F(U)^T[K_{G2}](U)$$

(3.25)

where

$$[K_{G1}] = \int_0^{\ell} [N_y']^T [N_y'] \, dx \tag{3.26}$$

$$[K_{G2}] = \int_0^{\ell} \frac{x}{\ell} [N_y']^T [N_y'] \, dx \tag{3.27}$$

The total kinetic energy of the system is

$$T = \sum_{i=1}^{nl} \left(\sum_{e=1}^{n} T_e \right)_i \tag{3.28}$$

where nl is the number of links of the mechanical system, and n is the number of elements in a link.

Similarly, the total strain energy of the system is

$$V = \sum_{i=1}^{nl} \left(\sum_{e=1}^{n} V_e \right)_i \tag{3.29}$$

The ith generalized constraint equations may be written

$$\phi_i = \phi(q_1, q_2, \cdots, q_\ell, u_1, u_2, \cdots, u_{3(N+1)}) \tag{3.30}$$

where there are ℓ inertial generalized coordinates q_ℓ, and there are $3(N+1)$ elastic generalized coordinates $u_{3(N+1)}$. N is defined as the number of elements.

The first and the second time derivative of the constraint equations are

$$\dot{\phi} = \sum_{i=1}^{\ell} \frac{\partial \phi}{\partial q_i} \dot{q}_i + \sum_{j=1}^{3(N+1)} \frac{\partial \phi}{\partial u_j} \dot{u}_j \tag{3.31}$$

$$\ddot{\phi} = \sum_{i=1}^{\ell}\sum_{k=1}^{\ell} \frac{\partial^2 \phi}{\partial q_i \partial q_k} \dot{q}_i \dot{q}_k + \sum_{i=1}^{\ell} \frac{\partial \phi}{\partial q_i} \ddot{q}_i + \sum_{j=1}^{3(N+1)}\sum_{\ell=1}^{3(N+1)} \frac{\partial^2 \phi}{\partial u_j \partial u_\ell} \dot{u}_j \dot{u}_\ell + \sum_{j=1}^{3(N+1)} \frac{\partial \phi}{\partial u_j} \ddot{u}_j \tag{3.32}$$

To find the equations of motion of the mechanical system, the generalized Lagrange's equation is employed in the inertial generalized coordinates and the Lagrange's equation without Lagrange multipliers is employed in the elastic generalized equation. These two equations are

$$\frac{d}{dt}\left(\frac{\partial T}{\partial \dot{q}_i}\right) - \frac{\partial T}{\partial q_i} + \frac{\partial V}{\partial q_i} - \sum_{j=1}^{nc} \lambda_j \frac{\partial \phi_j}{\partial q_i} = Q_i, \quad i=1,2,\cdots,\ell \tag{3.33}$$

where nc denotes the number of constraint equations

$$\frac{d}{dt}\left(\frac{\partial T}{\partial \dot{u}_k}\right) - \frac{\partial T}{\partial u_k} + \frac{\partial V}{\partial u_k} = Q_k \ , \quad k=1,2,\cdots,3(N+1) \tag{3.34}$$

Employing equations(3.33) and (3.34) and introducing the second time derivative constraint equation(3.32), yields the equations of motion

$$\begin{bmatrix} [M_{qq}] & [\frac{\partial \phi}{\partial q}] & [M_{qu}] \\ [\frac{\partial \phi}{\partial q}]^T & 0 & 0 \\ [M_{qu}]^T & 0 & [M_{uu}] \end{bmatrix} \begin{bmatrix} \ddot{q} \\ -\lambda \\ \ddot{u} \end{bmatrix} + \begin{bmatrix} 0 & 0 \\ 0 & [KK] \end{bmatrix} \begin{bmatrix} q \\ -\lambda \\ u \end{bmatrix} = \begin{bmatrix} [g] \\ [f] \\ [h] \end{bmatrix} \tag{3.35}$$

where

$$[KK] = [K] + [KG_1] + [KG_2] \tag{3.36}$$

$$g_k = \sum_{i=1}^{p} F_i \cdot \frac{\partial r_i}{\partial q_k} - [\dot{M}_{qq}\ \dot{M}_{qu}] \begin{bmatrix} \dot{q} \\ 0 \end{bmatrix} \quad , \ k=1,2,\cdots,\ell \tag{3.37}$$

$$f_p = \sum_{i=1}^{\ell} \sum_{k=1}^{\ell} \frac{\partial^2 \phi_p}{\partial q_i \partial q_k} \dot{q}_i \dot{q}_k + \sum_{j=1}^{3(N+1)} \sum_{\ell=1}^{3(N+1)} \frac{\partial^2 \phi_p}{\partial u_j \partial u_\ell} \dot{u}_j \dot{u}_\ell$$

$$+ \sum_{j=1}^{3(N+1)} \frac{\partial \phi_p}{\partial u_j} \dot{u}_j \quad , \ p=1,2,\cdots,nc \tag{3.38}$$

$$h_Q = \sum_{i=1}^{p} F_i \cdot \frac{\partial r_i}{\partial u_Q} + \frac{1}{2} [\dot{q}\ \dot{u}] \left[\frac{\partial M}{\partial u_Q} \right] \begin{bmatrix} \dot{q} \\ \dot{u} \end{bmatrix} - [\dot{M}_{qu}^T\ M_{uu}] \begin{bmatrix} 0 \\ \dot{u} \end{bmatrix}$$

$$, \ Q=1,2,\cdots,3(N+1) \tag{3.39}$$

In equation (3.35) the differential equations are represented as a set of simultaneous, linear algebraic equations in the variables $\ddot{q}_i$, λ_p and $\dot{u}_k$, and the coefficient matrix can be conveniently partitioned into four submatrices. The upper-left submatrix is symmetric and can be divided into four more submatrices, $[M_{qq}]$, $\left(\frac{\partial \phi}{\partial q} \right)$ and its transpose, and zero-matrix. $[M_{qq}]$ is symmetric but no longer constant, unlike the rigid-link mechanisms, which are the coefficients of the second-order inertial acceleration terms in the Lagrange's equations, while $\left(\frac{\partial \phi}{\partial q} \right)$ is the system Jacobian which is formed directly from the second-order terms of the constraint equation, while its transpose is the coefficient of the Lagrange multipliers. Notice that the constraint equations are influenced by the deformation of the links. The matrix $[M_{qu}]$ is a coefficient matrice comes from the non-linear coupling of the

inertial motion and elastic deformation. $[M_{uu}]$ is well-known as a mass matrix and need only be calculated once in the procedure of computer simulation.

The second term in equation (3.35) is known as the stiffness matrix in structural dynamic problem which is formed from the deformation of the links. The second-order column vector contains the second-order derivatives of $\ddot{q}$ and $\ddot{u}$, and also the Lagrange multipliers which originated in the generalized Lagrange's equations. On the right-hand side of equation (3.35) the column vector contains displacement and velocity-dependent forces, $g(q,\dot{q})$, pertaining to the particular Lagrange's equations, of the constraint equation associated with the row in which they appear. The terms g_k and h_Q include the effect of all external forces, as well as the centripetal and Coriolis components, while the terms f_p contain the centripetal and Coriolis terms from the loop-closure equation for the mechanical system.

3.3 SOLUTION PROCEDURE

Equation (3.35) includes both the generalized inertial and generalized elastic coordinates. In order to solve the equations of motion efficiently these two generalized coordinates systems may be separated. Equation (3.40) relates to the inertial generalized coordinates while equation (3.41) relates to the elastic generalized coordinates.

$$\begin{bmatrix} [M_{qq}] & [M_{qu}] \\ [M_{qu}]^T & 0 \end{bmatrix} \begin{bmatrix} \ddot{q} \\ -\lambda \end{bmatrix} = \begin{bmatrix} [g] \\ [f] \end{bmatrix} - [M_{qu}] \begin{bmatrix} \ddot{u} \\ 0 \end{bmatrix} \qquad (3.40)$$

$$[M_{uu}] \{ \ddot{u} \} + [KK] \{ u \} = \{ h \} - [M_{qu}]^T \{ \ddot{q} \} \qquad (3.41)$$

For most structures, the exact form of damping matrix is unknown since the sources of energy loss are complicated. Generally, in the mode-superposition approach the damping is assumed to be uncoupled and is given in each mode as a percentage of the critical damping. The selection of realistic damping values for a particular structure is based on experimental measurements. Thus of the damping matrix is introduced [66] and is represented by [C], the equation (3.41) can be modified as

$$[M_{uu}] \{ \ddot{u} \} + [C] \{ \dot{u} \} + [KK] \{ u \} = \{ \bar{R} \} \qquad (3.42)$$

where $\{\bar{R}\} = \{ h \} - [M_{qu}]^T \{ \ddot{q} \}$, is denoted as external forces on the link.

To solve equation (3.40), the same numerical integration technique was employed as in section 2.6. The major difference is the selection of the initial values. To provide the inertial initial values, the dynamic analysis of a rigid-link mechanism was executed, and the elastic initial values were provided by the solution of equation (3.41).

Mode-superposition method was employed to solve equation (3.42). An effective transformation matrix is established using the displacement solutions of the free vibration equilibrium equations with damping neglected,

$$[M_{uu}] \{ \ddot{u} \} + [KK] \{ u \} = 0 \qquad (3.43)$$

The solution to equation (3.43) can be postulated to be of the form

$$u = \phi \sin \omega(t - t_0) \tag{3.44}$$

where ϕ is a vector of order n, t the time variable, t_0 a time constant, and ω a constant identified to represent the frequency of vibration (rad/sec) of the vector ϕ.

Substituting equation (3.44) into (3.43), the generalized eigen-problem is obtained, from which ϕ and ω must be determined:

$$[\ KK\ ]\ [\ \phi\ ] = \omega^2\ [\ M\ ]\ [\ \phi\ ] \tag{3.45}$$

The eigen-problem in equation (3.42) yields the n eigensolutions (ω_1^2,ϕ_1), (ω_2^2,ϕ_2), ····, (ω_n^2,ϕ_n), where the eigenvectors are M-orthonormalized. Thus $\phi^T K\phi = \Omega^2$ and $\phi^T M\phi = I$. using

$$u(t) = \phi\ \eta(t) \tag{3.46}$$

the equilibrium equations are obtained that correspond to the modal generalized displacements

$$\ddot{\eta} + \phi^T C\phi\dot{\eta} + \Omega^2\eta = \phi^T \bar{R} \tag{3.47}$$

The initial values on η are obtained using equation(3.46) and the M-orthonormality of ϕ; i.e., at time 0 we have

$$\eta_0 = \phi^T M u_0\ ;\ \dot{\eta}_0 = \phi^T M\dot{u}_0 \tag{3.48}$$

$\ddot{\eta}$ can be solved easily from equation (3.48) as

$$\ddot{\eta} = \phi^T \bar{R} - \phi^T C\phi\dot{\eta} - \Omega^2\eta \tag{3.49}$$

The displacement and velocity, η and $\dot{\eta}$, at t=t+1 were obtained by integrating $\ddot{\eta}$.

The solution procedure can be summarized by the following steps:

1. At t_0, based upon the given initial values, $\ddot{q}$ and λ are solved by employing PLU-decomposition. The inertial velocity and displacement characteristics $\dot{q}$ and q at t_1 are obtained by integrating $\ddot{q}$ from t_0 to t_1.

2. At the time t_0, equation(3.41) is solved by employing the mode-superposition method and employing the initial values. The elastic velocity and displacement characteristics $\dot{u}$ and u are obtained by integrating $\ddot{u}$ from t_0 to t_1.

3. The initial values of the next time-step are the final values obtained from the previous time-step.

4. Step 1 and step 2 are repeated until the end of the simulation.

The physical meaning of the above solution procedure can be interpreted as follows:

1. At t_0, the configuration of the mechanism was fixed by applying the given initial values, and then the mechanism was allowed to move from t_0 to t_1 without changing the shape of the links.

2. Based upon the elastic and inertial initial values given at t_0, the discretized elastic deformation of the links were calculated at t_1.

3. At t_1, the mechanism was re-set to the new configuration because of the deformation of the links. Based upon the new shapes of the links,

the mechanism was considered as a rigid-linked system again and the properties of the next time-step were calculated.

4. If the time-step is small enough, the error of the quasi-equilibrium solution can be neglected. Figure 3.4 demonstrates the above procedures.

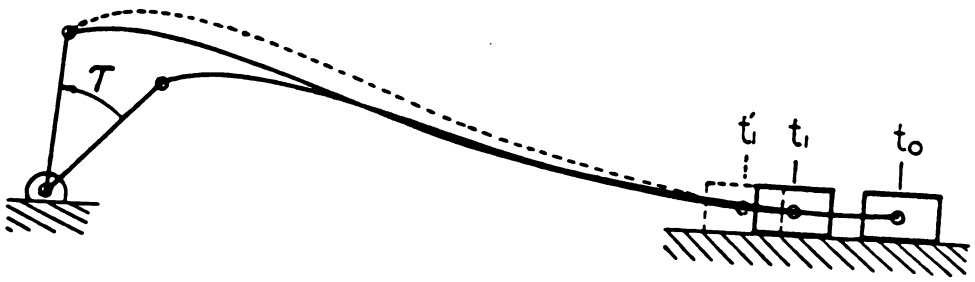

Figure 3.4 Quasi-static solution procedures

3.4 EXAMPLE - A slider-crank mechanism with a flexible connecting rod

A planar slider-crank mechanism with a flexible connecting rod was analyzed using the proposed methodology prior to comparing the theoretical results with experimental response data from an accompanying experimental program. A schematic of the mechanism is presented in Figure 3.5(a) and the relevant kinematic parameters are presented in Figure 3.5(b). Since the numerical solutions for more than six elements were found less improved and because of saving the computer cpu-time,

the connecting rod was divided into six elements as shown in Figure 3.6. The characteristics of the mechanism are shown in table 3.1.

Table 3.1 The characteristics of the experimental slider-crank mechanism

Items	symbol	magnitude	unit
Length of the crank-shaft	r_2	0.048	m
Length of the connecting rod	r_3	0.29318	m
Mass density	ρ	7860	Kg/m^3
Modulus of elasticity	E	200	GPa
Width of the connecting rod	WID	0.01905	m
Depth of the connecting rod	DEP	0.00127	m
Mass of the slider	M_s	0.63607	Kg

Two half-bridge strain gauges were attached on the link to detect the deformation of the link as shown in Figure 3.7. From the photograph, it is clearly shows that one of the strain gauges was located at the middle of the link while the other one was located at the quarter of the link.

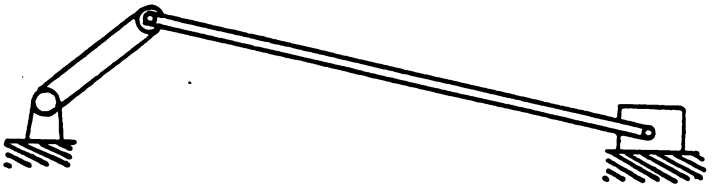

(a)

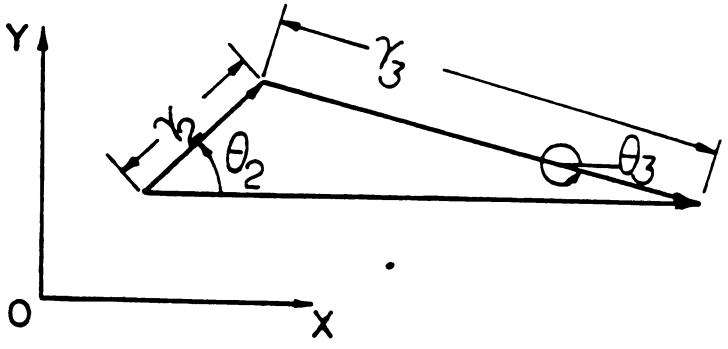

(b)

Figure 3.5 (a) The slider-crank mechanism with flexible connecting rod
(b) Vector-loop model of the mechanism

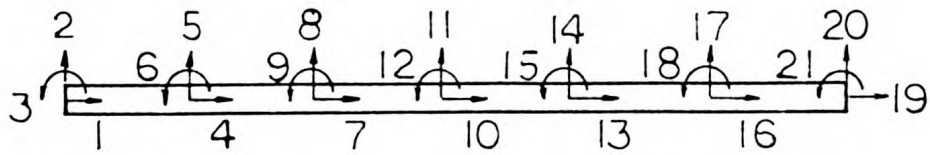

Figure 3.6 The six finite elements of the connecting rod

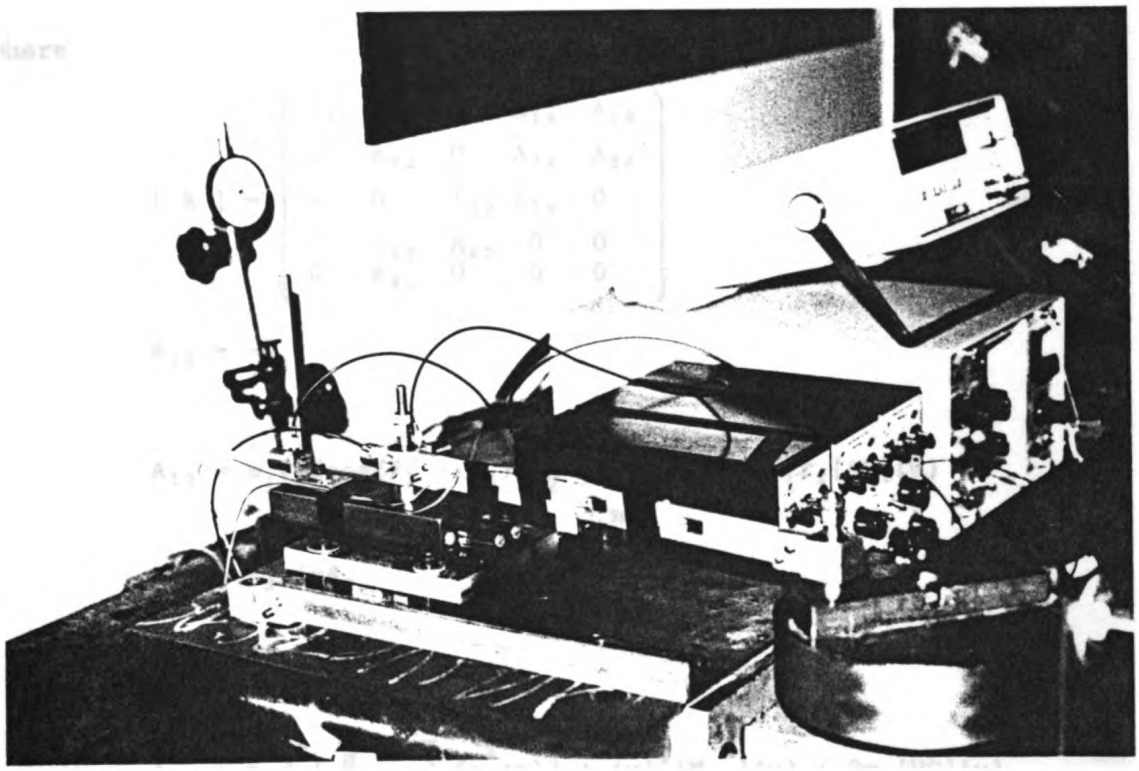

Figure 3.7 Photograph of the flexible connecting rod with strain gauges

3.4.1 Equations of motion

The dynamical behavior of the slider-crank mechanism is governed by a mixed set of differential and algebraic equations. By applying equations (3.5) - (3.31), two set of equations were obtained which are in inertial and elastic bases respectively;

$$[\,A\,]\,\{\,X\,\} = \{\,B\,\} \tag{3.50}$$

$$[M_{uu}]\,\ddot{\{u\}} + ([K]+F_1[KG_1]+\Delta F[KG_2]-\dot{\theta}_3^2\,[M_{uu}])\,\{u\}$$

$$=-m_1 r_2 \dot{\theta}_2^2[AG]^T - m_1\ddot{\theta}_3[FG]\{u\} - 2m_1\dot{\theta}_3[FG]\{\dot{u}\} - m_1\ddot{\theta}_3[EG]^T$$

$$+ m_1\dot{\theta}_3^2[HG]^T - [C]\{\dot{u}\} \tag{3.51}$$

where

$$[\,A\,] = \begin{bmatrix} A_{11} & A_{12} & 0 & A_{14} & A_{15} \\ 0 & A_{22} & 0 & A_{24} & A_{25} \\ 0 & 0 & A_{33} & A_{34} & 0 \\ 0 & A_{42} & A_{43} & 0 & 0 \\ 0 & A_{52} & 0 & 0 & 0 \end{bmatrix} \tag{3.52}$$

$$A_{11} = -1$$

$$A_{12} = m_1 r_2 \ell\cos(\theta_3 - \theta_2)\left(\frac{N}{2} + \sum_{n=1}^{N-1} n\right) - m_1 r_2[AG]\{u\}$$

$$A_{14} = r_2\sin\theta_2$$

$$A_{15} = -r_2\cos\theta_2$$

$$A_{22} = m_1\ell^2\left[\frac{N}{3} + \sum_{n=1}^{N-1}(n^2+n)\right] + \{u\}^T[M_{uu}]\{u\} + 2m_1[HG]\{u\}$$

$$A_{24} = (r_3 - \frac{1}{2}(u)^T[KG1]\{u\} + u_{19})\sin\theta_3$$

$$A_{25} = -(-r_3 + \frac{1}{2}(u)^T[KG1]\{u\} - u_{19})\cos\theta_3$$

$$A_{33} = M_s$$

$$A_{34} = 1$$

$$A_{42} = A_{24}$$

$$A_{43} = 1$$

$$A_{52} = A_{25}$$

$$\{X\} = [\lambda_3 \ \ddot{\theta}_3 \ \ddot{s} \ \lambda_1 \ \lambda_2 \ ] \tag{3.53}$$

$$\{B\} = [B_1 \ B_2 \ B_3 \ B_4 \ B_5] \tag{3.54}$$

$$B_1 = m_1 r_2 \ell \ddot{\theta}_3 \sin(\theta_3 - \theta_2)(\frac{N}{2} + \sum_{n=1}^{N-1} n) + m_1 r_2 \dot{\theta}_3^2 [BG]\{u\}$$

$$+ 2m_1 r_2 \dot{\theta}_3 [AG]\{\dot{u}\} - m_1 r_2 [BG]\{\ddot{u}\}$$

$$B_2 = -m_1 r_2 \ell \dot{\theta}_2^2 \sin(\theta_3 - \theta_2)(\frac{N}{2} + \sum_{n=1}^{N-1} n) - m_1 r_2 \dot{\theta}_2^2 [BG]\{u\}$$

$$- 2\dot{\theta}_3 \{\dot{u}\}[M]\{u\} - 2m_1 \dot{\theta}_3 [HG]\{\dot{u}\} - m_1 [EG]\{\ddot{u}\}$$

$$+ m_1 \{u\}^T [FG]\{\ddot{u}\}$$

$$B_3 = -(sgn)\mu M_s g$$

$$B_4 = -r_2\dot{\theta}_2^2\cos\theta_2 - r_3\dot{\theta}_3^2\cos\theta_3 - (\{\bar{u}\}[KG1]\{u\} + \{\dot{u}\}[KG1]\{\dot{u}\}$$

$$- \frac{1}{2}\dot{\theta}_3^2\{u\}^T[KG1]\{u\} - \bar{u}_{19} + u_{19}\dot{\theta}_3^2)\cos\theta_3$$

$$- (2\dot{u}_{19}\dot{\theta}_3 - 2\dot{\theta}_3\{\dot{u}\}^T[KG1]\{u\})\sin\theta_3$$

$$B_5 = -r_2\dot{\theta}_2^2\sin\theta_2 - r_3\dot{\theta}_3^2\sin\theta_3 - (\{\bar{u}\}[KG1]\{u\} + \{\dot{u}\}[KG1]\{\dot{u}\}$$

$$- \frac{1}{2}\dot{\theta}_3^2\{u\}^T[KG1]\{u\} - \bar{u}_{19} + u_{19}\dot{\theta}_3^2)\sin\theta_3$$

$$- (-2\dot{u}_{19}\dot{\theta}_3 + 2\dot{\theta}_3\{\dot{u}\}^T[KG1]\{u\})\cos\theta_3$$

$$[AG]_i = \frac{1}{2}\,[-\cos(\theta_3-\theta_2) \quad \sin(\theta_3-\theta_2) \quad \frac{\ell}{6}\sin(\theta_3-\theta_2)$$

$$-\cos(\theta_3-\theta_2) \quad \sin(\theta_3-\theta_2) \quad -\frac{\ell}{6}\sin(\theta_3-\theta_2)]$$

$$[BG]_i = \frac{1}{2}\,[\sin(\theta_3-\theta_2) \quad \cos(\theta_3-\theta_2) \quad \frac{\ell}{6}\cos(\theta_3-\theta_2)$$

$$\sin(\theta_3-\theta_2) \quad \cos(\theta_3-\theta_2) \quad -\frac{\ell}{6}\cos(\theta_3-\theta_2)]$$

$$[EG]_i = [0 \ (\frac{3\ell}{20} + \frac{n\ell}{2}) \ (\frac{\ell^2}{30} + \frac{n\ell^2}{12}) \ 0 \ (\frac{7\ell}{20} + \frac{n\ell}{2}) \ (\frac{-1}{20}\ell^2 - \frac{n\ell^2}{12})]$$

$$, n-i-1$$

$$[FG]_i = \begin{bmatrix} 0 & -\frac{7}{20} & -\frac{\ell}{20} & 0 & -\frac{3}{20} & \frac{\ell}{30} \\ \frac{7}{20} & 0 & 0 & \frac{3}{20} & 0 & 0 \\ \frac{\ell}{20} & 0 & 0 & \frac{\ell}{30} & 0 & 0 \\ 0 & -\frac{3}{20} & -\frac{\ell}{30} & 0 & -\frac{7}{20} & \frac{\ell}{20} \\ \frac{3}{20} & 0 & 0 & \frac{7}{20} & 0 & 0 \\ -\frac{\ell}{30} & 0 & 0 & -\frac{\ell}{20} & 0 & 0 \end{bmatrix}$$

$$[KG1]_i = \begin{pmatrix} 0 & 0 & 0 & 0 & 0 & 0 \\ 0 & \frac{6}{5\ell} & \frac{1}{10} & 0 & -\frac{6}{5\ell} & \frac{1}{10} \\ 0 & \frac{1}{10} & \frac{2\ell}{15} & 0 & -\frac{1}{10} & -\frac{\ell}{30} \\ 0 & 0 & 0 & 0 & 0 & 0 \\ 0 & -\frac{6}{5\ell} & \frac{1}{10} & 0 & \frac{6}{5\ell} & -\frac{1}{10} \\ 0 & \frac{1}{10} & -\frac{\ell}{30} & 0 & -\frac{1}{10} & \frac{2\ell}{15} \end{pmatrix}$$

$$[KG2]_i = \begin{pmatrix} 0 & 0 & 0 & 0 & 0 & 0 \\ 0 & \frac{3}{5\ell} & \frac{1}{10} & 0 & -\frac{3}{5\ell} & 0 \\ 0 & \frac{1}{10} & \frac{\ell}{30} & 0 & -\frac{1}{10} & -\frac{\ell}{60} \\ 0 & 0 & 0 & 0 & 0 & 0 \\ 0 & -\frac{3}{5\ell} & -\frac{1}{10} & 0 & \frac{3}{5\ell} & 0 \\ 0 & 0 & -\frac{\ell}{60} & 0 & 0 & \frac{\ell}{10} \end{pmatrix}$$

$$[HG]_i = \ell[(\tfrac{1}{2}n + \tfrac{1}{6}) \quad 0 \quad 0 \quad (\tfrac{1}{2}n + \tfrac{1}{3}) \quad 0 \quad 0], \; n=i-1$$

$\ell \approx$ Length of one element

N ≈ Number of elements

$m_i \approx$ Mass of one element

$$[M_{uu}] = \frac{\rho_e A_e \ell}{420} \begin{pmatrix} 140 & 0 & 0 & 70 & 0 & 0 \\ 0 & 156 & 22\ell & 0 & 54 & -13\ell \\ 0 & 22\ell & 4\ell^2 & 0 & 13\ell & -3\ell^2 \\ 70 & 0 & 0 & 140 & 0 & 0 \\ 0 & 54 & 13\ell & 0 & 156 & -22\ell \\ 0 & -13\ell & -3\ell^2 & 0 & -22\ell & 4\ell^2 \end{pmatrix}$$

$$[K] = \frac{1}{\ell^3}\begin{bmatrix} EA\ell^2 & 0 & 0 & -EA\ell^2 & 0 & 0 \\ 0 & 12EI & 6\ell EI & 0 & -12EI & 6\ell EI \\ 0 & 6\ell EI & 4\ell^2 EI & 0 & -6\ell EI & 2\ell^2 EI \\ -EA\ell^2 & 0 & 0 & EA\ell^2 & 0 & 0 \\ 0 & -12EI & -6\ell EI & 0 & 12EI & -6\ell EI \\ 0 & 6\ell EI & 2\ell^2 EI & & -6\ell EI & 4\ell^2 EI \end{bmatrix}$$

In equation (3.53) does not feature $\ddot{\theta}_2$, since the crank is assumed to operate with a constant angular velocity which requires the angular acceleration of the crank-shaft to be zero. This situation mandates the introduction of the Lagrange multiplier λ_3 which represents the torque required to maintain this constant crank frequency. The Lagrange multipliers λ_1 and λ_2 in (3.53) represent, F_{s3x}, the force imposed on link 3 by the slider in OX direction, and, F_{s3y}, the force imposed on link 3 by the slider in the OY direction respectively.

3.4.2 Some remarks on the elastodynamic behavior of a flexible connecting rod

The effective natural frequency and the damping of the flexible connecting rod were dependent upon the time dependent axial force in the member. Figure 3.8 shows the relationship between the effective natural frequency of the link and the axial forces. A tensile force increases the frequency of vibration while a compressive force reduces the frequency of vibration. Figure 3.9 shows the effect of the axial force on the structural damping in the member. The damping factor

reduced from 0.0114 to 0.00949 while the tensile force varied from 0 lbf to 10 lbf. The above results were obtained by applying the external compressive and tensile forces, in the axial direction of the link, on the slider while the mid-span of the link was given an initial deformation. The damping factor of the link was calculated by employing the logarithmic decrement method which is defined as the natural logarithm of the ratio of any two successive amplitudes. Thus, the logarithmic decrement is defined

$$\delta = \frac{1}{n} \ell_n \frac{x_0}{x_n} \tag{3.55}$$

where x_0 represents the magnitude of the first wave and x_n denotes the magnitude after n cycles have elapsed. The logarithmic decrement can be expressed as

$$\delta = \xi \omega_n \tau_d = \frac{2\pi\xi}{\sqrt{(1-\xi^2)}} \tag{3.56}$$

where ω_n is the natural frequency of the link and τ_d is the period of the damped vibration.

If ξ is less than 0.3, then $\sqrt{(1-\xi^2)} \approx 1$, and the damping factor can be expressed as

$$\xi = \frac{\delta}{2\pi} \tag{3.57}$$

Upon reviewing equation (3.51) the stiffness matrix was affected by the axial force as well as the angular velocity of the connecting rod. In order to investigate the theoretical effectiveness of the axial force on the natural frequency of the link, free vibration

test was obtained by zeroing the dynamic external forces and only static axial force was applied in the end of the link.

Figure 3.10 was obtained when 5 lbf of static tensile force was applied and 0.009 of the damping factor was employed while Figure 3.11 was obtained when 5 lbf of the compressive force was applied and 0.015 of the damping factor was given. Upon reviewing Figure 3.10, 20.7 cycles were obtained during a period of 0.6 seconds. Thus the natural frequency was calculated 34.5 Hz, while the original natural frequency was 30 Hz without any external force. Similarly, Figure 3.11 shows 25.83 Hz of compressive natural frequency. These results matched the experimental test shown in Figure 3.8.

Equation (3.51) was solved by employing mode-superposition method in which three modes were chosen for the solution. The first three modes were plotted in Figure 3.12. The vibrational natural frequency of each mode was also investigated during the simulation. Figure 3.13 shows the variation of the first-mode natural frequency during one crank cycle, in which three crank speed were recorded. Figure 3.11 shows the higher the crank speed the bigger the change in the natural frequency. It is easy to understand that the axial force imposed on the link is bigger at higher crank speed. Three curves in Figure 3.13 intersect at 85 and 275 degrees of crank angle, where the axial force is zero. The corresponding natural frequency is 30 Hz. The second-mode and the third-mode were undertaken the same investigation as shown in Figure 3.14 and 3.15. From Figure 3.13 to 3.15, it is evident that the first mode has the biggest variation on the natural frequency while the third mode has the smallest variation on the natural frequency.

The mode shape did not change during one crank cycle but its natural frequency changed continuously. In Figure 3.16 shows the first mode shape did not change at 0, 45, 180, and 225 degree of crank angle.

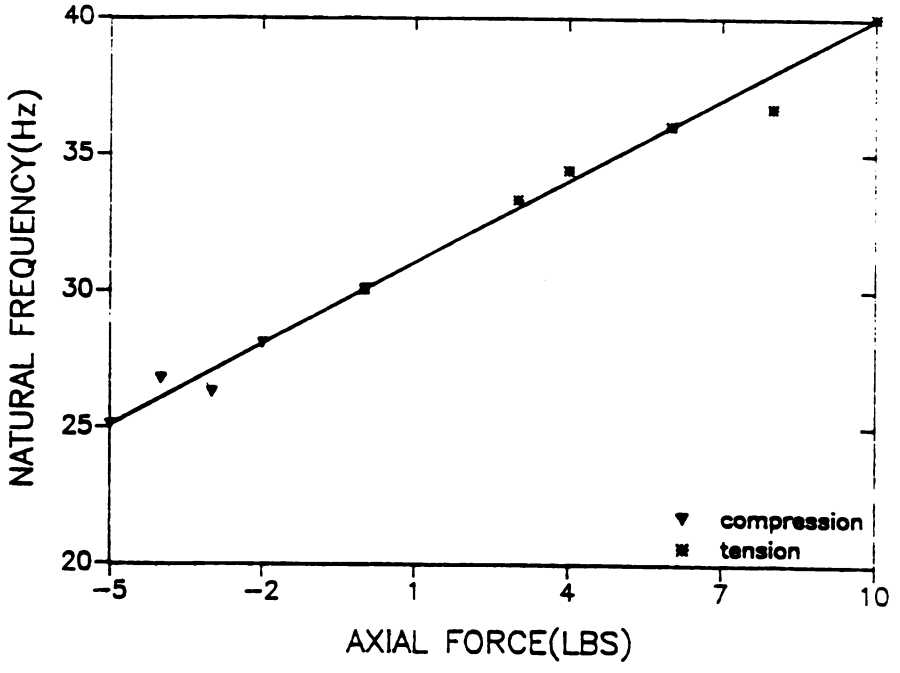

Figure 3.8 The relationship between the natural frequency and the axial force

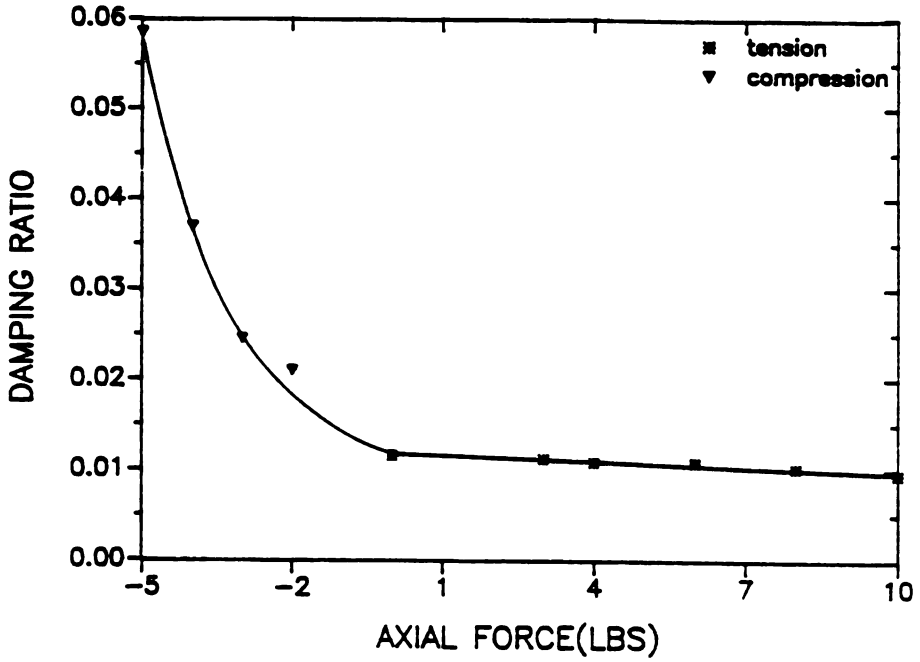

Figure 3.9 The relationship between the damping factor and the axial force

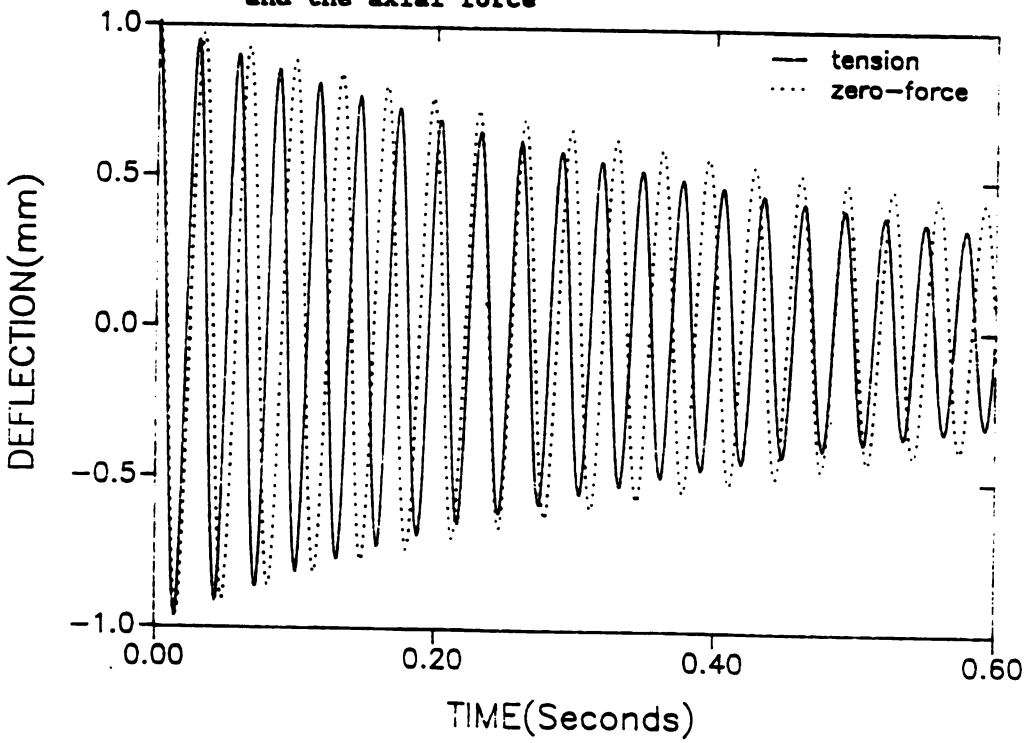

Figure 3.10 Simulation of a simply-supported beam by applying an external tensile force

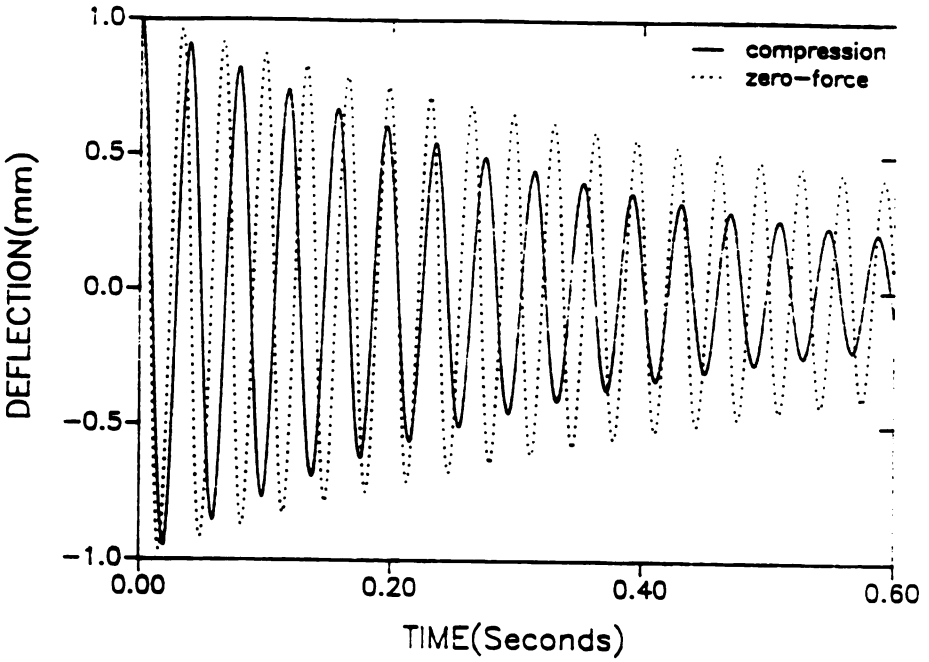

Figure 3.11 Simulation of a simply-supported beam by applying an external compressive force

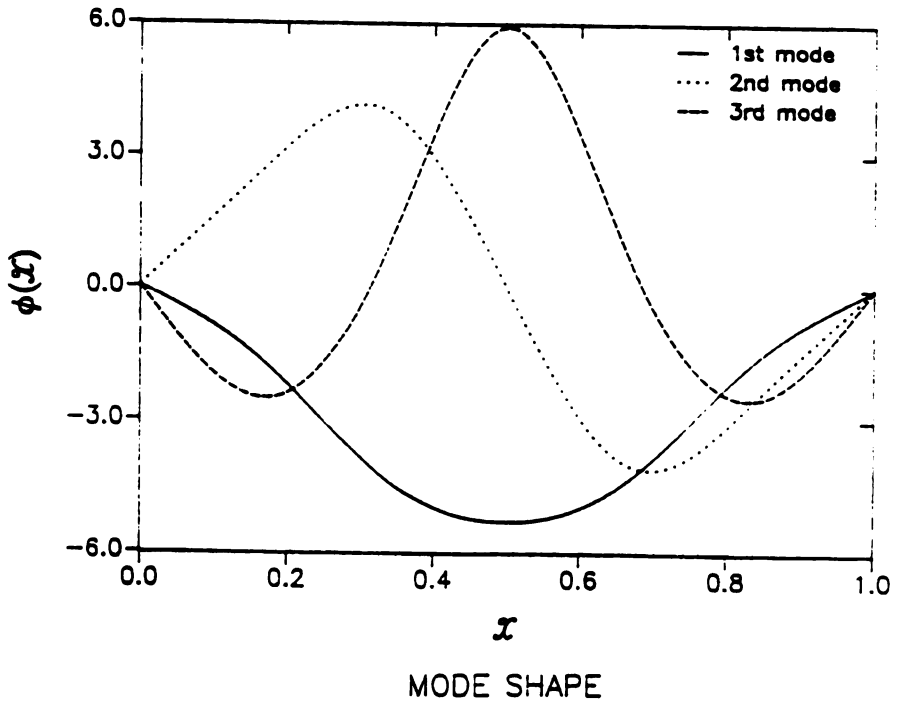

Figure 3.12 The mode shape of the first three modes

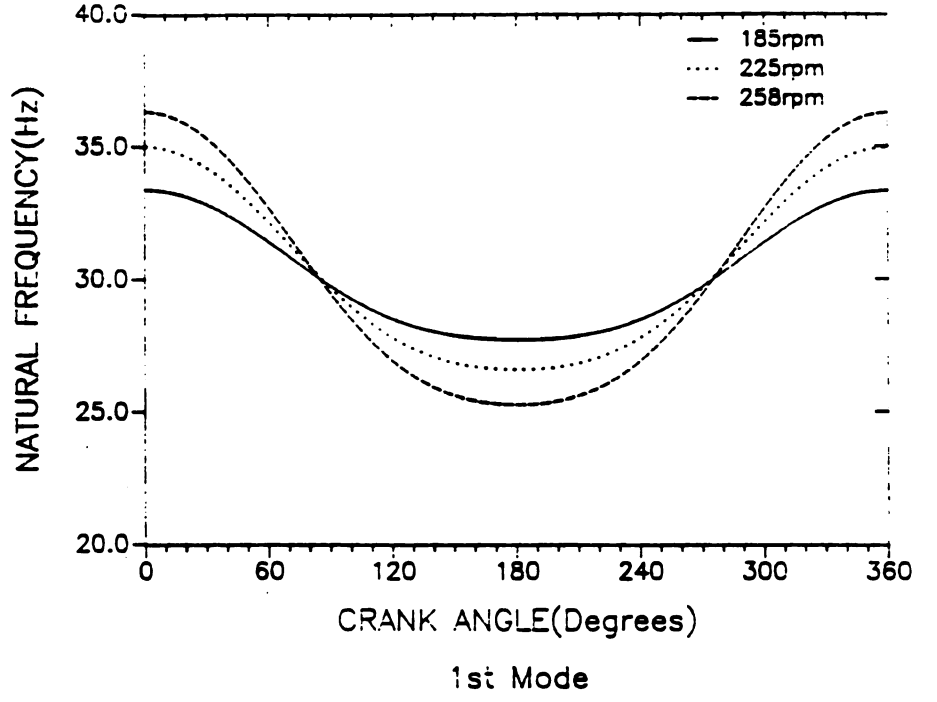

Figure 3.13 The variation of the natural frequency: the first mode

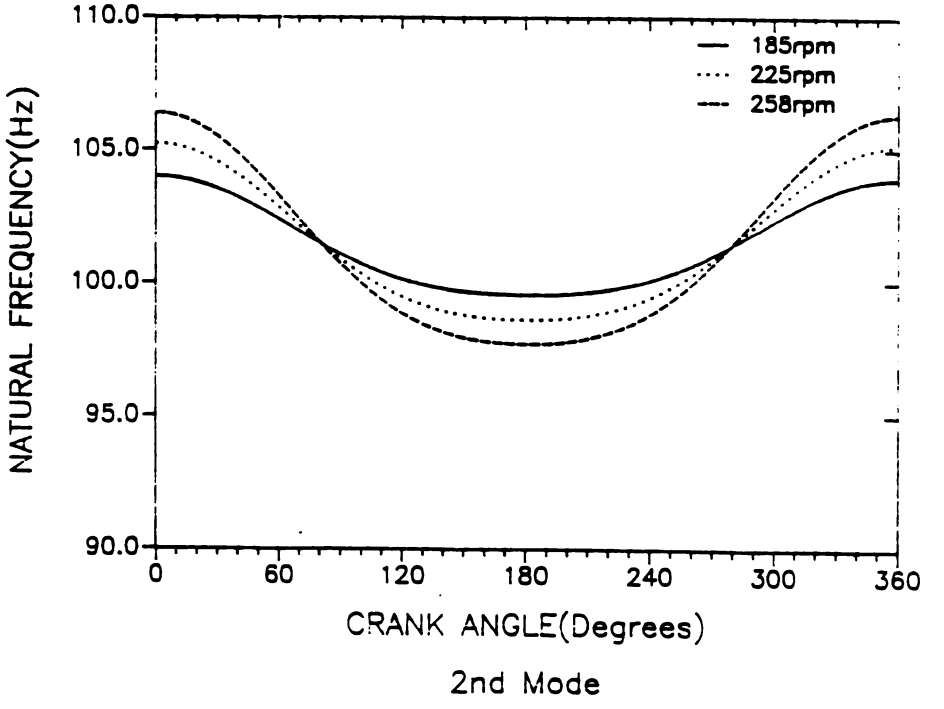

Figure 3.14 The variation of the natural frequency: the second mode

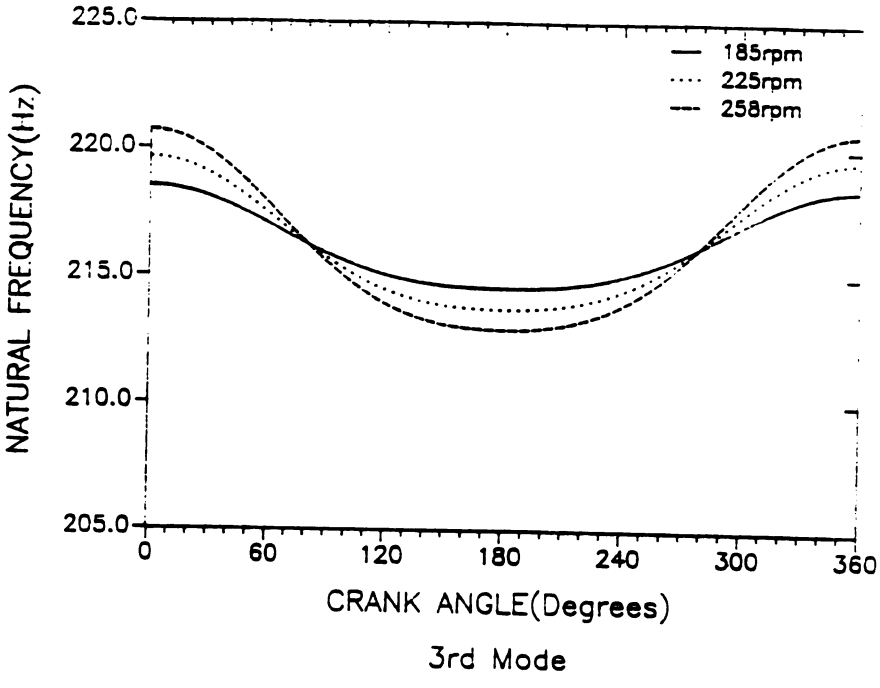

Figure 3.15 The variation of the natural frequency: the third mode

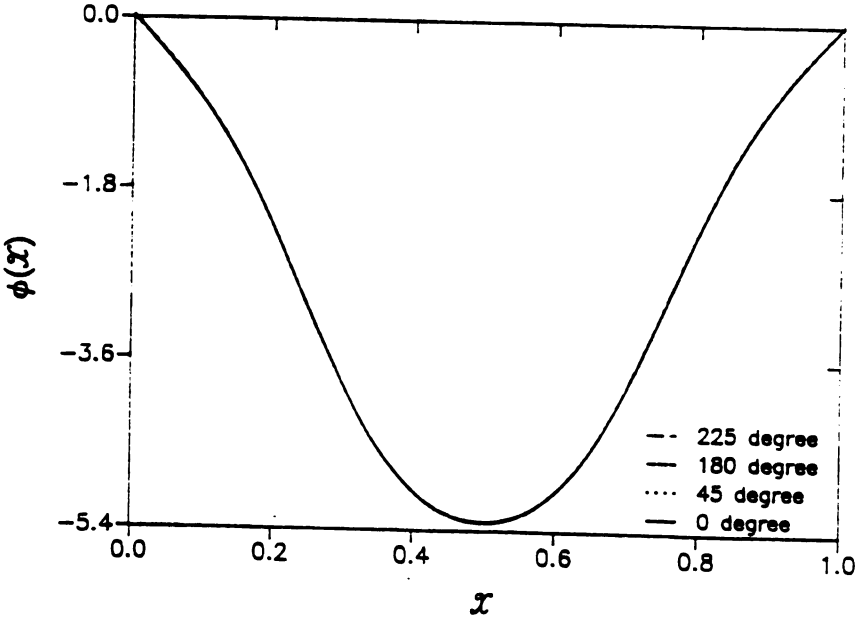

Figure 3.16 The mode shape of the first-mode at 0, 45, 180, and 225 degrees of crank angle. Mechanism operating speed 185 rpm

3.4.3 Experimental and theoretical results

The same procedures as described in Chapter two were employed on this experimental work. The mid-span deflection of the connecting rod, the tangential and transverse accelerations of the connection-rod and the acceleration of the slider were recorded.

Figures 3.17 - 3.19 represent the mid-span deflection of the connecting rod at 185, 225 and 258 rpm crank speed, respectively. The solid line shows the experimental result while the dash line represents the theoretical result. These curves show an excellent correlation not only in the magnitude of the deflection but also in the frequency of the vibration.

Figure 3.20 represents the acceleration of the slider at 258 rpm crank speed. The solid line shows the experimental result while the dash line represents the theoretical result. Figure 3.21 represents the acceleration of the slider at 185 rpm crank speed. The solid line shows the theoretical simulation with rigid connecting rod while the dash line shows the theoretical simulation with flexible connecting rod. The difference can not be distinguished between these two curves in Figure 3.21. But Figure 3.22 shows the difference between these two curves in which the acceleration response of rigid-link system was subtracted by the acceleration response of flexible-link system. The accelerations of the slider at 225 rpm and 258 rpm show the same characteristics as at 185 rpm. Hence the acceleration of the slider at 225 and 258 rpm are not presented here, only the variation of the rigid-link system and flexible-link system were presented. Figure 3.23 shows the variation of the acceleration of the slider at 225 rpm while Figure 3.24 shows those

at 258 rpm. Upon reviewing these Figures, the curves show twice the vibration frequency as the connecting rod. Therefore, it is evident that these differences were caused by the flexibility of the connecting rod.

The magnitude and direction of the pin force, F_{g3}, at gudgeon-pin bearing is shown in Figure 3.25 and 3.26, respectively. The operating speed of the mechanism was 185 rpm. Again, no differences can be seen from the Figures, but the microscopic view of the differences were presented by Figure 3.27 and 3.28. Figure 3.27 shows the difference of the pin force while Figure 3.28 shows the difference of the force angle.

3.5 CONCLUSIONS OF THE CHAPTER

A displacement finite element formulation has been derived for undertaking the nonlinear vibrational analysis of general flexible linkage mechanisms. This formulation incorporates geometrical nonlinearities and also terms coupling the rigid-body kinematics and the elastic deformations. The numerical simulation is based upon two sets of equations of motion which obtained from the inertial and elastic frame, respectively.

The comparison of the dynamical characteristics between the rigid-link mechanisms and flexible-link mechanisms have been studied by taking a slider-crank mechanism as an example. The time-dependent stiffness of the system and the mid-span deflection show a good correlation between simulation and experimental results.

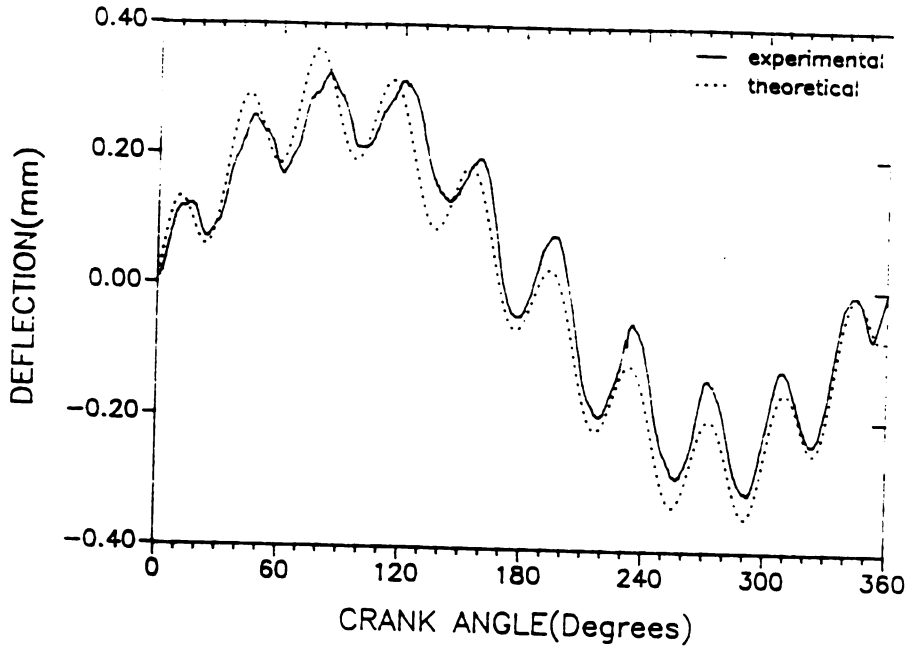

Figure 3.17 The mid-span deflection of the connecting rod. Mechanism operating speed 185 rpm

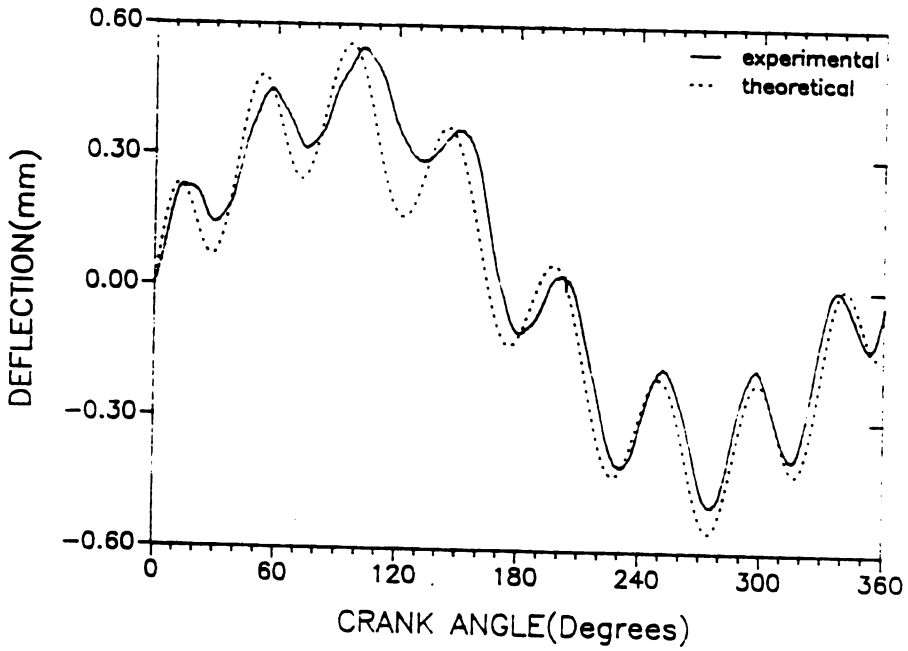

Figure 3.18 The mid-span deflection of the connecting rod. Mechanism operating speed 225 rpm

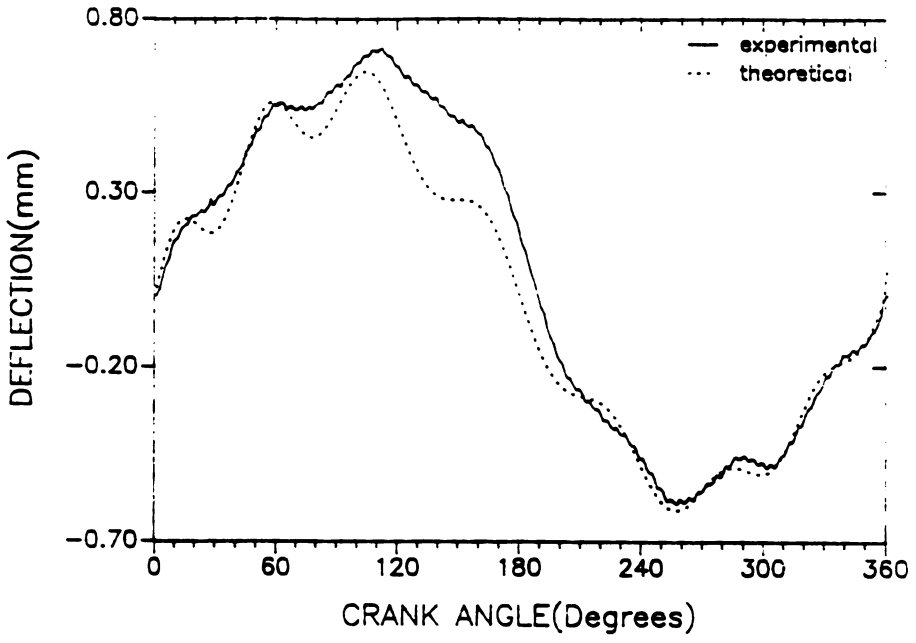

Figure 3.19 The mid-span deflection of the connecting rod. Mechanism operating speed 258 rpm

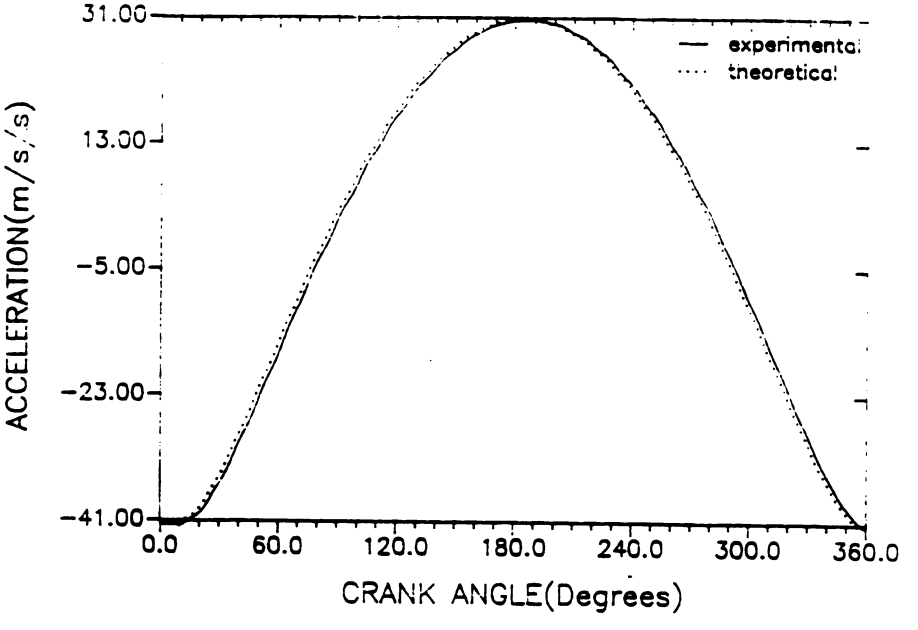

Figure 3.20 The acceleration of the slider. Mechanism operating speed 258 rpm

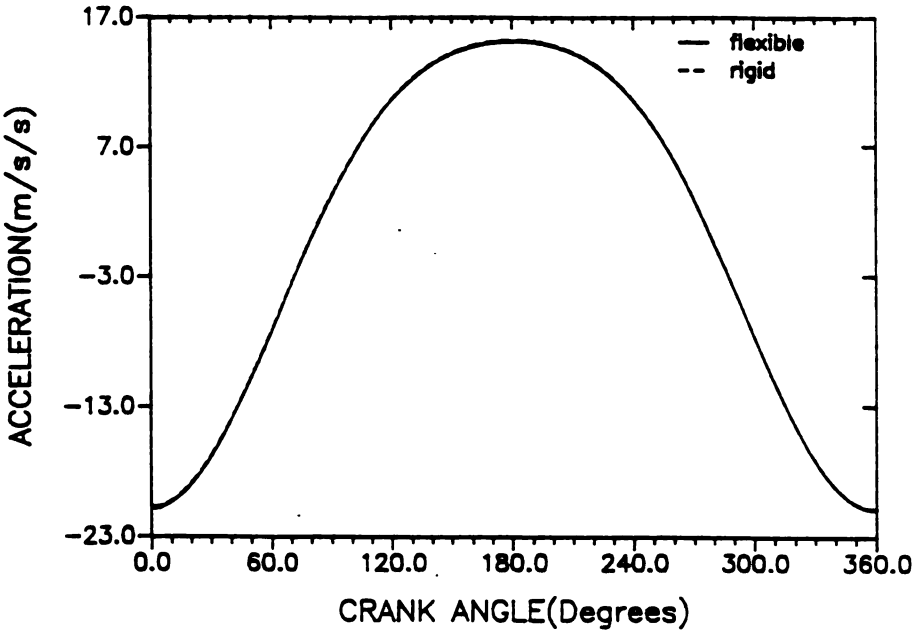

Figure 3.21 The acceleration of the slider. Mechanism operating speed 185 rpm

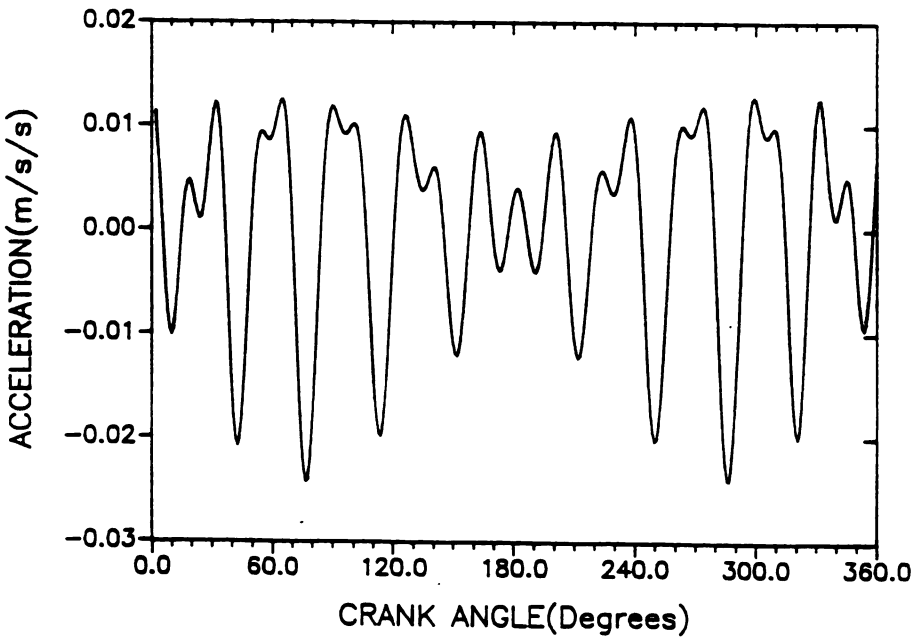

Figure 3.22 The variation of the acceleration of the slider between the rigid-link and flexible-link of a slider-crank mechanism. Mechanism operating speed 185 rpm

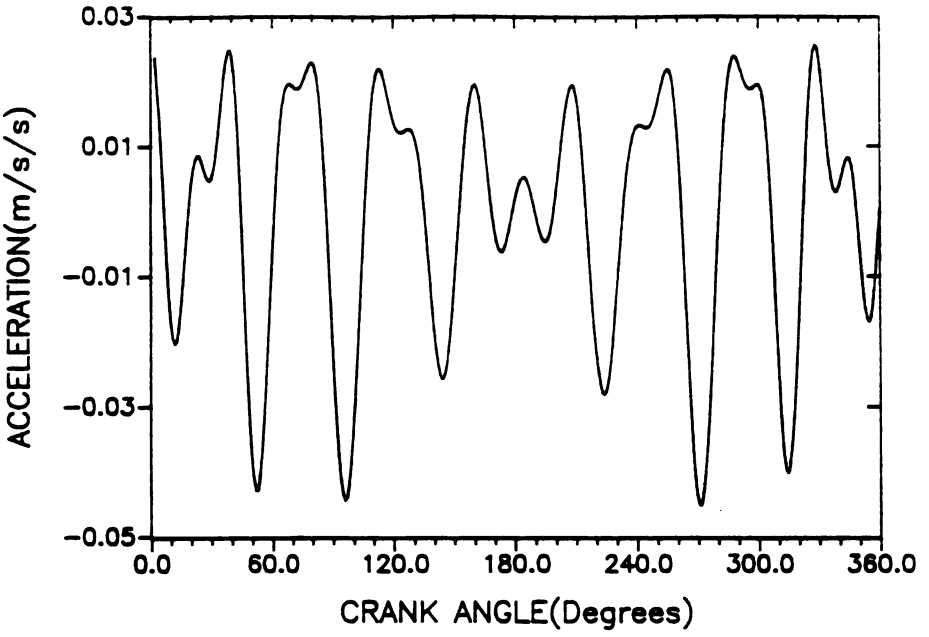

Figure 3.23 The variation of the acceleration of the slider between the rigid-link and flexible-link of a slider-crank mechanism. Mechanism operating speed 225 rpm

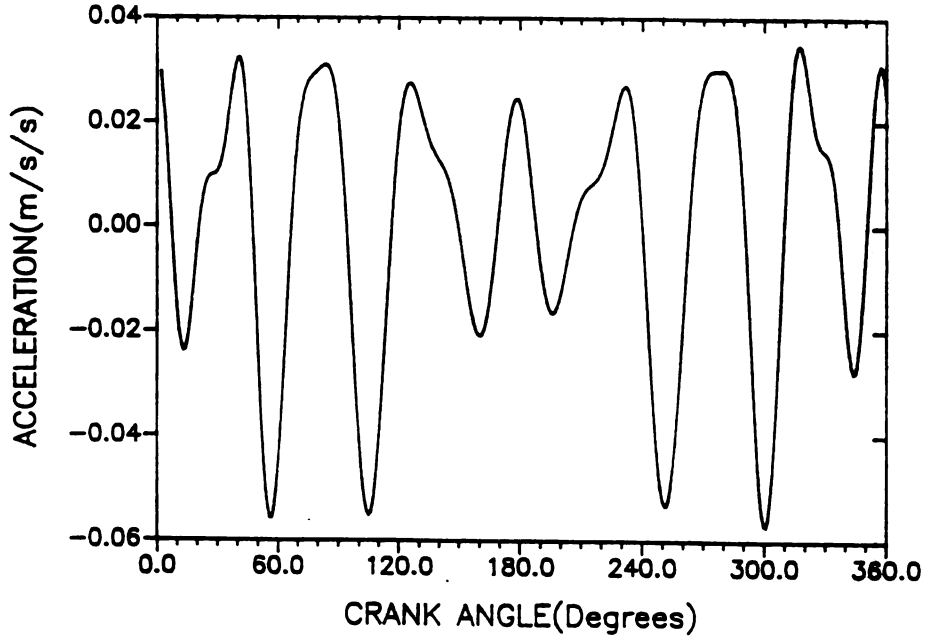

Figure 3.24 The variation of the acceleration of the slider between the rigid-link and flexible-link of a slider-crank mechanism. Mechanism operating speed 258 rpm

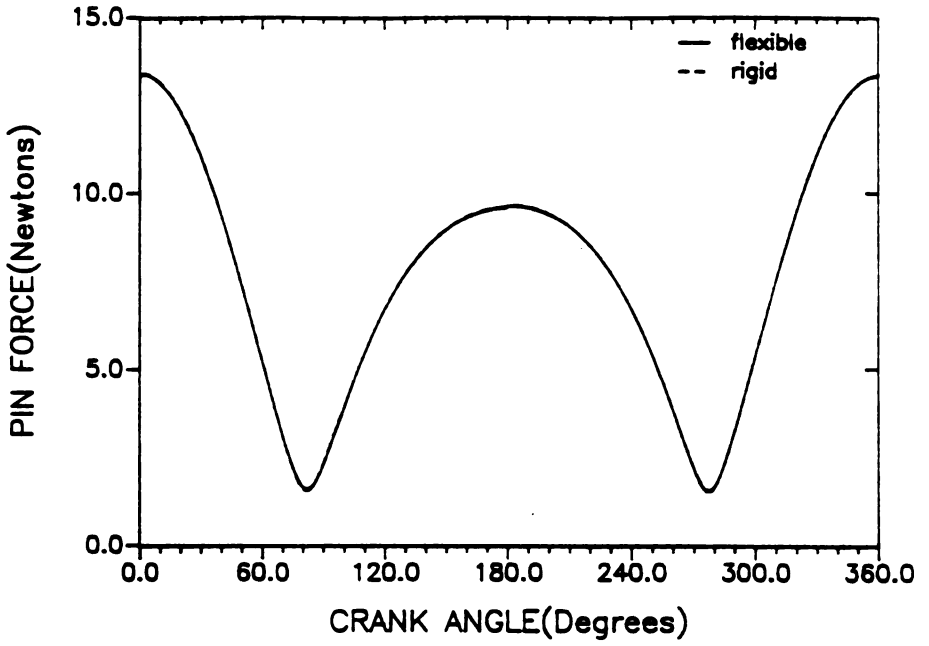

Figure 3.25 The magnitude of the pin force in gugeon-pin bearing Mechanism operating speed 185 rpm

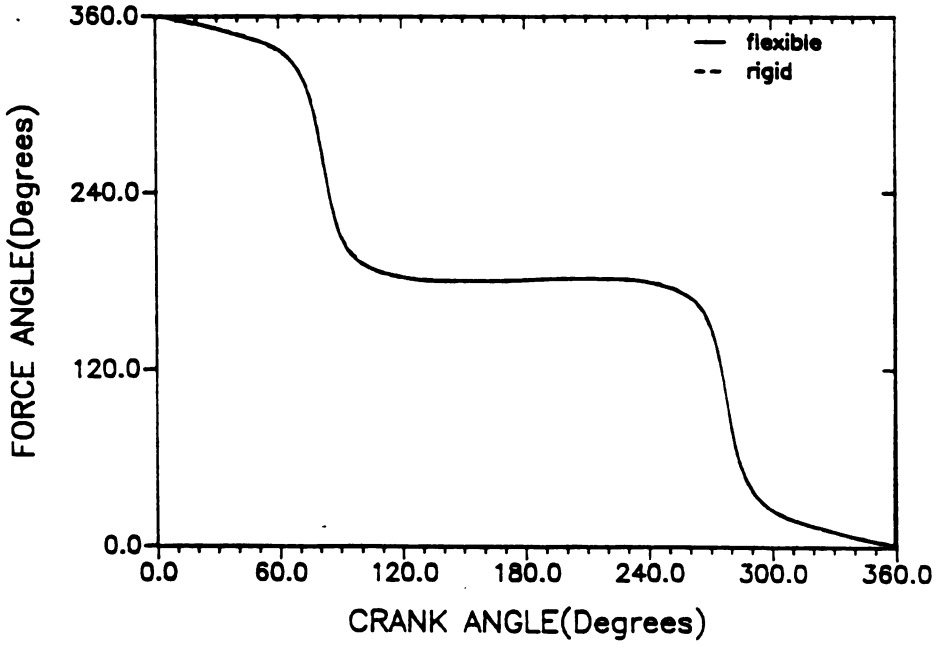

Figure 3.26 The force angle of the pin force in gugeon-pin bearing Mechanism operating speed 185 rpm

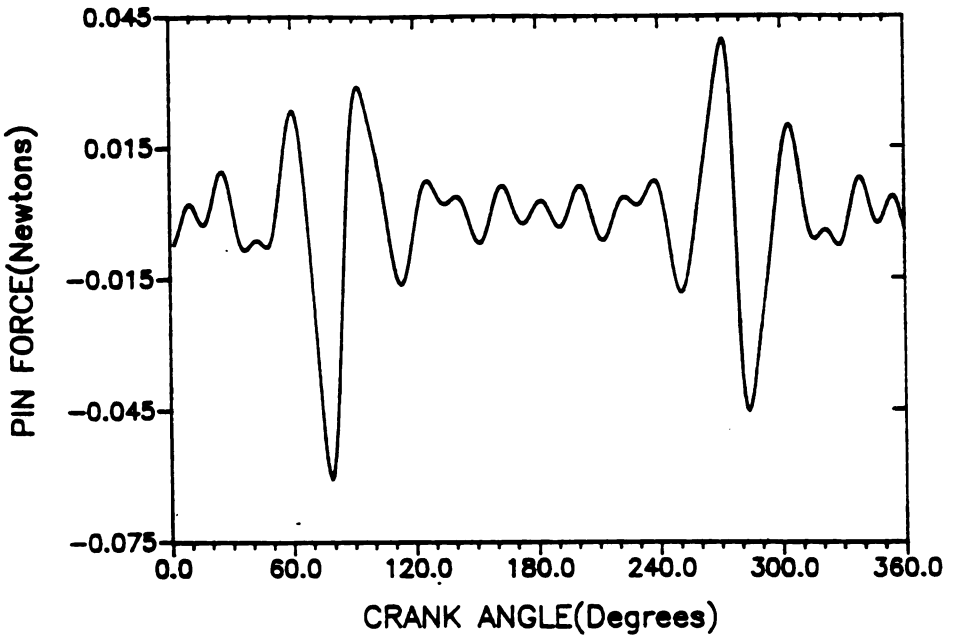

Figure 3.27 The variation of the pin force in the gudgeon-pin bearing between the rigid-link and flexible-link slider-crank mechanism. Mechanism operating speed 185 rpm

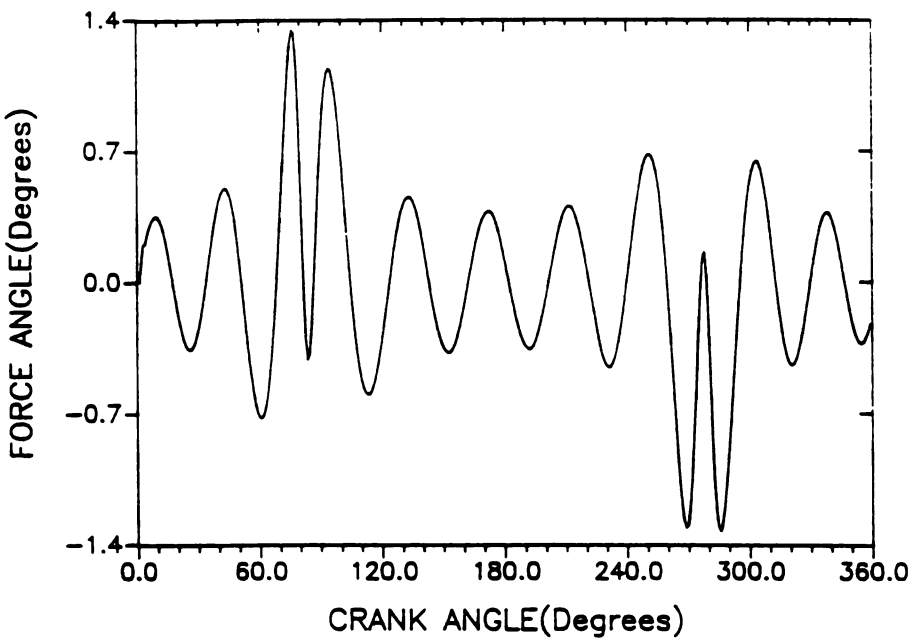

Figure 3.28 The variation of the force angle in the gudgeon-pin bearing between the rigid-link and flexible-link slider-crank mechanism. Mechanism operating speed 185 rpm

Chapter IV

ELASTODYNAMIC ANALYSIS OF A GENERAL PLANAR MECHANISM FEATURING FLEXIBLE-LINKS WITH RADIAL CLEARANCES IN THE REVOLUTE JOINTS

4.1 INTRODUCTION

The major purpose of this chapter is to formulate a general analytical model to predict the vibration of the links and the dynamical characteristics of a general planar mechanical system featuring flexible-links and bearing clearances. Subsequent to the development of this general methodology, two illustrative examples are presented in order to predict the elastodynamic response of these systems and compare these theoretical results with experimental results obtained from complementary experimental programs. The first example is a compound pendulum with prescribed initial dynamical conditions which is subjected to a sudden impact from a fixed mechanical stop. The second example is a slider-crank mechanism with a flexible connecting rod and featuring a prescribed radial clearance in the gudgeon-pin bearing.

4.2 MODEL OF A GENERAL PLANAR MECHANISM FEATURING FLEXIBLE-LINKS AND REVOLUTE JOINTS WITH BEARING CLEARANCES

A general planar mechanism system incorporating joints with bearings with radial clearances undergoes several different phenomenological responses which are associated with the relative motion of the pin and journal in each joint. The four-mode model, as proposed in Chapter Two, was extended in order to incorporate elastodynamic effects and employed to described the elastodynamical response of this general planar mechanical system. These four modes are classified as the contact-mode, the free-flight-mode, the impact-mode and the transient-mode, and these modes were schematically presented in Figure 2.3.

The mathematical descriptions of these four modes for a rigid-linked system are described in Chapter Two. In order that these formulations are applicable to flexible-linked systems several additional constraints must be appended to these definitions in order to accommodate flexibility effects.

The four-mode model is described as follows:

(i) Contact-Mode:

In this mode, the pin and the journal are in contact and a sliding motion relative to each other is assumed to exist. The contact surface is assumed to be rigid, smooth and frictionless, thus there is no energy loss in this mode.

Two criteria must be satisfied by the pin and journal of a joint in order that the bearing behavior be described by the contact-mode: firstly, the kinematic constraint equations for the contact-mode

must be satisfied. Secondly, the contact force between the pin and the journal must be compressive force. The second criterion is one of the two criteria which dictate the termination of the contact-mode. The other criterion for initiating the free-flight-mode is the rate of change of the force angle. Note that the termination of the contact-mode always leads to the simulation control initiating the free-flight-mode. If all of the joints in a mechanism in which the behavior of the joints are governed by the contact-mode, then each flexible-link of the system would be treated as a Euler-Bernoulli beam with the assumption that the thickness-to-length ratio is very small. Contact stresses at the pin-journal interface are not included in the formulation.

(ii) Free-Flight-Mode:

In the free-flight-mode, the pin and the journal in a specific joint are not in contact, hence there are no reaction forces between these two members. Thus a constraint equations different from those employed for the contact-mode must be developed. During the free-flight-mode, the flexible-link will be treated as a pin-free beam. The tip position of the link is calculated and continuously monitored during the simulation process in order to determine when the free-flight-mode is terminated. This event occurs when the tip of the link, which is the location of the pin, again contacts the inner surface of the journal. The duration of the free-flight-mode is governed by the flexibility and dynamical behavior of the kinematic chain subjected to analysis.

(iii) Impact-Mode:

A significant impactive force is developed in a bearing when the pin and the journal contact suddenly. This behavior is the basis for

the impact-mode, and this phenomenon is modeled by invoking a momentum-exchange approach which incorporates the coefficient of restitution. During the impact duration, the joint is treated as being in the contact-mode, thus the constraint equations governing the contact-mode must be satisfied. The coefficient of restitution, which captures the material properties of the impacting bodies, are dependent upon the stiffness of the contacting materials, the roughness of the contact surfaces, the geometrical shape of the impacting bodies, and also the velocities of the bodies prior to impact. The value of the coefficient of restitution is generally determined experimentally.

(iv) Transient-Mode:

The transient-mode begins at the first impact between the pin and the journal in a specific joint, and ends with the restoration of contact between these members. Thus this mode generally comprises a sequence of several free-flight-modes of progressively smaller duration and also several impact-modes. This progressively attenuating vibrational response is also governed by the flexibility of the links of the system.

The subsequent sections present the mathematical apparatus for modeling each mode.

4.3 GOVERNING EQUATIONS OF THE SYSTEM

Two adjacent links, i and j, in a general planar mechanical system with flexible-links incorporating revolute joints which featuring a distinct radial clearance can be modeled as shown in Figure 4.1. Axes

OXY denotes the inertial reference frame, while $o_i x_i y_i$ denote the moving frame fixed in the body in an undeformed reference state. At any instant t, a general point in the ith link was denoted as p_i and p_i' before and after deformation. Therefore, the general point p after deformation can be expressed as

$$r_i = r_{oi} + r_{Ri} + u_i \tag{4.1}$$

where r_{oi} are the components measured in the $o_i x_i y_i$ frame of the position vector of the origin of the body axes relative to the origin of the inertial frame. Similarly, r_{Ri} denotes the position vector of point p in the reference state relative to the origin of the body axes and u_i is the deformation displacement vector, may be expressed as $u_x e_1 + u_y e_2$, where u_x is the axial deformation in the ox direction and u_y is the transverse deformation in the oy direction. Terms e_1 and e_2 are the unit vectors in the ox and oy direction measured relative to the moving reference frame, respectively.

The constraint equation can be obtained from the closed-loop vector

$$r_{oi} + r_{Ri} + u_i + \xi_{ij} + r_{oj} + r_{Rj} + u_j = 0 \tag{4.2}$$

where ξ_{ij} denotes the clearance vector in the revolute joint which connecting the ith link and jth link. Note that the clearance vector is a position vector which is zero if the bearing is assumed to be devoid of clearance.

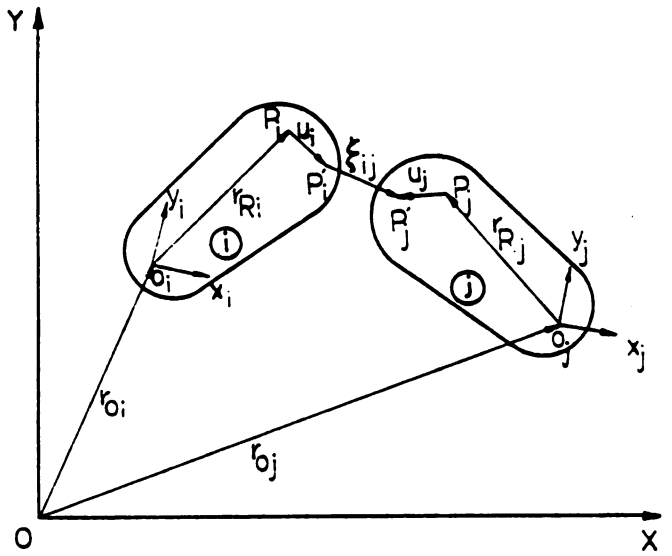

Figure 4.1 Generalized coordinate of two adjacent links

In general, the constraint equation can be expressed as

$$\phi_i = \phi(q_1, q_2, \cdots q_\ell, \xi_1, \xi_2, \cdots, \xi_m, , u_1, u_2, \cdots, u_{3(N+1)}) \tag{4.3}$$

where there are ℓ inertial generalized coordinates, m inertial clearanced coordinates and 3(N+1) elastic generalized coordinates, N is the number of finite elements employed to model the mechanism system. For convenience, q_i and ξ_k can be represented by a set of inertial generalized coordinates, η_j. Thus the general constraint equation can be rewritten as

$$\phi_i = \phi(\eta_1, \eta_2, \cdots, \eta_p, u_1, u_2, \cdots, u_{3(N+1)}) \tag{4.4}$$

where $p = \ell + m$

The finite element method is incorporated in the derivation of the equations of motion of each link which is assumed herein to be modeled as a beam rather the shell or plate. Each link can be divided into many finite elements and the elastic deformation of each element described by six nodal displacements, u_1 - u_6, which represent the axial, transverse and rotating deformation at each node as illustrated in Figure 3.2. The deformed state of a general point p in the element can be expressed relative to the inertial reference frame by the expression

$$R_i = [X_A + (x+u_x)\cos\theta - u_y\sin\theta]i + [Y_A + (x+u_x)\sin\theta - u_y\cos\theta]j \tag{4.5}$$

where $X_A i + Y_A j$ is the position vector of point A relative to the inertial frame.

The corresponding velocity, thus, is

$$\dot{R}_i = [\dot{X}_A + \dot{u}_x\cos\theta - (x+u_x)\dot{\theta}\sin\theta - \dot{u}_y\sin\theta + u_y\dot{\theta}\cos\theta]i$$
$$+ [\dot{Y}_A + \dot{u}_x\sin\theta + u_x\dot{\theta}\cos\theta + \dot{u}_y\cos\theta - u_y\dot{\theta}\sin\theta]j \tag{4.6}$$

Equations (4.5) and (4.6) can be expressed in the rotating frame,

$$r_i = (X_A\cos\theta + Y_A\sin\theta + x + u_x)e_1 + (-X_A\sin\theta + Y_A\cos\theta + u_y)e_2 \tag{4.7}$$

$$\dot{r}_i = (\dot{X}_A\cos\theta + \dot{Y}_A\sin\theta - u_y\dot{\theta} + \dot{u}_x)e_1$$
$$+ [-\dot{X}_A\sin\theta + \dot{Y}_A\cos\theta + (x+u_x)\dot{\theta} + \dot{u}_y]e_2 \tag{4.8}$$

The displacement at any point in the element can be expressed in terms of the nodal displacements as

$$u(x,t) = [\ N\ ]\ \{\ U\ \} \tag{4.9}$$

where [N] is the shape function and is dependent upon the position only, while {U} is the column vector of nodal displacement which is function of time.

The deformation in the e_1 and e_2 directions can now be expressed as

$$u_x = [N_x]\ \{U\} \tag{4.10}$$

and,

$$u_y = [N_y]\ \{U\} \tag{4.11}$$

where

$$[N_x] = [N_1\ 0\ 0\ N_4\ 0\ 0]$$

$$[N_y] = [0\ N_2\ N_3\ 0\ N_5\ N_6]$$

$$\{U\}^T = \{u_1\ u_2\ u_3\ u_4\ u_5\ u_6\}$$

$$N_1 = 1 - \zeta$$

$$N_2 = 1 - 3\zeta^2 + 2\zeta^3$$

$$N_3 = \ell(\zeta - 2\zeta^2 + \zeta^3)$$

$$N_4 = \zeta$$

$$N_5 = 3\zeta^2 - 2\zeta^3$$

$$N_6 = \ell(-\zeta^2 + \zeta^3),\ \zeta = x/\ell$$

Equation(4.8) can be expressed in the following form by introducing equation (4.10) and (4.11),

$$\dot{r} = (\dot{x}_A - [N_y](U)\dot{\theta} + [N_x](\dot{U}))e_1 + (\dot{y}_A + x\dot{\theta} + [N_x](U)\dot{\theta} + [N_y](\dot{U}))e_2 \quad (4.12)$$

where $\dot{x}_A = \dot{X}_A\cos\theta + \dot{Y}_A\sin\theta$, and $\dot{y}_A = -\dot{X}_A\sin\theta + \dot{Y}_A\cos\theta$

For convenience, equation(4.10) can be rewritten in matrix form as

$$\begin{bmatrix} \dot{r}_x \\ \dot{r}_y \end{bmatrix} = [\, I \; A \; B \,] \begin{bmatrix} \dot{p} \\ \dot{\theta} \\ \dot{u} \end{bmatrix} \quad (4.13)$$

where

$$I = \begin{bmatrix} 1 & 0 \\ 0 & 1 \end{bmatrix}, \quad A = \begin{bmatrix} -[N_y](U) \\ x+[N_x](U) \end{bmatrix}, \quad B = \begin{bmatrix} [N_x] \\ [N_y] \end{bmatrix},$$

and $\dot{p} = \begin{bmatrix} \dot{x}_A \\ \dot{y}_A \end{bmatrix}$

If the link is assumed to be homogeneous with constant cross sectional area (A_e) and mass density (ρ_e), the kinetic energy of an element can be expressed as

$$T_e = \frac{1}{2}\rho_e A_e \int_0^{\ell} \dot{r}_i \cdot \dot{r}_i \, dx$$

$$= \frac{1}{2}\rho_e A_e \int_0^{\ell} [\, \dot{p}^T \; \dot{\theta} \; \dot{u} \,] \begin{bmatrix} I \\ A^T \\ B^T \end{bmatrix} [I \; A \; B] \begin{bmatrix} \dot{p} \\ \dot{\theta} \\ \dot{u} \end{bmatrix} dx$$

$$= \frac{1}{2}\rho_e A_e [\, \dot{p}^T \dot{\theta} \; \dot{u} \,] \left\{ \int_0^{\ell} \begin{bmatrix} I & A & B \\ A^T & A^T A & A^T B \\ B^T & B^T A & B^T B \end{bmatrix} dx \right\} \begin{bmatrix} \dot{p} \\ \dot{\theta} \\ \dot{u} \end{bmatrix} \quad (4.14)$$

The kinetic energy of each link, therefore, is

$$T_i = \sum_{e=1}^{n} T_e \quad \text{, where n is the number of elements in each link} \tag{4.15}$$

In equation(4.14), defining $\dot{\eta} = [\dot{p}\ \dot{\delta}]$, where η denotes the generalized coordinate. Therefore, equation (4.14) can be expressed as

$$T_e = \frac{1}{2} [\dot{\eta}\ \dot{u}] \begin{bmatrix} M_{\eta\eta} & M_{\eta u} \\ M_{\eta u}^T & M_{uu} \end{bmatrix} \begin{bmatrix} \dot{\eta} \\ \dot{u} \end{bmatrix}$$

$$= \frac{1}{2} [\dot{\eta}\ \dot{u}]\ [M] \begin{bmatrix} \dot{\eta} \\ \dot{u} \end{bmatrix} \tag{4.16}$$

where

$$[M] = \begin{bmatrix} M_{\eta\eta} & M_{\eta u} \\ M_{\eta u}^T & M_{uu} \end{bmatrix} \tag{4.17}$$

$$M_{\eta\eta} = \rho_e A_e \int_0^{\ell} \begin{bmatrix} I & A \\ A^T & A^T A \end{bmatrix} dx \tag{4.18}$$

$$M_{\eta u} = \rho_e A_e \int_0^{\ell} \begin{bmatrix} B \\ A^T B \end{bmatrix} dx \tag{4.19}$$

$$M_{uu} = \rho_e A_e \int_0^{\ell} \left[B^T B \right] dx \tag{4.20}$$

The strain energy of the element can be expressed as

$$V_e = \frac{1}{2} \int_0^{\ell} EI \left(\frac{\partial^2 u_y}{\partial x^2} \right)^2 dx + \frac{1}{2} \int_0^{\ell} EA \left(\frac{\partial u_x}{\partial x} \right)^2 dx$$

$$+ \frac{1}{2} \int_0^{\ell} F(x) \left(\frac{\partial^2 u_y}{\partial x} \right)^2 dx \tag{4.21}$$

The first and the second terms in equation(4.21) are the strain energy due to the transverse and axial deformations of the link respectively, while the the third term is the work done by the axial force F(x) due to the change in the horizontal projection of an element.

Introduction of equations (4.10) and (4.11) into equation (4.21), the strain energy in each finite element can be written as

$$V_e = \frac{1}{2}\int_0^{\ell} EI\{u\}^T[N_y'']^T[N_y'']\{u\}dx + \frac{1}{2}\int_0^{\ell} EA\{u\}^T[N_x']^T[N_x']\{u\}dx$$

$$+\frac{1}{2}\int_0^{\ell} F(x)\{u\}^T[N_y']^T[N_y']\{u\}dx$$

$$= \frac{1}{2}\{u\}^T[K]\{u\} + \frac{1}{2}\int_0^{\ell} F(x)\{u\}^T[N_y']^T[N_y']\{u\}dx \qquad (4.22)$$

where [K] is the stiffness matrix which is defined by

$$\int_0^{\ell} EI[N_y'']^T[N_y'']dx + \int_0^{\ell} EA[N_x']^T[N_x']dx \qquad (4.23)$$

Note that (') denotes the spatial derivative with respect to x, while (") represents the second spatial derivative with respect to x.

The axial force at any point in the link may be expressed as,

$$F(x) = F_1 + (F_2 - F_1)\frac{x}{\ell} = F_1 + \Delta F\frac{x}{\ell} \qquad (4.24)$$

where the terms are defined relevant to Figure 3.3.

Redefining equation(4.24) to incorporate equation(4.23), the strain energy of the link can be rewritten as

$$V_e = \frac{1}{2}\{u\}^T[K]\{u\} + \frac{1}{2}F_1\{u\}^T[K_{G1}]\{u\} + \frac{1}{2}\Delta F\{u\}^T[K_{G2}]\{u\} \qquad (4.25)$$

where

$$[K_{G1}] = \int_0^{\ell} [N_y']^T [N_y'] \, dx \tag{4.26}$$

$$[K_{G2}] = \int_{0\ell}^{\ell x} [N_y']^T [N_y'] \, dx \tag{4.27}$$

The total kinetic energy of the system may be written

$$T = \sum_{i=1}^{nl} T_i \tag{4.28}$$

where nl is the number of links of the mechanical system.

Similarly, the total strain energy of the system may be written

$$V = \sum_{i=1}^{nl} \left(\sum_{e=1}^{n} V_e \right)_i \tag{4.29}$$

The first and the second time derivative of the constraint equations, equation(4.4), may be written

$$\dot{\phi} = \sum_{i=1}^{p} \frac{\partial \phi}{\partial \eta_i} \dot{\eta}_i + \sum_{j=1}^{3(N+1)} \frac{\partial \phi}{\partial u_j} \dot{u}_j \tag{4.30}$$

$$\ddot{\phi} = \sum_{i=1}^{p} \sum_{k=}^{p} \frac{\partial^2 \phi}{\partial \eta_i \partial \eta_k} \dot{\eta}_i \dot{\eta}_k + \sum_{i=1}^{p} \frac{\partial \phi}{\partial \eta_i} \ddot{\eta}_i + \sum_{j=1}^{3(N+1)} \sum_{\ell=1}^{3(N+1)} \frac{\partial^2 \phi}{\partial u_j \partial u_\ell} \dot{u}_j \dot{u}_\ell$$

$$+ \sum_{j=1}^{3(N+1)} \frac{\partial \phi}{\partial u_j} \ddot{u}_j \tag{4.31}$$

4.3.1 Equations of motion for the contact-mode

The equations of motion for a mechanical system in the contact-mode are developed herein by utilizing the generalized Lagrange's equation and expressing all terms relative to the inertial generalized coordinates . The Lagrange's equation is employed in the elastic generalized equation. These two equations are

$$\frac{d}{dt}\left(\frac{\partial T}{\partial \dot{\eta}_i}\right) - \frac{\partial T}{\partial \eta_i} + \frac{\partial V}{\partial \eta_i} - \sum_{j-1}^{nc} \lambda_j \frac{\partial \phi_j}{\partial \eta_i} = Q_i \tag{4.32}$$

$$\frac{d}{dt}\left(\frac{\partial T}{\partial \dot{u}_k}\right) - \frac{\partial T}{\partial u_k} + \frac{\partial V}{\partial u_k} = Q_k \tag{4.33}$$

where nc denotes the number of constraint equations

Employing equations(4.32) and (4.33) and introducing the second time derivative constraint equation(4.31), yields the equations of motion for the adjacent flexible links where the pin and journal as the kinematic pair are describing the contact mode

$$\begin{bmatrix} [M_{\eta\eta}] & [\frac{\partial \phi}{\partial \eta}] & [M_{\eta u}] \\ [\frac{\partial \phi}{\partial \eta}]^T & 0 & 0 \\ [M_{\eta u}]^T & 0 & [M_{uu}] \end{bmatrix} \begin{bmatrix} \ddot{\eta} \\ -\lambda \\ \ddot{u} \end{bmatrix} + \begin{bmatrix} 0 & 0 \\ 0 & [KK] \end{bmatrix} \begin{bmatrix} \eta \\ -\lambda \\ u \end{bmatrix}$$

$$= \begin{bmatrix} \{g\} \\ \{f\} \\ \{h\} \end{bmatrix} \tag{4.34}$$

where

$$[KK] = [K] + [KG_1] + [KG_2] \tag{4.35}$$

$$g_k = \sum_{i=1}^{nf} F_i \cdot \frac{\partial r_i}{\partial \eta_k} - [\dot{M}_{\eta\eta} \quad \dot{M}_{\eta u}] \begin{bmatrix} \dot{\eta} \\ \dot{u} \end{bmatrix}, k=1,2,\cdots,p \qquad (4.36)$$

where nf denotes the number of external forces

$$f_k = \sum_{i=1}^{p} \sum_{k=1}^{p} \frac{\partial^2 \phi_k}{\partial \eta_i \partial \eta_k} \dot{\eta}_i \dot{\eta}_k + \sum_{j=1}^{3(N+1)} \sum_{\ell=1}^{3(N+1)} \frac{\partial^2 \phi_k}{\partial u_j \partial u_\ell} \dot{u}_j \dot{u}_\ell$$

$$+ \sum_{j=1}^{3(N+1)} \frac{\partial \phi}{\partial u_j} \ddot{u}_j \quad , k=1,2,\cdots,nc \qquad (4.37)$$

where nc denotes the number of constraint equations

$$h_Q = \sum_{i=1}^{nf} F_i \cdot \frac{\partial r_i}{\partial u_Q} + \frac{1}{2} [\dot{\eta} \ \dot{u}] \left[\frac{\partial M}{\partial u_Q} \right] \begin{bmatrix} \dot{\eta} \\ \dot{u} \end{bmatrix} - [\dot{M}^T_{\eta u} \ \dot{M}_{uu}] \begin{bmatrix} \dot{\eta} \\ \dot{u} \end{bmatrix}$$

$$, Q=1,2,\cdots,3(N+1) \qquad (4.38)$$

In equation (4.34) the differential equations are represented as a set of simultaneous, linear algebraic equations in the variables $\ddot{\eta}_i$, λ_p and $\ddot{u}_k$ and the coefficient matrix can be conveniently partitioned into four submatrices. The upper-left submatrix is symmetric and can be divided into four more submatrices, $[M_{\eta\eta}]$, $\left[\frac{\partial \phi}{\partial \eta} \right]$, and its transpose $\left[\frac{\partial \phi}{\partial \eta} \right]^T$, and null-matrix. Submatrix $[M_{\eta\eta}]$ is symmetric but no longer constant, unlike in the analysis of rigid-linked mechanisms, which are the coefficients of the second-order inertial acceleration terms in the Lagrange's equations, while $\left[\frac{\partial \phi}{\partial \eta} \right]$ is the system Jacobian which is formed directly from the second-order terms of the constraint equation, while its transpose is the coefficient of the Lagrange

multipliers. Notice that the constraint equations are influenced by the deformation of the links. The matrix $[M_{\eta u}]$ is a coefficient matrix describing the non-linear coupling of the inertial motion associated with the articulating system and elastic deformation associated with the flexible member. Submatrix $[M_{uu}]$ is the mass matrix and need only be calculated once in the procedure of computer simulation.

The coefficient submatrix [KK] in equation (4.34) is the stiffness matrix which is frequently encountered in solving problems of structural dynamics and is dependent upon the deformation of the links and the axial force in the element. The second-order column vector contains the second-order derivatives of $\ddot{\eta}$ and $\ddot{u}$, and also the Lagrange multipliers which originated in the generalized Lagrange's equations. On the right-hand side of equation (4.34) the sub-column vector contains the displacement and velocity-dependent forces, $g(\eta,\dot{\eta},u,\dot{u})$, pertaining to the particular Lagrange's equations, or the constraint equation associated with the row in which they appear. The terms g_k and h_Q include the effect of all external forces, as well as the centripetal and Coriolis components, while the terms f_k contain the centripetal and Coriolis terms from the loop-closure equation for the general mechanical system being analyzed.

4.3.2 Equations of motion for the free-flight-mode

During the free-flight-mode, in a specific revolute joint with clearance, the constraints imposed at the joint during the contact mode are not enforced during the short time duration in which relative motion between the pin and the journal occurs as the pin moves across the bearing clearance. Consequently the Lagrange multipliers, imposing the constraints at these joints, disappear for those joints in which contact has been lost and the free-flight-mode initiated. The equations of motion for the free-flight-mode assume the same general format as equation (4.34). Thus they may be obtained by deleting the columns and rows associated with those Lagrange multipliers which are zero in order to relax the associated constraints. If there are several joints, "a", which are governed by the free-flight-mode, the equations of motion become

$$\begin{bmatrix} [M^f_{\eta\eta}] & [\frac{\partial \phi}{\partial \eta}^f] & [M^f_{\eta u}] \\ [\frac{\partial \phi}{\partial \eta}^f]^T & 0 & 0 \\ [M^f_{\eta u}]^T & 0 & [M^f_{uu}] \end{bmatrix} \begin{bmatrix} \ddot{\eta}^f \\ -\lambda^f \\ \ddot{u}^f \end{bmatrix} + \begin{bmatrix} 0 & 0 \\ 0 & [KK]^f \end{bmatrix} \begin{bmatrix} \eta^f \\ -\lambda^f \\ u^f \end{bmatrix}$$

$$= \begin{bmatrix} (g)^f \\ (f)^f \\ (h)^f \end{bmatrix} \tag{4.39}$$

where

$$[KK]^f = [K]^f + [KG_1]^f + [KG_2]^f \tag{4.40}$$

$$g_k^f = \sum_{i=1}^{nf} F_i \cdot \frac{\partial r_i}{\partial \eta_k^f} - [\dot{M}_{\eta\eta}^f \quad \dot{M}_{\eta u}^f] \begin{pmatrix} \dot{\eta}^f \\ \dot{u}^f \end{pmatrix}, k=1,2,\cdot\cdot,p-a \qquad (4.41)$$

$$f_k^f = \sum_{i=1}^{p-a} \sum_{j=1}^{p-a} \frac{\partial^2 \phi_k^f}{\partial \eta_i^f \partial \eta_j^f} \dot{\eta}_i^f \dot{\eta}_j^f + \sum_{j=1}^{3(N+1)} \sum_{i=1}^{3(N+1)} \frac{\partial^2 \phi_k^f}{\partial u_j^f \partial u_i^f} \dot{u}_j^f \dot{u}_i^f$$

$$+ \sum_{j=1}^{3(N+1)} \frac{\partial \phi^f}{\partial u_j^f} \ddot{u}_j^f \quad , k=1,2,\cdots,nc \qquad (4.42)$$

$$h_Q^f = \sum_{i=1}^{nf} F_i \cdot \frac{\partial r_i}{\partial u_Q^f} + \frac{1}{2} [\dot{\eta}^f \ \dot{u}^f] \left[\frac{\partial M^f}{\partial u_Q^f} \right] \begin{pmatrix} \dot{\eta}^f \\ \dot{u}^f \end{pmatrix} - [\dot{M}_{\eta u}^{fT} \ \dot{M}_{uu}^f] \begin{pmatrix} \dot{\eta}^f \\ \dot{u}^f \end{pmatrix}$$

$$, Q=1,2,\cdots,3(N+1) \qquad (4.43)$$

where the superscript "f" denotes the characteristics in free-flight-mode, and there are "m-a" joints which are governed by contact, transient or impact conditions.

4.3.3 Equations of motion for the impact-mode

The discontinuities associated with mechanical systems with bearing clearances, create impulsive phenomena when the two principal members of a revolute joint suddenly contact. The equations of motion governing the impact-mode can be obtained by integrating equations(4.32) and (4.33) over an arbitrarily small time interval τ,

$$\left(\frac{\partial T}{\partial \dot{\eta}_k} \right)^* - \left(\frac{\partial T}{\partial \dot{\eta}_k} \right) = \hat{Q}_k^{\eta} + \sum_{p=1}^{nc} \hat{\lambda}_p \frac{\partial \phi_p}{\partial \eta_k} \qquad (4.44)$$

and

$$\left[\frac{\partial T}{\partial \dot{u}_\ell}\right]^* - \left[\frac{\partial T}{\partial \dot{u}_\ell}\right] = \hat{Q}^u_\ell \ , \tag{4.45}$$

where the asterisk, (*), denotes the post-collision property, and

$$\frac{\partial T}{\partial \dot{\eta}_k} = \begin{bmatrix} M_{\eta\eta} \\ M^T_{\eta u} \end{bmatrix} \{ \dot{\eta}_k \} \tag{4.46}$$

$$\frac{\partial T}{\partial \dot{u}_\ell} = \begin{bmatrix} M_{\eta u} \\ M_{uu} \end{bmatrix} \{ \dot{u}_\ell \} \tag{4.47}$$

$$\hat{Q}^\eta_k = \int_t^{t+\tau} \bar{Q}^\eta_k \, dt = \sum_{j=1}^{nf} \hat{F}_j \ \frac{\partial \mathbf{r}_j}{\partial \eta_k} \cdot \mathbf{n}_j \ , \ k=1,2,\cdots,p \tag{4.48}$$

$$\hat{Q}^u_\ell = \int_t^{t+\tau} \bar{Q}^u_\ell \, dt = \sum_{j=1}^{nf} \hat{F}_j \ \frac{\partial \mathbf{r}_j}{\partial u_\ell} \cdot \mathbf{n}_j \ , \ \ell=1,2,\cdots,3(N+1) \tag{4.49}$$

and $\hat{F}_j$ is defined as the impulse in the $\mathbf{n}_j$ direction.

In order to develop sufficient equations for determining the unknown quantities ($\dot{\eta}^*_i$, $\dot{u}^*_i$, $\hat{\lambda}_i$, $\hat{F}_i$), a velocity constraint relationship must be developed and also a relationship for the kinematic behavior before and after the impact must also be formulated. The first requirement is satisfied by employing equation (4.30) and the second requirement is satisfied by developing an expression incorporating the

coefficient of restitution ϵ at each joint. Equation (4.30) may be applied to model the impact phenomenon by utilizing the expression

$$\dot{\phi}_r^* - \dot{\phi}_r - \sum_{i=1}^{p} \frac{\partial \phi_r}{\partial \eta_i} (\dot{\eta}_i^* - \dot{\eta}_i) + \sum_{j=1}^{3(N+1)} \frac{\partial \phi_r}{\partial u_j} (\dot{u}_j^* - \dot{u}_j) = 0. \qquad (4.50)$$

which describes the velocity constraint relationship before and after impact.

The general expression defining the coefficient of restitution is

$$\epsilon = - \frac{(\dot{r}_{Qa}^* - \dot{r}_{Qb}^*)\cdot n}{(\dot{r}_{Qa} - \dot{r}_{Qb})\cdot n} \quad , \text{ where } \dot{r} = \sum_{i=1}^{p} \frac{\partial r}{\partial \eta_i} \dot{\eta}_i + \sum_{i=1}^{3(N+1)} \frac{\partial r}{\partial u_i} \dot{u}_i \qquad (4.51)$$

where the relative velocity after impact is $(\dot{r}_{Qa}^* - \dot{r}_{Qb}^*)$ while $(\dot{r}_{Qa} - \dot{r}_{Qb})$ is the relative velocity before impact. The subscript Q denotes the impact point while a and b denote the impacting bodies. Since $\dot{r}_{Qa}$ and $\dot{r}_{Qb}$ are both dependent on $\dot{r}(\eta_i, \dot{\eta}_i, u_i, \dot{u}_i)$, equation (4.51) can be rewritten as

$$\epsilon = - \frac{\left(\sum_{i=1}^{p} \frac{\partial r_k}{\partial \eta_i} \dot{\eta}_i^* \cdot n_k + \sum_{j=1}^{3(N+1)} \frac{\partial r_k}{\partial u_j} \dot{u}_j^* \cdot n_k \right)}{\left(\sum_{i=1}^{p} \frac{\partial r_k}{\partial \eta_i} \dot{\eta}_i \cdot n_k + \sum_{j=1}^{3(N+1)} \frac{\partial r_k}{\partial u_j} \dot{u}_j \cdot n_k \right)} \qquad (4.47)$$

whi

rel

gov

The

whe

which expresses the energy dissipation coefficient, ϵ, in terms of the relevant system parameters.

Equations (4.44), (4.50) and (4.52) are the equations governing the impact-mode in a revolute joint with radial clearance. These expressions can be conveniently expressed in matrix form as

$$\begin{bmatrix} M_{\eta\eta} & \frac{\partial \Phi}{\partial \eta} & \frac{\partial R}{\partial \eta} & M_{\eta u} \\ \left(\frac{\partial \Phi}{\partial \eta}\right)^T & 0 & 0 & \frac{\partial \Phi}{\partial u} \\ \left(\frac{\partial R}{\partial \eta}\right)^T & 0 & 0 & \frac{\partial R}{\partial u} \\ M_{\eta u}^T & 0 & \left(\frac{\partial R}{\partial u}\right)^T & M_{uu} \end{bmatrix} \begin{Bmatrix} \dot{\eta}^* \\ -\hat{\lambda} \\ -\hat{F} \\ \dot{u}^* \end{Bmatrix} = \begin{Bmatrix} (e) \\ (f) \\ (g) \\ (h) \end{Bmatrix} \tag{4.53}$$

where

$\left[\frac{\partial \Phi}{\partial \eta}\right]$ - system Jacobian matrix associated with the Lagrange multipliers

$\left[\frac{\partial R}{\partial \eta}\right]$ - system Jacobian matrix associated with the impulse formulation

$$\{\dot{\eta}^*\} = \{\dot{\eta}_1^*, \dot{\eta}_2^*, \cdots, \dot{\eta}_p^*\}^T$$

$$\{\hat{F}\} = \{\hat{F}_1, \hat{F}_2, \cdots\cdots, \hat{F}_{nf}\}^T$$

$$\{\hat{\lambda}\} = \{\hat{\lambda}_1, \hat{\lambda}_2, \cdots\cdots, \hat{\lambda}_{nc}\}^T \tag{4.54}$$

$$\{ e \} = \{e_1, e_2, \cdots\cdots, e_p\}^T$$

$$\{ f \} = \{f_1, f_2, \cdots\cdots, f_{nc}\}^T$$

$$\{ g \} = \{g_1, g_2, \cdots\cdots, g_{nf}\}^T$$

$$\{ e \} = [M_{\eta\eta}] \{ \dot{\eta} \} + [M_{\eta u}] \{ \dot{u} \} \tag{4.55}$$

$$f_j = \sum_{i=1}^{p} \frac{\partial \phi_i}{\partial \eta_i} \dot{\eta}_i + \sum_{i=1}^{3(N+1)} \frac{\partial \phi_i}{\partial u_i} \dot{u}_i \ , \quad j = 1, 2, \cdots\cdots, nc \tag{4.56}$$

$$g_k = -\epsilon \left\{ \sum_{j=1}^{p} \left(\frac{\partial r_k}{\partial \eta_j} \cdot n_k\right) \dot{\eta}_j + \sum_{j=1}^{3(N+1)} \left(\frac{\partial r_k}{\partial u_j} \cdot n_k\right) \dot{u}_j \right\},$$

$$k = 1, 2, \cdots\cdots, nf \tag{4.57}$$

$$\{ h \} = [M_{\eta u}^T] \{ \dot{\eta} \} + [M_{uu}] \{ \dot{u} \} \tag{4.58}$$

Equation (4.58) completes the development of the mathematical apparatus necessary for predicting the elastodynamic behavior of a four-mode model of a kinematic pair comprising flexible links and a revolute joints with radial clearance.

The equations of motion of a planar general mechanism system with flexible links and bearing clearances have been developed. Attention now focuses upon applying this proposed approach to predict the dynamical response of two mechanical systems in order to illustrate the approach.

4.4 ILLUSTRATIVE EXAMPLE 1 - DYNAMIC BEHAVIOR OF A COMPOUND PENDULUM SUBJECTED TO IMPACT

A general mathematical model for predicting the elastodynamic behavior of impacting bodies has been developed in the previous sections of this chapter. In order to evaluate the predictive capabilities of this model, two illustrative examples are considered in which the theoretical results are compared with experimental results from a complementary experimental investigation. The first example examines the elastodynamic behavior of a compound pendulum in which a beam accelerates from rest under gravitational loading prior to impacting a stationary mechanical stop. A schematic diagram of the principal elements of this system is presented in Figure 4.2.

This simple test was undertaken to verify the four-mode model. The four-mode model can be applied to any kind of mechanism describing intermittent motion. In this illustrative example, the free-flight mode describes the major motion of the compound pendulum as it rotates from the initial point θ to impulsively contact the stationary mechanical stop. The impact-mode and the contact-mode exist only for a very short time period during each impact while the transient-mode is initiated by the first impact until the equilibrium position is attained.

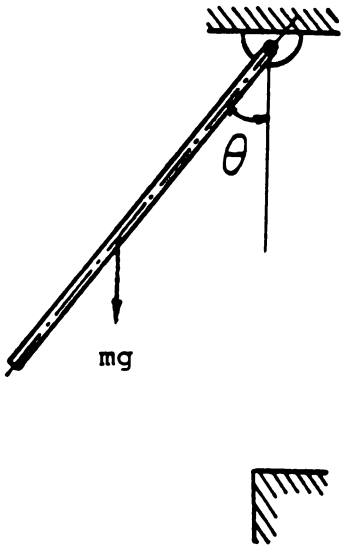

Figure 4.2 A schematic diagram of a compound pendulum articulating under gravitational loading prior to impacting with a fixed mechanical stop

4.4.1 Equations of motion for the free-flight-mode

The dynamical behavior of the pendulum in the free-flight-mode can be obtained by using equations(4.14) through (4.34), in which the frictional torque of the bearing is neglected. Constraint equation (4.4) is not employed in the derivation since the angular position θ is the major factor for determining the termination of the free-flight-mode rather than the pin force which occurs when $\theta = 0$. The pendulum was divided into six elements as before.

The final set of equations of motion in the inertial frame is

$$(m_i \ell^2 (n^2 + n + \tfrac{1}{3}) + \{u\}^T [M] \{u\} + 2m_i [H_G]\{u\})\ddot{\theta} =$$

$$-m_i g(n\ell + \tfrac{1}{2}\ell)\sin\theta - 2\dot{\theta}\{\dot{u}\}^T[M]\{u\} - 2m_i\dot{\theta}[H_G]\{\dot{u}\} - m_i[E_G]\{\ddot{u}\}$$

$$+ m_i\{u\}^T[F_G]\{\ddot{u}\} \qquad (4.59)$$

while the set of equations of motion in the elastic frame is

$$[M]\{\ddot{u}\} - [C]\{\dot{u}\} + ([K] + [k_{G2}] - \dot{\theta}^2[M])\{u\} -$$

$$-m_i\ddot{\theta}[F_G]\{u\} - 2m_i\dot{\theta}[F_G]\{\dot{u}\} - m_i\ddot{\theta}(E_G)^T + m_i\dot{\theta}^2(H_G)^T \qquad (4.60)$$

where

$m_i = \rho_e A_e \ell$

ℓ = the length of one finite element

$n = N-1$

N = the number of finite elements

θ = the angle between the center-line of the pendulum and the vertical direction

$\dot{\theta}$ = the angular velocity of the pendulum

$\ddot{\theta}$ = the angular acceleration of the pendulum

g = gravitational force, assumed to be 9.8 m/sec^2

$$[M]_i = \frac{\rho_e A_e \ell}{420}\begin{bmatrix} 140 & 0 & 0 & 70 & 0 & 0 \\ 0 & 156 & 22\ell & 0 & 54 & -13\ell \\ 0 & 22\ell & 4\ell^2 & 0 & 13\ell & -3\ell^2 \\ 70 & 0 & 0 & 140 & 0 & 0 \\ 0 & 54 & 13\ell & 0 & 156 & -22\ell \\ 0 & -13\ell & -3\ell^2 & 0 & -22\ell & 4\ell^2 \end{bmatrix}$$

$$\{HG\}_i = \ell\{(\tfrac{1}{2}k + \tfrac{1}{6}) \;\; 0 \;\; 0 \;\; (\tfrac{1}{2}k + \tfrac{1}{3}) \;\; 0 \;\; 0\}, \; k=i-1$$

$$\{EG\}_i = \{0 \;\; (\tfrac{3\ell}{20} + \tfrac{k\ell}{2}) \;\; (\tfrac{\ell^2}{30} + \tfrac{k\ell^2}{12}) \;\; 0 \;\; (\tfrac{7\ell}{20} + \tfrac{k\ell}{2}) \;\; (\tfrac{-1}{20}\ell^2 - \tfrac{k\ell^2}{12})\}$$

$$, k=i-1$$

$$[FG]_i = \begin{bmatrix} 0 & -\frac{7}{20} & -\frac{\ell}{20} & 0 & -\frac{3}{20} & \frac{\ell}{30} \\ \frac{7}{20} & 0 & 0 & \frac{3}{20} & 0 & 0 \\ \frac{\ell}{20} & 0 & 0 & \frac{\ell}{30} & 0 & 0 \\ 0 & -\frac{3}{20} & -\frac{\ell}{30} & 0 & -\frac{7}{20} & \frac{\ell}{20} \\ \frac{3}{20} & 0 & 0 & \frac{7}{20} & 0 & 0 \\ -\frac{\ell}{30} & 0 & 0 & -\frac{\ell}{20} & 0 & 0 \end{bmatrix}$$

$$[KG1]_i = \begin{bmatrix} 0 & 0 & 0 & 0 & 0 & 0 \\ 0 & \frac{6}{5\ell} & \frac{1}{10} & 0 & -\frac{6}{5\ell} & \frac{1}{10} \\ 0 & \frac{1}{10} & \frac{2\ell}{15} & 0 & -\frac{1}{10} & -\frac{\ell}{30} \\ 0 & 0 & 0 & 0 & 0 & 0 \\ 0 & -\frac{6}{5\ell} & \frac{1}{10} & 0 & \frac{6}{5\ell} & -\frac{1}{10} \\ 0 & \frac{1}{10} & -\frac{\ell}{30} & 0 & -\frac{1}{10} & \frac{2\ell}{15} \end{bmatrix}$$

$$[KG2]_i = \begin{bmatrix} 0 & 0 & 0 & 0 & 0 & 0 \\ 0 & \frac{3}{5\ell} & \frac{1}{10} & 0 & -\frac{3}{5\ell} & 0 \\ 0 & \frac{1}{10} & \frac{\ell}{30} & 0 & -\frac{1}{10} & -\frac{\ell}{60} \\ 0 & 0 & 0 & 0 & 0 & 0 \\ 0 & -\frac{3}{5\ell} & -\frac{1}{10} & 0 & \frac{3}{5\ell} & 0 \\ 0 & 0 & -\frac{\ell}{60} & 0 & 0 & \frac{\ell}{10} \end{bmatrix}$$

$$[K]_i = \frac{1}{\ell^3} \begin{bmatrix} EA\ell^2 & 0 & 0 & -EA\ell^2 & 0 & 0 \\ 0 & 12EI & 6\ell EI & 0 & -12EI & 6\ell EI \\ 0 & 6\ell EI & 4\ell^2 EI & 0 & -6\ell EI & 2\ell^2 EI \\ -EA\ell^2 & 0 & 0 & EA\ell^2 & 0 & 0 \\ 0 & -12EI & -6\ell EI & 0 & 12EI & -6\ell EI \\ 0 & 6\ell EI & 2\ell^2 EI & & -6\ell EI & 4\ell^2 EI \end{bmatrix}$$

[C] = the damping matrix, which is obtained from experimental results

4.4.2 Equations of motion of the contact-mode

The tip of the pendulum is assumed to have the same kinematic characteristics as the stationary stop at the moment of impact. Therefore, the angular position, angular velocity and angular acceleration are all zero at the initiation of the contact-mode. The compound pendulum can be treated as a simply-supported beam in this condition. Hence, the equation of motion of the pendulum in inertial frame is

$$\ddot{\theta} = 0 \tag{4.61}$$

and the equations of motion in the elastic frame are same as equation (4.60). Note that while the global form of the equations of motion are the same in both the free-flight-mode and the contact-mode, the elements of these matrices are different. The elastic equations of motion will yield a solution which will be different in each mode, since different boundary conditions will be applied in each different mode.

4.4.3 Equations of motion in impact-mode

By employing equations (4.44) - (4.53), the equations of motion for the impact-mode is obtained

$$\begin{bmatrix} A_{11} & \underline{A}_{12} & A_{13} \\ & \underline{A}_{22} & \underline{A}_{23} \\ \text{symmetric} & & A_{33} \end{bmatrix} \begin{bmatrix} \dot{\theta}^* \\ \dot{\underline{u}}^* \\ \hat{F} \end{bmatrix} - \begin{bmatrix} B_1 \\ \underline{B}_2 \\ B_3 \end{bmatrix} \tag{4.62}$$

where

$$A_{11} = m_i \ell^2 (n^2 + n + \tfrac{1}{3}) + (u)^T [M] (u) + 2m_i [H_G](u)$$

$$\underline{A}_{12} = m_i (E_G) - m_i (u)^T [F_G]$$

$$A_{13} = r_3 - \tfrac{1}{2} (u)^T [K_{G1}](u) + u_L$$

$$\underline{A}_{22} = [M]$$

$\dot{\theta}^*$ - the rebound angular velocity after impact

$\dot{\underline{u}}^*$ - the velocity characteristics of the link after impact

$\hat{F}$ - impactive force between the pendulum and the block

$$B_1 = [A_{11}] \dot{\theta}_3 + [A_{12}] (\dot{u})$$

$$B_2 = [A_{21}] \dot{\theta}_3 + [A_{22}] (\dot{u})$$

$$B_3 = -\epsilon \dot{\theta} A_{13}$$

u_L - axial displacement at the tip node of the link

Note that the under-line may denotes a submatrix, a sub-row vector or a sub-column vector.

4.4.4 Solution procedures

Equations of motion for the compound pendulum subjected to impact have been developed. This section describes the solution procedures of the equations of motion.

Equation (4.59) can be rewritten as

$$[A]\ [\ddot{\theta}] = [B] \tag{4.63}$$

in which

$$[A] = (m_i \ell^2 (n^2 + n + \tfrac{1}{3}) + (u)^T [M] (u) + 2m_i[H_G](u))$$

and

$$[B] = -m_i g(n\ell + \tfrac{1}{2}\ell)\sin\theta - 2\dot{\theta}[\dot{u}]^T[M][u] - 2m_i\dot{\theta}[H_G][\dot{u}] - m_i[E_G][\ddot{u}]$$

$$+ m_i[u]^T[F_G][\ddot{u}]$$

Thus, [A] is function of the beam inertia and also u, the deformation of the pendulum ,and [B] is function of θ, $\dot{\theta}$, u, $\dot{u}$, $\ddot{u}$.

Similarly, equation (4.60) can be expressed in the standard form as

$$[M](\ddot{u}) + [C](\dot{u}) + [KK](u) = (R) \tag{4.64}$$

where

$$[KK] = [K] + [k_{G2}] - \dot{\theta}^2[M]$$

$$(R) = -m_i\ddot{\theta}[F_G](u) - 2m_i\dot{\theta}[F_G](\dot{u}) - m_i\ddot{\theta}[E_G]^T + m_i\dot{\theta}^2[H_G]^T$$

To solve the equations of motion (4.63) and (4.64), the following procedures are employed:

1. The initial values, $\dot{\theta}$, u, $\dot{u}$, and $\ddot{u}$ associated with the initial angle θ of the pendulum are set equal to zero since the pendulum is stationary prior to initiating the experiment.

2. In equation(4.63), the angular acceleration, $\ddot{\theta}$, is calculated, and the angular velocity and angular displacement of the pendulum are obtained by integrating $\ddot{\theta}$.

3. At the same time, equation(4.64) is solved by employing the mode-superposition method. The first three modes are chosen for the solution.
4. The angular displacement θ is calculated and monitored continuously during the simulation. If the angular displacement is found to equal zero, the simulation switches to the impact-mode.
5. During the impact-mode, equation(4.62) is solved and the impactive velocity characteristics, $\dot{\theta}^*$ and $\dot{u}^*$, are calculated in addition to impulse $\hat{F}$.
6. The simulation is switched to the contact-mode immediately after the completion of the impact-mode. An impact duration of 0.008 seconds, which is the total time duration of the contact-mode, was obtained from the experimental results, and used for the simulation of the contact-mode.
7. The final calculated-values of the previous time-step are employed as the initial conditions for calculating the values of the subsequent time-step.

Figure 4.3 presents the experimental equipment employed in this study, in which the compound pendulum is clamped in a test fixture by using a precision bearing, which is the same bearing described in Chapter Two. The compound pendulum was initially released from a given angular positions, θ, of 30 degrees and 60 degrees. The tip of the compound pendulum articulated through these angles prior to impacting a stationary block. This impact phase followed by a transient response phase in which the pendulum repeatedly impacted and rebounded from the mechanical stop prior to attaining equilibrium.

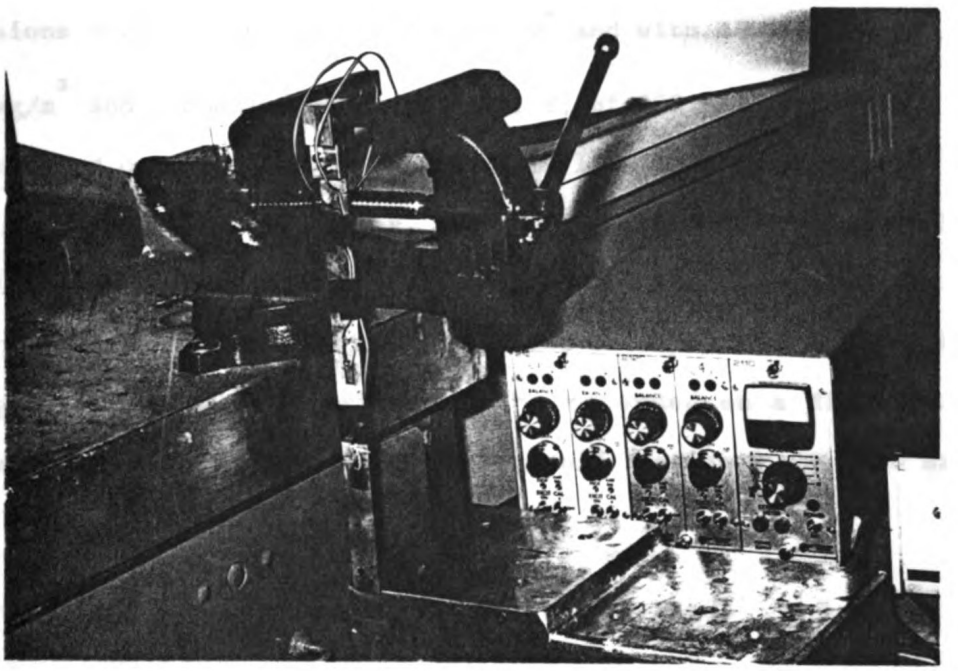

Figure 4.3 Photograph of the compound pendulum and stationary mechanical stop

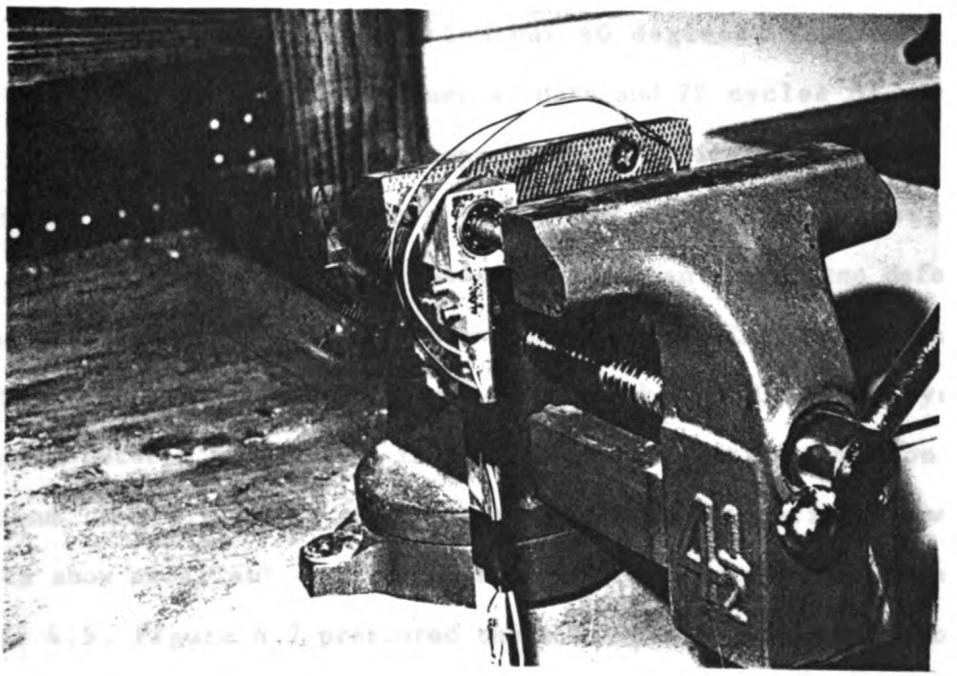

Figure 4.4 Photograph of experimental compound pendulum showing the pin and the bearing

The pendulum was fabricated from a low carbon steel with the dimensions 0.29318 x 0.01905 x 0.00127 m^3 and with a mass density, ρ, of 7860 kg/m^3 and a modulus of elasticity, E, of 200 GPa. The strain gauges were mounted on the mid-span the flexible link in a bending half-bridge configuration. The foil gauges, type CEA-13-250UW-350, were supplied by the Micromeasurements Group of Vishay Inc. and the signal was fed into Vishay 2120 portable strain conditioner and then into a Wavetek HI/LO analog filter, model 432, prior to being recorded on a MicroVax-based digital-data-acquisition system. The cut-off frequency was 1000 Hz.

4.4.5 Experimental and theoretical results

Figure 4.5 shows the experimental results for the transverse deformation of the mid-span of the pendulum for a two seconds duration when the initial angular position was 60 degrees. Four impacts are clearly evident from this experimental data and 22 cycles of vibration were observed between the two impacts which indicates a damped natural frequency of 52.63 Hz. Figures 4.6 - 4.8 show the corresponding simulation results. Figure 4.6 shows the mid-span transverse deformation of the pendulum during the two second period following the initiation of the free-flight-mode. Four impacts are observed and 22 cycles of vibration between two impacts is also observed. The deformation of the pendulum, the vibration of the pendulum and the period between two impacts show excellent correlation with the experimental results in Figure 4.5. Figure 4.7 presented the corresponding angular velocity of the pendulum during the same time period and Figure 4.8 presents the angular displacement of the pendulum.

When the initial angular position of the pendulum was set to 30 degrees prior to releasing the pendulum, the subsequent experimental mid-span deformation of the pendulum following impact are presented in Figure 4.9. Figures 4.10 - 4.12 present the corresponding simulation results. Figure 4.10 shows the calculated mid-span deformation of the pendulum, Figure 4.11 represents the angular velocity and Figure 4.12 shows the angular position of the pendulum during the first two seconds time period of the simulation. Again, the results show an impressive predictive capability for the proposed mathematical model.

The conclusion to be drawn from this first illustrative example is that the mathematical formulation developed herein can accurately predict the elastodynamic response of a compound pendulum released from rest and accelerating under a gravitational field prior to impacting a stationary mechanical stop.

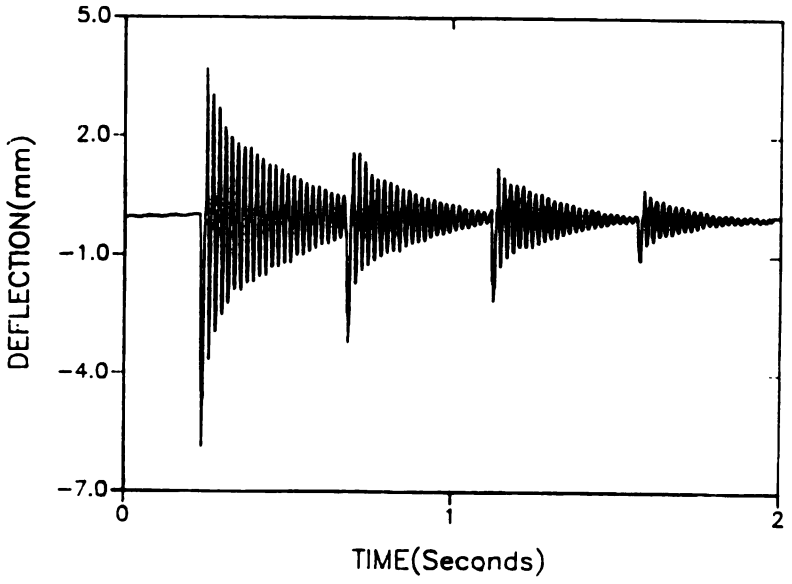

Figure 4.5 The experimental mid-span deformation of the pendulum. The intial angular position 60 degrees

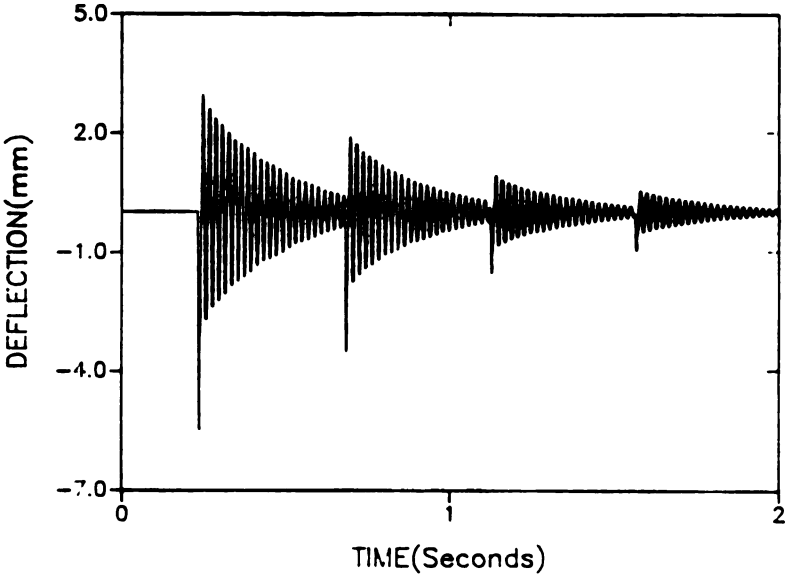

Figure 4.6 The theoretical mid-span deformation of the pendulum. The intial angular position 60 degrees

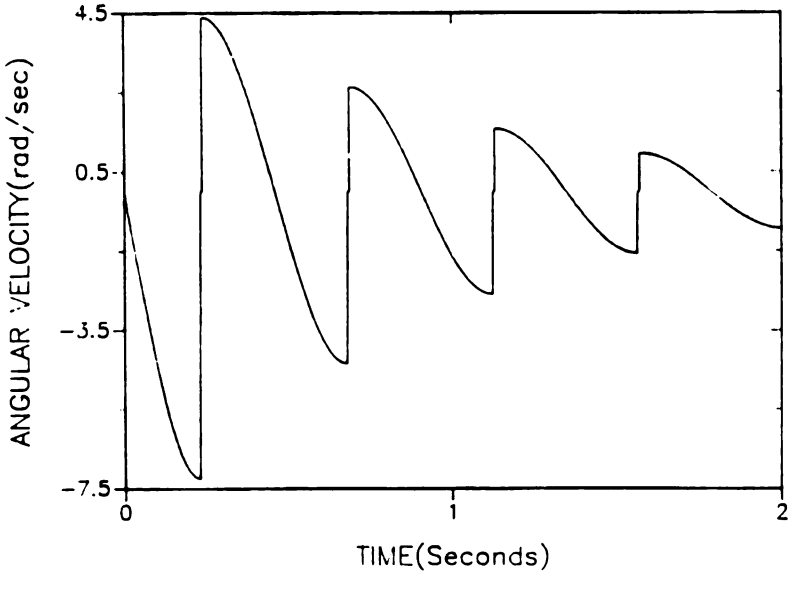

Figure 4.7 The theoretical angular velocity of the pendulum. The initial angular position 60 degrees

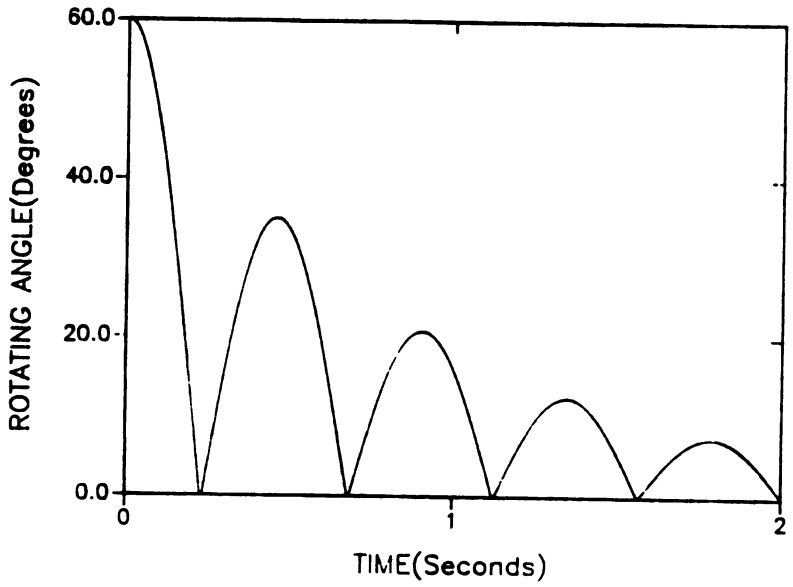

Figure 4.8 The theoretical angular position of the pendulum. The initial angular position 60 degrees

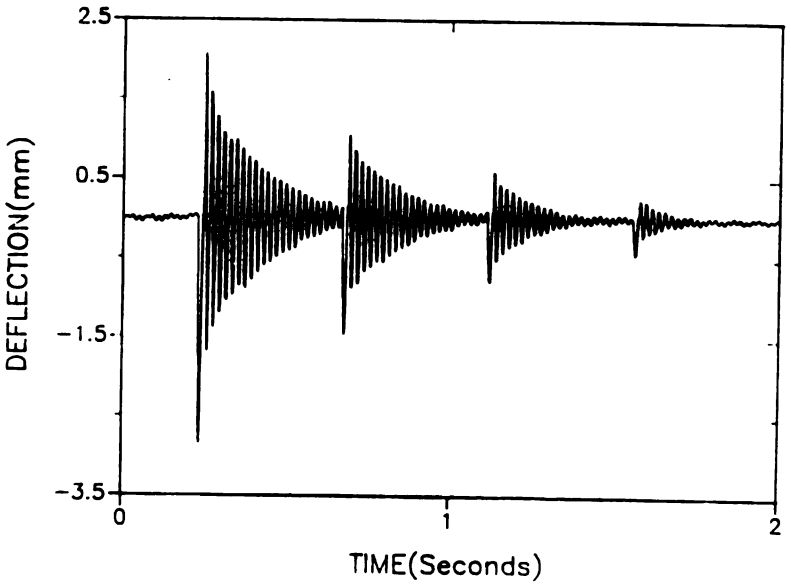

Figure 4.9 The experimental mid-span deformation of the pendulum. The intial angular position 30 degrees

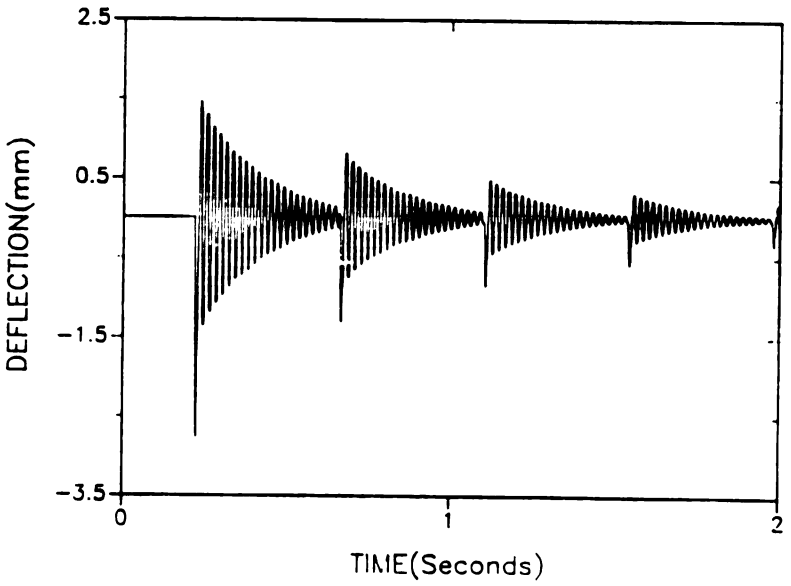

Figure 4.10 The theoretical mid-span deformation of the pendulum. The intial angular position 30 degrees

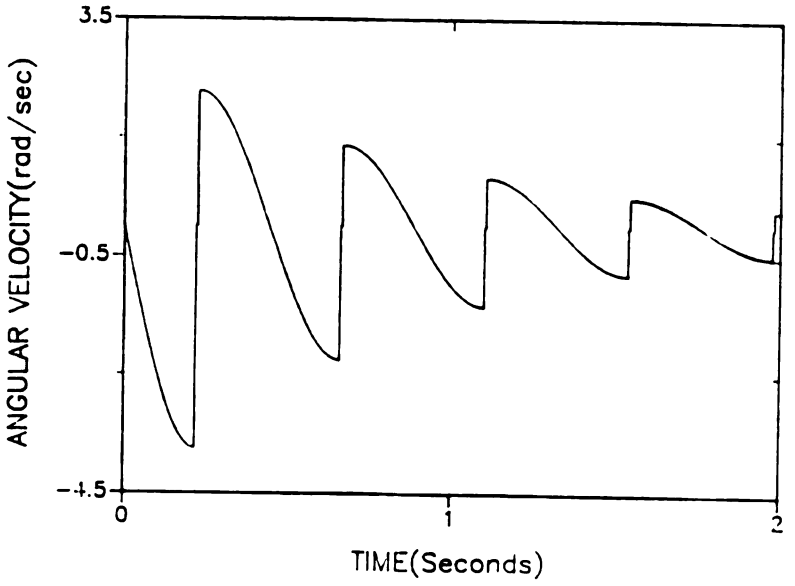

Figure 4.11 The theoretical angular velocity of the pendulum. The initial angular position 30 degrees

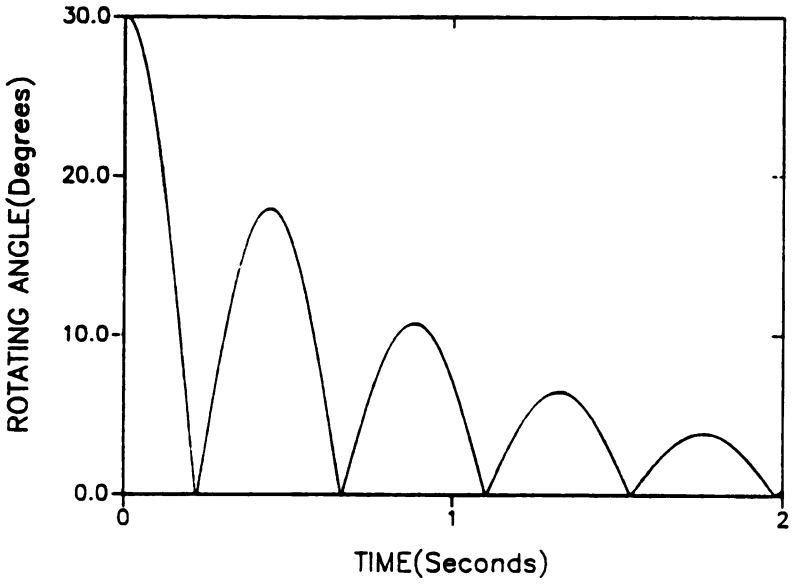

Figure 4.12 The theoretical angular position of the pendulum. The initial angular position 30 degrees

4.5 ILLUSTRATIVE EXAMPLE 2 - A slider-crank mechanism with flexible connecting-rod featuring radial clearance in the gudgeon-pin joint

A planar slider-crank mechanism with flexible connecting-rod and featuring radial clearance in the gudgeon pin joint was analyzed using the proposed methodology prior to comparing the theoretical results with experimental results. A schematic of the mechanism is presented in Figure 4.13(a) and the relevant kinematic parameters are presented in Figure 4.13(b). The characteristics of the mechanism are shown in table 3.1.

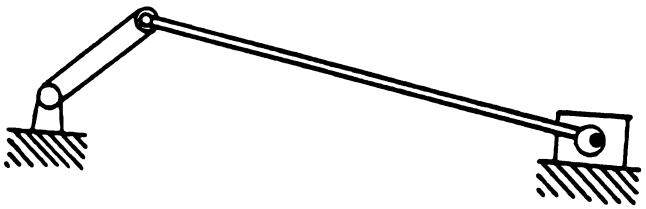

(a)

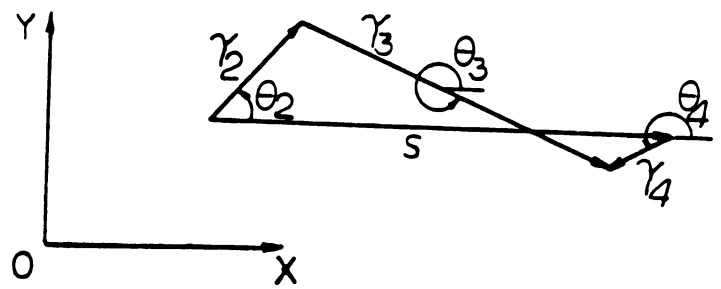

(b)

Figure 4.13 (a) The slider-crank mechanism with flexible connecting rod showing dominant clearance at the gudgeon-pin bearing
(b) Vector-loop model of the mechanism

4.5.1 Equations of motion for the contact-mode

The dynamical behavior of the slider-crank mechanism in the contact-mode is governed by a set of independent simultaneous second-order differential equations which are established using equations (4.14)-(4.34). Two set of equations were obtained which are in inertial and elastic bases respectively;

$$[A_1]\{X_1\} = \{B_1\} \tag{4.65}$$

and

$$[M_{uu}]\{\ddot{u}\} + ([K]+F_1[KG_1]+\Delta F[KG_2]-\dot{\theta}_3^2[M_{uu}])\{u\}$$
$$=-m_1 r_2 \dot{\theta}_2^2[AG]^T - m_1\ddot{\theta}_3[FG]\{u\} - 2m_1\dot{\theta}_3[FG]\{\dot{u}\} - m_1\ddot{\theta}_3[EG]^T$$
$$+ m_1\dot{\theta}_3^2[HG]^T - [C]\{\dot{u}\} \tag{4.66}$$

where

$$[A_1] = \begin{pmatrix} A^1_{11} & A^1_{12} & 0 & 0 & A^1_{14} & A^1_{15} \\ 0 & A^1_{22} & 0 & 0 & A^1_{24} & A^1_{25} \\ 0 & 0 & 0 & 0 & A^1_{35} & A^1_{36} \\ 0 & 0 & 0 & A^1_{44} & A^1_{45} & 0 \\ 0 & A^1_{52} & A^1_{53} & A^1_{54} & 0 & 0 \\ 0 & A^1_{62} & A^1_{63} & 0 & 0 & 0 \end{pmatrix} \tag{4.62}$$

$$A^1_{11} = -1$$

$$A^1_{12} = m_1 r_2 \ell\cos(\theta_3 - \theta_2)\left(\frac{N}{2} + \sum_{n=1}^{N-1} n\right) - m_1 r_2[AG]\{u\}$$

$$A^1_{15} = r_2 \sin\theta_2$$

$$A^1_{16} = -r_2 \cos\theta_2$$

$$A^1_{22} = m_1 \ell^2 \left[\frac{N}{3} + \sum_{n=1}^{N-1} (n^2+n) \right] + \{u\}^T [M_{uu}] \{u\} + 2m_1 [HG] \{u\}$$

$$A^1_{25} = \left(r_3 - \frac{1}{2} \{u\}^T [KG1] \{u\} + u_{19} \right) \sin\theta_3$$

$$A^1_{26} = -\left(-r_3 + \frac{1}{2} \{u\}^T [KG1] \{u\} - u_{19} \right) \cos\theta_3$$

$$A^1_{35} = -r_4 \sin\theta_4$$

$$A^1_{36} = r_4 \cos\theta_4$$

$$A^1_{44} = M_s$$

$$A^1_{45} = 1$$

$$A^1_{52} = A^1_{25}$$

$$A^1_{53} = A^1_{35}$$

$$A^1_{54} = 1$$

$$A^1_{62} = A^1_{26}$$

$$A^1_{63} = A^1_{36}$$

$$\{X_1\} = [\lambda_3 \ \bar{\theta}_3 \ \bar{\theta}_4 \ \bar{s} \ \lambda_1 \ \lambda_2 \ ] \qquad (4.68)$$

$$\{B_1\} = [B^1_1 \ B^1_2 \ B^1_3 \ B^1_4 \ B^1_5 \ B^1_6] \qquad (4.69)$$

$$B_1^1 = m_1 r_2 \ell \ddot{\theta}_3 \sin(\theta_3 - \theta_2)\left(\frac{N}{2} + \sum_{n=1}^{N-1} n\right) + m_1 r_2 \dot{\theta}_3^2 [BG]\{u\}$$

$$+ 2m_1 r_2 \dot{\theta}_3 [AG]\{\dot{u}\} - m_1 r_2 [BG]\{\ddot{u}\}$$

$$B_2^1 = -m_1 r_2 \ell \dot{\theta}_2^2 \sin(\theta_3 - \theta_2)\left(\frac{N}{2} + \sum_{n=1}^{N-1} n\right) - m_1 r_2 \dot{\theta}_2^2 [BG]\{u\}$$

$$- 2\dot{\theta}_3 \{\dot{u}\}[M]\{u\} - 2m_1 \dot{\theta}_3 [HG]\{\dot{u}\} - m_1 [EG]\{\ddot{u}\}$$

$$+ m_1 \{u\}^T [FG]\{\ddot{u}\}$$

$$B_3^1 = 0$$

$$B_4^1 = -(sgn)\mu M_s g$$

$$B_5^1 = -r_2 \dot{\theta}_2^2 \cos\theta_2 - r_3 \dot{\theta}_3^2 \cos\theta_3 - (\{\ddot{u}\}[KG1]\{u\} + \{\dot{u}\}[KG1]\{\dot{u}\}$$

$$- \frac{1}{2} \dot{\theta}_3^2 \{u\}^T [KG1]\{u\} - \ddot{u}_{19} + u_{19} \dot{\theta}_3^2)\cos\theta_3$$

$$- (2\dot{u}_{19} \dot{\theta}_3 - 2\dot{\theta}_3 \{\dot{u}\}^T [KG1]\{u\})\sin\theta_3 + r_4 \dot{\theta}_4^2 \cos\theta_4$$

$$B_6^1 = -r_2 \dot{\theta}_2^2 \sin\theta_2 - r_3 \dot{\theta}_3^2 \sin\theta_3 - (\{\ddot{u}\}[KG1]\{u\} + \{\dot{u}\}[KG1]\{\dot{u}\}$$

$$- \frac{1}{2} \dot{\theta}_3^2 \{u\}^T [KG1]\{u\} - \ddot{u}_{19} + u_{19} \dot{\theta}_3^2)\sin\theta_3$$

$$- (-2\dot{u}_{19} \dot{\theta}_3 + 2\dot{\theta}_3 \{\dot{u}\}^T [KG1]\{u\})\cos\theta_3 + r_4 \dot{\theta}_4^2 \sin\theta_4$$

4.5.2 Equations of motion for the free-flight-mode

The loss of contact between the connecting rod and the slider in the free-flight-mode mandates that the mechanism to be modeled as two

systems. One system is the double-pendulums arrangement of the crank and the connecting rod which moves independently of the second system which comprises the slider. Thus, the pin force at the gudgeon-pin joint is zero, since there is no contact between the pin and journal of this bearing. Utilizing the Lagrange's equation again, two sets of second-order differential equations govern this mode corresponding to the inertial frame and elastic frame respectively and they can be written, in matrix form, as

$$[A_2] \{ X_2 \} = \{ B_2 \} \tag{4.70}$$

and

$$\begin{aligned}&[M_{uu}] \{\ddot{u}\} + ([K]+F_1[KG_1]+\Delta F[KG_2]-\dot{\theta}_3^2 [M_{uu}]) \{u\} \\ &=-m_1 r_2 \dot{\theta}_2^2[AG]^T - m_1\ddot{\theta}_3[FG]\{u\} - 2m_1\dot{\theta}_3[FG]\{\dot{u}\} - m_1\ddot{\theta}_3[EG]^T \\ &\quad + m_1\dot{\theta}_3^2[HG]^T - [C]\{\dot{u}\}\end{aligned} \tag{4.71}$$

where

$$[A_2] = \begin{bmatrix} A_{11}^2 & A_{12}^2 & 0 \\ 0 & A_{22}^2 & 0 \\ 0 & 0 & A_{33}^2 \end{bmatrix} \tag{4.72}$$

$$\{ X_2 \} = [\lambda_1 \ \ddot{\theta}_3 \ \ddot{s} \ ]^T \tag{4.73}$$

and,

$$\{ B_2 \} = [B_1^2 \ B_2^2 \ B_3^2 \ ]^T \tag{4.74}$$

$$A_{11}^2 = -1$$

$$A_{12}^2 = m_1 r_2 \ell \cos(\theta_3 - \theta_2)\left(\frac{N}{2} + \sum_{n=1}^{N-1} n\right) - m_1 r_2 [AG]\{u\}$$

$$A_{22}^2 = m_1 \ell^2 \left[\frac{N}{3} + \sum_{n=1}^{N-1} (n^2+n)\right] + \{u\}^T [M_{uu}]\{u\} + 2m_1 [HG]\{u\}$$

$$A_{33}^2 = M_s$$

$$B_1^2 = m_1 r_2 \ell \ddot{\theta}_3 \sin(\theta_3 - \theta_2)\left(\frac{N}{2} + \sum_{n=1}^{N-1} n\right) + m_1 r_2 \dot{\theta}_3^2 [BG]\{u\}$$

$$+ 2m_1 r_2 \dot{\theta}_3 [AG]\{\dot{u}\} - m_1 r_2 [BG]\{\ddot{u}\}$$

$$B_2^2 = -m_1 r_2 \ell \dot{\theta}_2^2 \sin(\theta_3 - \theta_2)\left(\frac{N}{2} + \sum_{n=1}^{N-1} n\right) - m_1 r_2 \dot{\theta}_2^2 [BG]\{u\}$$

$$- 2\dot{\theta}_3 \{\dot{u}\}[M]\{u\} - 2m_1 \dot{\theta}_3 [HG]\{\dot{u}\} - m_1 [EG]\{\ddot{u}\}$$

$$+ m_1 \{u\}^T [FG]\{\ddot{u}\}$$

$$B_3^2 = -(sgn)\mu M_s g$$

where μ is the coefficient of friction between the slider and the guide.

4.5.3 Equations of motion for the impact-mode

The equations of motion governing the impact behavior between the pin and the journal in the gudgeon-pin bearing are established using equations (4.44)-(4.53). Upon applying these general equations to the planar slider-crank mechanism, the following equations emerge

$$[\ A_3\ ]\ \{\ X_3\ \} - \{\ B_3\ \} \tag{4.75}$$

where

$$[\ A_3\ ] - \begin{bmatrix} A^3_{11} & A^3_{12} & A^3_{13} & 0 & A^3_{15} \\ 0 & A^3_{22} & A^3_{23} & 0 & A^3_{25} \\ 0 & A^3_{32} & A^3_{33} & 0 & A^3_{35} \\ 0 & 0 & 0 & A^3_{44} & A^3_{45} \\ 0 & A^3_{52} & A^3_{53} & A^3_{54} & 0 \end{bmatrix}, \tag{4.76}$$

$$\{\ X_3\ \} - [\hat{T}_{or}\ \ \theta^*_3\ \ \dot{u}^*\ \ \dot{s}^*\ \ \hat{F}\ ]\ , \tag{4.77}$$

and,

$$[\ B_3\ ] - [B^3_1\ B^3_2\ B^3_3\ B^3_4\ B^3_5\ ]^T \tag{4.78}$$

where

$$A^3_{11} - -1$$

$$A^3_{12} - m_1 r_2 \ell \cos(\theta_3 - \theta_2)\left(\frac{N}{2} + \sum_{n=1}^{N-1} n\right) - m_1 r_2 [AG]\{u\}$$

$$A^3_{13} - m_1 r_2 [B_G]$$

$$A^3_{15} - r_2 \sin(\theta_4 - \theta_2)$$

$$A^3_{22} - m_1 \ell^2 \left[\frac{N}{3} + \sum_{n=1}^{N-1} (n^2+n)\right] + \{u\}^T [M_{uu}]\{u\} + 2m_1 [HG]\{u\}$$

$$A^3_{23} - m_1 ([E_G] - [u]^T [F_G])$$

$$A^3_{25} = \left(r_3 - \frac{1}{2}\{u\}^T[KG1]\{u\} + u_{19}\right)\sin(\theta_4-\theta_3)$$

$$\underline{A}^3_{32} = \underline{A}^{3T}_{23}$$

$$\underline{A}^3_{33} = [M]$$

$$\underline{A}^3_{35} = -[K_{G1}]\{u\}\cos(\theta_4-\theta_3)$$

$$A^3_{44} = M_3$$

$$A^3_{45} = \cos\theta_4$$

$$A^3_{52} = A^3_{25}$$

$$\underline{A}^3_{53} = \underline{A}^{3T}_{35}$$

$$A^3_{54} = A^3_{45}$$

$$B^3_1 = A^3_{12}\dot{\theta}_3 + [A^3_{13}]\{\dot{u}\}$$

$$B^3_2 = A^3_{22}\dot{\theta}_3 + [A^3_{23}]\{\dot{u}\}$$

$$\underline{B}^3_3 = \underline{A}^3_{32}\dot{\theta}_3 + [A^3_{33}]\{\dot{u}\}$$

$$B^3_4 = \mu M_3 \dot{s}$$

$$B^3_5 = -\epsilon\left\{r_2\dot{\theta}_2\sin(\theta_4-\theta_2) + A^3_{52}\dot{\theta}_3 + [A^3_{53}]\{\dot{u}\} + \dot{s}\cos\theta_4\right\}$$

$$+r_2\dot{\theta}_2\sin(\theta_4-\theta_2)$$

Note that the under-line may denotes a matrix, a row vector or a column vector.

The coefficient of restitution, ϵ, which is an energy-dissipation parameter was experimentally determined to be 0.46 for the gudgeon-pin bearing by dynamically stimulating the bearing in a

carefully controlled environment in order to replicate the impactive dynamical environment imposed on the journal and pin by the articulating mechanism.

4.5.4 Equations of motion for the transient-mode

The transient-mode, which is clearly evident in the experimental response profiles furnished by the transducers from the complementary laboratory investigation, comprises a series of impact and free-flight-modes which are terminated when the contact-mode is initiated. The governing equations are therefore documented in the previous sections.

4.5.5 Simulation protocols

This section of the thesis documents the mathematical formulations which define the bounds of the different behavioral modes described previously for revolute joints with radial clearance, and also the subtleties incorporated into the simulation software.

(i) Contact Loss

Two criteria were employed in order to trigger the change from the contact-mode to the free-flight-mode. First, in every time-step of the simulation, the resultant contact force between the pin and journal at the gudgeon-pin joint was calculated using the expression,

$$F_s = \lambda_1 \cos \theta_4 + \lambda_2 \sin \theta_4 \qquad (4.79)$$

The physical system remains in the contact-mode provided that the resultant contact force between the pin and the journal, F_s, is compressive. Thus from a mathematical standpoint, where compressive forces are assumed to be negative, this notation mandates that F_s will always be less than zero when the pin and journal are in the contact-mode. Experience accrued in the complementary experimental investigation clearly indicated that this criterion is only valid at crank speeds below 100 rpm for the specific slider-crank mechanism under investigation. The generality of this observation is unknown. A second criterion was, therefore, introduced in order to overcome the lack of generality associated with the first criterion. This second criterion states that a loss of contact will occur when F_s assumes a minimum value and, in addition, the rate-of-change of the pressure angle is high relative to other values of this parameter, where the pressure angle is defined as the angle of the resultant force vector F_s relative to the inertial reference frame OXY. This criterion is the result of both theoretical and experimental observations. If only the pin force criterion alone is employed to predict the loss of contact, then the simulation software will predict that the pin and journal remain in the contact-mode provided that F_s is negative, no matter how rapidly the pressure angle changes with time. However, experimental results both herein, and also in references [12,25,26], clearly contradict this observation since contact loss is normally characterized by a high rate of change of pressure angle. Consequently, the simulation software package predicts that contact between the pin and the journal of a revolute joint will be lost when the contact force at the joint is small

and also the angular rate-of-change of the force vector is high. These criteria capture the instability characteristics associated with this dynamical state.

(ii) Termination of the Free-Flight-Mode

The pin of a revolute joint is assumed to be in the free-flight-mode relative to the journal until the following geometrical inequality criterion is violated whereupon the impact-mode is initiated,

$$0 < (\Delta x^2 + \Delta y^2)^{1/2} - \xi. \tag{4.80}$$

where ξ denotes the radial clearance. This constraint relates the locations of the geometrical centers of the pin and the journal relative to the radial clearance in the joint. The terms Δx and Δy are obtained from the loop closure constraint. Namely,

$$\Delta x = r_2\cos\theta_2 + (r_3 - \{u\}^T[K_{G1}]\{u\} + u_L)\cos\theta_3 - r_4\cos\theta_4 - s \tag{4.81}$$

$$\Delta y = r_5 + r_2\sin\theta_2 + (r_3 - \{u\}^T[K_{G1}]\{u\} + u_L)\sin\theta_3 - r_4\sin\theta_4 \tag{4.82}$$

Ideally, if $(\Delta x^2 + \Delta y^2)^{1/2} = \xi$, the system is in the impact-mode, since this mode is assumed to follow the free-flight-mode. However, in all digital simulation work, computational round-off errors accumulate and a tolerance must inevitably be introduced in order to accommodate these small inaccuracies in the numerical results. Thus, the system was assumed to be in the impact-mode if the following inequality was satisfied

$$|1.0 \times 10^{-8}| \leq [\ (\Delta x^2 + \Delta y^2)^{1/2} - \xi\ ] \qquad (4.83)$$

(iii) Restoration of the Contact-Mode

The software was written to incorporate the constraint that the motion of the pin and journal are governed by the free-flight-mode following the impact-mode provided that the duration of the flight-time of the pin and journal between contact-loss and the re-establishment of contact subtends more than a twentieth of a degree of crank rotation. If contact between the pin and journal is re-established within a twentieth of a degree of crank rotation and there is also an insignificant difference between the original contact point and the new contact point, then the simulation control switches to the contact-mode.

(iv) Solution Procedure

A flow chart documenting the logic of the simulation software for predicting the elastodynamic response of planar mechanisms incorporating bearing clearances is presented in Figure 4.14. The initial conditions for simulating the dynamical behavior of the slider-crank mechanism were based upon the assumption that the position vector representing the clearance in the gudgeon-pin joint had the same direction as the angle of the resultant force in the bearing. The magnitude of this angle was obtained from an analysis of the mechanism incorporating a gudgeon-pin bearing with zero clearance, and in addition, the angular velocity of the clearance-vector was assumed to equal the rate-of-change of the angle of the resultant force. The initial values for the elastic deformations were obtained from experimental results. The step-by-step simulation, therefore, began in the contact-mode, and the equations of motion were expressed in matrix form as presented by equations (4.65) and (4.66). Upon determining the

appropriate initial values for the system, the coefficients of, $[A_1]$ and $\{B_1\}$ were then evaluated prior to calculating the vector $\{X_1\}$ which included the terms $\ddot{\theta}_3$, $\ddot{\theta}_4$, $\ddot{s}$, λ_1, λ_2, and λ_3. PLU-factorization was employed in conjunction with forward and backward substitution in order to undertake this task. Subsequently, the second-order variables $\ddot{\theta}_3$, $\ddot{\theta}_4$, and $\ddot{s}$ were transformed into a set of first-order equations, and a subroutine "DGEAR" in the IMSL subroutine library was employed to integrate these second-order derivatives and obtain values of $\dot{\theta}_1$, θ_1, $\dot{s}$, and s. The elastic equations of motion were solved by using the mode-superposition method. The first three modes were included in the simulation. The link was treated as a simple-supported beam system in the contact-mode. The joint force and the rate-of-change of the angle of the resultant force were also calculated at each time-step. Simulation control switched to the free-flight-mode once the criteria for contact loss were satisfied, and equations (4.70) and (4.66) were then solved. Notice that the link was treated as a pin-free beam system and thus the initial values for the free-flight-mode have to be recalculated. The equation governing the impact-mode, equation (4.75) was solved, once the inequality relationship (4.80) was satisfied. After the first impactive motion, the simulation entered the transient-mode, and following a series of relatively brief free-flight and impactive-mode states, the control returned to the contact-mode again provided the criteria for the restoration of the contact-mode were satisfied.

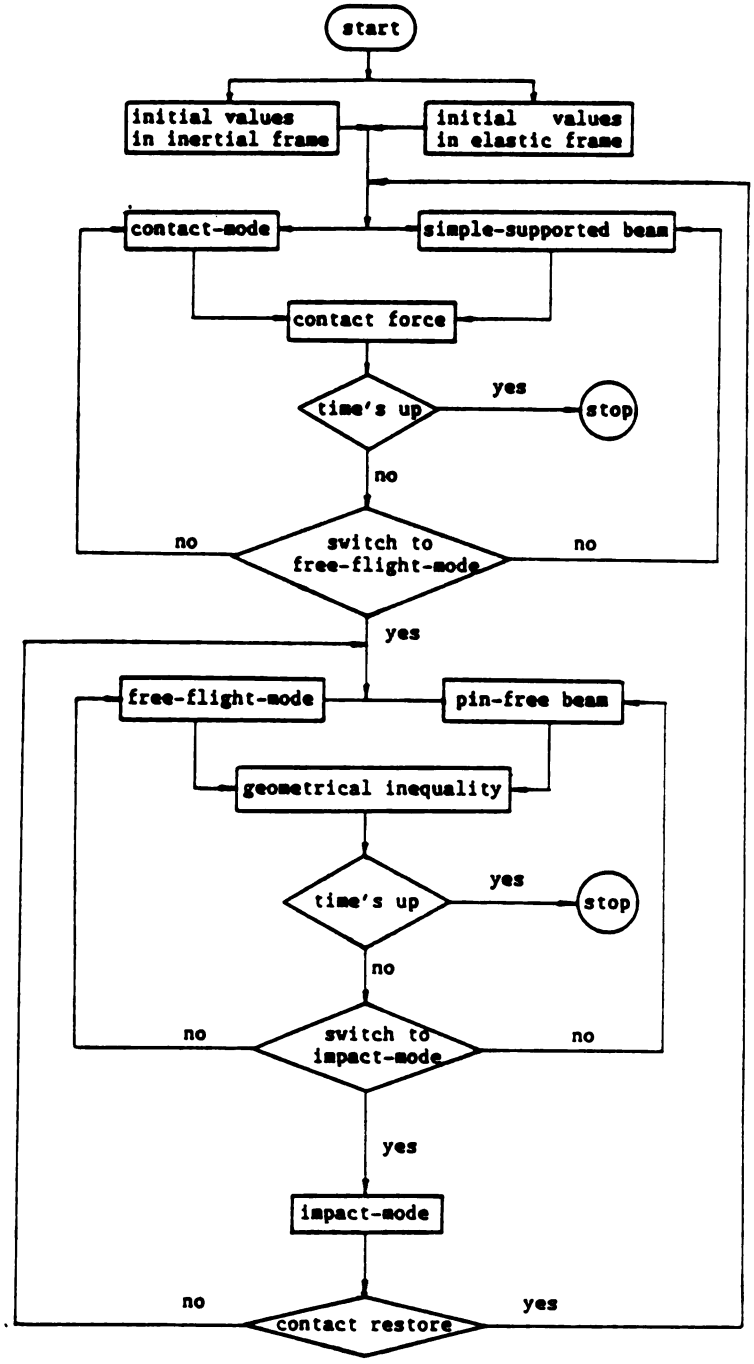

Figure 4.14 Flow chart for the computer simulation

4.5.6 Comparison of experimental and theoretical results

Figures 4.15 - 4.22 present experimental and theoretical response data for the slider-crank mechanism operating at crank frequencies of 185, 199, 225 and 258 rpm. The radial clearance is 0.127 mm at the gudgeon-pin bearing for all response profiles. Figures 4.15 - 4.18 present the accelerations of the slider at 185, 199, 225 and 258 rpm respectively, while Figures 4.19 - 4.22 present the corresponding tangential accelerations of the connecting rod. As the same reason which mentioned in Chapter two, frequencies above 60 Hz were removed by analog filtering. In order to develop a viable environment for comparing the analytical and experimental results, the numerical results were subjected digital filtering, LSP$FILTER_NONREC, which is a nonrecursive, finite impulse, filtering software on a DEC MicroVax II/GPX workstation [90].

Upon reviewing the acceleration profiles presented in Figures 4.15 - 4.22, it is clearly evident that there is very good correlation between the theoretical and experimental results for a broad range of operating conditions. The pin and journal loose contact and undergo major excursions relative to each other twice during each revolution of the crank shaft, and the restoration of contact occurs at the end of the transient-mode. The first separating generally occurred at approximately 80 degrees of crank rotation and the second separating occurred at approximately 280 degrees of crank rotation. Figures 4.19 - 4.22 indicate that the most severe impact conditions occur at 95 degrees and 295 degrees of crank rotation, while the experimental results indicate that the most serious impact occurs at 100 degrees and 298 degrees of

crank rotation. This is an impressive predictive capability for such a complex nonlinear mechanical system.

Figures 4.23 - 4.25 present the elastic response of the connecting rod. Figure 4.23 shows the mid-span deflection of the connecting rod at 185 rpm, Figure 4.24 presents the mid-span deflection of the connecting rod at 199 rpm and Figure 4.25 shows the mid-span deflection of the connecting rod at 258 rpm. Upon reviewing the theoretical results in Figures 4.23 - 4.25, it is clearly evident that two suddenly change in the deflection profile are found in each revolute cycle. The first change, which occurs at about 100 degrees of crank rotation, is bigger than the second change, which occurs at approximately 295 degrees of crank rotation. Upon reviewing the experimental results in Figures 4.23 and 4.25, it is clearly evident that the first impact changes the deflection profile at about 105 degrees of crank rotation, and the effect of the second impact is not obviously presented but little change on the deflection profile. Generally speaking, the elastic response of the theoretical results are impressive, since the phase of the vibrational response and most parts of deflection matched very well as shown in the Figures. As author's knowledge, there is no report on the comparison of theoretical and experimental deflection of the link of a clearanced mechanism. Since the flexible link is easily affected by the environmental conditions, such as friction between the pin and journal, the elastic effects of cables for signals, which were neglected in simulation, the error may be possibly introduced in the experimental results.

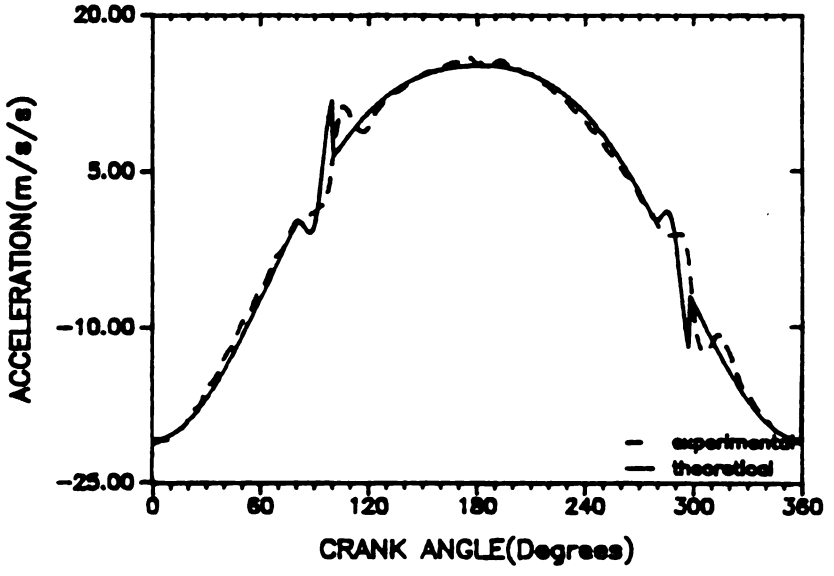

Figure 4.15 Slider acceleration. Mechanism operating speed 185 rpm

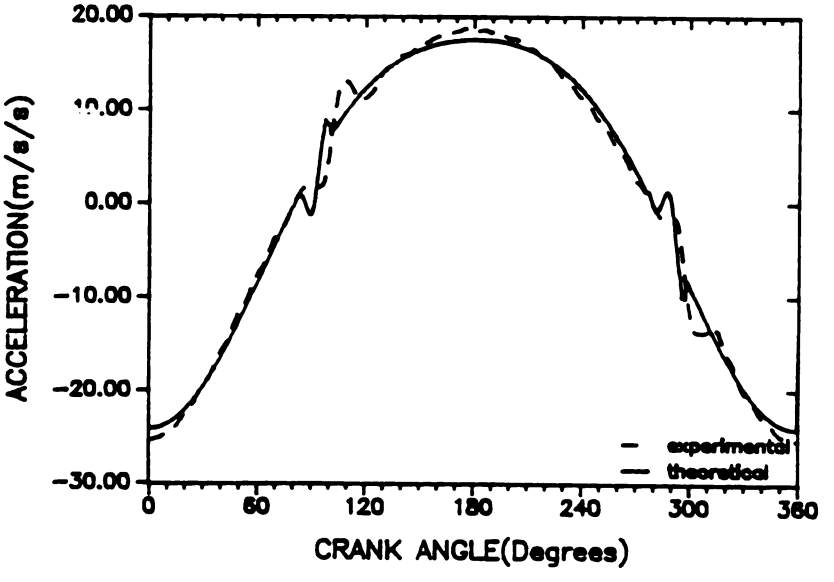

Figure 4.16 Slider acceleration. Mechanism operating speed 199 rpm

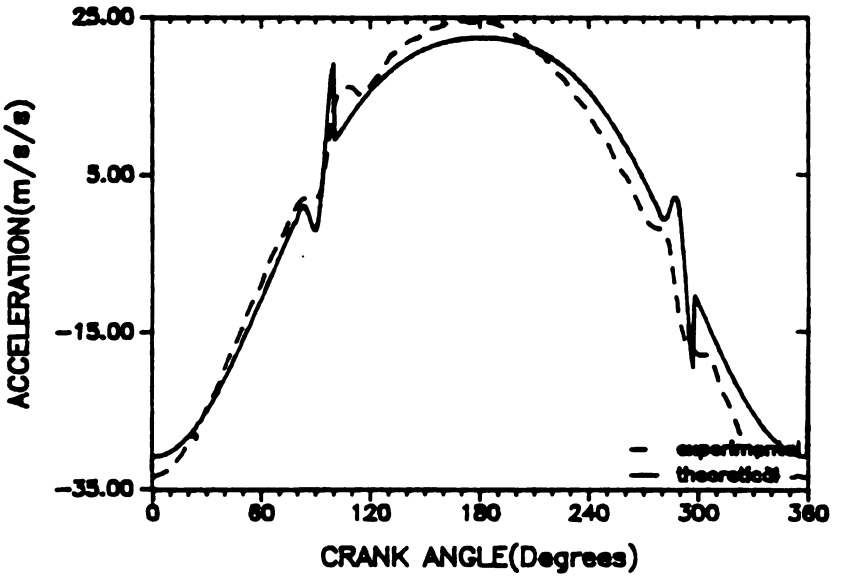

Figure 4.17 Slider acceleration. Mechanism operating speed 225 rpm

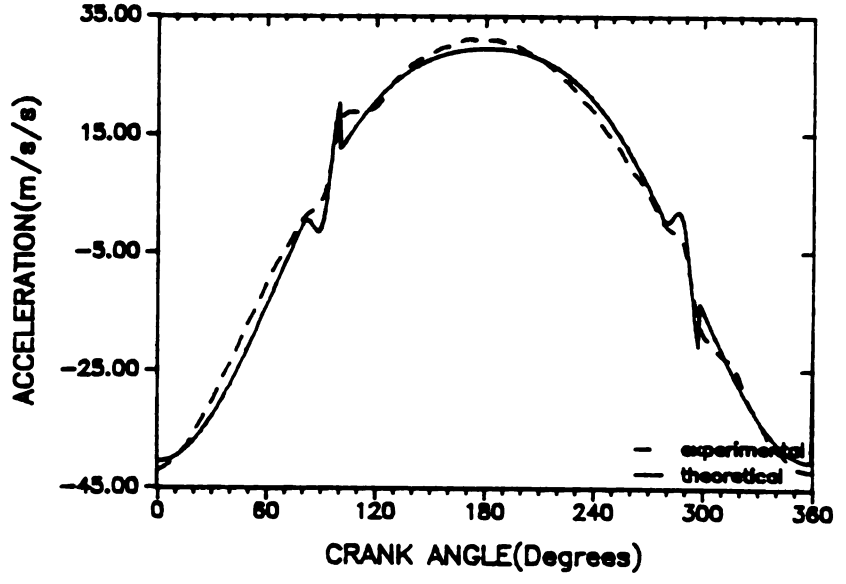

Figure 4.18 Slider acceleration. Mechanism operating speed 258 rpm

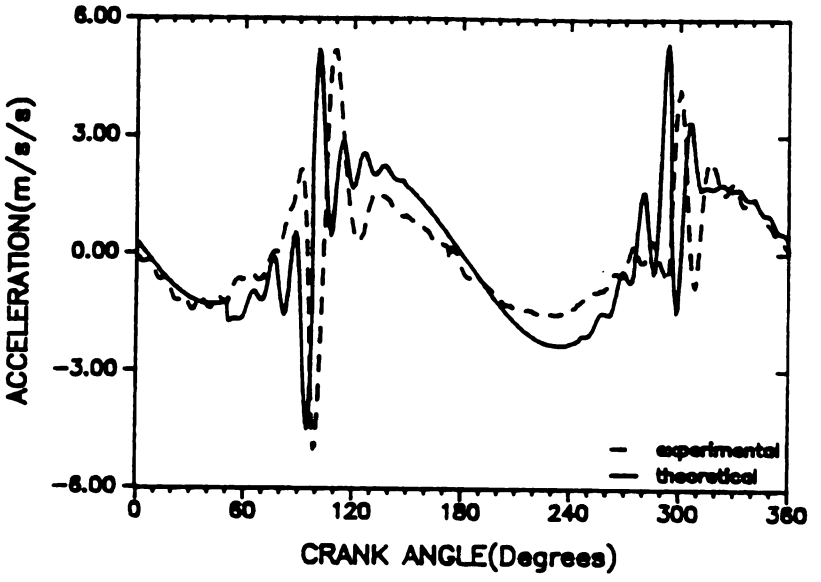

Figure 4.19 Connecting-rod tangential acceleration.
Mechanism operating speed 185 rpm

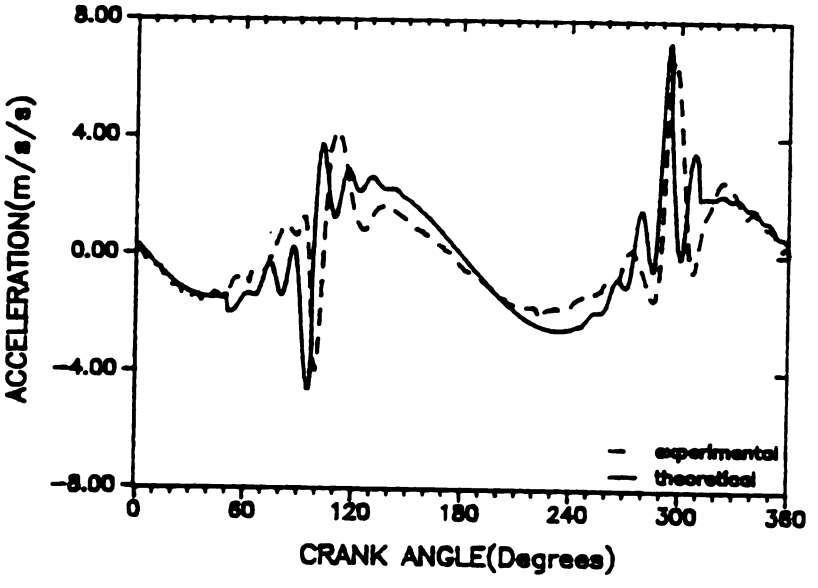

Figure 4.20 Connecting-rod tangential acceleration.
Mechanism operating speed 199 rpm

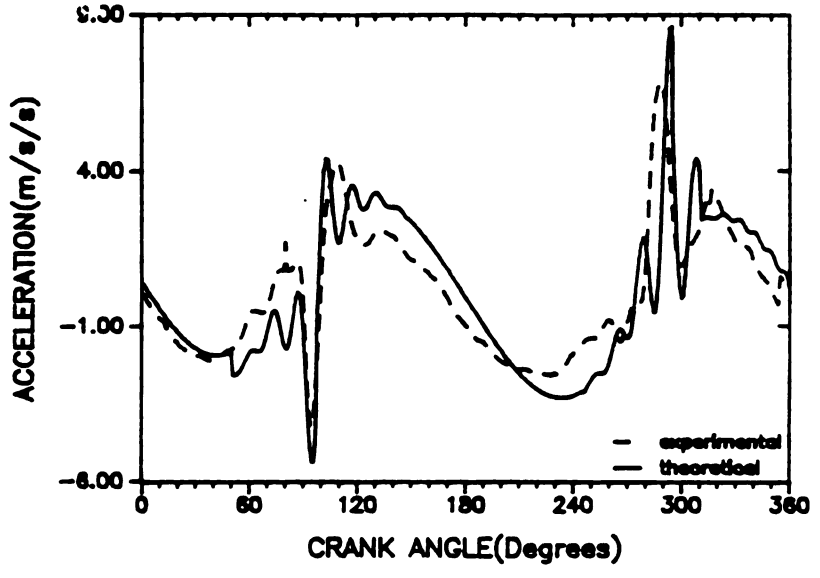

Figure 4.21 Connecting-rod tangential acceleration.
Mechanism operating speed 225 rpm

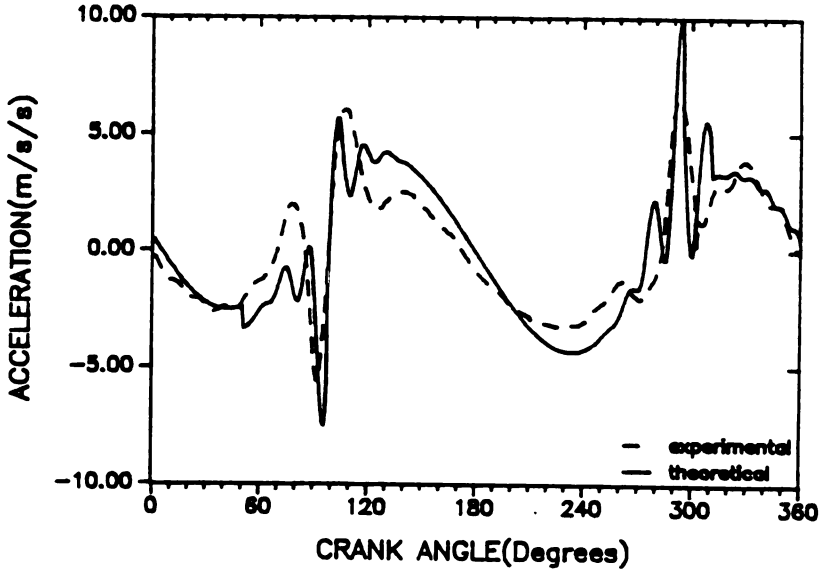

Figure 4.22 Connecting-rod tangential acceleration.
Mechanism operating speed 258 rpm

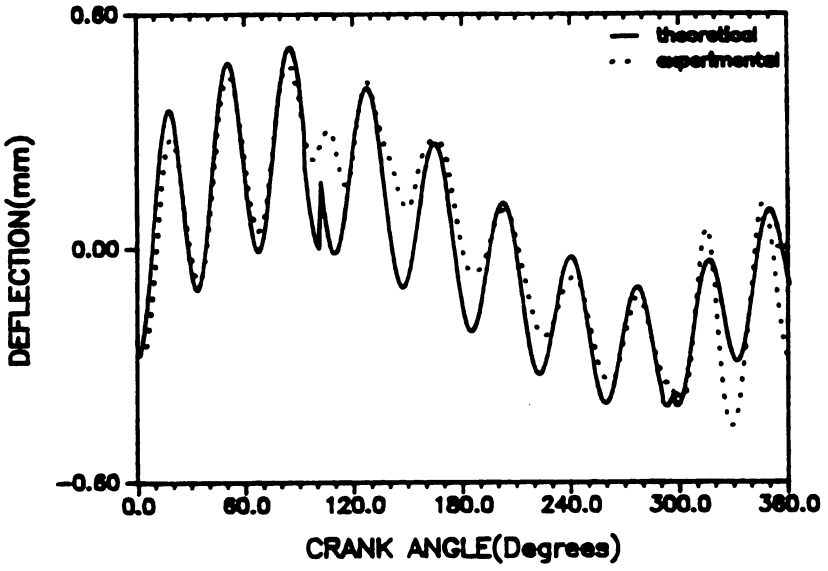

Figure 4.23 The mid-span deflection of the connecting-rod. Mechanism operating speed 185 rpm

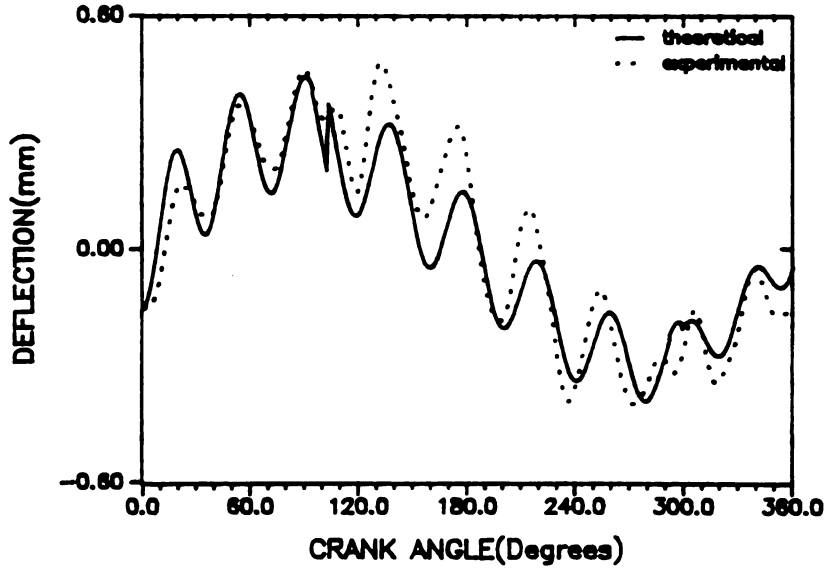

Figure 4.24 The mid-span deflection of the connecting-rod. Mechanism operating speed 199 rpm

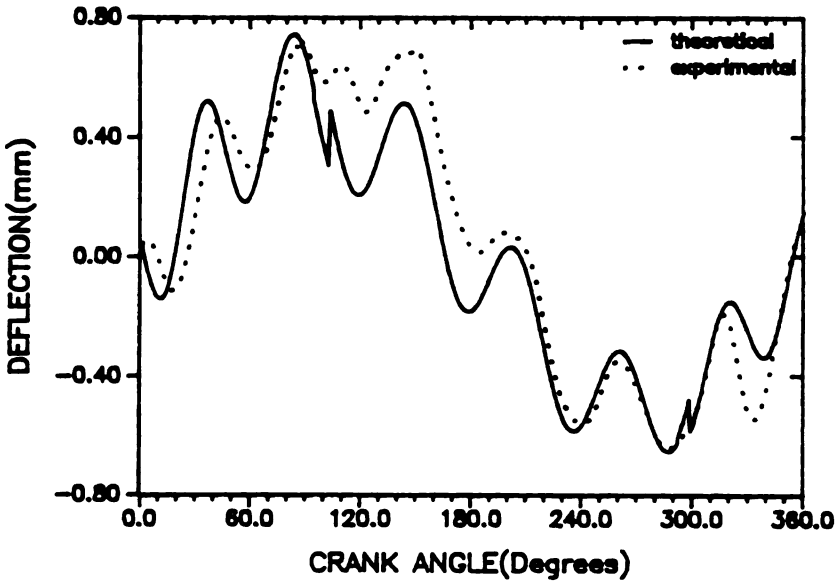

Figure 4.25 The mid-span deflection of the connecting-rod. Mechanism operating speed 258 rpm

4.6 CONCLUSIONS OF THE CHAPTER

Analytical and computational models of general planar mechanisms with flexible links and bearing clearances have been developed. The dynamical characteristics of the mechanisms have been described by a proposed four-mode model. The nonlinear equations of motion can be solved by a quasi-static procedure. As illustrative examples of the approach, a compound pendulum subjected to impact and a slider-crank mechanism with flexible connecting rod with radial clearance in the gudgeon-pin bearing were studied in a comprehensive analytical, computational and experimental program and the numerical results are in qualitative agreement with the results from a complementary experimental program.

CHAPTER V

CONCLUSIONS AND RECOMMENDATIONS

IMPACT ON THE TECHNOLOGY-BASE AND THE SCIENCE-BASE

The fundamental research prosecuted in this document has been undertaken in response to the insatiable demand in the international marketplace for viable design tools for predicting the dynamical and elastodynamical responses of articulating mechanical systems with radial clearances in the revolute joints of these systems. Such systems are extremely common and are numerous in the defense, automotive, aerospace and advanced manufacturing segments of the economy.

The design tools developed herein can be employed in an industrial setting to predict the dynamic and elastodynamic responses of general planar mechanical systems for systems with one revolute joint with clearance and one flexible link. Futher experimental work is needed in order evaluate the predictive capabilities of this methodology developed in this thesis, when applied to more demanding systems with multiple flexible links and also several links with bearing clearances. Naturally, further work is required in order to bring a software package

to the marketplace, but this research program has undoubtably enhanced the technology-base in this field.

In order to extend the technology-base, the research reported herein has involved extending the science-base. The science-base has been extended by the development of a four-mode model of the dynamically behavior of revolute joint with clearance which has been evaluated in several examples by comparing the theoretical results with experimental data. This work established a mathematical apparatus for each dynamical mode of the joint behavior, and also developed a viable simulation protocol for attaining a viable solution. Finally, new experimental evidence has been obtained by the monitoring of the dynamical and elastodynamical responses of planar mechanical systems with bearing clearances. These results should not only provide the basis for evaluating future mathematical models, but also motivate further theoretical studies on planar mechanisms with prescribed radial clearances in the joints.

5.1 CONCLUSIONS OF THE THESIS

5.1.1. The equations of motion of a general planar linkage mechanism with rigid links, or flexible links, featuring revolute joints with, or without bearing clearances have been developed by employing a general Lagrange's equations formulation. This formulation results in the establishment of a mixed set of partial differential equations and algebraic equations which must be solved in order to predict the dynamical behavior of the rigid-linked system. If the system comprises an assemblage of flexible members then the elastodynamic behavior of the

system is obtained by developing a mixed set of ordinary differential equations, using the displacement finite element method, and also algebraic constraint equations. These sets of equations are solved using the Adams numerical integration scheme.

5.1.2. A four-mode model has been proposed to describe the phenomenological behavior of a revolute joint with a prescribed radial clearance between the pin and the journal. Such a model is relevant to antifriction bearings which are worn, journal bearings, plain bearings and bushings which require a prescribed radial clearance in order to function correctly. The four modes are the contact-mode, the free-flight-mode, the impact-mode and the transient-mode. The four-mode formulation describes the dynamical response of every kind of intermittent motion. For example , the formulation can be applied to predict the dynamical response of an aircraft landing on an airport runway. The aircraft is in the free-flight-mode when flying in the air and then switches to the impact-mode when touching the ground. The simulation control transfers to the transient-mode when the aircraft bounces back into the air and then touch down on the runway again and again until finally this bouncing phenomenon ceases. Finally the simulation is in the contact-mode when the aircraft cruises down the runway.

5.1.3. The criteria for switching the modes have been carefully defined. The termination of the contact-mode is controlled by contact loss which is determined by the contact force between the pin and the journal in each joint. In addition, the contact loss is also determined

by the magnitude of the contact force and the rate of change of the force angle. Physically, the higher the rate of change of the force angle posseses bigger turbulent energy and contact loss happens when the contact force is small and can not maintain the contact any more. The termination of the free-flight-mode is controlled by the geometrical constraints of the mechanism from which two contact points in each members are at the same position. The contact restoration is determined by the fact that the contact point has not change very much even a free-flight-mode is assumed.

5.1.4. The initial values for the inertial generalized coordinate are determined by performing a dynamical analysis of the general planar mechanism without bearing clearance. For example, in slider-crank mechanism with bearing clearance in gudgeon-pin joint, the angular velocity of the position vector defining the clearance in the revolute joint with clearance is assumed to equal the rate of change of the angle of the contact force vector in that joint.

5.1.5. The initial values for the elastic generalized coordinates are determined by employing the first vibrational mode of the flexible link. The mode shapes of the flexible link be compatible with the boundary conditions of that member. For example, in the contact-mode, the flexible connecting rod of a slider-crank mechanism is modeled as simply-supported beam while in the free-flight-mode the link is modeled as pin-free beam.

5.1.6. In order to model the continuously varying natural frequency during the operating cycle of the mechanism, a geometrical nonlinearity formulation had to be incorporated into the formulation.

5.1.7. A quasi-static solution procedure has been employed to solve the inertial equations of motion and the elastic equations of motion in order to reduce the dimension of the equations of motion, and also the computing time. The error can be neglected when the time step is small enough.

5.2 RECOMMENDATIONS FOR FUTURE WORK

5.2.1. The methodology derived in this doctoral work can be generalized from planar two-dimensional systems to more complex spatial three-dimensional mechanical systems relevant to robot arms design and automotive suspension systems.

5.2.2. The plain journal bearing which was studied herein can be replaced by other kinds of bearings such as ball bearings, hydraulic thrust bearings, ··,etc., in which the interaction between pin and journal is more complicated.

5.2.3. The contact stress in the bearing, fatigue life, failure criteria and the acoustic radiation resulting from a bearing with the clearance, are worth developing. However, the phenomena is quite complicated.

5.2.4. If the bearing is not well-aligned, an out-of-plane motion may occur. Thus it is necessary to extend the planar bearing analysis to study the three-dimensional spatial response of these bearings.

5.2.5. Throughout the theoretical work reported herein, the coefficient of restitution is experimentally determined and employed in the equations of motion. Thus the impact duration can not be entirely predicted theoretically. A more detailed formulation, such as the Kelvin-Voigt model may be included in the impact-mode to improve the analysis, but the stiffness constant and damping coefficient still have to be determined experimentally.

5.2.6. In this thesis the surface of the bearing was assumed smooth. Friction may be added in the formulation to improve the model if the effects of the roughness of the surface become serious.

5.2.7. In the illustrative examples, the mechanical system featured only one bearing with clearance. The research program may, therefore, be extended to more complicated mechanism systems featuring mechanisms with multiple bearing clearances and multiple flexible links. Again, a coherent program of analytical, computational and experimental work is needed.

5.2.8. The pin force and the relative motion between the pin and journal have not been measured in this study due to technical problems. A special design of the kinematic pair is needed, and high speed cinematography may be necessary.

APPENDIX

LIST OF PUBLICATIONS

1. Liao, D.X., Sung, C.K., Thompson, B.S. and Soong K.
"An Experimental Study to Document the Response Regimes of a Class of Flexible Four-bar Linkages."
Ninth Applied Mechanisms Conference, Oklahoma State University Held in Kansas city, Oct.,1985. pp.III-1 - III-6

2. Thompson, B.S., Soong, K. and Sung, C.K.
"An Experimental Bread-Board Model for a Class of Intelligent High-Speed Machinery: Some Preliminary Results"
Ninth Applied Mechanisms Conference, Oklahoma State University Held in Kansas city, Oct.,1985. pp.IV-1 - IV-4

3. Liao, D.X., Sung, C.K., Thompson, B.S. and Soong, K.
"A Note On The Quasi-Static Response, Dynamic Responses, and The Super-harmonic Resonances of Flexible Linkage: Some Experimental Results"
ASME Paper No. 86-DET-146, ASME Conference, Columbus, OH, Oct. 1986.

4. Soong, K., Sunappan, D. and Thompson, B.S.
"The Elastodynamic Response Of A Class Of Intelligent Machinery, Part I, Theory"
ASME Design Technology Conferences, 1987. Held in Boston, Sep. 27-30, DE-Vol.8, ADVANCED TOPICS IN VIBRATIONS, pp.147 - 154

5. Sunappan, D., Soong, K. and Thompson, B.S.
"The Elastodynamic Response Of A Class Of Intelligent Machinery, Part II, Computational and Experimental Results"
ASME Design Technology Conferences, 1987. Held in Boston, Sep. 27-30, DE-Vol. 8, ADVANCED TOPICS IN VIBRATIONS, pp.155 -160

6. Soong, K. and Thompson, B.S.
"An Experimental Investigation Of The Dynamic Response Of A Mechanical System With Bearing Clearance"
ASME Design Technology Conferences, 1987. Held in Boston, Sep. 27-30, DE-Vol. 10-2, ADVANCES IN DESIGN AUTOMATION -1987, Volume Two, Robotics, Mechanisms, and Machine Systems. pp.411 - 419

7. Soong, K. and Thompson, B.S.
"An Experimental and Analytical Investigation of The Dynamic Response Of A Slider-Crank Mechanism With Controlled Radial Clearance At The Gudgeon-pin Joint."
10th Applied Mechanisms Conference. Held in New Orleans, Louisiana. Dec. 6-9, 1987, Vol. 3, pp. 9A-III.1 - 9A-III.9

8. Brown, J.M.B., Soong, K., Borthwick, W.K.D. Gandhi, M.V. and Thompson, B.S.
"Effects Of Intermittent Contact In Mechanisms Of The Performance Of Numerical Integration Methods."
10th Applied Mechanisms Conference. Held in New Orleans, Louisiana. Dec. 6-9, 1987, Vol. 3, pp. 8C-IV.1 - 8C-IV.7

9. Soong, K., Sunappan, D. and Thompson, B.S.
"The Elastodynamic Response Of A Class Of Intelligent Machinery, Part I, Theory"
ASME Journal of Vibration, Acoustics, Stress and Reliability in Design, in press.

10. Sunappan, D., Soong, K. and Thompson, B.S.
"The Elastodynamic Response Of A Class Of Intelligent Machinery, Part II, Computational and Experimental Results"
ASME Journal of Vibration, Acoustics, Stress and Reliability in Design, in press.

11. Brown, J.M.B., Soong, K., Borthwick, W.K.D. Gandhi, M.V. and Thompson, B.S.
"The Effects Of Intermitten Contact In Flexible Mechanism Systems On the Performance Of Numerical Integration Methods."
Mechanism and Machine Theory, under review.

12. Soong, K. and Thompson, B.S.
"A Theoretical and Experimental Investigation of the Dynamic Response of Planar Mechanisms with Radial Clearances in the Revolute Joints."
(Accepted by ASME Mechanism Conference. To be held in Orlando, Florida, Sep. 25 - 28, 1988)

AN EXPERIMENTAL STUDY TO DOCUMENT THE RESPONSE REGIMES OF A CLASS OF FLEXIBLE FOUR-BAR LINKAGES

AN EXPERIMENTAL STUDY TO DOCUMENT THE RESPONSE REGIMES OF A CLASS OF FLEXIBLE FOUR-BAR LINKAGES

D.X. Liao*, C.K. Sung+, B.S. Thompson×, and K. Soong‡
Department of Mechanical Engineering
Michigan State University
East Lansing, MI 48824-1226

*Visiting Scholar and Associate Professor,
Huazhong University of Science and Technology, Wuhan, China

+Graduate Research Assistant

×Associate Professor

‡Graduate Student

Abstract

This investigation focuses on the response of flexible four bar linkages comprising two flexible links, the coupler link and the rocker link. The crank and ground link are both taken to be rigid bodies. An experimental apparatus and the associated instrumentation is described for studying the midspan transverse deflections of flexible coupler and rocker links of four bar mechanisms for a wide range of operating speeds and link length combinations. Hence a range of forcing frequencies and natural frequencies were studied. The results are documented and presented in this paper which demonstrates that the vibrational characteristics may be grouped into quasi-static, and dynamic regimes, and also conditions of resonance.

Introduction

A debate has raged in academic circles for some years concerning the modeling of flexible linkage mechanisms. The focus has primarily concerned the nature of the flexural response of the members, and to some extent a secondary debate has centered on the frequency response of these flexible articulating systems. Since much of the discussion has been based on theoretical presentations, the authors have attempted herein, to furnish the participants in the debating chamber with some experimental results in order to provide an unbiased foundation for further interactions.

The main theme of the debate has centered on whether the analyst must undertake an elastodynamic analysis or a quasi-static analysis for predicting the response of a flexible mechanism [1-3]. The first class of analyses are computationally more time-consuming, and hence expensive, than the second group of techniques but they provide more accurate results from a mathematical standpoint.

The difference in the two formulations may be illustrated by considering the finite element equations for a general flexible linkage mechanism, which may be written as.

$$[K]\{U\} + [C]\{\dot{U}\} + [M]\{\ddot{U}\} = \{Q\} \qquad (1)$$

In equation (1), [K], [C] and [M] are the global stiffness, damping and mass matrices, column vector {Q} represents the loading imposed on the system, {U} represents the discretized deformation displacement field, and the overdot denotes the time derivative. Equation (1) is generally solved in its entirety by numerical integration or modal superposition techniques to yield the elastodynamic response of the system.

In contrast to this approach, a quasi-static solution may be sought by simplifying equation (1). This approximate solution is sought by first neglecting the terms characterized by {$\dot{U}$} and {$\ddot{U}$}, prior to solving the equation

$$[K]\{U\} = \{Q\} \qquad (2)$$

by Gaussian elimination or some other technique in linear algebra. This philosophy models a dynamic system as a static system, and hence is characterized by the term "quasi-static."

The flexural response of a flexible linkage mechanism is generally the dominate mode of vibration. The waveform comprises a periodic response at the operating frequency of the mechanism, upon which is superimposed a higher frequency component. From a mathematical standpoint, a quasi-static analysis will only predict the periodic response at the lower frequency, while an elastodynamic response will predict both the low-frequency component and also the high-frequency response superimposed upon it. Hence when the amplitude of the high-frequency component is small, the elastodynamic response and the quasi-static response are nominally the same. Under these conditions the designer can legitimately simplify the mathematical model and hence reduce the computational costs associated with the analysis. The fundamental question, the kernel of the debate, centers upon the conditions under which this simplification is admissible.

Having described the salient features of the debate on the elastodynamic and quasi-static responses of flexible mechanisms, attention now focusses on the second, somewhat less volatile topic for discussion which centers on the frequencies at which flexible mechanisms respond. Modeling the frequency response of a flexible multi-link mechanism involves considerations of the forcing frequency (the crank speed) and the natural frequencies of the individual links in their anticipated response mode (flexural, torsional, etc.) and the natural frequencies of the assemblage of flexible bodies. The situation is complicated somewhat by the periodically changing configuration of the mechanism as the assemblage articulates, and this presents one of the fundamental differences between a structure, such as a portal frame, and a linkage mechanism. The final complication is associated with the exaggerated flexibility of many laboratory systems which introduces additional nonlinear phenomena [4-6].

The purpose of this paper is to present experimental data relevant to the two debates described above. This is accomplished by operating

a class of flexible four bar linkages through a range of crank speeds and recording the resulting flexural responses of the members. Specifically, the investigation focuses on the response of flexible four bar linkages with flexible coupler and rocker links. The midspan transverse deflections of these flexible links are presented for a wide range of operating speeds and link length combinations. Thus a range of forcing frequencies and natural frequencies are investigated.

Experimental Apparatus

A photograph of the experimental four bar linkage apparatus used in this study is presented in Figure 1, from which it is clear that it incorporated two flexible members, the coupler and the rocker links. This apparatus was designed to accommodate a wide range of link lengths for the coupler and rocker links, but the crank and ground link were always held constant at 63.5mm and 412.8mm, respectively. The crank was assumed to be rigid since it was manufactured from steel bar stock of cross-sectional dimensionals 25.4mm x 25.4mm.

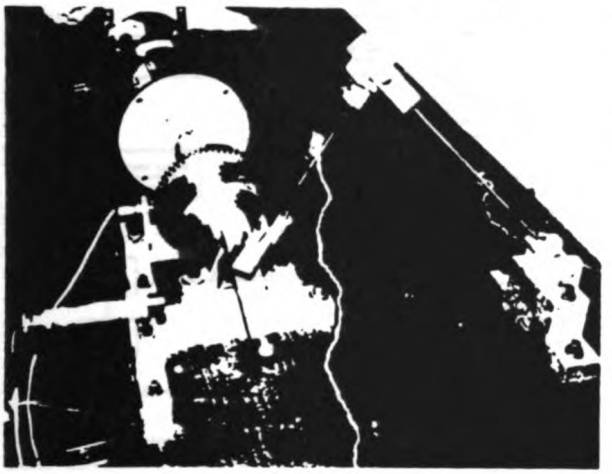

Fig. 1 Photograph of Experimental Four-Bar Linkage

Three classes of mechanism were examined in this study and these kinematic chains are defined in Table 1. The rocker and coupler links were both manufactured from steel strip material and link specimens were interchangeable so that a variety of kinematic chains could be studied. Two classes of steel strip were employed with the following length, width and depth dimensions: 268.0 mm x 19.05 mm x 1.27 mm and 165.0 mm x 25.4 mm x 1.14 mm.

The coupler and rocker links of the experimental four-bar linkage apparatus were both manufactured from strip steel material and the ends of each specimen were clamped to the respective bearing housings by two socket screws. The clamping loads were distributed over the ends by flat plates which are clearly visible on the coupler link in Figure 1. These small clamping plates were found to be essential components of the mechanism since they ensured a smooth load transfer between the three principal components of each link.

Table 1: Linkage Classification

Linkage Classification Number	Ground Link (mm)	Crank (mm)	Coupler (mm)	Rocker (mm)
1	412.8	63.5	308.0	309.5
2	412.8	63.5	308.0	206.5
3	412.8	63.5	205.0	309.5

Identical aluminum bearing housings were manufactured for the rocker link where it was retained on the ground-link/rocker joint, and also for the coupler where it was retained on the crank pin joint. The dimension of the housings in the longitudinal direction of their respective links were 38.1mm from the end of the housing adjacent to the threaded holes for the socket screws and the centerline of the bearings. The masses of these components including bearings, socket screws and clamping plates was 0.05kg.

The coupler and rocker links were supported on matched pairs of 6.4mm bore R3 DB R12 instrument ball bearings supplied by FAG Bearings Limited. Each bearing housing in the mechanism was preloaded using a Dresser Industries torque limiting screw driver calibrated to ±0.113 N·m which permitted bearing clearance to be eliminated since the impactive loading associated with bearing clearances would have resulted in larger link deflections. Conversely, if the bearings were subjected to large axial preloads, then the deflections would be attenuated.

The two flexible links articulated in the same plane in order to eliminate the complications of nonlinear torsional coupling terms which characterize co-planar flexible linkages. This was accomplished using a cleavage bearing design that is clearly visible in the top center of Figure 1. The housings were fabricated in a aluminum alloy and the longitudinal dimension of the housing comprising part of the coupler was 38.1mm from the bearing centerline to the end of the housing adjacent to the threaded holes used to clamp the link specimen. The mass of this assembly, including bearings, socket screws and clamping plate was 0.052 kg. The cleavaged component of the coupler-rocker joint was bolted to the rocker link. The axial dimension of this part from the bearing centerline was 44.5 mm and the mass was 0.063 kg including the spindle, washers and nuts.

The mechanism was bolted to a large cast-iron test stand which was bolted to the floor and also to the wall of the laboratory to provide a substantial rigid foundation. A 0.75 h.p. Dayton variable speed D-C electric motor (model 22846) which was bolted to the test stand, powered the linkage through a 15.9 mm diameter shaft supported by Fafnir pillow block bearings. A 100 mm diameter flywheel was keyed to the shaft thereby providing a large inertia to ensure a constant crank frequency, when operating in unison with the motor's speed controller.

Instrumentation

A schematic of the instrumentation used in the experimental investigation is presented in Figure 2. The rated speed of the electric motor was 2500 rpm and this was directly measured in revolutions per minute by a Hewlett Packard 5314A universal counter which was activated by a digital-magnetic pickup, model 58423, manufactured by Electro Corporation sensing a sixty tooth spur gear mounted on the drive shaft of each rig. This large gear is clearly visible in Figure 1. The aforementioned arrangement provided visual feedback to the operator when the speed controller of the motor was being adjusted to establish a desired speed.

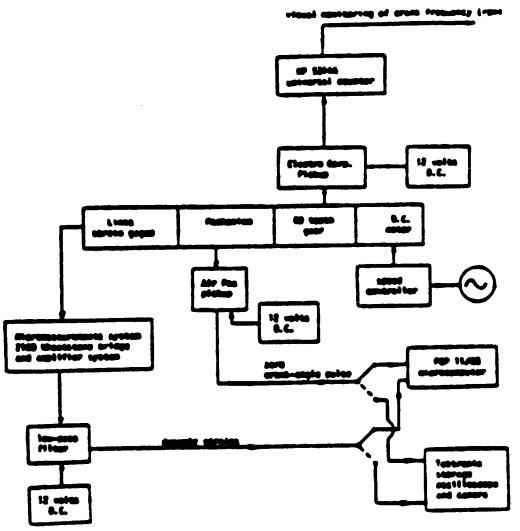

Fig. 2 Schematic Diagram of Instrumentation

The flexural deflections at the midspan of each link specimen were monitored by Micromeasurements Groups Inc. type EA-06-125AD-120 strain gages bonded to each link at the midspan location. Bending half-bridge configurations were adopted, using one gage on each side of the specimen, and they were used in conjunction with a Micromeasurements Group Inc., strain gage conditioner/amplifier system, type 2100. In addition, the deflection at the one-quarter span location was also monitored by strain gauges. This transducer arrangement was considered important in order to monitor potential second-mode flexural responses of the links.

In order to relate the strain gage signal to the configuration of the particular mechanism being studied, a third transducer arrangement was established. An Airpax type 14-0001 zero velocity digital pickup was employed to sense the bolt head at the end of the crank when the mechanism was in the conventional zero-degree crank angle position. This long hexagonal transducer is again clearly visible in Figure 1.

This mechanism configuration signal and the output from the gages were fed to a Digital Equipment Corporation PDP11/03 microcomputer with a LSI 11/23 processor. This digital-data-acquisition system featured 256 kB of memory for post-processing data and also a 5 mB hard disk for storage. A dual port floppy disk system was also available. The experimental response curves were displayed on a Digital Equipment Corporation VT100 terminal with retrographics enhancement.

The BNC cables from each experimental apparatus were connected to a input-output module, bolted to the cabinet of the computer, which was built by the Electronic and Computer Services Department at NSU. This instrument featured 16 analog-digital channels, 4 digital-analog channels and two Schmidt triggers. Using software developed specifically for digital data acquisition purposes, the flexural response signal was recorded from the zero crank angle position through 360 degrees by firing one of the Schmidt triggers. In order to activate the trigger, a 100 μF capacity was used to modify the square-wave output from the Airpax pickup.

Experimental results were obtained by implementing the following procedure. The signal from the strain gage instrumentation was passed through a first-order analog low-pass filter in order to remove the electrically or mechanically inducted noise prior to being digitized by the analog-to-digital converter and recorded by the PDP 11/03 microcomputer. This low-pass filter also prevented aliasing problems when employing a rectangular data window, and a sampling rate of $(2578)^{-1}$ seconds, which was considered to be at least twice the highest frequency component of the pure elasto-dynamic response signal.

Results

The experimental results contained in Figures 3-8 present the flexural response of the coupler and rocker links over a wide range of crank frequencies for a variety of link-length combinations. Upon undertaking a cursory review of these results it is evident that a broad spectrum of response histories are presented, and clearly some classification is desirable in order to aid the design engineer. A classification is defined herein in an arbitrary manner to characterize each response regime.

Response Classification

The flexural response of four-bar linkages may be classified by three response regimes, and these are now defined (albeit, somewhat arbitrarily) for the purposes of this study.

Dynamic Response This response history is characterized by two waveforms comprising a low-frequency periodic waveform (at the crank frequency) upon which is superimposed a high-frequency sinusoidal waveform at approximately the same frequency of the link being monitored. The amplitude of the high frequency component is generally of the same order of magnitude as the amplitude of the low-frequency component.

Quasi-Static Response This response regime is only characterized by the low-frequency periodic waveform at the crank frequency. For the purposes of this study, responses were classified as "quasi-static" when the amplitude of any high-frequency ripple superimposed upon the low-frequency carrier was less than 10 percent of the amplitude of the carrier response.

Resonance Conditions of resonance were defined by the amplitude of the response at a specific crank frequency being significantly larger than the amplitude of the response at adjacent crank frequencies. While this appears to be a somewhat unscientific and an ill-defined statement, in practice it was quite appropriate for the phenomena observed in this study.

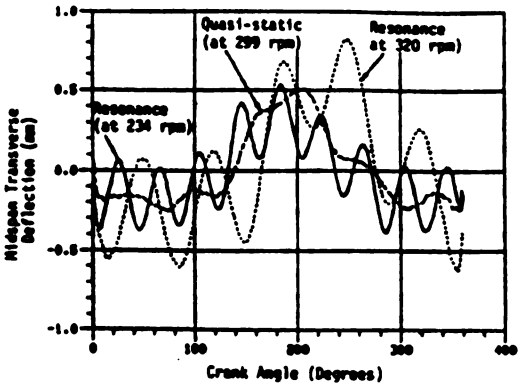

Fig. 3 Class 1 Mechanism; Rocker Link Midspan Transverse Deflections at Three Operating Speeds

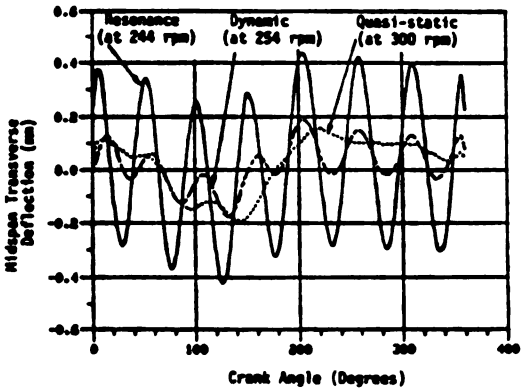

Fig. 4 Class 2 Mechanism; Coupler Link Midspan Transverse Deflections at Three Operating Speeds

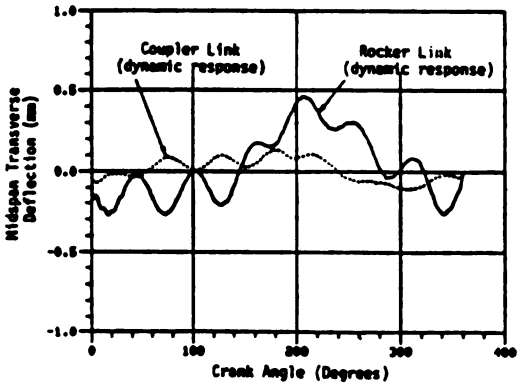

Fig. 5 Class 2 Mechanism; Coupler and Rocker Midspan Transverse Deflections at 268 rpm

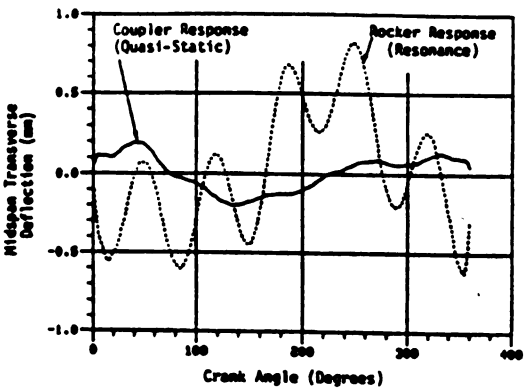

Fig. 6 Class 1 Mechanism; Coupler and Rocker Midspan Transverse Deflections at 321 rpm

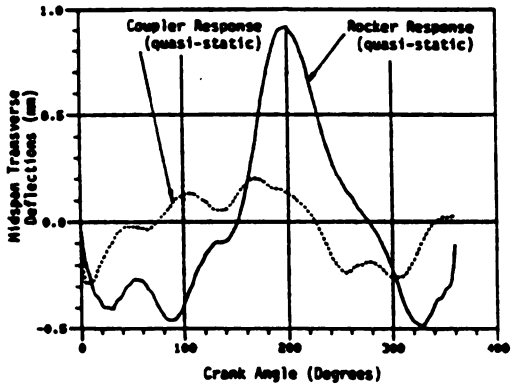

Fig. 7 Class 1 Mechanism; Coupler and Rocker Midspan Transverse Deflections at 357 rpm

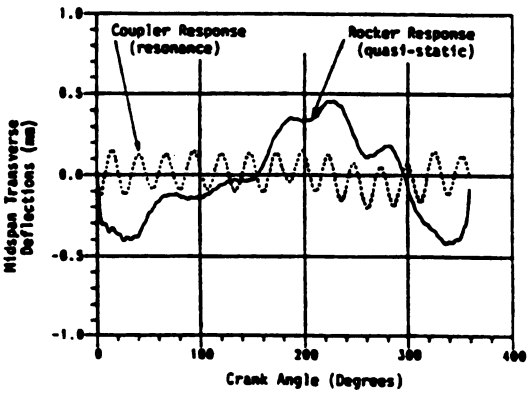

Fig. 8 Class 3 Mechanism; Coupler and Rocker Midspan Transverse Deflections at 281 rpm

Discussion

Figures 3-11 present only a glimpse of the data collected during this experimental investigation, but nevertheless these response histories permit some interesting observations to be recorded. For example, Figure 3 presents the midspan flexural responses of the rocker link of a class 1 mechanism operating at 234, 299 and 320 rpm. Two classes of response are presented, with the amplitude of the response condition at 320 rpm (a condition of resonance) being greater than that at 234 rpm (a second state of resonance). Figure 4 presents a similar set of data for the midspan flexural response of the coupler link of a class 2 mechanism. Three classes of response regime are presented in Figure 4 with the resonance condition at 244 rpm dominating. The amplitude of the vibrations at 244 rpm are larger than the amplitude of the dynamic response at 254 rpm and the quasi-static response at 300 rpm.

Figures 5-8 each present simultaneously the response histories of both the coupler and rocker links of a variety of mechanisms operating at different crank frequencies in order to demonstrate the variety of response regimes developed by this class of four-bar linkage. Thus for example, Figure 5 presents the response of a Class 1 of mechanism in which both the coupler and rocker simultaneously develop a dynamic response. Figure 6 records an interesting condition whereby at 321 rpm a Class 1 mechanism exhibits a resonant condition of the rocker link while the coupler responds quasi-statically. At 357 rpm the same mechanism develops a quasi-static rocker response and also a quasi-static coupler response, and these are presented in Figure 7. Figure 8 presents the response of a class 1 mechanism operating at 281 rpm where the rocker exhibits a quasi-static response while the coupler is in a state of resonance. Thus, it is clearly evident the operating frequency significantly affects the response behavior.

Figures 9-11 present the response regimes of some of the links studied in this investigation. For the mechanisms systems tested, the flexural response was generally of a dynamic nature with resonance conditions observed at the indicated speeds. Quasi-static regimes were generally confined to narrow bands, but this was not universally the case as indicated by Figure 9 where this link did not develop a quasi-static response. The observed resonance conditions are also indicated.

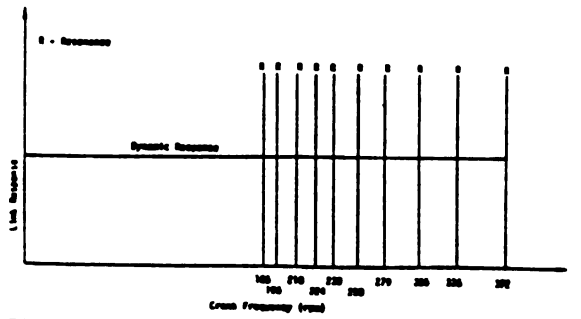

Fig. 9 Class 3 Mechanism; Coupler Response Regimes

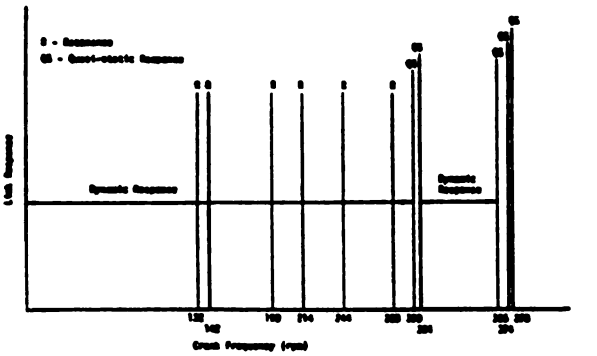

Fig. 10 Class 2 Mechanism; Coupler Response Regimes

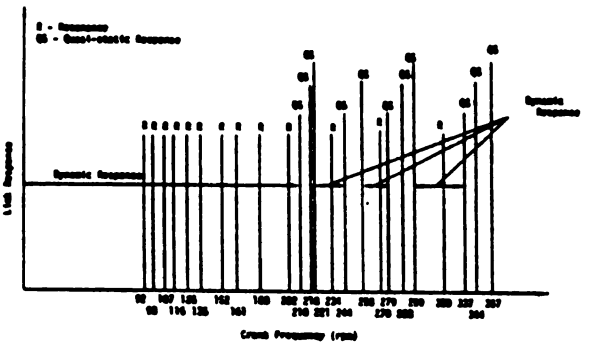

Fig. 11 Class 1 Mechanism; Rocker Response Regimes

Conclusions

An experimental study of flexible four-bar linkages has been presented which documents the different classes of flexural midspan elastodynamic responses of the coupler and rocker links. It is evident that these responses comprise three types: quasi-static, dynamic and resonant. Moreover, it was also observed that adjacent links may be responding quite differently. Thus, for example, the response of a coupler link may be classified as quasi-static response, while at the same speed the adjacent rocker link may be in a state of resonance. The development of theoretical tools to explain these nonlinear vibrational phenomena appear to be quite challenging.

References

1. Willmert, K.D., Thornton, W.A. and Khan, M.R., "A Hierarchy of Methods for Analysis of Elastic Mechanism with Design Application," ASME Paper No. 78-DET-56.

2. Sanders J.R., and Tesar, D., "The Analytical and Experimental Evaluation of Vibratory Oscillations in Realistically Proportioned Mechanisms," ASME, Journal of Mechanical Design, Vol. 100, p. 762 (1978).

3. Haines, R.S., "On Predicting Vibrations in Realistically Proportioned Linkage Mechanisms," ASME, Journal of Mechanical Design, Vol. 103, p. 706 (1981).

4. Thompson, B.S., and Sung, C.K., "A Variational Formulation for the Nonlinear Finite Element Analysis of Flexible Linkages: Theory, Implementation, and Experimental Results," ASME, Journal of Mechanisms, Transmissions, and Automation in Design, Vol. 106, p. 482 (1984).

5. Sung, C.K., Thompson, B.S., Xing, T.M., and Wang, C.H., "An Experimental Study on the Nonlinear Elastodynamic Response of Linkage Mechanisms," Mechanism and Machine Theory (in press) (1985).

6. Turcic, D.A., and Midha, A., "Dynamic Analysis of Elastic Mechanism Systems, Part I: Application, and Part II: Experimental Result," ASME, Journal of Dynamic System, Measurements, and Control, Vol. 106, p. 249 (1984).

AN EXPERIMENTAL BREAD-BOARD MODEL FOR A CLASS OF INTELLIGENT HIGH-SPEED MACHINERY: SOME PRELIMINARY RESULTS

AN EXPERIMENTAL BREAD-BOARD MODEL FOR A CLASS OF INTELLIGENT HIGH-SPEED MACHINERY: SOME PRELIMINARY RESULTS

B.S. Thompson‡, K. Soong*, and C.K. Sung×

Department of Mechanical Engineering
Michigan State University
East Lansing, MI 48824-1226

‡Associate Professor
*Graduate Student
×Graduate Research Assistant

Abstract

The elastodynamic response of high-speed machinery is governed by the mass, stiffness and damping characteristics of the links, and also the inertial loading imposed upon these members. For a specific mechanism, the physical link characteristics are of course invariant and the response is governed by the kinematic variables upon which the inertial loading depends. Herein, preliminary work is described which concerns the control of the inertial loading imposed on flexible mechanisms in order to achieve a desired response. The philosophy is directed towards developing computer-controlled intelligent machinery which are capable of both reducing link deflections and also operating with more versatile path-generation capabilities.

Introduction

The vast majority of industrial machine systems have one rigid-body degree of freedom and one power source which are responsible for creating a single distinct output characteristic. This output characteristic will generally satisfy the criteria imposed on the performance of the machine, but the machine will be generally dedicated to performing a limited class of operations.

This paper reports on some preliminary work directed towards stimulating the evolution of a new generation of computer-controlled intelligent machine systems which are more versatile, more adaptable and more cost-effective than the current generation of machine systems available in the marketplace. This new generation of products will enable single machines to generate a number of different classes of performance characteristics that currently must be undertaken by several individual machines. An example of this is the variety of different coupler curves generated by the tracer points of several different four-bar linkages. The work described herein is directed towards replacing these different classes of four-bar linkages by a reduced number of more versatile mechanisms which can generate all of the coupler curves of the separate four-bar mechanisms.

A second class of problem concerns the synthesis of high-speed machinery. These systems develop elastodynamic effects which may contaminate the performance characteristics and prevent the machine from satisfying prescribed design specifications. Alternatively, bearing degradation may result in a machine operating outside the performance envelope after operating for a period of time. The work reported herein is directed towards resolving these situations by developing a methodology for designing intelligent machines. The methodology requires the machine's performance to be continually monitored by sensors on the principal elements of the system, with the response data being fed to a controller or microprocessor which has the capability of modifying the machine's performance by activating a secondary force input to the system. Thus the output characteristics would then be the result of a primary and a secondary excitation. By this means it is anticipated that the desired response would be achieved.

While this approach to adaptive control is the goal of this project, currently an open-loop mode of operation is employed rather than the closed-loop philosophy proposed above. Herein the current status of the project is documented and some preliminary results presented.

Proposed Methodology

The proposed methodology is based on the approach described in reference [1], which utilizes a four-bar linkage in which the constraints imposed at the rocker/ground-link joint are relaxed. This relaxation involves replacing this normally stationary revolute joint by a sliding joint which permits translational motion to occur in the horizontal direction OX as shown schematically in Fig. 1. This modification creates a linkage with two rigid-body degrees-of-freedom and hence provides the option for two inputs to the mechanism; one due to the crank rotation and one due to a prescribed motion at the sliding joint. The nature of these excitations govern the performance characteristics of the linkage.

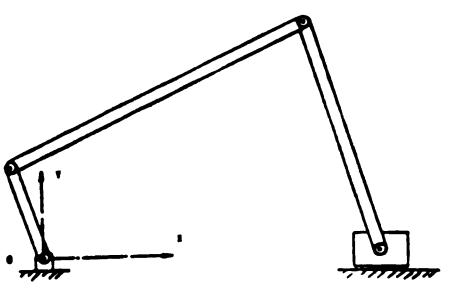

Fig. 1 Intelligent Mechanism: Basic Kinematic Chain

Path-Generation Capabilities

Consider, for example, the operation of a four-bar linkage in a path-generation mode where the tracer-point is located at the midspan of the coupler link. A single coupler curve is generated by this mechanism system. However, if the length of the ground link is either lengthened or shortened to create a number of discrete ground link lengths; then a number of coupler curves may be developed as indicated in Fig. 2. Moreover, by employing the single system described schematically in Fig. 1, then any of the these curves may be generated by first changing the ground link length to a prescribed value and then activating the mechanism. The proposed system has the additional advantage of permitting any point to within the work-envelope presented in Fig. 2 to be accessed by the tracer-point. This is achieved by coordinating the motions of the slider and crank members of the system described in Fig. 1. Not only can these points be accessed, but the two degrees of freedom permit a variety of coupler-curves within that work-envelope to be generated. These inputs may, of course, be computer-controlled.

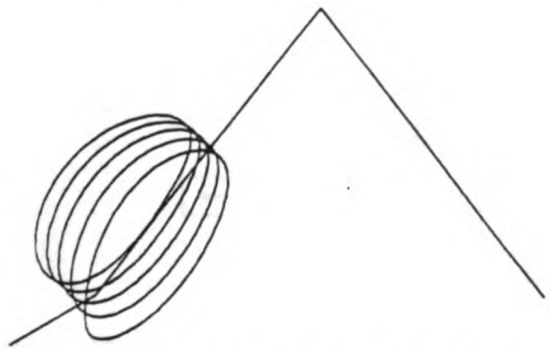

Fig. 2 Family of Coupler Curves Developed by the Intelligent Mechanism

Elastodynamic-control Capabilities

The motion of the tracer-point of a high-speed, or flexible, linkage will not generate the smooth coupler curves shown in Fig. 2. Instead, an elastodynamic deflection will be imposed on the curves, as indicated in Fig. 3. It is clearly plausible for this deflection and the associated stresses to be unacceptable, because of potential fatigue failure or inaccurate coupler-curve generation. Under these circumstances, the linkage system proposed in Fig. 1 may provide a solution whereby the motion of the slider would be computer-controlled in a prescribed manner in order to reduce the deflections of the coupler midspan. Thus the forcing function exciting the response of the link would be fine-tuned through a careful orchestration of the crank motion and the slider motion.

From a mathematical standpoint the boundary conditions and force fields imposed upon the assemblage of articulating beam-shaped bodies are being continuously modified. Thus a variety of dynamical mixed boundary-value problems are being solved to create a suite of response characteristics.

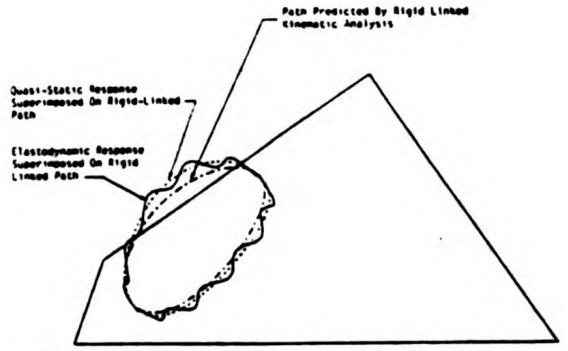

Fig. 3 Coupler Curve Components for a Flexible Four-Bar Linkage

This philosophy is examined herein by studying the response of an experimental four-bar linkage with a flexible coupler link (see Fig. 4). The midspan transverse deflection of the coupler is first recorded for the system operating in a conventional four-bar mode. Then the shaker is excited, using a waveform based on the quasi-static response of the coupler, in order to attenuate the amplitude of this deflection.

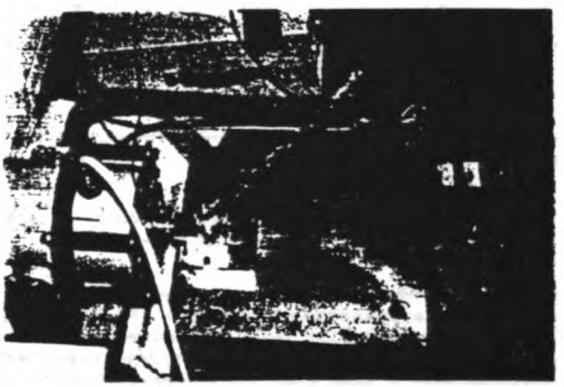

Fig. 4 Photograph of Intelligent Mechanism Model.

While the mechanism was designed to accommodate a range of link lengths, this investigation was undertaken with an initial ground link length of 381 mm, a crank length of 50 mm, a coupler of length

Experimental Apparatus and Instrumentation

The proposed class of adaptive four-bar linkages was studied by constructing the system presented in Figs. 4 and 5. Figure 5 schematically presents the final system configuration for the project, but at this time the system runs open-loop, with the controller module being the investigator. Gravitational loading is perpendicular to the plane of the mechanism.

293.6 mm and a rocker of length 305 mm. The coupler was a very flexible link of cross-sectional dimensions 0.838 mm x 10.2 mm while the rocker was a much more substantial member of cross-sectional dimensions 6.25 mm x 19.43 mm.

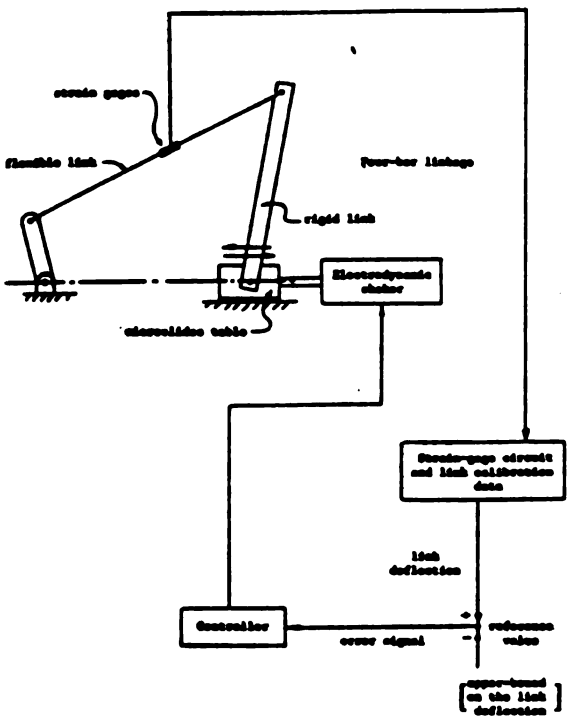

Fig. 5 Final System Configuration

The bearings of the system were carefully preloaded to eliminate radial clearance and the coupler/rocker joint was a cleavage design. One end of the rocker link was connected to a Microslides Inc., type A-2020 cross-roller slide assembly which permitted translational motion in the OX direction in Fig. 1 to occur. This precision assembly was then bolted to a Bruel and Kjaer force transducer, type 8200, which permitted the force exerted by the electrodynamic shaker on the mechanism to be carefully monitored.

This shaker was an air-cooled Ling Dynamic Systems, type V411 exciter. The acceleration imposed by the exciter upon the slide-assembly was monitored by a Bruel and Kjaer accelerometer, type 4731, mounted on the slide-assembly. The output from this transducer was fed to a Bruel and Kjaer conditioning amplifier, type 2635, which enabled the velocity and displacement characteristics of the slide-assembly to be monitored.

The output from the transducers were either fed to an oscilloscope for preliminary evaluation of the response data, or fed to a DEC PDP 11/03 microcomputer for storage and post-processing using FFT algorithms.

Experimental Procedure, Results and Discussion

The experimental procedure involved first operating the mechanism at a constant crank frequency with the cross-rolled slide assembly clamped in order to create a classical four-bar linkage system. Strain gauges mounted at the midspan of the coupler monitored the lateral deflections of the link and the data was fed through an analog filter prior to storing in the PDP 11/03 microcomputer. Upon completing a digital filtering operation and multiplying the resulting data by a link calibration factor relating the transverse deflection and the corresponding voltage, the resulting response history for the mechanism operating at 189 rpm is presented in Fig. 6. The waveform comprises two components: the quasi-static response at the mechanism's operating frequency and a high-frequency component at approximately the link's fundamental natural frequency in flexure. It may be classified as an elastodynamic response.

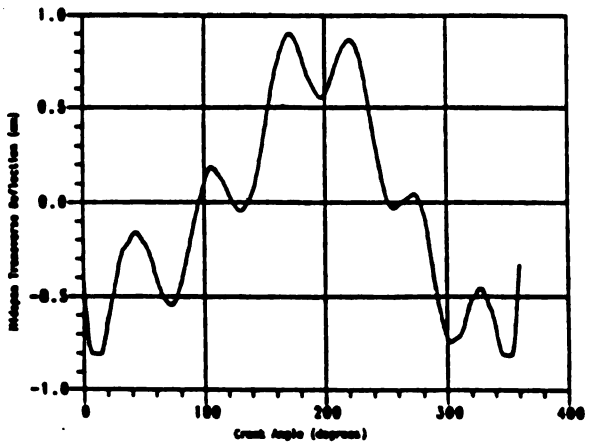

Fig. 6 Coupler Midspan Transverse Deflection of Four-Bar Linkage

In this current open-loop mode of operation, this data was then post-processed again by simulating a low-pass digital filter in order to yield the quasi-static response of the coupler at 189 rpm prior to programming the data into a Wavetek digital arbitrary waveform generator, model 275. This device permits arbitrary waveforms to be generated for a wide range of frequencies. For this study the generator was programmed to synthesize the inverse of the quasi-static response of the coupler midspan transverse deflection. This waveform was proposed as being a viable motion with which to excite the shaker in this inverse force-deflection problem, although there is little justification other than the algorithm proposed in reference [1].

Thus, using the waveform described by the inverse of the quasi-static deflection, the shaker was then excited at the crank frequency (189 rpm). Thus the coupler link was being excited by an inertial force field, due to the motion of the articulating mechanism, and also a second input due to the force field imposed by the shaker. These combined excitations, in addition to the different boundary conditions at the ground-link/rocker joint which create a kinematic chain with a time-dependent configuration, yield the results presented in Fig. 7. This is a quasi-static response.

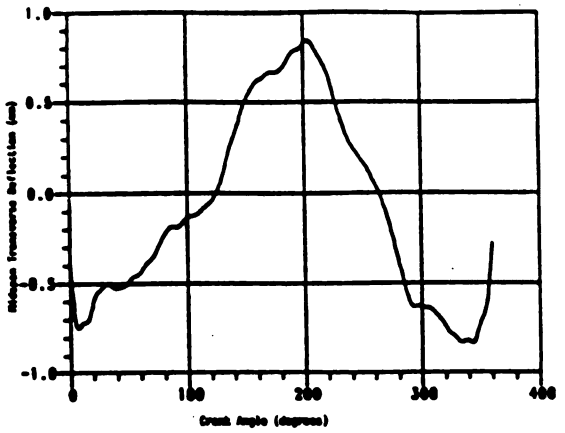

Fig. 7 Coupler Midspan Transverse Deflection of "Four-Bar Linkage" with Shaker Activated

This response history is for the coupler midspan transverse deflection at 189 rpm. The high-frequency component is absent and the maximum deflection has been reduced by 7 percent through the shaker excitation of the modified linkage. The resultant force at the shaker/slider connection, as monitored by the Bruel and Kjaer force transducer, is presented in Fig. 8. This force profile is comprised of a force component due to the articulating motion of the mechanism and also the force component generated by exciting the shaker. The corresponding displacement profile of the crossed-roller slide assembly developed during one revolution of the crank at 3.15 Hz (189 rpm) is presented in Fig. 9.

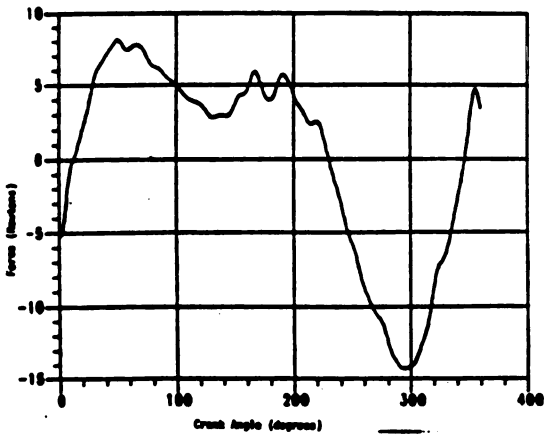

Fig. 8 Force Response at the Shaker/Mechanism Interface

These preliminary experimental results provide a boost in confidence for the original proposition that a more versatile class of machines can be developed, based on the four-bar linkage chain with an additional input at the normally fixed ground-link/rocker joint. Clearly more work must be undertaken to document the control algorithms for the active control of these distributed parameter systems since the input from the shaker must be carefully orchestrated with the primary forcing function provided by the crank motion, in order to avoid combination resonances and other undesirable elastodynamic phenomena.

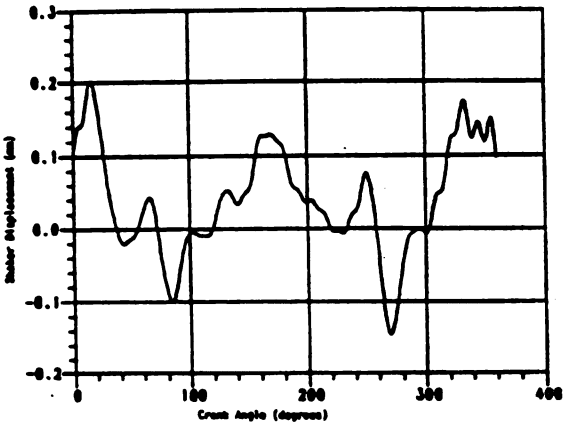

Fig. 9 Displacement Response of the Reciprocating Slide Assembly

Conclusions

An experimental investigation into a class of adaptive flexible linked mechanisms with two forcing inputs has been presented. By operating in an open-loop mode, this bread-board model for a class of intelligent machines has demonstrated that link deflections may be reduced by controlling the force excitation of the linkage system using an electrodynamic shaker.

Acknowledgements

The authors wish to acknowledge with thanks the financial support for this project in the Machinery Elastodynamics Laboratory that has been provided by the Division of Engineering Research at Michigan State University.

References

1. Oliver, J.H., Wysocki, D.A., and Thompson, B.S., "The Synthesis of Flexible Linkage by Balancing the Tracer Point Quasi-Static Deflection's using Microprocessor and Advanced Materials Technologies," Mechanism and Machine Theory, Vol. 20, No. 2, pp. 103-114, 1985.

A NOTE ON THE QUASI-STATE RESPONSE, DYNAMIC RESPONSES, AND THE SUPER-HARMONIC RESONANCES OF FLEXIBLE LINKAGE: SOME EXPERIMENTAL RESULTS

THE AMERICAN SOCIETY OF MECHANICAL ENGINEERS
345 E. 47 St., New York, N.Y. 10017
86-DET-146

The Society shall not be responsible for statements or opinions advanced in papers or in discussion at meetings of the Society or of its Divisions or Sections, or printed in its publications. Discussion is printed only if the paper is published in an ASME Journal. Papers are available from ASME for fifteen months after the meeting.
Printed in USA.

A Note on the Quasi-Static Responses, Dynamic Responses, and the Super-Harmonic Resonances of Flexible Linkages: Some Experimental Results

D. X. LIAO, C. K. SUNG, B. S. THOMPSON, and K. SOONG
Department of Mechanical Engineering
Michigan State University
East Lansing, MI 48824-1226

ABSTRACT

This paper reports on several experimentally-observed vibration phenomena in flexible four-bar linkages that have not appeared before in the literature. These nonlinear vibrational responses, which cannot be predicted using state-of-the-art computer models, will, it is anticipated, trigger renewed theoretical activities in this aspect of linkage design.

The investigation focuses on the response of flexible four-bar linkages comprising two flexible links, the coupler link and the rocker link. An experimental approach is described for measuring the midspan transverse deflections of these links for a wide range of operating speeds and different link length combinations. The experimental response data presented herein demonstrates that the vibrational characteristics at the link midspans may be grouped into quasi-static and dynamic regimes, and also conditions of super-harmonic resonance.

INTRODUCTION

A debate has raged in academic circles for some years concerning the appropriate mathematical apparatus for modeling flexible linkage mechanisms. The focus has primarily concerned the nature of the flexural response of the members, and to some extent a secondary debate has centered on the frequency response of these flexible articulating systems. Since much of the discussion has been based on theoretical presentations, the authors have attempted herein, to furnish experimental results which should provide an unbiased foundation for further academic interactions.

The focus of the debate has centered on whether the analyst must undertake an elastodynamic analysis, or a quasi-static analysis, for predicting the response of a flexible mechanism [1-3]. The first class of analyses are computationally more time-consuming, and hence expensive, than the second group of techniques but they provide more accurate results from a mathematical standpoint.

The difference in the two formulations may be illustrated by considering the finite element equations of motion for a general flexible linkage mechanism, which may be written as

$$[K]\{U\} + [C]\{\dot{U}\} + [M]\{\ddot{U}\} = \{Q\} . \qquad (1)$$

In equation (1), $[K]$, $[C]$ and $[M]$ are the global stiffness, damping and mass matrices respectively, column vector $\{Q\}$ represents the loading imposed on the system, $\{U\}$ represents the discretized deformation displacement field, and the overdot denotes the time derivative. Equation (1) is generally solved in its entirety by numerical integration or modal superposition techniques to yield the elastodynamic response of the system.

In contrast to this approach, a quasi-static solution may be sought by simplifying equation (1). This approximate solution is sought by first neglecting the terms characterized by $\{\dot{U}\}$ and $\{\ddot{U}\}$, prior to solving the equation

$$[K]\{U\} = \{Q\} \qquad (2)$$

by Gaussian elimination or some other technique in linear algebra. This philosophy models a dynamic system as a static system, and hence is characterized by the term "quasi-static."

The flexural response of a flexible linkage mechanism is the dominant mode of vibration. The waveform often comprises a periodic response at the operating frequency of the mechanism, upon which is superimposed a higher frequency component. From a mathematical standpoint, a quasi-static analysis will only predict the periodic response at the lower frequency, while an elastodynamic response will predict both the low-frequency component and also the high-frequency response superimposed upon it. Hence when the amplitude of the high-frequency component is small, the elastodynamic response and the quasi-static response are nominally the same. Under these conditions the designer can legitimately simplify the mathematical model and hence reduce the computational costs associated with the analysis. The fundamental

Presented at the Design Engineering Technical Conference
Columbus, Ohio — October 5-8, 1986

question, the kernel of the debate, centers upon the conditions under which this simplification is admissible. At this time, there are no design guidelines to provide assistance with this decision.

Having described the salient features of the debate on the elastodynamic and quasi-static responses of flexible mechanisms, attention now focuses on the second, somewhat less volatile topic for discussion which centers on critical operating speeds and the frequencies at which flexible mechanisms respond. Modeling the frequency response of a flexible multi-link mechanism involves considerations of the forcing frequency (the crank speed), the natural frequencies of the individual links in their anticipated response mode (flexural, torsional, etc.), and the natural frequencies of the assemblage of flexible bodies. The situation is complicated somewhat by the periodically changing configuration of the mechanism as the assemblage articulates, and this presents one of the fundamental differences between a structure, such as a portal frame, and a linkage mechanism.

The early work in this area reported on linkages with only one flexible member [4-6]. The approaches generally involved transforming the governing linkage equations into a set of uncoupled Mathieu-Hill's equations. This class of equations have received considerable attention in the literature. References [7] and [8] presented and used Mathieu-Hill equations and [9] used Floquet theory for the solution of the Hill's equations resulting from the analysis of a four-bar mechanism with an elastic rocker link. Subsequently finite element analyses have been developed for predicting the critical running speeds and dynamic instabilities in linkages comprising several flexible links [10-11]. While these mathematical models are indeed valuable contributions to the mechanisms literature, they are unable to predict the experimentally-observed nonlinear phenomena reported herein. It is therefore anticipated that these experimental results will hopefully catalyse further theoretical studies in this area.

The experimental results were obtained by operating a class of flexible four-bar linkages through a range of crank speeds and recording the resulting flexural responses of the members. Specifically, the investigation focuses on the response of four-bar linkages with flexible coupler and rocker links. The midspan transverse deflections of these flexible links are presented for a wide range of operating speeds and link-length combinations in order to demonstrate the generality of the observed phenomena and also provide some classification of the responses. Three classes of link configuration have been studied: class 1 has the same link characteristics for both coupler and rocker links while classes 2 and 3 possess different link characteristics. The reason for employing two different cross-sectional links is to observe the possible mode interaction between two links.

EXPERIMENTAL APPARATUS

A photograph of the experimental four bar linkage apparatus used in this study is presented in Figure 1, from which it is clear that it incorporated two flexible members, the coupler and the rocker links. This apparatus was designed to accommodate a wide range of coupler and rocker links lengths, but the crank and ground link were always held constant at 63.5mm and 412.8mm, respectively. The crank was assumed to be rigid since it was manufactured from steel bar stock of cross-sectional dimensions 25.4mm x 25.4mm.

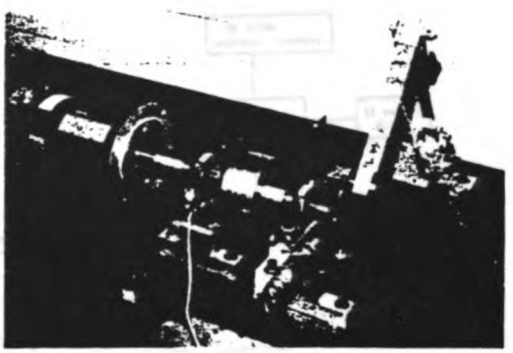

Fig. 1 Photograph of Experimental Four-Bar Linkage

Three classes of four-bar mechanism were examined in this study and these kinematic chains are defined in Table 1. The rocker and coupler links were both manufactured from steel strip material, and link specimens were interchangeable so that a variety of kinematic chains could be studied. Two classes of steel strip were employed with the following length, width and depth dimensions: (268.0 mm x 19.05 mm x 1.27 mm) and (165.0 mm x 25.4 mm x 1.14 mm).

Table 1: Link Classification

Link Characteristics		Ground Link	Crank	Coupler	Rocker
Length (mm)	1	412.8	63.5	308.0	309.5
	2	412.8	63.5	308.0	206.5
	3	412.8	63.5	205.0	309.5
Cross-section (mm x mm)	1		25.4x25.4	19.05x1.27	19.05x1.27
	2		25.4x25.4	19.05x1.27	25.4x1.14
	3		25.4x25.4	25.4x1.14	19.05x1.27
Natural Frequency (H_z)	1			28.5	27.0
	2			28.5	50.2
	3			55.6	26.8

The coupler and rocker links of the experimental four-bar linkage apparatus were both manufactured from strip steel material and the ends of each specimen were clamped to the respective bearing housings by two socket screws. The clamping loads were distributed over the ends by flat plates which are clearly visible on the coupler link in Figure 1. These small clamping plates were found to be essential components of the mechanism since they ensured a smooth load transfer between the three principal components of each link.

Identical aluminum bearing housings were manufactured for the rocker link where it was retained on the ground-link/rocker joint, and also for the coupler where it was retained on the crank pin joint. The dimension of the housings in the longitudinal direction of their respective links were 38.1mm from the end of the housing adjacent to the threaded holes for the socket screws and the centerline of the bearings. The masses of these components including bearings, socket screws and clamping plates was 0.05kg.

The coupler and rocker links were supported on matched pairs of 6.4mm bore R3 DB R12 instrument ball bearings supplied by FAG Bearings Limited. Each bearing housing in the mechanism was preloaded using a Dresser Industries torque limiting screw driver calibrated to ±0.113 N·m which permitted bearing clearance to be eliminated since the impactive loading associated with bearing clearances would have resulted in larger link deflections. Conversely, if the bearings were subjected to large axial preloads, then the deflections would be attenuated.

The two flexible links articulated in the same plane in order to eliminate the complications of nonlinear torsional coupling terms which characterize co-planar flexible linkages. This was accomplished using a cleavage bearing design that is clearly visible in the top center of Figure 1. The housings were fabricated in a aluminum alloy and the longitudinal dimension of the housing comprising part of the coupler was 38.1mm from the bearing centerline to the end of the housing adjacent to the threaded holes used to clamp the link specimen. The mass of this assembly, including bearings, socket screws and clamping plate was 0.052 kg. The cleavaged component of the coupler-rocker joint was bolted to the rocker link. The axial dimension of this part from the bearing centerline was 44.5 mm and the mass was 0.063 kg including the spindle, washers and nuts. In this investigation, the driving frequencies are rather small comparing to the natural frequencies of both links, therefore, the deflection is mainly dominant by the first mode of vibration. In addition, the bearings and the link-bearing connections are placed on both ends of the links, so the influence on the natural frequencies of the individual links is small.

The mechanism was bolted to a large cast-iron test stand which was bolted to the floor and also to the wall of the laboratory to provide a substantial rigid foundation. A 0.75 h.p. Dayton variable speed D-C electric motor (model 2Z846) which was bolted to the test stand, powered the linkage through a 15.9 mm diameter shaft supported by Fafnir pillow block bearings. A 100 mm diameter flywheel was keyed to the shaft thereby providing a large inertia to ensure a constant crank frequency, when operating in unison with the motor's speed controller.

INSTRUMENTATION

A schematic of the instrumentation used in the experimental investigation is presented in Figure 2. The rated speed of the electric motor was 2500 rpm and this was directly measured in revolutions per minute by a Hewlett Packard 5314A universal counter which was activated by a digital-magnetic pickup, model 58423, manufactured by Electro Corporation sensing a sixty tooth spur gear mounted on the drive shaft of each rig. This large gear is clearly visible in Figure 1. The aforementioned arrangement provided visual feedback to the operator when the speed controller of the motor was being adjusted to establish a desired speed.

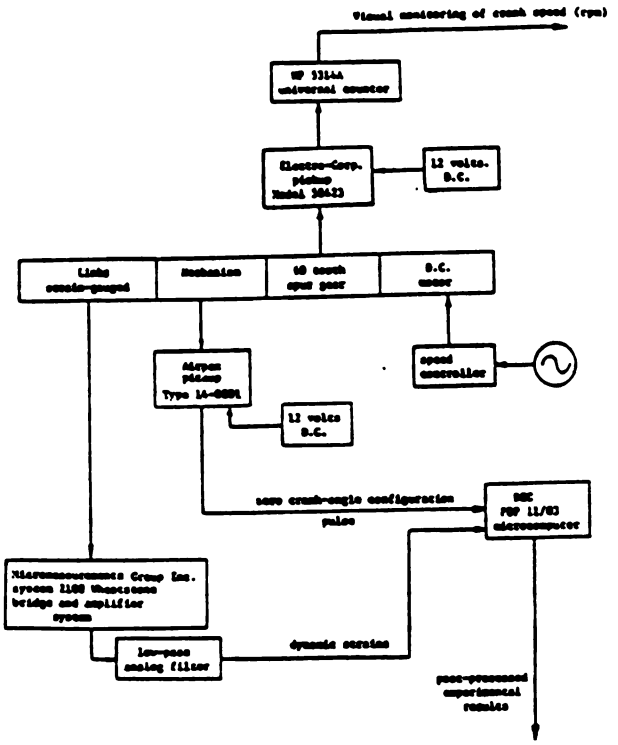

Fig. 2 Schematic Diagram of Instrumentation

The flexural deflections at the midspan of each link specimen were monitored by Micromeasurements Groups Inc. type EA-06-125AD-120 strain gages bonded to each link at the midspan location. Bending half-bridge configurations were adopted, using one gage on each side of the specimen, and they were used in conjunction with a Micromeasurements Group Inc., strain gage conditioner/amplifier system, type 2100. In addition, the deflection at the one-quarter span location was also monitored by strain gauges. This transducer arrangement was considered important in order to monitor potential second-mode flexural responses of the links.

In order to relate the strain gage signal to the configuration of the particular mechanism being studied, a third transducer arrangement was established. An Airpax type 14-0001 zero velocity digital pickup was employed to sense the bolt head at the end of the crank when the mechanism was in the conventional zero-degree crank angle position. This long hexagonal transducer is again clearly visible in Figure 1.

This mechanism configuration signal and the output from the gages were fed to a Digital Equipment Corporation PDP11/03 microcomputer with a LSI 11/23 processor. This digital-data-acquisition system featured 256 kB of memory for post-processing data and also a 5 mB hard disk for storage. A dual port floppy disk system was also available. The experimental response curves were displayed on a Digital Equipment Corporation VT100 terminal with retrographics enhancement.

The BNC cables from each experimental apparatus were connected to a input-output module, bolted to the

cabinet of the computer, which was built by the Electronic and Computer Services Department at MSU. This instrument featured 16 analog-digital channels, 4 digital-analog channels and two Schmidt triggers. Using software developed specifically for digital data acquisition purposes, the flexural response signal was recorded from the zero crank angle position through 360 degrees by firing one of the Schmidt triggers. In order to activate the trigger, a 100 μF capacity was used to modify the square-wave output from the Airpax pickup.

Experimental results were obtained by implementing the following procedure. The signal from the strain gage instrumentation was passed through an analog variable low-pass filter manufactured by Wavetek Inc., type 432, in order to remove the electrically or mechanically inducted noise prior to being digitized by the analog-to-digital converter and recorded by the PDP 11/03 microcomputer. This low-pass filter also prevented aliasing problems when employing a rectangular data window, and a sampling rate of $(2578)^{-1}$ seconds, which was considered to be at least twice the highest frequency component of the pure elastodynamic response signal.

CLASSIFICATION OF RESULTS

The experimental results contained in Figures 3-8 present the flexural responses of the coupler and rocker links over a wide range of crank frequencies for a variety of link-length combinations. Upon undertaking a cursory review of these results it is evident that a broad spectrum of response histories are presented, and clearly some classification is desirable for discussion purposes. A classification is defined herein in a somewhat arbitrary manner to characterize each response regime.

Response Classification

The flexural response of four-bar linkages may be classified into three response regimes, and these are now defined (albeit, somewhat arbitrarily) for the purposes of this investigation.

Dynamic Response

This response history is characterized by two waveforms comprising a low-frequency periodic waveform (at the crank frequency) upon which is superimposed a high-frequency sinusoidal waveform at approximately the same frequency of the link being monitored. The amplitude of the high frequency component is generally of the same order of magnitude as the amplitude of the low-frequency component.

Quasi-Static Response

This response regime is only characterized by the low-frequency periodic waveform at the crank frequency. For the purposes of this study, responses were classified as "quasi-static" when the amplitude of any high-frequency ripple superimposed upon the low-frequency carrier waveform was less than 10 percent of the amplitude of the carrier response.

Resonance

Conditions of resonance were defined by the amplitude of the response at a specific crank frequency being significantly larger than the amplitude of the response at adjacent crank frequencies. While this appears to be a somewhat unscientific and an ill-defined statement, in practice it was quite appropriate for the phenomena observed in this study.

DISCUSSION

Figures 3-11 present experimental response histories measured during this laboratory investigation. Upon undertaking a cursory review of these responses, it is immediately evident that there are a variety of different waveforms. For example, Figure 3 presents the midspan flexural responses of the rocker link of a class 1 mechanism operating at 234, 299 and 320 rpm. Two classes of response are presented, with the amplitude of the resonance condition at 320 rpm being greater than the resonant response at 234 rpm. Figure 4 presents a similar set of data for the midspan flexural response of the coupler link of a class 2 mechanism. Three classes of response regime are presented in Figure 4 with the resonance condition at 244 rpm dominating. In fact, the amplitude of the vibrations at 244 rpm are larger than the amplitude of the dynamic response at 254 rpm and the quasi-static response at 300 rpm. It is clear, therefore, that the response profile, the stress-levels and hence the fatigue life are all dependent upon the operating speed of the mechanism.

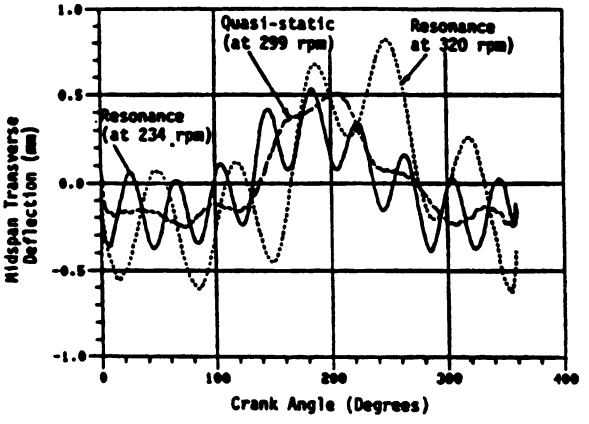

Fig. 3 Class 1 Mechanism; Rocker Link Midspan Transverse Deflections at Three Operating Speeds

Having previously focused on the responses of a particular link at a variety of operating speeds, attention now focuses on the responses of both the coupler and rocker links of a specific mechanism operating at some specific crank frequencies. These experimental results are presented in figures 5-8 which demonstrate the variety of response regimes developed by three dissimilar classes of four-bar linkage operating at different speeds. It is clearly evident from these results, that while the flexible coupler and rocker links have a common joint, which may imply some commonality of response format, that these adjacent links can respond quite differently. Results demonstrating these effects have not previously appeared in the literature.

Figure 5 presents the response of a Class 1 of mechanism in which both the coupler and rocker simul-

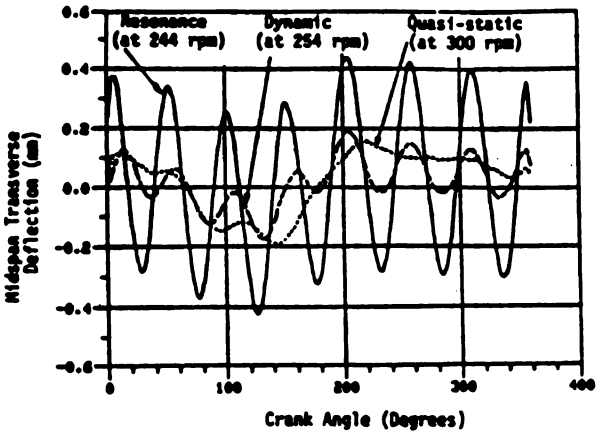

Fig. 4 Class 2 Mechanism; Coupler Link Midspan Transverse Deflections at Three Operating Speeds

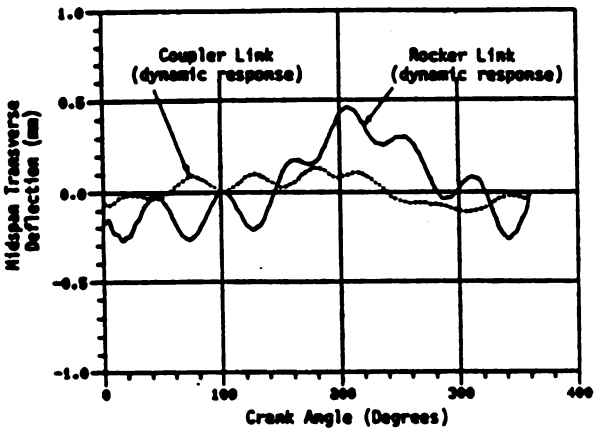

Fig. 5 Class 1 Mechanism; Coupler and Rocker Midspan Transverse Deflections at 268 rpm

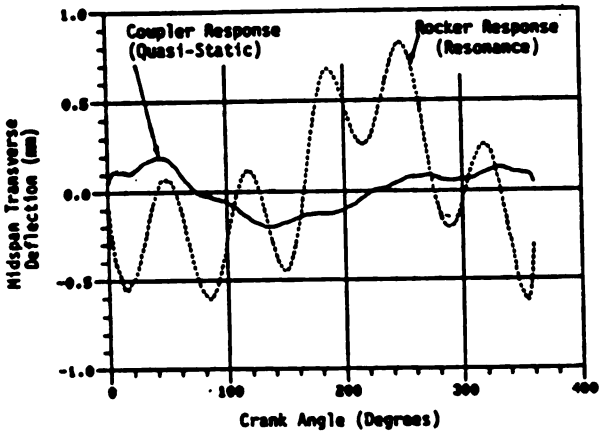

Fig. 6 Class 1 Mechanism; Coupler and Rocker Midspan Transverse Deflections at 321 rpm

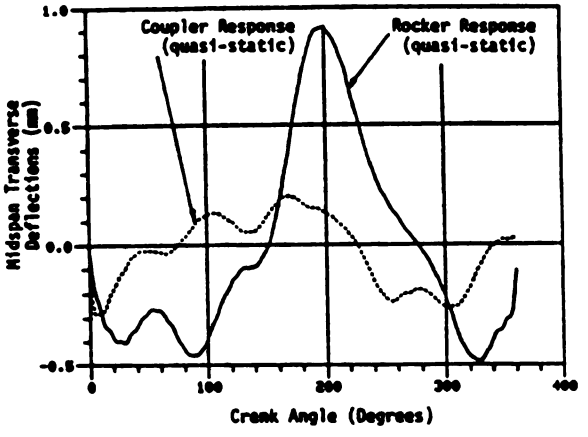

Fig. 7 Class 1 Mechanism; Coupler and Rocker Midspan Transverse Deflections at 357 rpm

taneously develop a dynamic response at 268 rpm. Figure 6, however, records an interesting condition whereby at 321 rpm the rocker link of a Class 1 mechanism vibrates vigorously in a state of resonance, while the adjacent coupler link responds in a quasi-static manner with minimal vibrational behavior. State-of-the-art computer models are unable to predict this phenomenon. In sharp contrast to this, at 357 rpm the same mechanism develops a quasi-static rocker response and also a quasi-static coupler response. These deformation histories are presented in Figure 7. If design guidelines existed for predicting such a response profile, then this response could have been predicted by undertaking a quasi-static finite element analysis, prior to the fabrication of the experimental mechanism. Such a guideline does not exist at this time.

Figure 8 presents the response histories of a class 3 mechanism operating at 281 rpm. The rocker link response is quasi-static in nature while the adjacent coupler link vibrates in a state of resonance. Again, design guidelines do not exist for predicting such a response. Thus, it is clearly evident from this comprehensive experimental investigation that the frequency at which the mechanism operates significantly affects the response behavior.

At this time, the design engineer lacks analytical tools for predicting whether a dynamic finite element model of a mechanism should be utilized, or whether a simplified quasi-static analysis is justified prior to the manufacture and testing of a product. Furthermore, the ability to predict whether a specific link

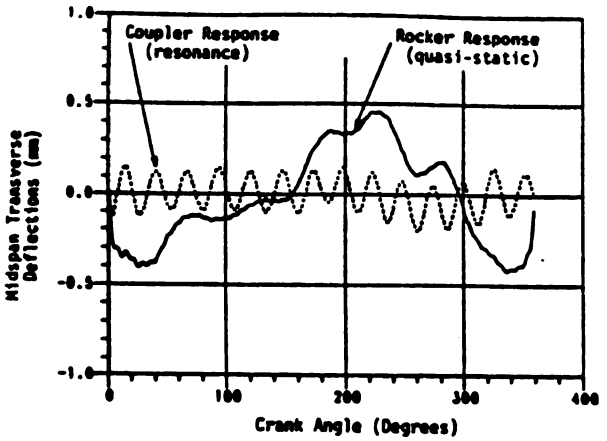

Fig. 8 Class 3 Mechanism; Coupler and Rocker Midspan Transverse Deflections at 281 rpm

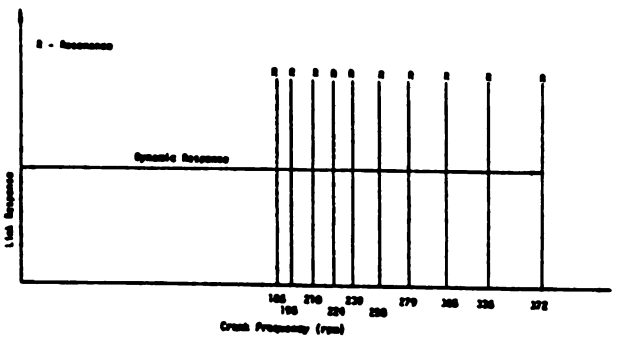

Fig. 9 Class 3 Mechanism; Coupler Response Regimes

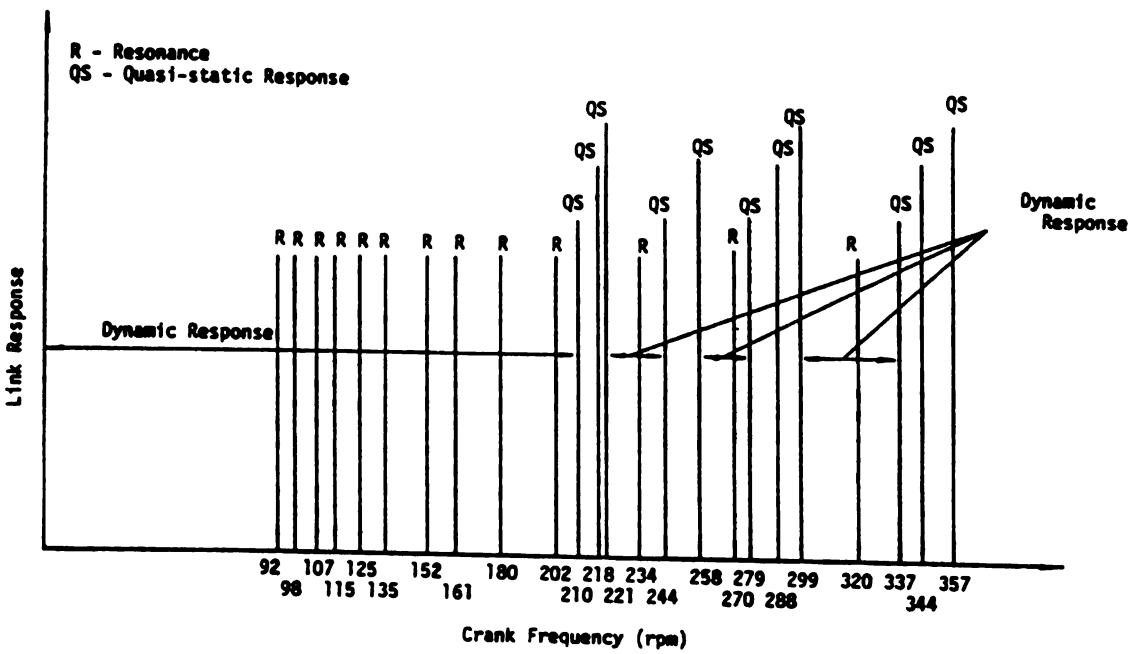

Fig. 10 Class 2 Mechanism; Coupler Response Regimes

will vibrate in a quasi-static regime, a dynamic regime, or in a state of super-harmonic resonance is also lacking.. Clearly design guidelines must be developed to address this significant void in the literature.

Figures 9-11 present the global response regimes of some of the links of the mechanisms studied in this investigation. The complex nature of the responses, which has been demonstrated in the previous figures, is again clearly evident upon reviewing these three sets of data. For the mechanisms systems tested, the flexural response was generally of a dynamic nature with resonance conditions observed at the indicated speeds. A typical set of response-regime data is presented in Figure 9. Quasi-static regimes were generally confined to narrow bands as demonstrated in Figures 10 and 11, but this was not universally the case as indicated by Figure 9 where this link did not develop a quasi-static response for the speed range tested. The observed resonance conditions are also indicated. The theoretical explanations for these perplexing situations undoubtedly requires a detailed nonlinear vibrational analysis.

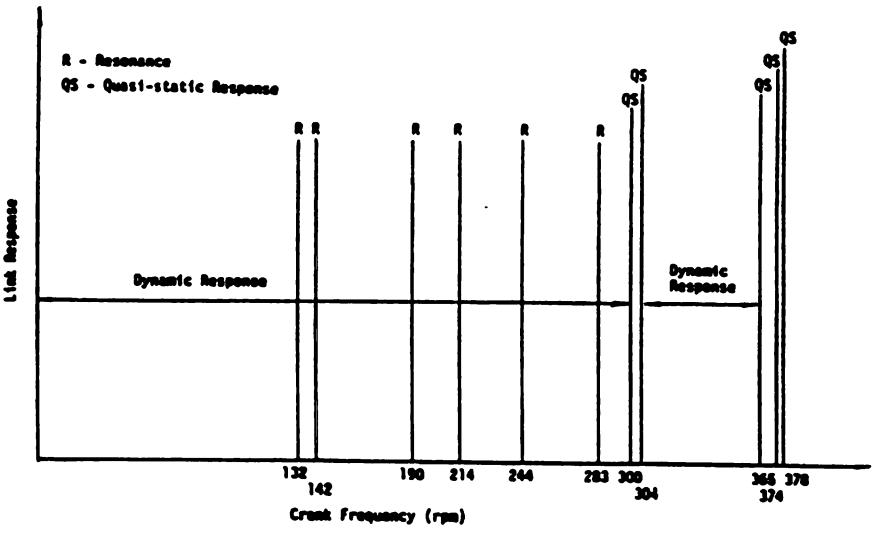

Fig. 11 Class 1 Mechanism; Rocker Response Regimes

CONCLUSIONS

An experimental study of flexible four-bar linkages has been presented which documents the different classes of flexural midspan elastodynamic responses of the coupler and rocker links, as being quasi-static, dynamic and resonant. While this terminology has been employed in the flexible mechanisms for some time, this investigation has uncovered for the first time a wide variety of response conditions which have not appeared in the literature before. It is anticipated that this experimental evidence will stimulate renewed theoretical activities in this area, from which design guidelines will be distilled for practicing engineers.

REFERENCES

1. Willmert, K.D., Thornton, W.A. and Khan, M.R., "A Hierarchy of Methods for Analysis of Elastic Mechanism with Design Application," ASME Paper No. 78-DET-56, 1978.

2. Sanders J.R., and Tesar, D., "The Analytical and Experimental Evaluation of Vibratory Oscillations in Realistically Proportioned Mechanisms," ASME, Journal of Mechanical Design, Vol. 100, 1978, pp. 762-768.

3. Haines, R.S., "On Predicting Vibrations in Realistically Proportioned Linkage Mechanisms," ASME, Journal of Mechanical Design, Vol. 103, 1981, pp. 706-711.

4. Thompson, B.S. and Ashworth, R.P., "Resonance in Planar Linkage Mechanisms Mounted on Vibrating Foundations," Journal of Sound and Vibration, Vol. 49, No. 3, 1976, (403-414).

5. Smith, M.R. and Maunder, L., "Stability of a Four-bar Linkage with Flexible Coupler," Journal of Mechanical Engineering Science, Vol. 13, No. 4, 1971, pp. 237-242.

6. Badlani, M. and Kleinhenz, W., "Dynamic Stability of Elastic Mechanisms," ASME Journal of Mechanical Design, Vol. 101, No. 1, 1979, pp. 149-153.

7. Bolotin, V.V., The Dynamic Stability of Elastic Systems, Holden-Day, San Francisco, 1964.

8. McLachlan, N.W., Theory and Application of Mathieu Function, Dover, New York, 1964.

9. Jandrasits, W.G. and Lowen, G.G., "The Elastic-dynamic Behavior of a Counterweighted Rocker Link with an Overhanging Endmass in a Four-bar Linkage," Part I: Theory; Part II: Application and Experiment, ASME Journal of Mechanical Design, Vol. 101, No. 1, 1979, pp. 77-78.

10. Kalaycioglu S. and Bagci, C., "Determination of the Critical Operating Speeds of Planar Mechanisms by the Actual Line Elements and Lumped Mass Systems," ASME Journal of Mechanical Design, Vol. 101, No. 2, 1979, pp. 210-223.

11. Cleghorn, W.L., Tabarrok, B., and Fenton, R.G., "Critical Running Speeds and Stability of High-Speed Flexible Mechanisms," Mechanism and Machine Theory, Vol. 19, No. 3, 1984, pp. 307-317.

THE ELASTODYNAMIC RESPONSE OF A CLASS OF INTELLIGENT MACHINERY, PART I, THEORY

THE ELASTODYNAMIC RESPONSE OF A CLASS OF INTELLIGENT MACHINERY – PART I: THEORY

K. Seong, D. Sunappan, Graduate Students and B. S. Thompson, Professor
Machinery Elastodynamics Laboratory
Department of Mechanical Engineering
Michigan State University
East Lansing, Michigan

ABSTRACT

A methodology is proposed, herein, for reducing the elastodynamic response of high-speed machine systems by introducing a retrofitment scheme which permits these systems to be subjected to an additional dynamical perturbational input which is computer-controlled. This paper is first of two companion papers which describe a comprehensive analytical and experimental investigation on a bread-board model of the concept, in which the objective is to reduce the vibrational response at the midspan of a flexible rocker link of a four-bar mechanism. A variational formulation is employed to develop the equations of motion governing the response of the flexible member which is subjected to combined parametric and forcing functions. In Part II of these companion papers, these equations are solved numerically and the viability of the approach is validated by comparing the analytical predictions with response data from a complementary experimental program.

INTRODUCTION

Intelligent machine systems have been the subject of numerous publications, principally in the context of robotic manipulators, but of course this terminology really pertains to a very broad class of machinery products which incorporate sensors and computers. The research reported herein, addresses the design of intelligent machinery in this broader context by proposing a general methodology for suppressing the elastodynamic response of linkage machinery.

The current generation of robotic systems are capable of undertaking many diverse tasks, and these significant capabilities are obtained by integrating a broad a spectrum of diverse technologies ranging from instrumentation, controls, computing and artificial intelligence to materials and machine dynamics [1,2]. In contrast to these robotics-orientated publications, herein, the focus of attention is the reduction of the elastodynamic response of flexible linkage machinery. This class of machinery features in a very broad range of both industrial and commercial machines and equipment, and these mechanism systems are prone to generate a vibrational response when operating in a high-speed mode. This response characteristic is attributed to the time-dependent inertial loading imposed upon the members of the articulating system, which are inherently an assemblage of flexible, not rigid, bodies. Typical contributions to this field include references [3-8].

The objective, herein, is to develop and then experimentally test the viability of a proposed methodology for reducing the elastodynamic response of flexible members of linkage mechanisms through the introduction of an additional microprocessor-controlled input into the original kinematic chain. The concept is evaluated by studying a bread-board model of the proposed methodology which comprises a retrofitted planar four-bar linkage with a flexible rocker link. The retrofitment involves modifying the normally stationary ground-link/rocker-link revolute joint to incorporate an additional prismatic joint whose perturbational motion is controlled by an electrodynamic shaker which is driven by an microprocessor-controlled arbitrary waveform/function generator. The resulting linkage can function as a classical four-bar mechanism by locking the prismatic joint, or alternatively, as a five-bar linkage when this locking device is released. In this latter mode, the system has two nominally rigid-body degrees of freedom with one input provided by the crank rotation and the second input provided by the motion of the microprocessor-controlled shaker. The equations of motion and the relevant boundary conditions for the flexible rocker link are derived, herein, using a variational technique, and the steady-state response is obtained using an approach developed in reference [9].

PROBLEM STATEMENT AND PROPOSED SOLUTION STRATEGY

Elastodynamic deflections, dynamic stresses, and fatigue considerations are all important design factors which must be carefully accounted for in the development of the next generation of machinery to operate in the international marketplace. The trend towards ultra-high operating speeds as a method for increasing productivity has exacerbated the design of modern machine systems and as a consequence of these

stimuli, the research community has responded by developing more sophisticated modeling techniques [10,11]. In addition to the enhanced predictive capabilities, described in the above review articles, the academic community has also developed two design methodologies for reducing the elastodynamic response of linkage machinery. The first advocates that the articulating members of these mechanical systems should be designed with optimal cross-sectional geometries and fabricated in the commercial metals [6,12,13]. The second advocates that the articulating members should be designed with polymeric composite laminates which are optimally-tailored for the specific application [14-16]. When implemented, the foregoing methodologies achieve a reduction in the levels of the dynamic response by increng the stiffness-to-weight ratios of the members by tailering the geometrical and material properties of the articulating members.

The rationale can be clarified by examining the terms in the approximate linear finite element equations of a general machine system presented below,

$$[M]^{-1}[K][U] + [M]^{-1}[C][\dot{U}] + [I][\ddot{U}] = -[I][\ddot{R}] \quad . \qquad (1)$$

In equation (1), [M], [K] and [C] are the global mass, stiffness and damping matrices respectively of the system, [I] is the identity matrix, (U) represents the discretized deformation field, the overdot denotes the time derivative and $(\ddot{R})$ represents the discretized rigid-body acceleration field. Thus for a prescribed machine system operating at a prescribed speed the elastodynamic response is principally dictated by the stiffness-to-mass ratio of the links.

In contrast to the foregoing methodologies [6,12-16] which focus on increasing the stiffness-to-mass ratio term on the left-hand-side of equation (1), the methodology proposed herein focuses on the right-hand-side of equation (1); namely the kinematic variables $(\ddot{R})$ which provide the principal system excitation in a high-speed mode of operation. Thus it is argued, if the magnitude of these variables can be reduced, then the magnitude of the forcing function will also be reduced, with a corresponding reduction in the elastodynamic response. This reduction in the elastodynamic response translates into a reduction in the dynamic deflections of the articulating members, a reduction in the associated dynamic stresses and also a reduction in the severity of the fatigue environment in which the members must operate. The idea was first reported in a theoretical publication [17] and some preliminary experimental work was presented in reference [18].

The proposed methodology would be implemented in practice by invoking the following procedure. The machine system under review would be operated at a prescribed speed and the elastodynamic response of a specific member, such as the output link, would be carefully monitored by strategically positioning sensors on the member. The sensor output would then be sampled, stored, and post-processed by a microprocessor prior to utilizing the profile of the dynamic deflection to suppress the motion of the vibrating link post-processed. This general vibration-suppression methodology would be implemented at any operating speed by feeding the experimental response-data to an arbitrary waveform function generator which would automatically synthesize the appropriate excitation voltage for an electrodynamic shaker. These latter operations would be performed by a microprocessor, hence, the term "intelligent machine." The shaker would then provide another dynamical input excitation to the output link via a retrofitment feature of the machine system. This retrofit scheme would involve replacing a normally fixed revolute joint by a prismatic joint, thereby permitting the introduction of a perturbational input to the system. Thus a machine system with n degrees of freedom would be retrofitted to generate (n+1) degrees of freedom. The perturbational input of the retrofitted system must be carefully orchestrated relative to the inputs of the original system in order to achieve the desired effect of reducing the elastodynamic response of the member targetted for response tailering.

The necessity for response tailoring, or actively suppressing the elastodynamic response of a machine system, are numerous and include the desire to reduce the severe elastodynamic responses associated with bearing degradation and dynamic instabilities resulting from the parasitic excitation of machine foundations; the need to control machine outputs in hostile hygrothermal environments; and to satisfy the demand for the development of a new generation of machines which generate more accurate output characteristics with more versatile performance envelopes.

ANALYTICAL MODEL OF AN INTELLIGENT MACHINE SYSTEM

The viability of the foregoing proposed general methodology for actively suppressing the elastodynamic response of distributed-parameter linkage systems was evaluated both analytically and experimentally by investigating the response of a bread-board laboratory model which operated open-loop. This model comprised a planar four-bar linkage with a flexible rocker link which was configured to principally vibrate in the plane of the mechanism. This classical single-input linkage system was retrofitted by introducing a second input at the revolute joint connecting the rocker-link and the ground-link, through the introduction of a prismatic joint. This prismatic joint permits the normally fixed ground-link length to be varied in a prescribed fashion when the five-bar linkage system operates in the computer-controlled mode, and in this mode, the system is termed an intelligent mechanism. The linkage system is shown schematically in Figure 1.

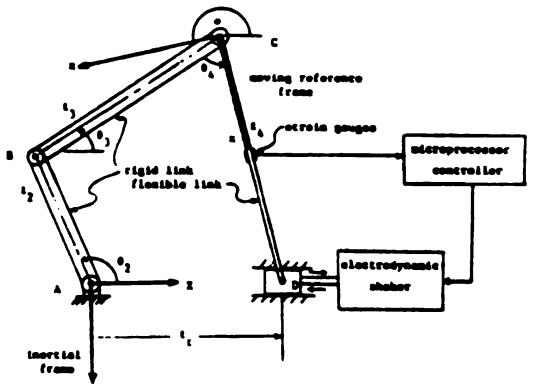

Figure 1. Schematic of Intelligent Mechanism.

An analytical model of the dynamical motion of the flexible rocker link of the intelligent machine system, which is subjected to both periodic and parametric forcing from the crank excitation and the perturbational excitation of the microprocessor-controlled shaker, was developed using a variational technique [19,20]. The technique is based on the introduction of approximating statements into a variational equation of motion prior to permitting arbitrary independent variations of the system variables which yields, as stationary conditions, the field equations and the associated boundary conditions for the particular boundary-value problem being investigated.

The relevant variational equation of motion [20] is

$$\delta J = \int_0^t \left\{ \int_V \left[-\rho\delta p_i [p_i - (\overset{*}{r}_{0i} + \overset{*}{u}_i + e_{ijk}\phi_j (r_{0k} + r_{Rk} + u_k))] \right.\right.$$

$$+ \delta\gamma_{ij}[\gamma_{ij} - (\partial W/\partial\gamma_{ij})]$$

$$+ \delta\tau_{ij}[\gamma_{ij} - \tfrac{1}{2}(u_{i,j} + u_{j,i} + u_{k,i}u_{k,j})]$$

$$\left. + \delta u_i [X_i + \tau_{ij,j} + u_{i,kj}\tau_{jk} + u_{i,k}\tau_{jk,j} - \rho\dot{p}_i]\right] dV$$

$$+ \int_{S_1} \delta u_i \, [\bar{g}_i - g_i - u_{i,k}g_k] dS_1$$

$$\left. - \int_{S_2} [\delta g_i + \delta u_{i,k}g_k + u_{i,k}\delta g_k] \, [\bar{u}_i - u_i] \, dS_2 \right\} dt = 0 \tag{2}$$

In equation (2), V defines the volume of an elastic body describing a general spatial motion relative to an inertial frame, while S_1 and S_2 sum to equal the total surface area, S, of the flexible body. The mass density is represented by ρ and p_i is the time rate of change of a position vector of a general point in the body. This position vector has components r_{0i}, which are the components relative to the moving body axes oxyz of the position vector of the origin of these body axes relative to the origin of the inertial frame, R_{Ri} which represent the position vector of a general point in the body in a reference state relative to the body axes and u_i, the deformation displacement vector.

The strain energy density is represented by W, γ_{ij} are the Lagrangian strain components, τ_{ij} are the stresses and X_i represent the body forces per unit volume. Prescribed surface tractions $\bar{g}_i$ are imposed on surface areas S_1 and prescribed surface displacements $\bar{u}_i$ on surface area S_2. The time rate of change of a quantity relative to the moving axes oxyz is represented by (*), ($\dot{}$) denotes the absolute rate of change and (,) defines spatial differentiation. Components of the angular velocity vector of the frame oxyz are represented by ϕ_i, and e_{ijk} is the alternating tensor.

This geometrically-nonlinear formulation has been selected for analyzing this class of flexible laboratory linkage because previous combined theoretical and experimental studies [4,8] have clearly demonstrated the superior predictive capabilities of the nonlinear model.

Approximations for the variables

Approximating statements for the system variables in equation (2) must be formulated so that it may be employed to construct the appropriate problem definition. The mechanism presented in 1 is assumed to have a rigid crank AB of length ℓ_2 which rotates at constant speed ϕ_2, a rigid coupler BC of length ℓ_3 and elastic rocker link CD of undeformed length ℓ_4 with a constant cross-sectional area A. The length of the ground link, ℓ_1, is time-dependent when the microprocessor activates the shaker. The system is assumed to be fabricated with smooth pin joints and the slider at point D is assumed to translate in a frictionless guide. Coordinates oxyz are Lagrangian axes fixed in the rocker link in an undeformed reference state which is defined by the angle ϕ_4 relative to the inertial frame OXYZ.

Deformations of the rocker link are restricted to simple axial and flexural components in the plane of the mechanism. The link is considered to be slender and the deformations small, hence the Euler-Bernoulli beam theory may be employed. The assumptions for the elastic deformations are

$$\begin{aligned} u_x &= u_o(x,t) - z\, w_{,x}(x,t) \\ u_y &= 0 \\ u_z &= w(x,t) \end{aligned} \tag{3}$$

The longitudinal stress τ_{xx} is assumed to consist of two components with the same format as the axial displacement. All other stresses are zero, except for τ_{xz}. Hence,

$$\begin{aligned} \tau_{xx} &= T_o(x,t) - zT_1(x,t) \\ \tau_{xz} &= T_2(x,t) \\ \tau_{yy} &= \tau_{zz} = \tau_{yz} = \tau_{xy} = 0 \end{aligned} \tag{4}$$

Similarly, for the strains,

$$\begin{aligned} \gamma_{xx} &= S_o(x,t) - zS_1(x,t) \\ \gamma_{yy} &= \gamma_{zz} = -\nu\,\gamma_{xx} \\ \gamma_{xy} &= \gamma_{yz} = 0 \\ \gamma_{xz} &= S_2(x,t) \end{aligned} \tag{5}$$

where ν is Poisson's ratio.

The velocity formats are assumed to be

$$\begin{aligned} p_x &= B(x,t) \\ p_y &= 0 \\ p_z &= C(x,t) \end{aligned} \tag{6}$$

The absolute angular velocity of the rotating frame oxyz relative to the inertial frame OXYZ is

$$\phi_x = 0 \quad , \quad \phi_y = \dot{\phi}_4 \quad , \quad \phi_z = 0 \tag{7}$$

The position vector describing the location of the origin of the moving axes oxyz relative to the inertial frame OXYZ has components

$$r_{ox} = \ell_t \cos\theta_4 - \ell_4$$
$$r_{oy} = 0$$
$$r_{oz} = \ell_t \sin\theta_4 \qquad (8)$$

measured relative to oxyz, and a general point P in the undeformed rocker link may be defined by the components

$$r_{Rx} = x$$
$$r_{Ry} = y$$
$$r_{Rz} = z \qquad (9)$$

Prescribed deformation displacements are to be imposed on a small region surrounding the centroid of the beam section at both the rocker-coupler joint and also the rocker-slider joint. The flexible link is considered to be a pinned-pinned beam, with the displacement constraints

$$\text{at} \quad x = 0, \quad \bar{u}_x = -zw_{,x} \quad \bar{u}_y = 0 \quad \bar{u}_z = 0 \qquad (10)$$

$$\text{and at } x = \ell_4 \quad \int_{S_3} (u_x \sin\theta_4 - u_z \cos\theta_4)\, dS_3 = 0.$$

This constraint equation defines the horizontal straight-line motion of the joint driven by the electromechanical shaker, and this constraint is imposed by the Lagrange multiplier $g_x/\cos\theta_4$. Prescribed surface tractions are imposed over the remainder of the sections at the ends of the link. Thus,

$$\text{at} \quad x = 0 \;, \quad \bar{g}_x = P(t)/A \;, \quad \bar{g}_y = 0 \;, \quad \bar{g}_z = Q(t)/A$$
$$\text{and at} \quad x = \ell_4 \;,$$

$$\bar{g}_x = \frac{1}{A}\left[N(t) \sin\theta_4 - F_s(t) \cos\theta_4 - M_s \dot{p}_x \right] \qquad (11)$$

$$\bar{g}_y = 0$$

$$\bar{g}_z = -\frac{1}{A}\left[N(t) \cos\theta_4 + F_s(t) \sin\theta_4 + M_s \dot{p}_z \right]$$

where P(t) and Q(t) are unknown pin force components, N(t) is the time-dependent reaction force exerted by the guide on the slider, $F_s(t)$ is the time-dependent force exerted by the shaker on the slider and M_s is the mass of the slider.

The flanks of the elastic link are assumed to be devoid of surface tractions. Hence

$$\bar{g}_x = \bar{g}_y = \bar{g}_z = 0 \qquad (12)$$

Construction of the problem definition

The equations of motion and boundary conditions are constructed by substituting the approximating statements (3) - (12) into the variational equation (2) prior to invoking the arbitrary independent nature of the variations in the system parameters. Upon substituting expressions (3) to (12) into the volume integrals in equation (2), this yields the expression

$$\int_x \Big\{ - \int_A \rho\delta B[B-(\dot{\ell}_t\cos\theta_4 - \ell_t\dot{\theta}_4\sin\theta_4 + \dot{u}_o - z\dot{w}_{,x}$$
$$+ \dot{\theta}_4(\ell_t\sin\theta_4 + z + w))]dA$$
$$- \int_A \rho\delta C[C-(\dot{\ell}_t\sin\theta_4 + \ell_t\dot{\theta}_4\cos\theta_4 + \dot{w}$$
$$- \dot{\theta}_4(\ell_t\cos\theta_4 - \ell_4 + x + u_o - zw_{,x}))]dA$$
$$+ \int_A [(\delta S_o - z\delta S_1)\Big\{T_o - zT_1 - \frac{\partial\chi}{\partial\tau_{xx}}$$
$$+ \nu\Big\{\frac{\partial\chi}{\partial\tau_{yy}} + \frac{\partial\chi}{\partial\tau_{zz}}\Big\}\Big\} + \delta S_2(2T_2 - 4GS_2)]dA$$
$$+ \int_A (\delta T_o - z\delta T_1)[S_o - zS_1 - \tfrac{1}{2}\{2(u_{o,x} - zw_{,xx}) + w^2_{,x}$$
$$+ (u_{o,x} - zw_{,xx})^2\}]dA$$
$$+ \int_A \delta T_2[S_2 - \tfrac{1}{2}(u_{o,x} - zw_{,xx})(-w_{,x})]dA$$
$$+ \int_A (\delta u_o - z\delta w_{,x})(\tau_{xj,j} + u_{x,jk}\tau_{kj}$$
$$+ u_{x,k}\tau_{kj,j} - \rho\dot{p}_x]dA$$
$$+ \int_A \delta w(\tau_{zj,j} + u_{z,jk}\tau_{kj} + u_{z,k}\tau_{kj,j}$$
$$- \rho\dot{p}_z]dA\Big\}\,dx = 0 \qquad (13)$$

The first two integrals yield the velocity statements

$$B = \dot{\ell}_t\cos\theta_4 + \dot{u}_o + w\dot{\theta}_4$$
$$C = \dot{\ell}_t\sin\theta_4 + \dot{w} - \dot{\theta}_4(x + u_o - \ell_4) \qquad (14)$$

which may be differentiated to provide the absolute acceleration components

$$\dot{B} = \ddot{\ell}_t\cos\theta_4 + 2\dot{w}\dot{\theta}_4 + w\ddot{\theta}_4 + \ddot{u}_o - \dot{\theta}_4^2(x + u_o - \ell_4)$$
$$\dot{C} = \ddot{\ell}_t\sin\theta_4 - 2\dot{u}_o\dot{\theta}_4 + \ddot{w} - w\dot{\theta}_4^2 - \ddot{\theta}_4(x + u_o - \ell_4) \qquad (15)$$

The link material from which the rocker is fabricated is assumed to be an elastic isotropic monolithic material. Hence by substituting the appropriate expression for the strain energy function W into the third integral of expression (13), the following statements emerge,

$$T_o = ES_o \,, \quad T_1 = ES_1 \,, \quad T_2 = 2GS_2 \tag{16}$$

where E is the Young's modulus and G is the modulus of rigidity.. The fourth and fifth integrals yield, upon integration,

$$\begin{aligned} S_o &= u_{o,x} + \tfrac{1}{2} u_{o,x}^2 + \tfrac{1}{2} w_{,x}^2 + \frac{I}{2A} w_{,xx}^2 \\ S_1 &= w_{,xx} (1 + u_{o,x}) \\ S_2 &= -\tfrac{1}{2} u_{o,x} w_{,x} \end{aligned} \tag{17}$$

where I is the second moment of area of the beam cross-section relative to the plane of bending. Upon neglecting the body force, X_i, the sixth and seventh integrals in equation (13) are integrated-by-parts to yield the equations of motion,

$$\begin{aligned} &\int_V \delta u_o [\tau_{xx,x} + (u_{x,x} \tau_{xx})_{,x} + (u_{x,z} \tau_{xz})_{,x} - \rho \dot{p}_x] \, dV \\ &+ \int_V \delta w \, [(u_{z,x} \tau_{xx})_{,x} - (u_{x,x} \tau_{xz})_{,x} + z \tau_{xx,xx} \\ &+ (z \, u_{x,x} \tau_{xx})_{,xx} \\ &+ (z \, u_{x,z} \tau_{xz})_{,xx} - z \rho \dot{p}_{x,x} - \rho \dot{p}_z] \, dV = 0 \end{aligned} \tag{18}$$

and the natural boundary terms,

$$\begin{aligned} &\int_x \int_y [\delta u_o - y \, \delta w_{,x}) \tau_{xz} (1 + u_{x,x}) + \delta w \, \tau_{xz} \, u_{z,x}]_z dxdy \\ &+ \int_z \int_y \delta w \, [\tau_{xz}(1 + u_{x,x}) - z \, [\tau_{xx,x} + (u_{x,x} \tau_{xx})_{,x} \\ &+ (u_{x,z} \tau_{xz})_{,x} - \rho \dot{p}_x] \,]_x dydz \end{aligned} \tag{19}$$

Upon substituting equations (15), (16) and (17) into equation (18) and then performing the integration, the final form of the coupled axial and flexural equations of motion emerge. The axial equation of motion is

$$\begin{aligned} &EA(u_{o,xx} + w_{,x} w_{,xx} + u_{o,x} u_{o,xx} + \frac{I}{A} w_{,xx} w_{,xxx}) \\ &+ \left\{ EAu_{o,x} [u_{o,x} + \tfrac{1}{2}(w_{,x}^2 + u_{o,x}^2 + \frac{I}{A} w_{,xx}^2)] \right. \\ &\left. + EIw_{,xx}^2 (1 + u_{o,x}) \right\}_{,x} + \left\{ AGu_{o,x} w_{,x}^2 \right\}_{,x} \\ &- \rho A \, [\ddot{\ell}_c \cos\theta_4 + \ddot{u}_o + \ddot{\theta}_4 w \\ &+ 2\dot{\theta}_4 \dot{w} - \dot{\theta}_4^2 (u_o + x - \ell_4)] = 0 \end{aligned} \tag{20}$$

and the flexural equation of motion is

$$\begin{aligned} &EI \left\{ w_{,xx} \left[1 + 2 \, u_{o,x} + \tfrac{1}{2} u_{o,x}^2 + \tfrac{1}{2} w_{,x}^2 + \frac{I}{2A} w_{,xx}^2 \right] \right\}_{,xx} \\ &- EA \left[w_{,x} \left(u_{o,x} + \tfrac{1}{2} u_{o,x}^2 + \tfrac{1}{2} w_{,x}^2 + \frac{I}{2A} w_{,xx}^2 \right)_{,x} \right] \\ &- AG \left(u_{o,x}^2 w_{,x} \right)_{,x} + \rho A \ddot{C} = 0 \end{aligned} \tag{21}$$

The boundary conditions associated with these equations of motion are established by combining the fifth and sixth terms in equation (2) with natural boundary terms (19), prior to the substitution of statements (10), (11) and (12).

At the rocker-coupler pin joint, prescribed deformations are imposed on a small region of the centroid of the section. Upon invoking the assumption of plane normal ends to the link, the kinematic boundary conditions at x=0 emerge. They are

$$u_o = w = 0 \tag{22}$$

Over the remainder of the section, the prescribed surface tractions must be combined with the natural boundary term in expression (19) to be evaluated at constant x. Integrating over the beam section yields the following expressions,

at x = 0,

$$\begin{aligned} &P(t) + EA[u_{o,x} + \tfrac{1}{2} u_{o,x}^2 + \tfrac{1}{2} w_{,x}^2 + \frac{I}{2A} w_{,xx}^2] (1 + u_{o,x}) \\ &+ EIw_{,xx}^2 (1 + u_{o,x}) + AGu_{o,x} w_{,x}^2 = 0 \\ &EIw_{,xx} [1 + 3u_{o,x} + \tfrac{3}{2} u_{o,x}^2 + \tfrac{1}{2} w_{,x}^2 + \frac{I}{2A} w_{,xx}^2] = 0 \end{aligned} \tag{23}$$

$$\begin{aligned} &Q(t) + EAw_{,x} [u_{o,x} + \tfrac{1}{2} u_{o,x}^2 + \frac{I}{2A} w_{,xx}^2 + \tfrac{1}{2} w_{,x}^2] \\ &- EI[w_{,xxx}[1 + u_{o,x}] - w_{,xx} [w_{,xxx} - u_{o,xx}]] (1 + u_{o,x}) \\ &+ AGu_{o,x}^2 w_{,x} - EI \left\{ w_{,xx} [u_{o,x} + \tfrac{1}{2} u_{o,x}^2 + \tfrac{1}{2} w_{,x}^2 \right. \\ &\left. + \frac{I}{2A} w_{,xx}^2] \right\}_{,x} = 0 \end{aligned}$$

On the beam flanks, the prescribed surface traction condition must be combined with the natural boundary terms in expression (19) to be evaluated at constant y. The result is identically zero.

Equation (10) yields

$$u_o \sin\theta_4 - w \cos\theta_4 = 0 \tag{24}$$

The statement for the prescribed surface tractions which are imposed on the major portion of the beam section at the rocker-slider pin must be combined with the natural boundary term and this yields, upon integration, the conditions at $x = \ell_4$. These statements are

$$N(t)\sin\theta_4 - F_s(t)\cos\theta_4 - M_s(\dot{p}_x)_{x=\ell_4}$$

$$- EA(1+u_{o,x})\left\{u_{o,x} + \tfrac{1}{2}u_{o,x}^2 + \tfrac{1}{2}w_{,x}^2 + \frac{I}{2A}(w_{,xx}^2)\right\}$$

$$- EIw_{,xx}^2(1 + u_{o,x}) - AGu_{o,x}w_{,x}^2 = 0$$

$$EIw_{,xx}(1 + 3u_{o,x} + \tfrac{3}{2}u_{o,x}^2 + \tfrac{1}{2}w_{,x}^2 + \frac{I}{2A}w_{,xx}^2 = 0 \quad (25)$$

$$-N(t)\cos\theta_4 - F_s(t)\sin\theta_4 - M_s(\dot{p}_z)_{x=\ell_4}$$

$$- EAw_{,x}(u_{o,x} + \tfrac{1}{2}u_{o,x}^2 + \tfrac{1}{2}w_{,x}^2)$$

$$+ \frac{I}{2A}w_{,xx}^2 + EI(w_{,xx}[1 + u_{0,x}]$$

$$- w_{,xx}[w_{,xxx} - u_{o,xx}])(1 + u_{o,x})$$

$$+ EI\left\{w_{,xx}[u_{o,x} + \tfrac{1}{2}u_{o,x}^2 + \tfrac{1}{2}w_{,x}^2 + \frac{I}{2A}w_{,xx}^2]\right\}_{,x} = 0$$

SOLUTION PROCEDURE

The problem definition is now complete since equations of motion and the corresponding boundary conditions have been constructed. Thus the objective now is to simplify the equations sufficiently to permit the use of a standard solution procedure. The approach involves adopting a model superposition approach prior to solving the resulting Hill's equation by a technique developed in reference [9].

The forcing frequency of a link is much lower than the first natural frequency in the axial mode, and hence the axial vibration may be neglected. If second and higher-order terms are assumed to be small in equation (20), then upon integration with respect to x yields a general statement for the axial force in the link. Thus

$$EAu_{0,x} = \rho A\ddot{\ell}_t\cos\theta_4(x - \ell_4) - \rho A\dot{\theta}_4^2[\tfrac{1}{2}x^2 - \ell_4 z + \ell_4^2]$$

$$+ N(t)\sin\theta_4 - F_s(t)\cos\theta_4 - M_s(\dot{p}_x)_{x=\ell_4} \quad (26)$$

Attention is now focussed on equation (21). Upon neglecting the shear term, second- and higher-order terms in the coefficient of EI and third-order terms in the coefficient of EA, this equation reduces to

$$EIw_{,xxxx} - EAu_{o,x}w_{,xx} - EAu_{o,xx}w_{,x} + \rho A\ddot{C} = 0 \quad (27)$$

Substituting (26) into (27) yields the governing coupled equation for the flexural motion of the rocker link

$$EIw_{,xxxx} - \left\{\rho Ax\ddot{\ell}_t\cos\theta_4 - \rho A\dot{\theta}_4^2(\tfrac{1}{2}x^2 - \ell_4 x)\right.$$

$$+ N(t)\sin\theta_4 - F_s(t)\cos\theta_4 - M_s(\dot{p}_x)_{x=\ell_4}$$

$$\left. - \rho A\ell_4\ddot{\ell}_t\cos\theta_4 - \tfrac{3}{2}\ell_4\dot{\theta}_4^2\right\}w_{,xx} + [-\rho A\ddot{\ell}_t\cos\theta_4$$

$$+ \rho A\dot{\theta}_4^2(x-\ell_4)]w_{,x} + \rho A[\ddot{\ell}_t\sin\theta_4 + \ddot{w} - w\dot{\theta}_4^2$$

$$- \ddot{\theta}_4(x-\ell_4)] = 0 \quad (28)$$

Equation (28) may be solved using a procedure employing normal modes. The standard form of the solution is

$$w(x,t) = \sum_{i=1}^{n} W_n(t)\,\phi_n(x) \quad (29)$$

where $W_n(t)$ are unknowns and $\phi_n(x)$ are the mode shapes. In accordance with the standard approach, the derivatives of equation (29) are substituted into equation (28) and upon invoking the orthogonality condition after multiplying by $\phi_m(x)$, yields the inhomogeneous Hill's equation

$$\ddot{W}(t) + W(t)\left[\frac{EIC_1}{\rho AC_7} - \frac{C_2+C_5}{C_7}\ell_4\dot{\theta}_4^2 + \frac{C_3+\frac{1}{2}C_6-C_7}{C_7}\dot{\theta}_4^2\right.$$

$$+ \frac{C_4}{\rho AC_7}\left[-N(t)\sin\theta_4 + F_s(t)\cos\theta_4 + \frac{m\ell_4}{2}\dot{\theta}_4^2\right]$$

$$\left. + \left\{+\frac{M_sC_4}{\rho AC_7} - \frac{C_2+C_5}{C_7} + \frac{C_4}{C_7}\ell_4\right\}\ddot{\ell}_t\cos\theta_4\right]$$

$$- \left[\frac{C_9-C_8\ell_4}{C_7}\right]\ddot{\theta}_4 - \frac{C_8}{C_7}\ddot{\ell}_t\sin\theta_4 \quad (30)$$

Thus, this linear inhomogeneous differential equation has periodic coefficients and the system is subjected to forcing excitations of a periodic nature. Restricting the investigation to the first mode response, the constants $C_i (i = 1,2,\ldots,9)$ are given by

$$C_1 = \int_o^{\ell_4}\phi_n\phi_n^{IV}\,dx \qquad C_5 = \int_o^{\ell_4}\phi_n\phi_n''\,x\,dx$$

$$C_2 = \int_o^{\ell_4}\phi_n\phi_n'\,dx \qquad C_6 = \int_o^{\ell_4}\phi_n\phi_n''\,x^2\,dx$$

$$C_3 = \int_o^{\ell_4}\phi_n\phi_n'\,x\,dx \qquad C_7 = \int_o^{\ell_4}\phi_n^2\,dx \quad (31)$$

$$C_4 = \int_o^{\ell_4}\phi_n\phi_n''\,dx \qquad C_8 = \int_o^{\ell_4}\phi_n\,dx$$

$$C_9 = \int_o^{\ell_4}\phi_n x\,dx$$

where (') denotes a spatial derivative with respect to x.
These constants may be evaluated using the tables in reference [21]. The first term in the coefficient of W in equation (30) yields the natural frequency ω_n of the stationary link. This observation permits the Hill's equation to be written in the simpler form,

$$\ddot{W}(t) + W(t)[\omega_n^2 + r(t)] = R(t) \tag{32}$$

The quasi-static response of the rocker link can be obtained simply by neglecting the dynamic term in W and solving the following algebraic relationship for the amplitude of the transverse deflection W(t),

$$W(t)[\omega_n^2 + r(t)] = R(t) \tag{33}$$

The elastodynamic response of the rocker link is obtained from the steady-state solution to equation (32). This is accomplished, herein, by employing the approach developed in reference [9].

Equation (32) is first written in the standard state-variable form as

$$\dot{x}(t) = C(t)x(t) + f(t) \tag{34}$$

where

$$x(t) = \begin{Bmatrix} x_1(t) \\ x_2(t) \end{Bmatrix} = \begin{Bmatrix} W(t) \\ \dot{W}(t) \end{Bmatrix}, \quad C(t) = \begin{bmatrix} 0 & 1 \\ -[\omega_n^2 + r(t)] & 0 \end{bmatrix},$$

$$f(t) = \begin{Bmatrix} 0 \\ R(t) \end{Bmatrix} \tag{35}$$

In the above equation x is a vector, C is real coefficient matrix periodic in t with period τ_o and f is also periodic vector in t but with period τ_f. For the intelligent mechanism being analyzed, τ_o would be the period of crank rotation and τ_f would be the period of the shaker excitation.

Let $\Phi(t)$ be the fundamental matrix for the solution of the homogeneous equation corresponding to equation (34). Furthermore, assume that the fundamental matrix equals the identity matrix at time t=0, and in addition, at this time f(t) is zero. The solution of equation (34) is then given by

$$x(t) = \Phi(t)(x(0) - (I - H)^{-1}Hg) + x_f(t) , \tag{36}$$

where the first term on the right-hand side is the solution to the homogeneous equation and $x_f(t)$ is the steady-state response which is given by the expression

$$x_f(t) = \Phi(t)\left\{\Phi^{-1}(s)f(s)ds + (I - H)^{-1}Hg\right\} \tag{37}$$

In equation (37), I is the identity matrix, and s is the dummy integral variable.

The quantities $\int_o^t \Phi^{-1}(s)f(s)ds$ and g appearing in equation (37) are evaluated by using the Trapezoidal rule of numerical integration. The final form of steady-state solution is given by

$$x_f(t_\kappa) = X_\kappa + \Phi(t_\kappa)(I - H)^{-1}X_\kappa, \quad \kappa = 0,1,2,\ldots,K \tag{38}$$

where

$$X_o = 0$$

$$X_\kappa = \Delta\left\{\frac{1}{2}\left[\prod_{j=1}^{\kappa}\varphi_j(\Delta)\right]f_o + \sum_{i=2}^{\kappa}\left[\prod_{i=2}^{\kappa}\varphi_i(\Delta)\right]f_{i-1} + \frac{1}{2}f_k\right\} \tag{39}$$

where the term Δ represents the time-step employed in the numerical integration. Furthermore,

$$H = \left[\prod_{j=1}^{\kappa}\varphi_j(\Delta)\right]$$

$$\Phi(0) = I,$$

$$\Phi(t_\kappa) = \prod_{j=1}^{\kappa}\varphi_j(\Delta), \quad \kappa = 1,2,\ldots,K \tag{40}$$

$$\Delta = \frac{\tau_o}{K}$$

$$f_j = f(t_j)$$

where for this investigation, K = 360 which governs the size of the timestep. The equations are written by assuming similar frequencies for the crank and shaker excitation.

An efficient expression for $\varphi_j(\Delta)$ may be evaluated using Scheme I of reference [9] which is given by

$$\varphi_j(\Delta) = \exp(C_j\Delta) \tag{41}$$

and permits equation (41) to be written as

$$\varphi_j(\Delta) = \begin{bmatrix} \cos\omega_j\Delta & \frac{1}{\omega_j}\sin\omega_j\Delta \\ -\omega_j\sin\omega_j\Delta & \cos\omega_j\Delta \end{bmatrix}\exp(-\Delta) \tag{42}$$

where $\omega_j = [\omega_n^2 + r_j(t)]^{1/2}$.

This completes the development of the mathematical apparatus necessary for predicting the elastodynamic response of the intelligent mechanism system schematically presented in Fig. 1 since upon substituting equations (39) - (42) into equation (38) the steady-state response or the amplitude of deflection of the rocker link may be evaluated at discrete time steps. In the companion paper [22] this proposed solution strategy is evaluated by comparing the results of the computer simulations with experimental results from a complementary investigation of a bread-model in the laboratory.

ACKNOWLEDGEMENTS

This material is based upon work supported by the Division of Engineering Research at Michigan State University. This funding is gratefully acknowledged.

REFERENCES

1. Robotics: Theory and Application, Paul, F.W., and Youcef-Toumi (eds.), ASME book DSC-Vol. 3, 1986.

2. Robotics Research and Advanced Applications, Book, W.J., (ed.), ASME Book H00236, 1982.

3. Shabana, A., and Wehage, R.A., "Variable Degree of Freedom Component Mode Analysis of Inertia Variant Flexible Mechanical Systems," ASME Journal of Mechanisms, Transmissions, and Automation in Design, Vol. 105, No. 3, 1983, pp. 371-378.

4. Turcic, D.A., and Midha, A., "Generalized Equations of Motion for the Dynamic Analysis of Elastic Mechanism Systems," ASME Journal of Dynamic Systems, Measurement and Control, Vol. 106, No. 4, 1984, pp. 243-248.

5. Midha, A., Erdman, A.G., and Frohrib, D.A., "Finite Element Approach to Mathematical Modeling of High-Speed Elastic Linkages," Mechanism and Machine Theory, Vol. 13, 1978, pp. 603-618.

6. Kakatsios, A.J., and Tricamo, S.J., "Integrated Kinematic and Dynamic Optimal Design of Flexible Planar Mechanisms," ASME Paper 86-DET-73, and ASME Journal of Mechanisms, Transmissions, and Automation in Design, (to appear).

7. Tennant, D.W., Willmert, K.D., and Sathymoorthy, M., "Finite Element Nonlinear Vibrational Analysis of Planar Mechanisms," Material Nonlinearity in Vibration Problems, ASME Book AMD-Vol. 71, M. Sathymoorthy, (ed.), pp. 79-89, 1985.

8. Thompson, B.S., and Sung, S.K., "A Variational Formulation for the Nonlinear Finite Element Analysis of Flexible Linkages: Theory, Implementation and Experimental Results," ASME Journal of Mechanisms, Transmissions, and Automation in Design, Vol. 106, No. 4, Dec. 1984, pp. 482-488.

9. Hsu, C.S., and Cheng, W.M., "Steady-State Response of a Dynamical System under Combined Parametric and Forcing Excitations," ASME Journal of Applied Mechanics, Vol. 41, 1974, pp. 371-378.

10. Lowen, G.G., and Chassapis, C., "The Elastic Behavior of Linkages: An Update," Mechanism and Machine Theory, Vol. 21, No. 1, 1986, pp. 33-42.

11. Thompson, B.S., and Sung, C.K., "A Survey of Finite Element Techniques in Mechanism Design," Mechanism and Machine Theory, Vol. 21, No. 4, 1986, pp. 351-359.

12. Cleghorn, W.L., Fenton, R.G., and Tabarrok, B., "Optimum Design of High Speed Flexible Mechanisms," Mechanism and Machine Theory, Vol. 16, No. 4, 1981, pp. 399-406.

13. Zhang, Ce, and Grandin, H.T., "Optimum Design of Flexible Mechanisms," ASME Journal of Mechanisms, Transmissions and Automation in Design, Vol. 105, 1983, pp. 267-272.

14. Sung, C.K., Thompson, B.S., Crowley, P. and Cuccio, J., "An Experimental Study to Demonstrate the Superior Response Characteristics of Mechanisms Constructed with Composite Laminates," Mechanism and Machine Theory, Vol. 21, No. 2, 1986, pp. 103-119.

15. Thompson, B.S. and Sung, C.K., "The Design of Robots and Intelligent Manipulators using Modern Composite Materials," Mechanism and Machine Theory, Vol. 20, No. 6, 1985, p. 471-482.

16. Sung, C.K. and Thompson, B.S., "A Theoretical and Experimental Study of the Response of Linkage Mechanisms Fabricated with Composite Laminates," Journal of Sound and Vibration, Vol. 111, No. 3, Dec. 1986, pp. 399-428.

17. Oliver, J.H., Wysocki, D.A., and Thompson, B.S., "The Synthesis of Flexible Linkages by Balancing Tracer Point Quasi-Static Deflections using Microprocessor and Advanced Materials Technologies," Mechanism and Machine Theory, Vol. 20, No. 2, 1985, pp. 103-114.

18. Thompson, B.S., Soong, K., and Sung, C.K., "An Experimental Bread-Board Model for a Class of Intelligent High-Speed Machinery," Proceedings of the Ninth OSU Applied Mechanisms Conference, Kansas City, MO, Oct. 1985, Vol. II, pp. IV-1 to IV-4.

19. Thompson, B.S., and Barr, A.D.S., "A Variational Principle for the Motion of Components of Elastic Mechanisms," Proceedings of the Fourth World Congress on the Theory of Machines and Mechanisms, Newcastle Upon Tyne, U.K., 1975, 2, pp. 235-239.

20. Thompson, B.S., "The Analysis of an Elastic Four-Bar Linkage on a Vibrating Foundation Using a Variational Method," ASME Journal of Mechanical Design, Vol. 120, No. 2, 1980, pp. 320-328.

21. Bishop, R.E.D., and Johnson, D.C., Vibration Analysis Tables, Cambridge University Press, London, 1956.

22. Sunappan, D., Soong, K., and Thompson, B.S., "The Elastodynamic Response of a Class of Intelligent Machinery, Part II: Computational and Experimental Results," submitted for publication in ASME Journal of Vibration, Acoustics, Stress and Reliability in Design.

THE ELASTODYNAMIC RESPONSE OF A CLASS OF INTELLIGENT MACHINERY, PART II, COMPUTATIONAL AND EXPERIMENTAL RESULTS

THE ELASTODYNAMIC RESPONSE OF A CLASS OF INTELLIGENT MACHINERY – PART II: COMPUTATIONAL AND EXPERIMENTAL RESULTS

D. Sanagpan, K. Seong, Research Students and B. S. Thompson, Professor
Machinery Elastodynamics Laboratory
Department of Mechanical Engineering
Michigan State University
East Lansing, Michigan

ABSTRACT

This paper, together with a companion paper [1], describes a comprehensive theoretical and experimental investigation on a methodology proposed for suppressing the elastodynamic response of flexible mechanisms. This methodology involves retrofitting the original mechanism by the introduction of a microprocessor-controlled perturbational motion at one of the normally fixed ground-link joints. The orchestration of this motion will, it is hypothesized, enable the inertial loading on the flexible members to be reduced and consequently the magnitude of the elastodynamic response will also be reduced. In Part I of two companion papers, the theoretical developments are presented. Part II presents an experimental investigation of a four-bar linkage with a flexible rocker link, which was then retrofitted to provide an additional, microprocessor-controlled, input. The magnitude of the midspan deflections of the retrofitted mechanism were less than those of the original mechanism over a broad range of operating speeds thereby validating the proposed methodology for this class of mechanism system.

INTRODUCTION

The design of high-speed machinery requires the development of methodologies which incorporate the assumption that these systems are assemblages of flexible bodies. Strategies for reducing the dynamic deflections and stresses associated with these systems have focussed on the design of link members with high stiffness-to-weight ratios, and two methodologies have been proposed for solving this class of problems. One methodology proposes the fabrication of links in monolithic materials and the other proposes the fabrication of links in advanced polymeric composite materials [2,3].

In sharp contrast to these strategies, which focus on the link materials and the geometrical configuration of the members, the strategy proposed herein is based on the proposition that if an additional, tailored dynamical input is introduced into the machine system, then the inertial loading on a specific member can be suppressed and consequently the peak amplitude of the elastodynamic response can also be reduced. This approach would therefore create more accurate output characteristics and a superior dynamical environment from a fatigue standpoint. More details on this proposed methodology are presented in Part I of these two-part companion papers [1].

In order to test the viability of the proposed methodology, a four-bar linkage with a flexible rocker link was studied. The objective of the study was to reduce the amplitude of the midspan transverse deflections of the link by retrofitting the rocker/ground-link joint with a prismatic joint whose translational motion was microprocessor-controlled. A variational approach was adopted in order to establish the equation of motion governing the flexural response of the rocker link as a function of the crank rotation and the characteristics of the microprocessor-controlled slider. Herein, the complementary experimental program is described, and response curves presented to validate both the methodology and also the proposed mathematical model for the flexible rocker link. This research strategy, based on the scientific method, has been adopted by other researchers in order to validate proposed methodologies. A flavor of this work is presented in references [4-7].

EXPERIMENTAL APPARATUS

A photograph of the experimental mechanism employed in this investigation is presented in Figure 1 from which it is evident that gravitational loading was perpendicular to the plane of the mechanism and the mechanism was bolted to a large cast-iron test stand to provide a substantial rigid foundation. A 0.75 h.p. Dayton variable speed d.c. electric motor which was also bolted to the test stand, powered the linkage through a 19.05 mm diameter shaft supported on a pair of Timken tapered roller bearings type TS4A-6. On the left-hand-side of Fig. 1, the 100 mm diameter flywheel which was keyed to the shaft is clearly evident. This flywheel provided a large inertia in the drive-train to ensure a constant crank frequency, when operating in unison with the speed controller of the motor.

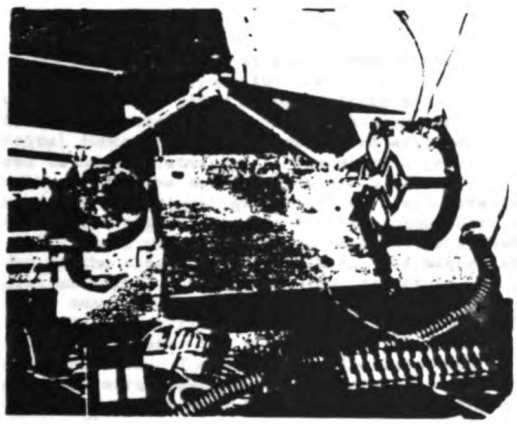

Fig. 1 Experimental Intelligent Mechanism

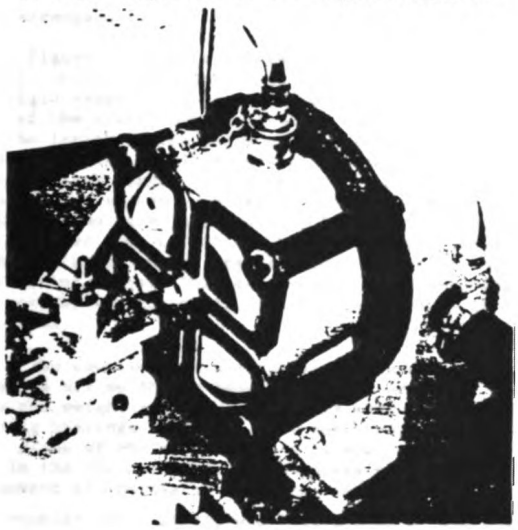

Fig. 2 Microprocessor-Driven Retrofittment

The microprocessor-controlled retrofitted joint of the intelligent mechanism is clearly illustrated on the right-hand-side of Figure 1. This joint was activated by a Ling Dynamic Systems V411 air-cooled vibrator with an auxiliary load-bearing platform type AX 400 which was driven by a Hafler power amplifier, model P500, which amplified signals from a Wavetek 12 MHz digital arbitrary function generator, model 275. Figure 2 presents a photograph of the microprocessor-driven retrofittment. The principal subassembly of the prismatic joint was an aluminum Microslides, Inc. crossed-roller slide assembly, model A-2020. This precision assembly was bolted to the vibrator head of the shaker using a fixture which incorporated a Bruel & Kjaer force transducer, type 8200, which permitted the force between the shaker and the slider to be carefully monitored. This arrangement was developed as a safety measure to protect the shaker against damage by the potentially large external forces developed by the mechanism. The acceleration imposed by the shaker upon the slide-assembly was monitored by a Bruel & Kjaer accelerometer type 4731, mounted directly on the reciprocating section of the slide-assembly. The output from the two transducers were fed to Bruel & Kjaer charge amplifiers, type 2635, which enabled the force, displacement, velocity and acceleration characteristics of the slide-assembly to be continuously monitored. Figure 3 presents a schematic of the instrumentation employed in the experimental investigation.

The speed of the electric motor powering the mechanism was directly measured in revolutions per minute by a Hewlett Packard 5314A universal counter which was activated by an electro-magnetic pickup, model 58423, manufactured by Electro Corporation which sensed a sixty tooth spur gear mounted on the crank shaft of the mechanism. This arrangement provided visual feedback to the operator by permitting the speed controller of the motor to be easily adjusted when establishing the desired operating frequency of the crank.

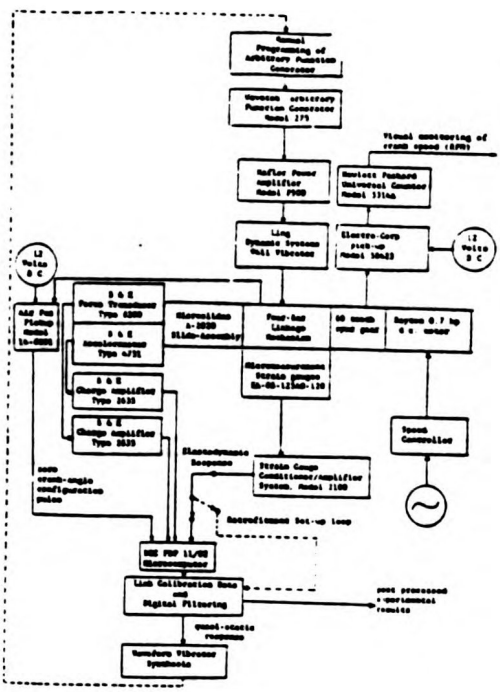

Fig. 3 Schematic Diagram of the Instrumentation and Apparatus

Electrical resistance strain gages, type EA-06-125AD-120 manufactured by Micromeasurements Inc., were bonded to the midspan of the flexible steel rocker link shown in the upper right-hand-corner of Figure 2, and the midspan deflections were monitored by a Micromeasurements Group Inc., strain gage conditioner/amplifier system type 2100. In order to relate the strain-gage signal to the configuration of the experimental mechanism, another transducer arrangement was established. An Airpax type 14-001 zero-velocity digital pickup was employed to sense the bolt-head at the end of the crank, when the mechanism is in the position of zero-degree crank angle.

The signal from the Airpax pickup in the zero-degree crank angle configuration was fed to the Wavetek function generator in order to orchestrate the excitation of the shaker in unison with crank motion. This digital function generator permitted arbitrary waveforms to be generated for a very wide range of frequencies. Once the desired waveform has been programmed into the signal generator, this waveform is triggered by the signal from the Airpax pickup prior to being amplified by the Hafler power amplifier and then being fed to the electrodynamic shaker. The mechanism configuration signal, the output from the strain gauges, the output from the accelerometer and the output from the force transducer were all fed to a DEC PDP 11/03 microcomputer for storage prior to post-processing the data. The midspan deflections were related to the strain-gauge voltages using a calibration fixture which permitted a series of known transverse deflections to be imposed on the isolated rocker link using a micrometer-attachment while recording the associated voltages in the wheatstone-bridge arrangement.

Figure 1 presents a clear exposition of the kinematic chain from which it is evident that the crank was a rigid member composite with the flywheel. The length of the crank, between bearing centerlines was 50mm, the length of the rigid coupler link was 305mm, the length of the flexible rocker link was 293.6mm and the ground link length of the four-bar linkage, without activating the shaker, was 381mm. In practice, this constant ground link length was achieved by employing a small plate at each end of the Microslides Inc. slide assembly which prevented translational motion of the reciprocating table. This was achieved by connecting the plates by two tie-bolts parallel to the axis of translation.

The coupler link was fabricated in aluminum with slots milled in the beam section in order to reduce the weight of the member. The mass of this link including bearings was 157gm, the depth perpendicular to the plane of the mechanism was 19.43mm, and the width in the plane of the mechanism was 6.25mm. The mass moment of inertia of the link, relative to the crank-coupler joint pivot, was 0.005286 $Kg\text{-}m^2$ and the location of the center of mass relative to that pivot was 0.176m.

The rocker link comprised a subassembly of three members with a total mass of 147.6gm. The mass of the rotating joint at the rocker-ground link joint was 36.05gm and the mass of the flexible strip component was 22.6gm. The depth of the flexible strip was 10.2mm perpendicular to the plane of the mechanism and the width in the plane of the mechanism was 0.838mm. The length of each of the bearing housings attached to the rocker link was 25mm parallel to the longitudinal axis of the link. The link was assumed to be fabricated in an alloy steel with a Young's modulus of 207GPa and a mass density of 9294.3 Kg/m^3. The second moment of area of the flexible strip was 3.9588 x 10^{-13} m^4 relative to the plane of bending.

The coupler-rocker joint incorporated matched pairs of 6.4mm bore R3 DB R12 instrument ball bearings manufactured by FAG Bearings Limited. These bearings were accurately preloaded using a Dresser Industries torque-limiting screwdriver calibrated to ±0.113 N·m. If these approach had not been implemented then inaccurate results would have been obtained due to either the backlash associated with bearing clearance, or else the increased resistive torques associated with preloaded bearings.

FOUR-BAR LINKAGE: THEORETICAL AND EXPERIMENTAL RESULTS

The first set of experimental results were obtained using a classical four-bar linkage in order to provide a reference set of data for subsequent comparison with the elastodynamic response of the microprocessor-controlled retrofitted mechanism. These reference results were obtained by first locking the crossed-roller slide assembly to create a four-bar linkage prior to operating the mechanism at several constant crank frequencies.

This reference data set were obtained by feeding the signal from the strain gage instrumentation monitoring the response of the rocker link to the PDP microcomputer prior to digitally filtering the results. This digital-filtering operation was implemented in order to remove spurious noise from the signal using a lower-bound cut-off frequency of 100 Hz. The data was then post-processed by multiplying the digitized response by a strain-deflection calibration factor for the rocker link specimen.

In order to evaluate the quality of the mathematical model developed for the flexible rocker link, the steady-state solution of the Hill's equation, equation (30) in reference [1], was obtained by setting the shaker input to zero and solving the equation for several crank frequencies. Some of the results are presented in Figures 4 and 5, which compare the predicted midspan transverse deflections with the corresponding experimental data. The good correlation between the sets of data at the differing speeds substantiate the assumptions embodied in the modeling process, and attention now focuses on implementing the retrofittment philosophy. A more comprehensive set of results are presented in reference [8].

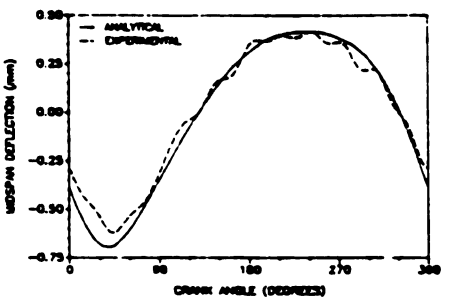

Fig. 4 Rocker Link Midspan Transverse Deflection at 148 rpm.

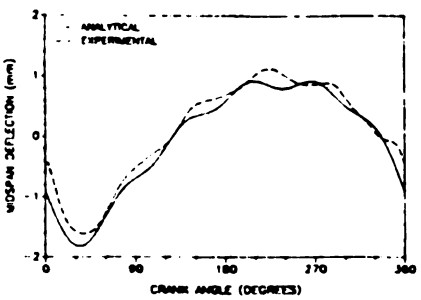

Fig. 5 Rocker Link Midspan Transverse Deflection at 215 rpm.

SYNTHESIS OF SHAKER MOTION

The current mode of operation of the single-input four-bar linkage may not satisfy the prescribed design specification; namely, the amplitude of the maximum deflection may exceed a prescribed limit. Under these circumstances, a linkage with two inputs may permit the deflections of the rocker link to be suppressed. This proposed methodology would involve carefully orchestrating the motion of the crank and also the motion of the proposed retrofitted slider attachment. However, this philosophy requires the ability to synthesize a suitable waveform for the shaker/slider motion $\ell_c(t)$. This task is the focus of attention in this section of the paper.

The transverse deflection of the flexible rocker link of the retrofitted four-bar linkage shown in Figure 1 is governed by the Hill's equation, equation (30) in reference [1], which may be written in a condensed form

$$\ddot{W}(t) + W\left\{\omega_n^2 + f_1(t) + f_2(t)\dot{\theta}_4^2 + f_3(t)\ell_c\right\} - f_4(t)\ddot{\theta}_4 + f_5(t)\ddot{\ell}_c \qquad (1)$$

where $f_i(t)$, $i = 1, 2, 3, 4, 5$ are the time-dependent coefficients in equation (30) in reference [1], ω_n is the transverse natural frequency of the link in flexure, $\dot{\theta}_4$ is the absolute angular velocity of the link, $\ddot{\theta}_4$ is the absolute angular acceleration of the link and $\ddot{\ell}_c$ is the absolute acceleration of the slider in the retrofitted mechanism.

In order to suppress the midspan transverse deflection W of the rocker link, the force-field imposed in the plane of the link must be continuously reduced in order to reduce the amplitude of this deflection. This, in turn, requires the absolute acceleration perpendicular to the link to be reduced. Thus it is argued, if the magnitude of the absolute acceleration can be reduced by a viable shaker motion, then so too will the elastodynamic response, since the absolute acceleration terms provide the principal forcing functions.

The elastodynamic response of a link comprises the sum of two waveforms; the first is termed a quasi-static response, and has the same frequency as the operating frequency of the mechanism, while the second waveform is a much higher frequency near the natural frequency of the link member [9]. The objective herein, is to reduce the amplitude of the quasi-static response and thereby reduce the amplitude of the resultant elastodynamic response.

The quasi-static response has a waveform with the same shape as the absolute acceleration perpendicular to the link member under review. Thus, while the appropriate slider motion of the retrofittment may be synthesized using a Fourier series representation, for example, the strategy adopted herein utilizes the measured elastodynamic response to provide the basis for the slider motion. Thus it is proposed, the elastodynamic response is first measured by strain gauges and is then stored in a microcomputer prior to being subjected to digitally filtering which yields the quasi-static response. This waveform then provides the basis for synthesizing the waveform to be programmed into the function generator prior to activating the electrodynamic shaker and slider attachment. While this bread-board model is based on an open-loop concept with human involvement, it can provide the basis for an automated closed-loop algorithm.

Figure 6 shows the results of the slider-waveform synthesis procedure, which presents the relationship between a typical quasi-static midspan deflection curve and the synthesized curve for the slider motion. The deflection profile provides the basis for the synthesis of the resulting slider motion characteristics which are then employed to reduce the amplitude of the quasi-static deflection curve. It is evident from Figure 6 that the synthesized shaker displacement function has basically the same amplitude and phase as the quasi-static deflection curve for the first 120 degrees of the crank cycle. Then, following a smoothing operation which subtends approximately 30 degrees of crank rotation, the shaker motion describes a mirror image of the quasi-static deflection profile about the zero displacement position prior to a second smoothing operation at approximately 330° into the cycle before repeating the periodic waveform. Thus the synthesized waveform is in phase with the quasi-static deflection profile for half of the crank revolution (0-150°, 330°-360°) and for the remainder of the cycle is a reflection of the quasi-static response about the zero deflection condition.

Waveforms with the same profile but with smaller amplitudes have negligible effect on the dynamic response of the flexible link, while much larger amplitudes excite a larger dynamic response. Thus, careful tailoring of the slider excitation is an essential ingredient of the retrofittment philosophy.

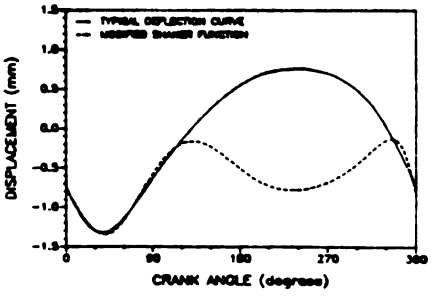

Fig. 6 Synthesis of Slider Waveform for the Retrofittment Scheme.

INTELLIGENT MECHANISM: EXPERIMENTAL AND COMPUTATIONAL RESULTS

The retrofittment methodology proposed in the previous sections was implemented in practice, and the experimental apparatus in presented in Figure 1. The approach involved operating the four-bar mechanism at a constant crank frequency, experimentally measuring the quasi-static response and then feeding the synthesized waveform to the shaker. The shaker, which was activated by a signal from the Airpax transducer with the crank in the zero crank angle configuration, was powered in a continuous mode in unison with the crank frequency to provide two types of excitation to the rocker link.

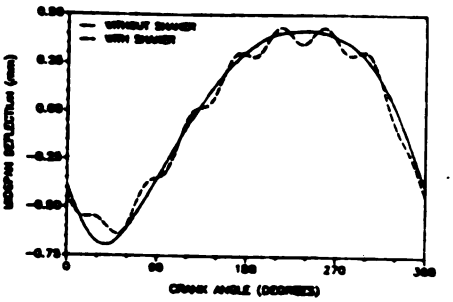

Fig. 7 Theoretical Elastodynamic Responses at 148 rpm for the Original and Microprocessor-Controlled Linkages

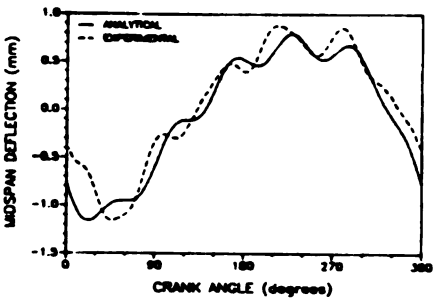

Fig. 8 Experimental Elastodynamic Responses at 148 rpm for the Original and Microprocessor-Controller Linkages.

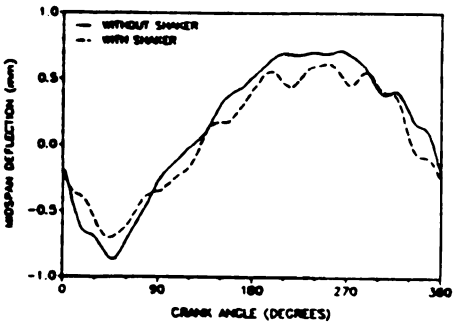

Fig. 9 Experimental Elastodynamic Responses at 170 rpm for the Original and Microprocessor-Controller Linkages.

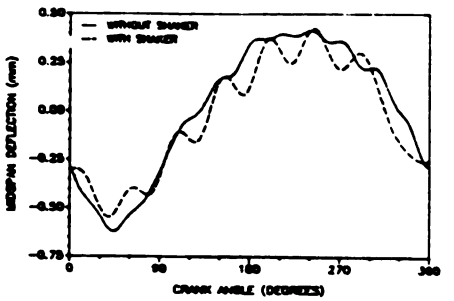

Fig. 10 Theoretical and Experimental Responses at 200 rpm for the Original and Microprocessor-Controller Linkages.

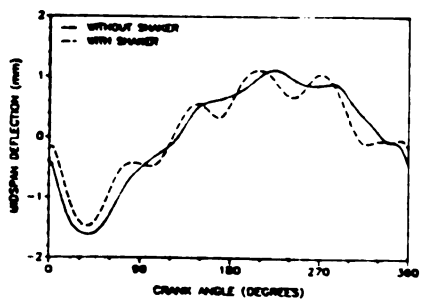

Fig. 11 Experimental Responses at 225 rpm for the Original and Microprocessor-Controller Linkages.

Figures 7 and 8 provide analytical and experimental results for the four bar mechanism and also the intelligent mechanism operating at 148 rpm. The response curves essentially validate the assumptions made in the modeling process for both systems and also the overall philosophy of employing a retrofittment which provides a perturbational input to the link. The experimental results in Figure 8 demonstrate a 12 percent reduction in the maximum amplitude of the midspan deflection.

Figures 9, 10, and 11 provide further evidence to establish the viability of the proposed methodology for the class of mechanism system studied over a range of operating speeds. At 170 rpm, Figure 9 shows that the intelligent machine system achieves an impressive 20 percent reduction in the maximum amplitude of the midspan transverse deflection and in the second half of the cycle the response is reduced on average by 12 percent. Figure 10 demonstrates that the analytical model of the intelligent mechanism is a viable approach for predicting the elastodynamic response of the system at 200 rpm, although the two waveforms have a small phase discrepancy. The experimental results presented in Figure 11 show that at 215 rpm the microprocessor-controlled system achieves an impressive reduction in the maximum rocker deflection of 16 percent.

This comprehensive theoretical and experimental investigation has clearly demonstrated that the introduction of a microprocessor-controlled perturbational input into the classical four-bar kinematic chain is capable of significantly reducing the amplitude of the elastodynamic response of the flexible rocker link. This crank frequency was limited to 230 rpm because of the very flexible link employed in the study, however, it is anticipated that the same approach is indeed a viable strategy for suppressing the elastodynamic response of more complex linkage mechanisms operating at different speeds.

CONCLUSIONS

A methodology was proposed, developed, and validated experimentally for suppressing the maximum amplitude of the elastodynamic response of flexible mechanism systems. The approach involved introducing a microprocessor-controlled perturbational input into the existing kinematic chain in order to control the inertial loading composed on a specific link member. The methodology was validated in a comprehensive experimental study of a flexible four bar linkage.

ACKNOWLEDGEMENTS

This material is based upon work supported by the Division of Engineering Research at Michigan State University. This funding is gratefully acknowledged.

REFERENCES

1. Soong, K., Sunappan, D., and Thompson, B.S., "The Elastodynamic Response of a Class of Intelligent Machinery, Part I: Theory," submitted for publication, ASME Journal of Vibrations, Acoustics, Stress and Reliability in Design.

2. Lowen, G.G., and Chassapis, C., "The Elastic Behavior of Linkages: An Update," Mechanism and Machine Theory, Vol. 21, No. 1, 1986, pp. 33-42.

3. Thompson, B.S. and Sung, C.K., "A Survey of Finite Element Techniques in Mechanism Design," Mechanism and Machine Theory, Vol. 21, No. 4, 1986, pp. 351-359.

4. Colebiewski, E.P. and Sadler, J.P., "Analytical and Experimental Investigation of Elastic Slider-Crank Mechanisms," ASME Journal of Engineering for Industry, Vol. 98, 1976, pp. 1266-1271.

5. Jandrasits, W.G. and Lowen, G.G., "The Elasto-Dynamic Behavior of a Counter-weighted Rocker Link with an Overhanging Endmass in a Four-bar Linkage, Part II: Application and Experiment," ASME Journal of Mechanical Design, Vol. 101, 1979, pp. 89-98.

6. Alexander, R.M. and Lawrence, K.L., "Experimentally Determined Dynamic Strains in an Elastic Mechanism," ASME Journal of Engineering for Industry, Vol. 97, 1975, pp. 791-794.

7. Turcic, D.A., Midha, A., Bosnik, J.R., "Dynamic Analysis of Elastic Mechanism Systems, Part II: Experimental Results," ASME Journal of Dynamic Systems, Measurement, and Control, Vol. 106, 1984, pp. 255-260.

8. Sunappan, D., "An Analytical and Experimental Investigation of the Elastodynamic Response of a Class of Intelligent Machinery," M.S. Thesis, Department of Mechanical Engineering, Michigan State University, February 1987.

9. Oliver, J.H., Wysocki, D.A., and Thompson, B.S., "The Synthesis of Flexible Linkages by Balancing Tracer Point Quasi-Static Deflections using Microprocessor and Advanced Materials Technologies," Mechanism and Machine Theory, Vol. 20, No. 2, 1985, pp. 103-114.

AN EXPERIMENTAL INVESTIGATION OF THE DYNAMIC RESPONSE OF A MECHANICAL SYSTEM WITH BEARING CLEARANCE

AN EXPERIMENTAL INVESTIGATION OF THE DYNAMIC RESPONSE OF A MECHANICAL SYSTEM WITH BEARING CLEARANCE

K. Soong, Graduate Student and B. S. Thompson, Professor
Machinery Elastodynamics Laboratory
Department of Mechanical Engineering
Michigan State University
East Lansing, Michigan

ABSTRACT

Numerous publications have been devoted to the development of analytical and computational models for predicting the dynamic response of mechanical systems comprising assemblages of rigid-bodies with clearance at the joints. However, there is a dearth of experimental investigations in this area which focus on furnishing complementary response data, consequently the predictive capabilities of these theoretical models are largely unknown. The experimental investigation presented herein, is motivated by this observation and is directed towards partially filling this significant void in the literature. In order to accomplish this goal, a comprehensive experimental study was undertaken of a slider-crank mechanism in which the radial clearance at the gudgeon-pin bearing was carefully controlled. Response data at different operating speeds are presented, along with an investigation of the bearing characteristics from which the coefficient of restitution, which features in many of the proposed mathematical models, was evaluated. Finally, design guidelines are distilled from the experimental data to relate the response of the system to the response of a similar system without bearing clearance.

INTRODUCTION

A large class of mechanical systems are characterized by discontinuous, or impective, motions which result in excessive vibrations, wear and the emission of high levels of acoustical radiation. While these phenomena are an inherent feature of specific classes of mechanical systems such as ratchets, escapements and geneva mechanisms, they are also present in a very large class of mechanical systems which are fabricated with journal bearings, and to a lesser extent, frictionless multi-element precision bearings. Both of these bearing systems feature a small radial clearance which is responsible for the intermittent motion characteristics of these mechanical systems as evidenced by discontinuities in the force fields and the kinematic characteristics.

Several texts in the literature address the problem of modeling impactive motions in constrained mechanical systems [1,2] and review articles [3] and [4] present comprehensive surveys of the field. This latter work focusses on the models employed to describe the relative motions between the principal components of revolute joints employed in planar mechanical systems and also the models proposed for simulating this impactive behavior. More recent literature includes references [5-12].

The comprehensive experimental study presented herein, on the dynamic response of a mechanical system with bearing clearance is motivated by the dearth of experimental studies in the literature on this subject References [13-16] provide a flavor of this experimental work which is devoted to studies of planar four-bar linkages. Thus, while numerous mathematical models have been proposed to predict the dynamic response of mechanical systems with intermittent impactive motions, the predictive capability of these models is largely unknown and untested. Since many of these papers include computer simulation results for the dynamic response of planar slider-crank mechanisms with a controlled radial clearance at one or more of the joints, such as for example [10,17,18,19], an experimental study of this mechanism was undertaken to furnish experimental data which may be employed to evaluate the proposed mathematical models. Response histories at different crank frequencies and with several different radial clearances are presented prior to presenting experimental data to determine the coefficient of restitution for these bearings. This coefficient features in the modeling process presented in a large number of theoretical papers [5-7,17,18,20-22].

EXPERIMENTAL APPARATUS

The principal subassembly in this experimental investigation was a planar slider-crank mechanism incorporating substantially rigid links which articulated in a plane perpendicular to the gravitational field. The essential features of the mechanism are presented in Figure 1. The crank, which had a length of 50mm, was fabricated as an integral part of a 146mm diameter flywheel. This heavy circular

disc was keyed to a 19.05mm (0.175 in) diameter drive-shaft, which was supported on a matched pair of Timken tapered roller bearings, type TS4A-6, and was powered by a 0.56Kw (0.75 h.p.) Dayton variable-speed dc motor, model 2Z846A. The slider of the slider-crank mechanism was represented by the translating table element of a Micro Slides, Inc., type 2050-RW-118-5 linear crossed-roller slide assembly which is a precision preloaded system without clearance.

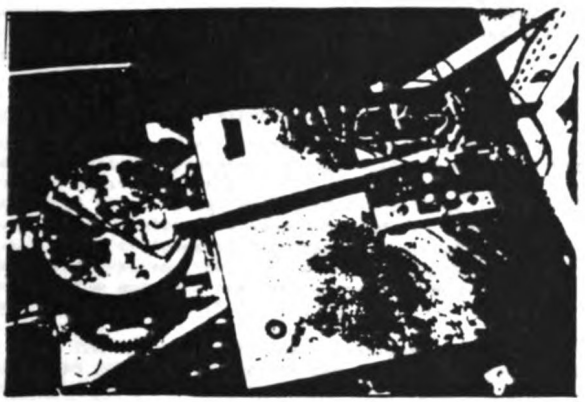

Fig. 1 Photograph of Experimental Apparatus

The connecting rod assembly comprised three components: a steel rod with dimensions 267 x 6 x 19mm^3, a crank-pin bearing, and a gudgeon-pin bearing. The total length of this link member was 293mm between bearing centerlines. The crank-pin bearing was designed to incorporate a matched pair of instrument ball bearings supplied by FAG Bearings Limited, type R4 DB 12. The spindle diameter was 6.35mm (0.25 inch). This bearing assembly was carefully preloaded using a Dresser Industries torque-limiting screw driver. This procedure enabled bearing clearance to be removed from the assembly, since the vibrational response associated with this clearance at the crank pin would have contaminated the experimental data from the transducers monitoring the dynamic response of the system at the gudgeon pin.

The gudgeon-pin bearing was fabricated as journal bearing with variable radial clearance. This was achieved by employing steel pins of diameter 6.35mm (0.250 inch) and 4.572mm (0.180 inch) which were each supported in a threaded hole in the reciprocating portion of the crossed-roller slide assembly. The journal element of the bearing was provided by a series of interchangeable brass bushings with internal diameters of 6.4mm (0.2520 inch), 6.5024mm (0.256 inch) and 6.604mm (0.260 inch) which permitted a variety of joints to be assembled with radial clearances of 1.016mm (0.040 inch), 0.127mm (0.005 inch), 0.0762mm (0.003 inch) and 0.0254mm (0.001 inch) respectively.

The experimental apparatus and the associated instrumentation is schematically presented in Figure 2. The operating speed of the mechanism was measured by a Hewlett Packard 5314A universal counter which was activated by an Electro Corporation digital-magnetic pickup, model 58423, which sensed a 60-tooth spur gear mounted on the crank shaft. This gear and the associated pickup are clearly evident in Figure 1.

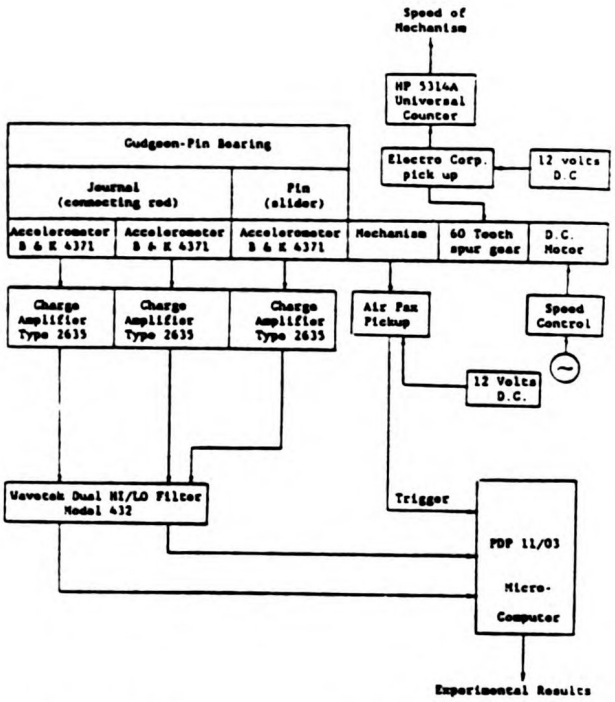

Fig. 2 Schematic of Experimental Apparatus and Associated Instrumentation.

The dynamic behavior of the slider and the connecting rod were monitored using three Bruel and Kjaer piezoelectric accelerometers, type 4371, which were each connected to a Bruel and Kjaer charge amplifier, type 2635. These accelerometers were positioned at the gudgeon-pin bearing in order to measure the dynamic response of the reciprocating slider and also the longitudinal and lateral motions of the connecting rod. This cluster of accelerometers are clearly evident in the right-hand-side of Figure 3. The signals from these accelerometers were fed to a Wavetek HI/LO analog filter, model 432, prior to being recorded on a PDP11-based digital-data-acquisition system. The cut-off frequency employed in this study was 60 Hz.

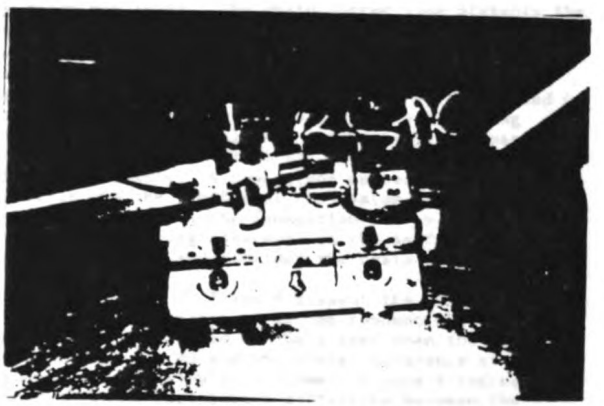

Fig. 3 Photograph of Accelerometer Configuration at the Gudgeon-Pin Bearing.

The response profiles measured by the accelerometers were related to the angle of the crankshaft using a third transducer arrangement, which featured an Airpax zero-velocity digital pickup, type 14-0001. This pickup was employed to sense the bolt head protruding from the flywheel when the crank was in the conventional zero crank-angle position, prior to firing the Schmidt triggers on the input/output panel of the data-acquisition system. Again, this arrangement is clearly presented in Figure 1. The highest sampling rate employed in this study was 2,500 samples per second.

In addition to the apparatus assembled to measure the dynamic response of the slider-crank mechanism with radial clearance at the gudgeon-pin joint, a second apparatus was assembled to evaluate the dynamic behavior of the joint. This strategy was motivated by the large number of theoretical publications which have been proposed for simulating the dynamic response of constrained rigid-linked mechanical systems, in which a coefficient of restitution approach has been adopted to model the impactive phenomena [5-7,17,18,20-22].

The objective of this investigation was to excite an impactive motion in the gudgeon-pin joint and then measure the velocities of both the pin and the journal before and after impact in order to distill an empirical expression for the coefficient of restitution from the experimental data. The approach involved exciting the Microslides table, and hence the pin of the bearing, by a Ling Dynamic Systems vibrator, model 411, which was driven by a Wavetek function generator, model 275, and a Hafler power amplifier, model P500. These tests were undertaken with the connecting-rod disconnected from the crank in order to isolate the motion between the two impacting machine elements. The connecting rod was configured so that the longitudinal axis was colinear with the axis of translation of the slider, and soft rubber springs were connected to it in order to ensure continued co-axial alignment during excitation.

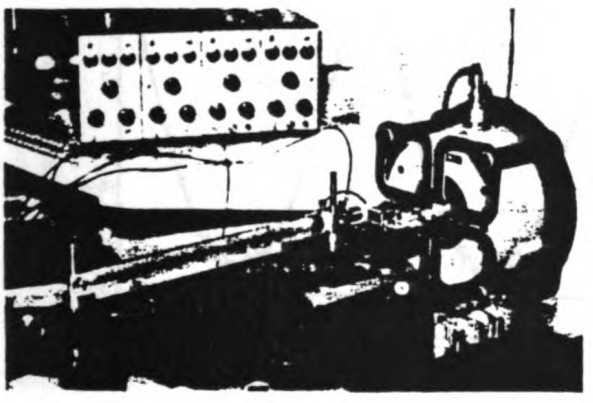

Fig. 4 Photograph of Experimental Apparatus for Evaluating the Impactive Forces and Determining the Coefficient of Restitution in the Gudgeon-Pin Bearing.

A Bruel and Kjaer force transducer, model 8200, was positioned between the shaker head and the sliding table in order to monitor the forcing function imposed upon the gudgeon-pin bearing. The motion of the journal and also the pin were carefully monitored by strategically locating Bruel and Kjaer piezoelectric accelerometers, type 4371, on the bearing assembly. These transducers were operated in conjunction with Bruel and Kjaer charge amplifiers, type 2635, which contain built-in integrators that permit velocity and displacement histories to be measured. Figure 4 presents a photograph of the experimental arrangement and Figure 5 presents a schematic diagram of the apparatus and the associated instrumentation.

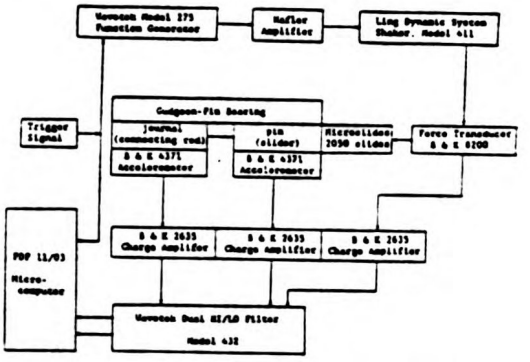

Fig. 5 Schematic Diagram of the Experimental Apparatus and Instrumentation for Determining the Coefficient of Restitution of the Bearing Elements.

DISCUSSION OF RESULTS

Figures 6-20 present experimental response histories from this experimental investigation for different operating speeds and different values of radial clearance at the gudgeon-pin bearing. The response is presented for two revolutions of the crank in order to illustrate the repetitive nature of the observed phenomena. In addition, each Figure presents two classes of dynamic response. The continuous line presents the response of the slider-crank mechanism with a controlled nonzero radial clearance at the gudgeon-pin joint. The chain-dotted line presents the experimental response of the slider-crank mechanism with zero clearance at the gudgeon-pin which provides the experimental response of an "ideal" or perfect system. These reference sets of data were obtained by monitoring the response of a gudgeon-pin bearing fabricated with a preloaded matched pair of instrument ball bearings, type R4 DB 12, manufactured by FAG Bearings Limited. A comparison between this response profile and the profile of the system with bearing clearance provides the foundation for evaluating the effects of bearing clearance on the performance of a given mechanism and provides the basis for discussion.

Figures 6, 7 and 8 present the normal and tangential accelerations of the connecting rod, and also the acceleration of the slider when the crank rotates at 150 rpm and the radial clearance at the gudgeon-pin bearing is 1.016mm. Figure 6 indicates that there is very little difference between the longitudinal accelerations of the connecting rod when the system contains a gudgeon pin joint with, or without, clearance at this crank frequency. Indeed, Figure 6 presents the worst-case situation, which

documents the response data for the case of the maximum deviation between the responses of systems with and without radial clearance at the gudgeon-pin bearing. At different operating speeds and with different values of radial clearance, the deviation between the two responses was less marked.

A bearing amplification factor (BAF) may be defined in order to relate the maximum acceleration at a specific point in a mechanical system with nonzero bearing clearance at a specific system configuration, to the maximum acceleration at the same point with the system containing zero bearing clearance. Thus,

$$BAF = \left| \frac{a^* - a}{a} \right| \qquad (1)$$

where a^* is the acceleration of a system with bearing clearance and a is the associated acceleration of the same system without clearance. Thus, Figure 6 indicates that BAF = 11 percent for the longitudinal acceleration component of the slider-crank mechanisms tested. Consequently, these response histories are not presented herein for brevity.

In sharp contrast to the profile in Figure 6, the tangential acceleration of the connecting rod and also the acceleration of the slider show very significant differences between the dynamic response histories of the systems with, and without, radial clearance at the gudgeon-pin joint. The most severe differences are evident in the tangential acceleration component where the peak value for the system with bearing clearance is approximately twenty times greater than that of the case without bearing clearance. The corresponding difference for the slider characteristic is approximately a 269 percent amplification. These experimental results clearly demonstrate the severe dynamical loading developed in a bearing with radial clearance, and they provide a qualitative measure of the associated severe fatigue environment in which the member must reliably operate.

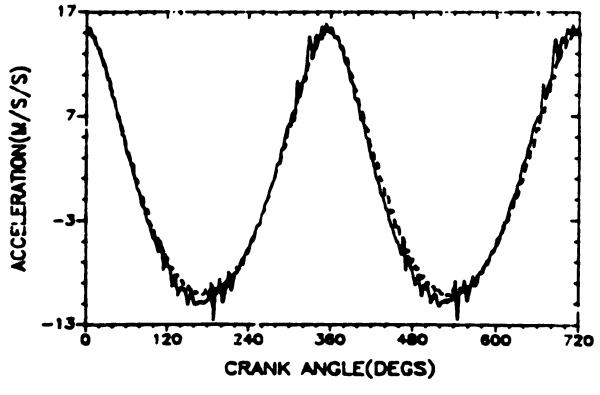

Fig. 6 Longitudinal Acceleration of the Connecting Rod. Mechanism Operating Speed 150 rpm, Radial Bearing Clearance 1.016mm.

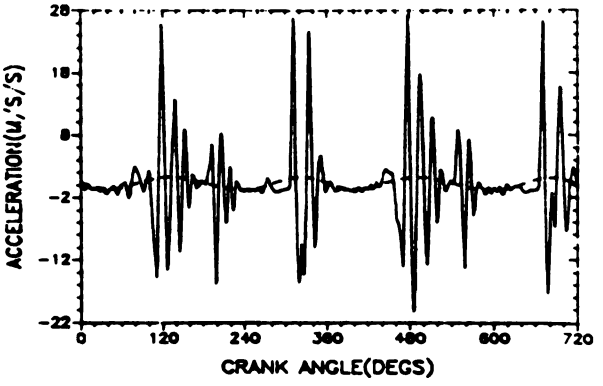

Fig. 7 Tangential Acceleration of the Connecting Rod. Mechanism Operating Speed 150 rpm, Radial Bearing Clearance 1.016mm.

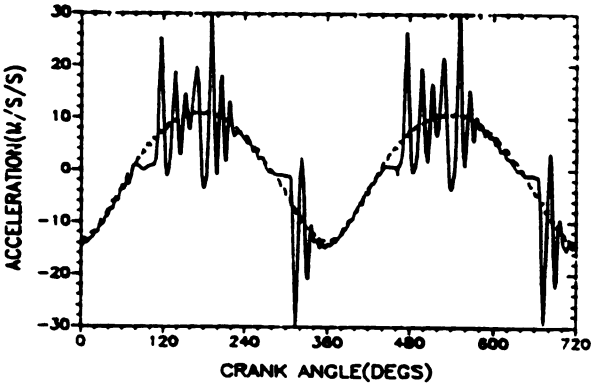

Fig. 8 Slider Acceleration. Mechanism Operating Speed 150 rpm, Radial Bearing Clearance 1.016mm.

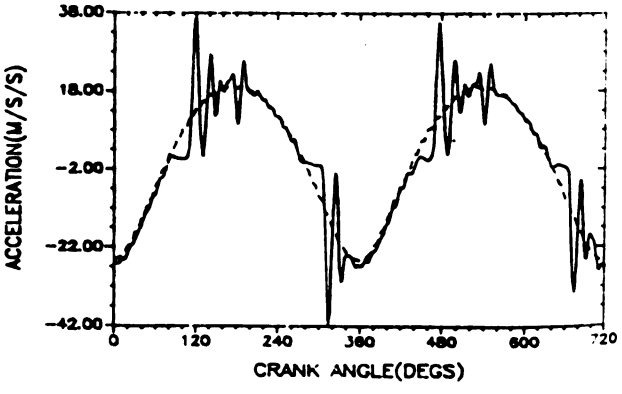

Fig. 9 Slider Acceleration. Mechanism Operating Speed 200 rpm, Radial Bearing Clearance 1.016mm.

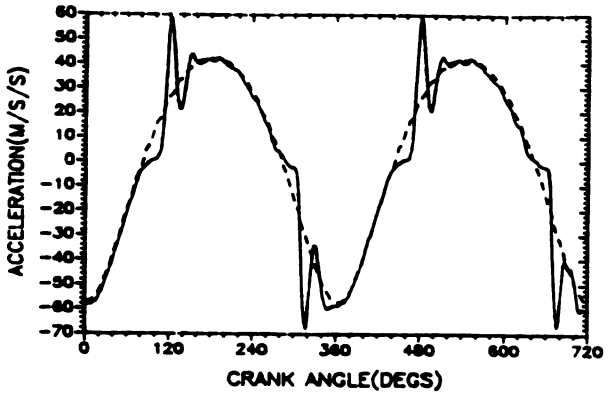

Fig. 10 Slider Acceleration. Mechanism Operating Speed 300 rpm, Radial Bearing Clearance 1.016mm.

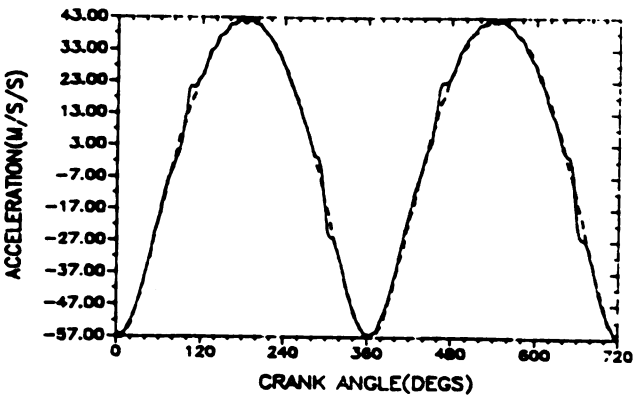

Fig. 13 Slider Acceleration. Mechanism Operating Speed 300 rpm, Radial Bearing Clearance 0.127mm.

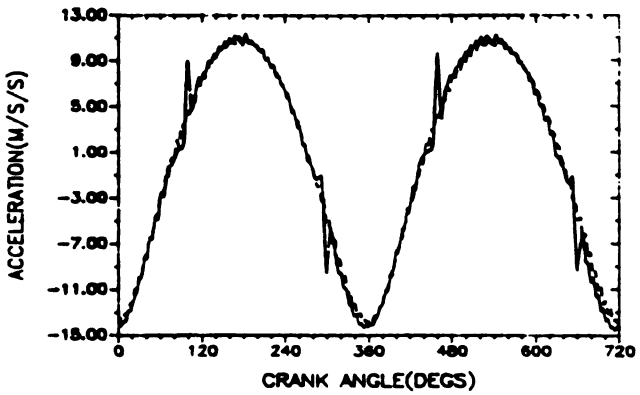

Fig. 11 Slider Acceleration. Mechanism Operating Speed 150 rpm, Radial Bearing Clearance 0.127mm.

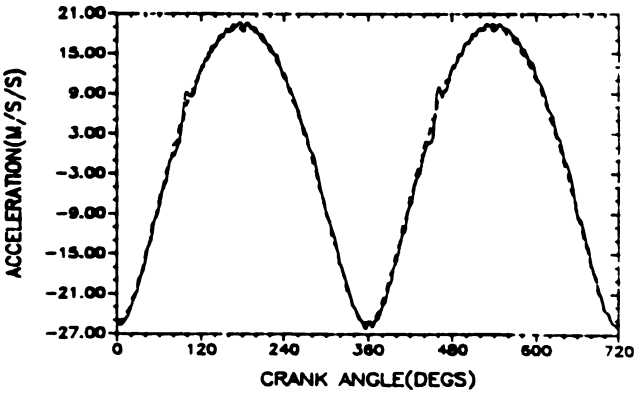

Fig. 14 Slider Acceleration. Mechanism Operating Speed 200 rpm, Radial Bearing Clearance 0.0762mm.

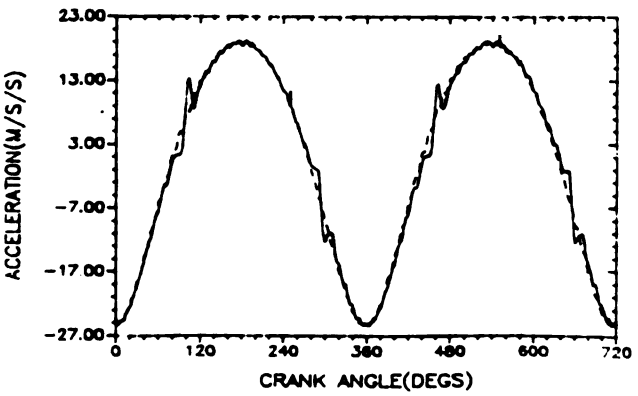

Fig. 12 Slider Acceleration. Mechanism Operating Speed 200 rpm, Radial Bearing Clearance 0.127mm.

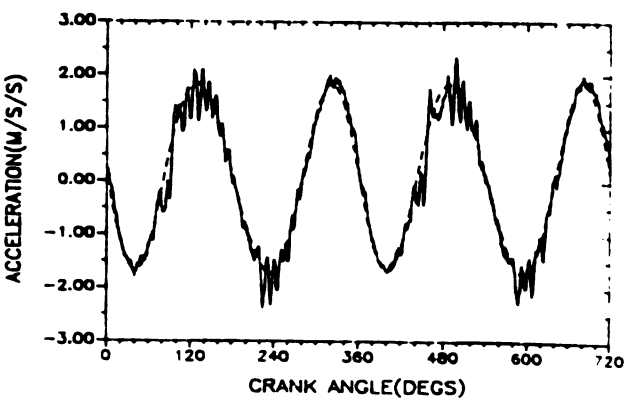

Fig. 15 Connecting-Rod Tangential Acceleration. Mechanism Operating Speed 200 rpm, Radial Bearing Clearance 0.0762mm.

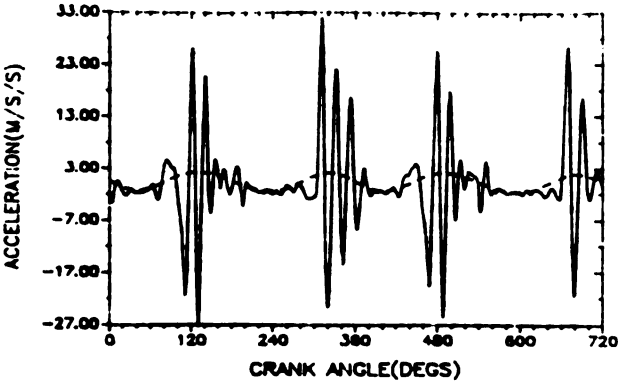

Fig. 16 Connecting-Rod Tangential Acceleration. Mechanism Operating Speed 200 rpm, Radial Bearing Clearance 1.016mm.

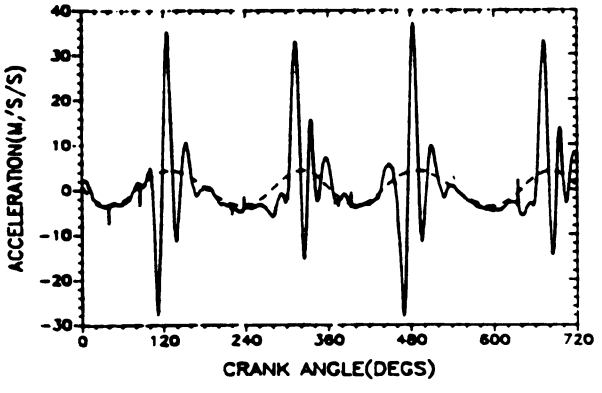

Fig. 17 Connecting-Rod Tangential Acceleration. Mechanism Operating Speed 300 rpm, Radial Bearing Clearance 1.016mm.

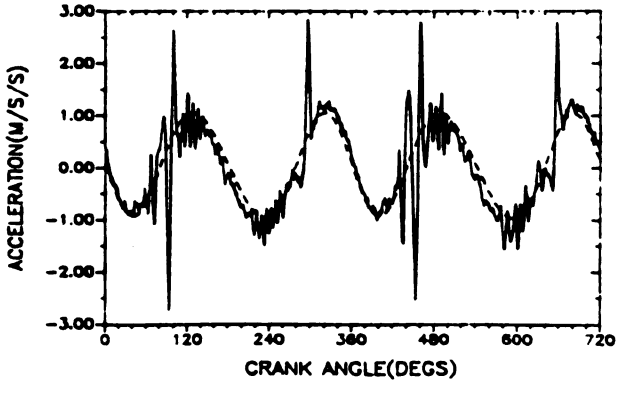

Fig. 18 Connecting-Rod Tangential Acceleration. Mechanism Operating Speed 150 rpm, Radial Bearing Clearance 0.127mm.

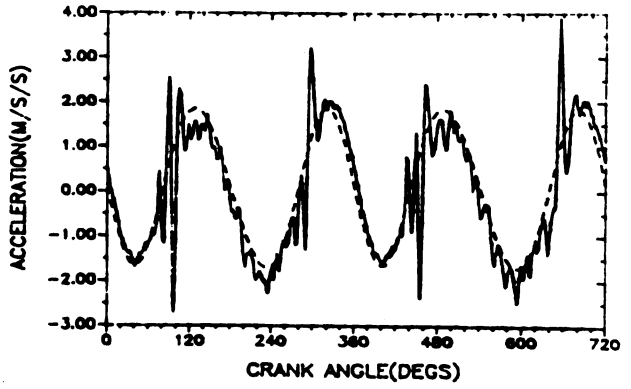

Fig. 19 Connecting-Rod Tangential Acceleration. Mechanism Operating Speed 200 rpm, Radial Bearing Clearance 0.127mm.

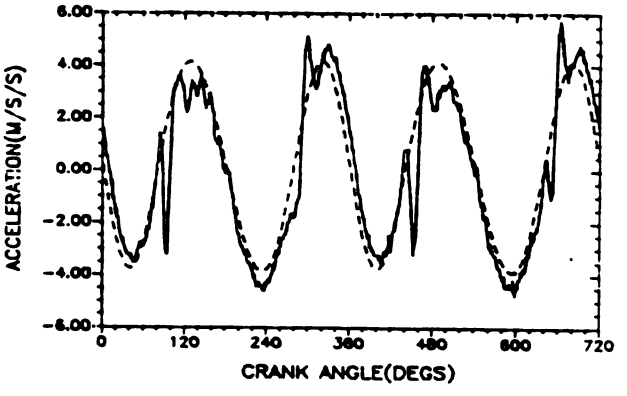

Fig. 20 Connecting-Rod Tangential Acceleration. Mechanism Operating Speed 300 rpm, Radial Bearing Clearance 0.127mm.

Figures 9-20 present similar sets of experimental response data for the mechanical system operating at different crank frequencies with different magnitudes of radial clearance at the gudgeon-pin. Figures 8, 9 and 10 show the effect of operating speed upon the dynamic response of the slider at 150 rpm, 200 rpm and 300 rpm with a radial clearance of 1.016mm. Figures 11, 12 and 13 present the acceleration histories of the slider when the mechanical system operates at 150, 200 and 300 rpm with a radial clearance of 0.127mm. Figure 14 presents the same kinematic characteristic for the system operating at 200 rpm which features a smaller gudgeon-pin radial clearance of 0.0762mm.

Upon reviewing Figures 8-14, which present the acceleration characteristics of the slider, it is evident that the most oscillatory response with the largest amplification factors are experienced by a mechanism incorporating a gudgeon-pin with a large clearance (1.016mm) while the system operates at relatively low speeds. As the speed increases the amplification-factor decreases, along with the oscillatory nature of the response. Hence the number of rebounds decrease as the operating speed increases; or alternatively a period of prolonged contact with be re-established sooner at higher operating speeds. The amplification factor is significantly reduced by

reducing the magnitude of the radial clearance as evidenced by comparing Figures 8 and 11 which present responses for the same mechanical system operating at 150 rpm but with difference radial clearance in the gudgeon-pin bearing.

Figure 8 clearly illustrates the loss of contact between the pin and journal during each revolution of the crankshaft when the crank angle is approximately 80 degrees and 280 degrees. The subsequent acceleration of the slider is approximately constant, as evidenced by the horizontal line, for approximately 30 degrees of crank rotation and 25 degrees, respectively. However, this is a special situation, because at different operating speeds and different clearances, the gradient of the graph, which measures the rate of change of acceleration, or jerk, changes considerably. Thus when contact is lost, and the pin and journal separate, the deviation angle subtended by the tangents to the zero-clearance response profile and the nonzero-clearance response profile at the point of separation, is dependent upon the operating speed and also the magnitude of the radial clearance in the joint. From the experimental data collected, it is evident that for a constant clearance, the deviation angle is approximately inversely proportional to operating speed; while for a constant speed, the deviation angle is proportional to the magnitude of the radial clearance.

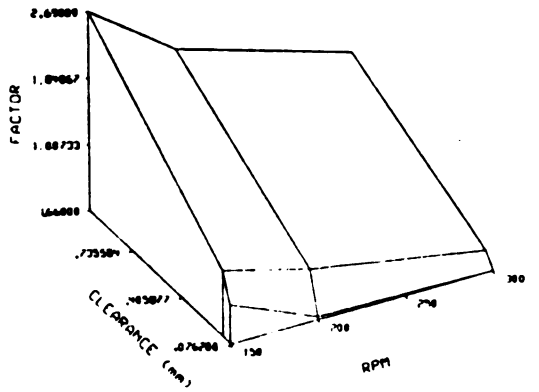

Fig. 21 Design Chart Relating Amplification Factor to Radial Bearing Clearance and Operating Speed for the Tangential Acceleration of the Connecting Rod.

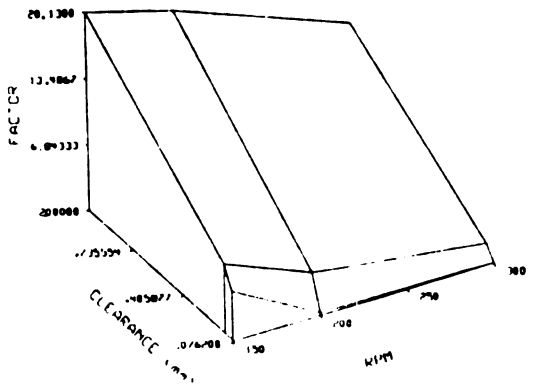

Fig. 22 Design Chart Relating Amplification Factor to Radial Bearing Clearance and Operating Speed for the Slider.

Figures 21 and 22 present three-dimensional design charts for the slider acceleration and the tangential acceleration of the connecting rod respectively, which relate the bearing amplification factor (BAF) to the magnitude of the radial bearing clearance and also the operating speed of the mechanical system. These contours, which were distilled from Figure 7-20, indicate that the slider is characterized by the largest amplification factors and hence the highest acceleration and force fields.

Upon reviewing Figures 8-14 it is evident that the pin and journal loose contact, or separate, twice during each revolution of the crank shaft. This phenomenon was evident for all of the crank frequencies investigated. The first separation generally occurred at approximately 80 degrees of crank rotation and this event was independent of operating speed and magnitude of radial clearance; lasting recontact between the pin and journal depended upon the operating speed and also the magnitude of the radial clearance. The crank angle at which the second separation occurred depended upon the radial clearance of the joint. For example, when the mechanical system operated at 200 rpm with a radial clearance of 1.016mm, contact was lost at a crank angle of 275 degrees; with a radial clearance of 0.127mm, contact was lost at 280 degrees of crank shaft rotation; and with a radial clearance of 0.0762mm, the loss of contact is unclear from the response data.

Upon reviewing the acceleration profiles of the slider, presented in Figures 8-14, it is evident that upon separation of the pin and the journal, there follows a response-regime characterized by large amplitude oscillatory behavior of impact and subsequent rebound. This portion of the cycle is more severe for the first case of contact loss, when the crank angle is less than 90 degrees, than for the second case of contact loss.

Figures 15-20 present experimental response data recording the tangential acceleration of the connecting rod at the gudgeon-pin as a function of the radial clearance and the frequency of operation of the crank shaft. Observations distilled from Figures 8-14 for the acceleration history of the slider generally also pertain to Figures 15-20. One significant difference occurs during the following mode [4] of the operating cycle of the mechanical system which is characterized by lasting contact between the pin and the journal [4]. This phase is characterized by a high-frequency, irregular ripple which is probably triggered by the surface roughness of the bearing.

Figures 23, 24, and 25 present results from some of the tests performed on the gudgeon-pin which permitted Figures 24 to be constructed, and hence an empirical value of the coefficient of restitution to be established. These results were obtained using the experimental apparatus presented in Figure 4, from which is evident that the gudgeon-pin joint was excited by an electrodynamic shaker. The Wavetek arbitrary function generator was programmed to provide a sinusoidal signal to the shaker, and in order to excite the gudgeon-pin bearing at different velocities, the frequency of excitation was varied from 10 Hz to 30 Hz. The amplitude of the excitation was approximately 1.6mm, and in all of the studies undertaken the radial clearance was maintained at 1.016mm. The signals from the accelerometers and the force transducer were subjected to low-pass filtering with a cut of frequency of 600 Hz prior to recording the signals on a PDP11 microcomputer using a sampling rate of 2500 samples per second.

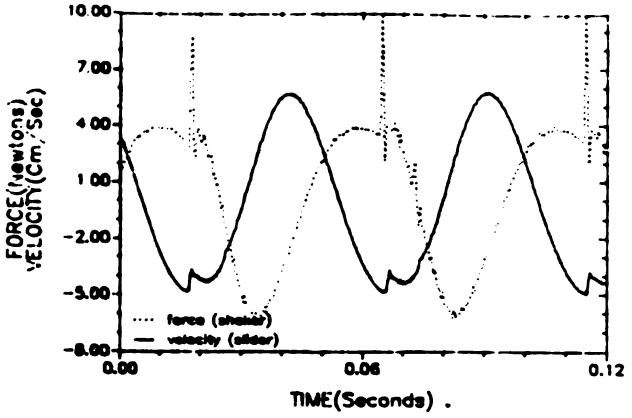

Fig. 23 Gudgeon-Pin Bearing Characteristics. Excitation Force Characteristic and Associated Velocity Characteristic of the Pin Impacting the Journal at a Frequency of 20 Hz.

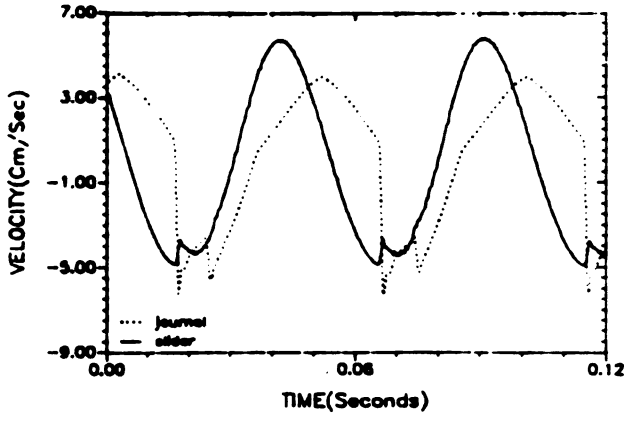

Fig. 24 Gudgeon-Pin Bearing Characteristics. Velocity Characteristics of the Impact Between Pin and Journal at a Pin Excitation Frequency of 20 Hz.

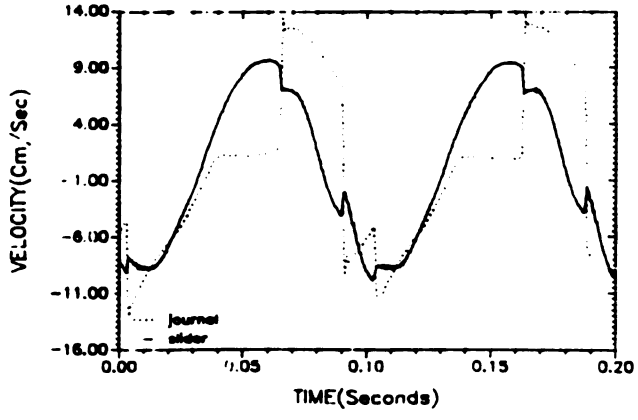

Fig. 25 Gudgeon-Pin Bearing Characteristics. Velocity Characteristics of the Impact Between Pin and Journal at a Pin Excitation Frequency of 10 Hz.

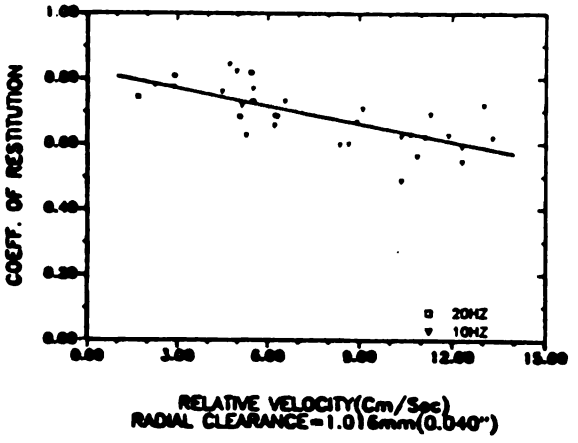

Fig. 26 Experimental Data Demonstrating the Relationship Between the Coefficient of Restitution and the Relative Velocity Before Impact of Pin and Journal.

The coefficient of restitution is dependent upon the material characteristics, the masses and shapes of the colliding bodies, and also the relative velocities of these bodies [23]. For the given conditions of a steel pin impacting on a brass bushing, the velocity characteristic provides the principal design variable. Thus, Figure 26 was developed to relate the relative velocity and the coefficient of restitution. A least-squares approach adopted in order to yield the following governing equation for the coefficient of restitution, e,

$$e = 0.8246 - 0.01836\ v \qquad (2)$$

where v is the relative velocity before impact.

CONCLUSIONS

A comprehensive experimental investigation of the dynamic response of a mechanical system incorporating radial clearance in one bearing has been undertaken. Kinematic and kinetic experimental data have been presented which will permit the predictive capabilities of the proposed mathematical models of these classes of systems to be evaluated and also motivate future work in this area. Design charts were developed for predicting the amplification of the acceleration characteristics as a function of bearing clearance and mechanism operating speed, in addition to distilling an empirical relationship for the coefficient of restitution.

REFERENCES

1. Kobrinskii, A.E., Dynamics of Mechanisms with Elastic Connections and Impact Systems, Fliffe Books Ltd., London, 1969.

2. Wittenberg, J., Dynamics of Systems of Rigid Bodies, B.G. Teubner, Stuttgart, 1977.

3. Kane, T.R. and Levinson, D.A., "Multibody Dynamics," ASME Journal of Applied Mechanics, Vol. 50, 1978, pp. 1071-1078.

4. Haines, R.S., "Survey: 2-Dimensional Motion and Impact at Revolute Joints," Mechanism and Machine Theory, Vol. 15, 1980, pp. 361-370.

5. Khulief, Y.A., "Restitution and Friction in Impact Analysis of Multibody Systems Executing Plane Motion," ASME paper 86-DET-50, 1986.

6. Khulief, Y.A., and Shabana, A.A., "Dynamic Analysis of a Constrained System of Rigid and Flexible Bodies with Intermittent Motion," ASME Journal of Mechanisms, Transmissions and Automation in Design, Vol. 108, 1986, pp. 38-45.

7. Khulief, Y.A. and Shabana, A.A., "Impact Responses of Multibody Systems with Consistent and Lumped Masses," Journal of Sound and Vibration, Vol. 104, 1986, pp. 187-207.

8. Bengisu, M.T., Hidayetoglu, T., and Akay, A., "A Theoretical and Experimental Investigation of Contact Loss in the Clearances of a Four-Bar Linkage," ASME Journal of Mechanisms, Transmissions and Automation in Design, Vol. 108, 1986, pp. 237-244.

9. Mostafi, A., and Dadbin, A., "Impact Type Loading Mechanisms," ASME paper 86-DET-170, 1986.

10. Dubowsky, S., Deck, J.F., Costello, H., "The Dynamic Modeling of Flexible Spatial Machine Systems with Clearance Connections," ASME Paper No. 86-DET-62, and ASME Journal of Mechanisms, Transmissions and Automation in Design, (in press).

11. DeRung, Wu., "Dynamic Response of the High Speed Mechanism with Clearance Connections," ASME paper 86-DET-171, 1986.

12. Bahgat, B.M., Osman, M.O.M., and Dukkipati, R.V., "On the Dynamic Gear Tooth Loading of Planetary Gearing as Affected by Bearing Clearances in High-Speed Machinery," ASME Journal of Mechanisms, Transmissions and Automation in Design, Vol. 107, 1985, pp. 430-436.

13. Haines, R.S., "An Experimental Investigation into the Dynamic Behavior of Revolute Joints with Varying Degrees of Clearance," Mechanism and Machine Theory, Vol. 20, 1985, pp. 221-231.

14. Dubowsky, S., and Moening, M.F., "An Experimental and Analytical Study of Impact Forces in Elastic Systems with Clearances," Mechanism and Machine Theory, Vol. 13, 1978, pp. 451-465.

15. Grant, S.J. and Fawcett, J.N., "Effects of Clearance at the Coupler-Rocker Bearing of a Four-Bar Linkage," Mechanism and Machine Theory, Vol. 14, 1974, pp. 99-110.

16. Shimojima, H., Ogawa, K., and Matsumoto, K., "Dynamic Characteristics of Planar Mechanism with Clearances," Bulletin of the Japanese Society of Mechanical Engineers, Vol. 21, 1978, pp. 303-308.

17. Wilson, R., and Fawcett, J.N., "Dynamics of the Slider-Crank Mechanism with Clearance in the Sliding Bearing," Mechanism and Machine Theory, 1974, Vol. 9, pp. 61-80.

18. Miedema, B. and Mansour, W.M., "Mechanical Joints with Clearance: a Three-Mode Model," ASME Journal of Engineering for Industry, Vol. 98, 1976, pp. 1319-1323.

19. Osman, M.O.M., Bahgat, B.M., and Sankar, T.S., "On the Prediction of Journal-Bearing Separation in High-Speed Mechanisms with Clearances," ASME paper 80-WA/DSC-36, 1980.

20. Mansour, W.M., and Townsend, M.A., "Impact Spectra and Intensities for High-Speed Mechanisms," ASME Journal of Engineering for Industry, Vol. 97, 1975, pp. 347-353.

21. Hunt, K.H. and Crossley, F.R.E., "Coefficient of Restitution Interpreted as Damping in Vibroimpact," ASME Journal of Applied Mechanics, Vol. 97, 1975, pp. 440-445.

22. Tatara, Y., "Effects of External Force on Contacting Times and Coefficients of Restitution in a Periodic Collision," ASME Journal of Applied Mechanics, Vol. 44, 1977, pp. 773-774.

23. Goldsmith, W., Impact: The Theory and Physical Behavior of Colliding Solids, Edward Arnold, London, 1960.

AN EXPERIMENTAL AND ANALYTICAL INVESTIGATION OF THE DYNAMIC RESPONSE OF A SLIDER-CRANK MECHANISM WITH CONTROLLED RADIAL CLEARANCE AT THE GUDGEON-PIN JOINT

AN EXPERIMENTAL AND ANALYTICAL INVESTIGATION OF THE DYNAMIC RESPONSE OF A SLIDER-CRANK MECHANISM WITH CONTROLLED RADIAL-CLEARANCE AT THE GUDGEON-PIN JOINT

by

K. Soong* and B.S Thompson+

* Graduate Research Assistant
+ Professor

Machinery Elastodynamics Laboratory
Department of Mechanical Engineering
Michigan State University
East Lansing, MI 48824

ABSTRACT

A mathematical model of a slider-crank mechanism with radial clearance at the joint connecting the slider and the connecting rod was developed prior to incorporating this three-mode model in a simulation software package for predicting the dynamic response of the mechanism under various operating conditions. Subsequent experimental work was undertaken in order to evaluate the predictive capabilities of this software design tool. The correlation between the theoretical and experimental results is impressive.

NOMENCLATURE

r_i	Length of the ith link
r_{Gi}	Length of the ith link from joint to mass center
λ_i	Lagrange multiplier
ϵ	Radial clearance
F_{ij}	The force imposed on link j by link i
s	Length of the ground link
T_i	Kinetic energy of the ith link
θ_i	Argument of the ith link
g	Gravitational acceleration
μ	Coefficient of friction between the ground and the slider
M_i	Mass of the ith link
T	System kinetic energy
ϕ_j	Scalar constraints
Q_k	Generalized force associated with coordinate q_k, including both conservative and nonconservative effects
q_k	Generalized coordiates
$\hat{Q}_k$	Generalized impulse associated with coordinate q_k
$\hat{F}$	Impulsive force
$\dot{q}_k$	First time derivative of the generalized coordinate q_k
*	Denotes post-collision parameter or characteristic
ϵ	Coefficient of restitution
$\vec{V}_{Q3}$	The velocity vector at the impact point Q on link 3
$\vec{V}_{Qs}$	The velocity vector at the impact point Q on the slider
θ_4	Argument of the clearance-link (Fig. 1b)
θ_4	The angle of the impact force w.r.t. the horizontal inertial coordinate (Fig. 3b)

INTRODUCTION

A large class of mechanical systems are characterized by discontinuous, or impactive, motions which result in excessive vibrations, wear and emission of high levels of acoustical radiation. While these phenomena are inherent feature of specific classes of mechanical systems such as ratchets, escapements and geneva mechanisms, they are also present in a very large class of mechanical systems which are fabricated with journal bearings, and to a lesser extent, frictionless multi-element precision bearings. Both of these bearing systems feature a small radial clearance which is responsible for the intermittent motion characteristics of these mechanical systems as evidenced by discontinuities in the force fields and the kinematic characteristics.

Several texts in the literature address the problem of modeling impactive motions in constrained mechanical systems [1,2] and review articles [3] and [4] present comprehensive surveys of the field. This latter work focusses on the models employed to describe the relative motions between the principal components of revolute joints employed in planar mechanical systems and also the models proposed for simulating this impactive behavior. More recent literature includes references [5-20].

In the present paper, a slider-crank mechanism with radial clearance in the gudgeon-pin joint, is employed to demonstrate the proposed approach to modeling these mechanism systems. The revolute joint between the pin and journal is assumed to be frictionless, thus the direction of the clearance link is assumed to coincide with the direction of the resultant bearing force at the joint. The dynamic analysis of the zero-clearance mechanism was employed to determine the initial values of the kinematic and kinetic parameters for simulating this class of mechanism problems. Criteria defining the different phases of the phenomena present in joints with radial clearance are also defined in the paper. A subroutine "DGEAR" in the IMSL subroutine library was employed to solve the set of second-order differential equation which govern this class of problems. The numerical results were then compared with experimental

results, from a complementary investigation with impressive correlation between theory and practice.

MATHEMATICAL MODEL

Figure 1(a) presents a schematic diagram and mathematical model of a slider-crank mechanism which features a radial clearance at the revolute joint between the connecting rod and the slider. The clearance shown in the Figure is grossly exaggerated for illustration purposes. The clearance is assumed to be present in a plain unlubricated journal bearing at the gudgeon pin. The end of the coupler is the journal, thus the pin is on the slider.

An exaggerated loop closure model is presented in Figure 1(b).

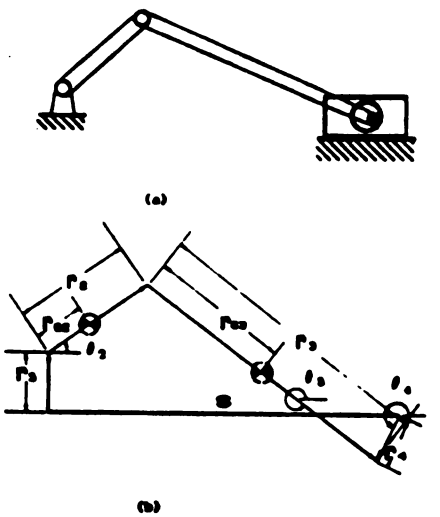

Fig. 1 (a) The slider-crank mechanism and the dominate clearance at the gudgeon-pin bearing. (b) Closed-loop of the mechanism.

The vector loop equation describing the geometric arrangement of the two-degree-of-freedom slider-crank mechanism may be written

$$\vec{r}_s + \vec{r}_2 + \vec{r}_3 - \vec{r}_4 - \vec{s} = 0 \qquad (1)$$

from which two geometric constraints were obtained:

$$\phi_1 = r_2 \cos\theta_2 + r_3 \cos\theta_3 - r_4 \cos\theta_4 - s \qquad (2a)$$

$$\phi_2 = r_2 \sin\theta_2 + r_3 \sin\theta_3 - r_4 \sin\theta_4 + r_s \qquad (2b)$$

A third constraint equation can be obtained by assuming that the crank rotates with constant angular velocity and hence the motion of the crank and coupler are related by the governing equation,

$$\phi_3 = \theta_2 - \dot{\theta}_2 t \qquad (2c)$$

In order to construct the equations of motion for the system, a constrained Lagrange equation may be employed. Thus

$$\frac{d}{dt}\left(\frac{\partial T}{\partial \dot{q}_k}\right) - \frac{\partial T}{\partial q_k} = \sum_{j=1}^{n} \lambda_j \phi_j - Q_k \qquad (3)$$

where

$$T = \frac{1}{2} \sum_{i=1}^{n} \sum_{j=1}^{n} m_{ij} \dot{q}_i \dot{q}_j \qquad (4)$$

$$Q_s = -(sgn)\mu M_s g \, ds \qquad (5)$$

in which

$$sgn = 1, \text{ if } \dot{s} > 0; \; -0, \text{ if } \dot{s} = 0; \; -1, \text{ if } \dot{s} < 0$$

DEFINITIONS

The dynamic phenomena evident in the response - behavior of a revolute joint with radial clearance may be captured by considering four different behavioral modes. These modes are: (i) The contact mode: The pin and the journal are in contact together and a sliding motion relative to each other is assumed to exist. The sliding surface is assumed to be smooth and thus no energy is dissipated. Since the clearance connection cannot transmit a tensile force in the contact mode at the pin-journal interface, this mode is terminated when the contact force between the pin and the journal becomes tensile [5], (ii) The free-flight mode: The pin and the journal loose contact in this mode, hence there are no constraints between these members. Under these conditions, the crank and connecting rod are treated as two compound pendula. Thus the system may be considered to be two independent dynamical systems, until a geometric constraint mandates the triggering of a different mode, (iii) The impact mode: At the termination of the free-flight mode, impactive behavior is triggered by the sudden contact of the pin and the journal. An exchange of momentum occurs between the two members, (iv) The transient phase: This phase begins at the first impact and ends with the restoration of the contact mode. The fundamental question associated with this transient mode is whether the system will return to the contact mode or enter the free-flight mode, after the termination of the impact mode. Herein the pin and the journal always assumed to separate after the impact mode. Thus the system is assumed to enter the free-flight mode. If the pin and journal re-establish contact in a "very short time" near the original contact point then the system is assumed to be in the contact mode. The magnitude of this "very short time" must be carefully quantified. Hence, this was ascertained from experimental data.

CRITERIA BETWEEN THE MODES

This section of the manuscript documents the mathematical formulations which define the different behavioral modes described previously for revolute joints with radial clearance.

Contact Loss

Two criteria were employed in order to simulate the change from the contact mode to the free-flight mode. First, in every step, the contact force between the pin and journal was calculated using the expression,

$$F_s = \lambda_1 \cos\theta_4 + \lambda_2 \sin\theta_4 \qquad (6)$$

The system is in the contact mode if $F_s \leq 0$.

Experience accrued in the complementary experimental investigation shows that this criterion is only valid at speeds below 100 rpm. The second criterion is defined as follows; the contact loss occurs when F_s is the minimum and the rate of the pressure angle changes rapidly. This empirical criterion is the result of both theoretical and experimental observations. Theoretical work suggests that F_s will always be greater than zero. This implies that contact will never be lost. However, experimental results clearly contradict this observation. In order to reconcile these conflicting states, the above criterion was established.

Termination of the Free-Flight Mode

The pin is assumed to be in free-flight mode until the following geometrical inequality is violated

$$0 < (\Delta x^2 + \Delta y^2)^{1/2} - \xi \tag{7}$$

where

$$\Delta x = r_2 \cos\theta_2 + r_3 \cos\theta_3 - r_4 \cos\theta_4 - s \tag{8}$$

$$\Delta y = r_8 + r_2 \sin\theta_2 + r_3 \sin\theta_3 - r_4 \sin\theta_4 \tag{9}$$

Ideally, if $(\Delta x^2 + \Delta y^2)^{1/2} - \xi$ the system is in the impact mode. In digital simulation work, a tolerance is inevitably introduced in order to accommodate computational round-off errors. Thus, the system is assumed to be in the impact mode if the following inequality is satisfied

$$|\ 1.0 \times 10^{-7}\ | \leq [\ (\Delta x^2 + \Delta y^2)^{1/2} - \xi\ ] \tag{10}$$

Transient Phase

As mentioned before, the system is assumed to be in free-flight mode after the impact mode. If the pin and journal make contact within a flight time which subtends more than a twentieth of a degree of crank rotation, then this assumption is valid. If contact between the pin and journal is re-established within a twentieth of a degree of crank rotation and there is an insignificance difference between the original contact point and the new contact point, the simulation switches to the contact mode. The subsequent sections present the equations of motion for the different behavioral modes of the mechanism.

EQUATIONS OF MOTION IN THE CONTACT-MODE

By equations (3) - (5), a set of independent simultaneous second order differential equations can be obtained, which can be expressed, in matrix form, as

$$[\ A_1\ ]\ [\ X_1\ ] = [\ B_1\ ] \tag{11}$$

where

$$[A_1] = \begin{bmatrix} -1 & m_3 r_3 r_{G3} \cos(\theta_3 - \theta_4) & 0 & 0 & r_3 \sin\theta_3 & -r_4 \cos\theta_4 \\ 0 & I_{G3} + m_3 r_{G3}^2 & 0 & 0 & r_3 \sin\theta_3 & -r_4 \cos\theta_4 \\ 0 & 0 & 0 & 0 & -r_4 \sin\theta_4 & r_4 \cos\theta_4 \\ 0 & 0 & 0 & m_3 & 1 & 0 \\ 0 & r_3 \sin\theta_3 & -r_4 \sin\theta_4 & 1 & 0 & 0 \\ 0 & -r_3 \cos\theta_3 & r_4 \cos\theta_4 & 0 & 0 & 0 \end{bmatrix} \tag{12}$$

$$[\ X_1\ ]^T = [\ \lambda_3\ \ddot{\theta}_3\ \ddot{\theta}_4\ \ddot{s}\ \lambda_1\ \lambda_2\ ] \tag{13}$$

$$[B_1] = \begin{bmatrix} m_3 r_3 r_{G3} \dot{\theta}_3^2 \sin(\theta_3 - \theta_4) \\ -m_3 r_3 r_{G3} \dot{\theta}_3^2 \sin(\theta_3 - \theta_4) \\ 0 \\ -(\mathrm{sgn})\mu N_3 g \\ -r_3 \cos\theta_3 \dot{\theta}_3^2 - r_4 \cos\theta_3 \dot{\theta}_3^2 + r_4 \cos\theta_4 \dot{\theta}_4^2 \\ -r_3 \sin\theta_3 \dot{\theta}_3^2 - r_4 \sin\theta_3 \dot{\theta}_3^2 + r_4 \sin\theta_4 \dot{\theta}_4^2 \end{bmatrix} \tag{14}$$

The Lagrangian multiplier λ_1 equals F_{s3x} (the force imposes on link 3 by the slider in x - direction) and λ_2 equals F_{s3y}, while λ_3 is the torque imposed on the crank.

A free-body diagram of the system can be employed to calculate the bearing forces, shown as Figure 2. Thus,

$$F_{32x} = \lambda_1 - m_3 a_{G3x} \tag{15}$$

$$F_{32y} = \lambda_2 - m_3 a_{G3y} \tag{16}$$

$$F_{12x} = m_2 a_{G2x} - F_{32x} \tag{17}$$

$$F_{12y} = m_2 a_{G2y} - F_{32y} \tag{18}$$

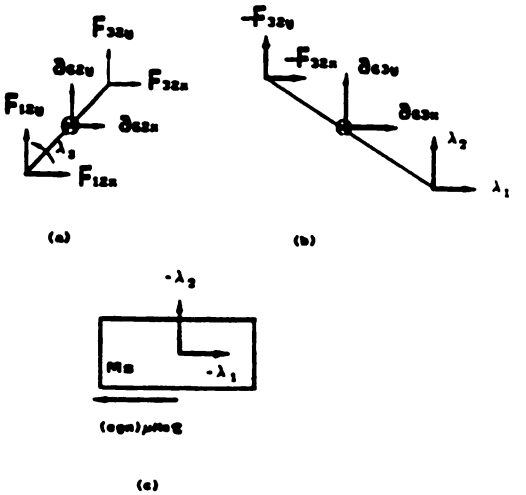

3. Fig. 2 Free-body diagram of the system in contact mode.

EQUATIONS OF MOTION IN FREE-FLIGHT MODE

In this mode, we treat the crank and the coupler as a set of double pendula. Therefore, the constraint force at the end of the coupler disappers. A torque is imposed on the crank to keep a constant angular velocity. By applying the constrained Lagrange equation again, only three second-order differential equations remain, which can be written, in matrix form, as

$$[\ A_3\ ]\ [\ X_3\ ] = [\ B_3\ ] \tag{19}$$

where

$$[A_3] = \begin{bmatrix} -1 & m_3 r_2 r_{G3}\cos(\theta_3 - \theta_2) & 0 \\ 0 & I_{G3} + m_3 r_{G3}^2 & 0 \\ 0 & 0 & m_3 \end{bmatrix} \tag{20}$$

$$[\ X_3\ ]^T = [\lambda_1\ \ddot{\theta}_3\ \ddot{s}\ ] \tag{21}$$

$$[B_3] = \begin{bmatrix} m_3 r_2 r_{G3}\dot{\theta}_3^2 \sin(\theta_3 - \theta_2) \\ -m_3 r_2 r_{G3}\dot{\theta}_3^2 \sin(\theta_3 - \theta_2) \\ -(\cos\theta_4) F_3 s \end{bmatrix} \tag{22}$$

EQUATIONS OF MOTION IN THE IMPACT MODE

If the impact duration, τ, is assumed to be arbitrarily small, the Lagrange equations of motion may be adapted , [19], and written

$$\left(\frac{\partial T}{\partial \dot{q}_k}\right)^* - \left(\frac{\partial T}{\partial \dot{q}_k}\right) = \int Q_k\, dt = \hat{Q}_k \tag{23}$$

the kinetic energy before and after impact can be expressed as

$$T = \frac{1}{2}(m_2 r_{G2}^2 + I_{G2})\dot{\theta}_2^2 + \frac{1}{2} m_3 (r_2^2 \dot{\theta}_2^2 + r_{G3}^2 \dot{\theta}_3^2 + 2 r_2 r_{G3}\dot{\theta}_2\dot{\theta}_3\cos(\theta_3 - \theta_2)) + \frac{1}{2} I_{G3}\dot{\theta}_3^2 + \frac{1}{2} m_3 \dot{s}^2 \tag{24}$$

$$T^* = \frac{1}{2}(m_2 r_{G2}^2 + I_{G2})\dot{\theta}_2^{*2} + \frac{1}{2} m_3 (r_2^2 \dot{\theta}_2^{*2} + r_{G3}^2 \dot{\theta}_3^{*2} + 2 r_2 r_{G3}\dot{\theta}_2^*\dot{\theta}_3^*\cos(\theta_3 - \theta_2)) + \frac{1}{2} I_{G3}\dot{\theta}_3^{*2} + \frac{1}{2} m_3 \dot{s}^{*2} \tag{25}$$

respectively. Referring to the free-body diagram presented as Figure 3 and applying the Lagrange equations of motion, (equation 23), three equations are obtained

$$m_3 r_2 r_{G3}(\dot{\theta}_3^* - \dot{\theta}_3)\cos(\theta_3 - \theta_2) = \hat{T}_{or} + \hat{F} r_2 \sin(\theta_2 - \theta_4) \tag{26}$$

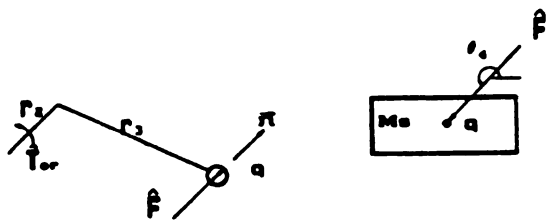

Fig. 3 Free-body diagram of the system in impact mode.

$$(m_3 r_{G3}^2 + I_{G3})(\dot{\theta}_3^* - \dot{\theta}_3) = \hat{F} r_3 \sin(\theta_3 - \theta_4) \tag{27}$$

$$m(\dot{s}^* - \dot{s}) = \hat{F}\cos\theta_4 \tag{28}$$

Thus there are four unknowns, $\hat{T}_{or}$, $\hat{F}$, $\dot{\theta}_3^*$, and $\dot{s}^*$, but only three equations. Hence an extra equation is required in order to determine a unique solution. The coefficient of restitution may be employed to provide the addition information. The resulting expression is

$$e = -\frac{(\vec{V}_{Q3}^* - \vec{V}_{Q4}^*)\cdot\vec{n}}{(\vec{V}_{Q3} - \vec{V}_{Q4})\cdot\vec{n}} \tag{29}$$

which may be written,

$$e = -\frac{r_2\dot{\theta}_2\sin(\theta_2 - \theta_4) + r_3\dot{\theta}_3^*\sin(\theta_3 - \theta_4)}{r_2\dot{\theta}_2\sin(\theta_2 - \theta_4) + r_3\dot{\theta}_3\sin(\theta_3 - \theta_4)} + \frac{\dot{s}^*\cos\theta_4}{\dot{s}\cos\theta_4} \tag{30}$$

Again, the above equations of motion can be expressed, in matrix form, as

$$[\ A_3\ ]\ [\ X_3\ ] = [\ B_3\ ] \tag{31}$$

where

$$[A_3] = \begin{bmatrix} -1 & m_3 r_2 r_{G3}\cos(\theta_3 - \theta_2) & 0 & -r_3\sin(\theta_3 - \theta_4) \\ 0 & m_3 r_{G3}^2 + I_{G3} & 0 & -r_3\sin(\theta_3 - \theta_4) \\ 0 & 0 & m_3 & -\cos\theta_4 \\ 0 & -r_3\sin(\theta_3 - \theta_4) & -\cos\theta_4 & 0 \end{bmatrix} \tag{32}$$

$$[\ X_3\ ]^T = [\hat{T}_{or}\ \ \dot{\theta}_3^*\ \ \dot{s}^*\ \ \hat{F}\ ] \tag{33}$$

$$[B_3] = \begin{bmatrix} m_3 r_2 r_{G3} \dot{\theta}_3 \cos(\theta_3 - \theta_4) \\ (m_3 r_{G3}^2 + I_{G3}) \dot{\theta}_3 \\ m_3 \dot{s} \\ + (r_2 \dot{\theta}_3 \sin(\theta_3 - \theta_4) + r_3 \dot{\theta}_3 \sin(\theta_3 - \theta_4) + \dot{s} \cos \theta_4) \\ + r_3 \dot{\theta}_3 \sin(\theta_3 - \theta_4) \end{bmatrix} \quad (34)$$

EXPERIMENTAL APPARATUS

The principal subassembly in this experimental investigation was a planar slider-crank mechanism incorporating substantially rigid links which articulated in a plane perpendicular to the gravitational field. The crank, which had a length of 50 mm, was fabricated as an integral part of a 146 mm diameter flywheel. This heavy circular disc was keyed to a 19.05 mm diameter drive-shaft, which was supported on a matched pair of Timken tapered-roller bearings, Type TS4A-6, and was powered by a 0.56KW (0.75 hp) Dayton variable-speed dc motor, model 2Z846A. The slider of the slider-crank mechanism was the translating table element of a Micro Slides, Inc., type 2050-RW-118-5 linear crossed-roller slide assembly which is a precision preloaded system without clearance.

The connecting rod assembly comprised three components: a steel bar with dimensions 267x6x19 mm^3, a crank-pin bearing, and a gudgeon-pin bearing. The total length of this link member was 293 mm between bearing centerlines. The crank-pin bearing was designed to incorporate a matched pair of instrument ball bearings supplied by FAG Bearings Limited, type R4DB12. The spindle diameter was 6.35 mm. This bearing assembly was carefully preloaded using a Dresser Industries torque-limiting screw driver. This procedure enabled bearing clearance to be removed from the assembly, since the vibrational response associated with this clearance at the crank pin would have contaminated the experimental data from the transducers monitoring the dynamic response of the system at the gudgeon pin.

The gudgeon-pin bearing was fabricated as journal bearing with variable radial clearance. This was achieved by employing steel pins of diameter 6.35 mm and 4.572 mm which were each supported in a threaded hole in the reciprocating portion of the crossed-roller slide assembly. The journal element of the bearing was provided by a series of interchangeable brass bushings with internal diameters of 6.4 mm, 6.5024 mm, 6.604 mm which permitted a variety of joints to be assembled with radial clearances of 1.016 mm, 0.127 mm, 0.0762 mm and 0.0254 mm respectively.

In addition, a second bearing assembly at the gudgeon pin was developed in order to design a joint with zero clearance. This would provide a reference set of data for comparison with the results of the experiments with non-zero clearance. This precision bearing assembly incorporated a matched pair of instrument ball bearings supplied by FAG Bearings Limited, type R4DB12. The spindle diameter was 6.35 mm.

The experimental apparatus and the associated instrumentation is schematically represented in Figure 4 and Figure 5. The dynamic behavior of the slider and the connecting rod were

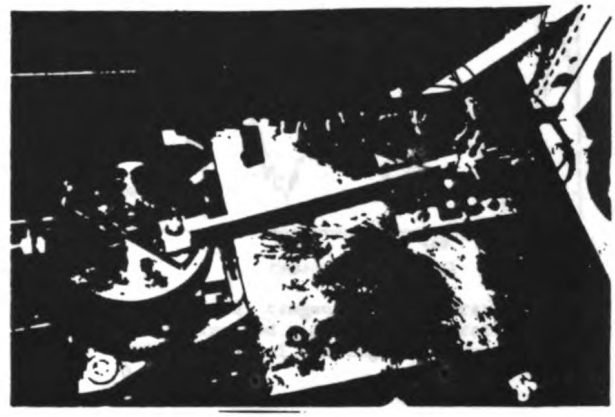

Fig. 4 Photograph of Experimental Apparatus

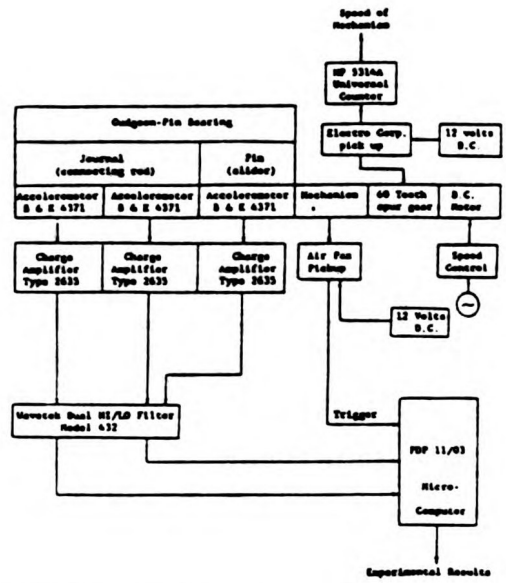

Fig. 5 Schematic of Experimental Appratus and Associated instrumentation.

monitored using three Bruel and Kjaer piezoelectric accelerometers, type 4371, which were each connected to a Bruel and Kjaer charge amplifier, type 2635. These accelerometers were positioned at the gudgeon-pin bearing in order to measure the dynamic response of the reciprocating slider and also the longitudinal and lateral motions of the connecting rod. The signals from these accelerometers were fed to a Wavetek HI/LO analog filter, model 432, prior to being recorded on a PDP11-based digital-data-acquisition system. The cut-off frequency employed in this study was 60 Hz.

The response profiles measured by the accelerometers were related to the angle of the crankshaft using a third transducer arrangement, which featured an Airpax zero-velocity digital pickup, type 14-0001. This was employed to sense the bolt head protruding from the flywheel when the

crank was in the conventional zero crank-angle position, prior to firing the Schmitt triggers on the input/output panel of the data-acquisition system. The highest sampling rate employed in this study was 2,500 samples per second.

NUMERICAL AND EXPERIMENTAL RESULTS

A slider-crank mechanism with r_2= 0.048 m, r_3= 0.293 m, m_2= 1.0 Kg, m_3= 0.21435 Kg, m_4= 0.63607 Kg, I_{G2}= 0.1 Kg-m^2, I_{G3}= 0.003883 Kg-m^2 and ϵ = 0.5 was used in this study.

The initial conditions for the computer simulations were based upon the assumption that the fictitious clearance link has the same direction as the pressure angle. The magnitude of this angle was obtained from an analysis of the mechanism incorporating a gudgeon pin bearing with zero clearance. In addition, the angular velocity of the clearance-link was assumed to equal the rate of change of the pressure angle. As mentioned in the previous section, the equations of motion were expressed in the matrix form $[A_1][X_1] = [B_1]$. If the proper initial values are given, then $[A_1]$ and $[B_1]$ can be calculated in order to solve for $[X_1]$. PLU-factorization was employed together with forward and backward substitution in order to achieve this task. In this example, $[X_1]$ includes some second-order terms, such as $\ddot{\theta}_3$, $\ddot{\theta}_4$ and $\ddot{s}$, and Lagrange multipliers. By converting the second-order equations into a first-order system, a subroutine "DGEAR" in the IMSL subroutine library was employed to integrate the second-order derivatives. Thus $\dot{\theta}_1$, θ_1, $\dot{s}$, and s were obtained. The initial conditions for each time-step in the computer simulations were obtained from the previous time-step. The average CPU-time for one cycle was 2 minutes and 50 seconds on a Vax-11/750 computer.

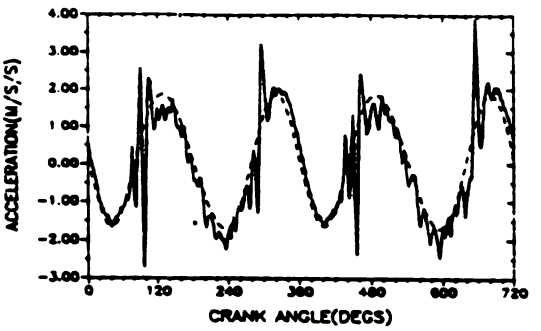

Fig. 6 Experimental tangential acceleration of the connecting rod. Mechanism operating speed 200 rpm, radial bearing clearance 0.000127 m.

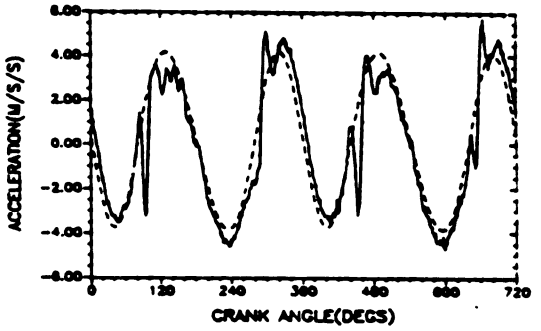

Fig. 7 Experimental tangential acceleration of the connecting rod. Mechanism operating speed 300 rpm, radial bearing clearance 0.000127 m.

RESULTS

Space limitations only permit some of the experimental and analytical results to be presented herein. Figures 6-9 present experimental response histories from this experimental investigation for 200 and 300 rpm. The radial clearance is 0.127 mm at the gudgeon-pin bearing for all response profiles. Figures 6 and 7 present the tangential accelerations of the connecting rod at 200 and 300 rpm respectively while Figures 8 and 9 present the corresponding accelerations of the slider. Figures 10-13 present the analytical results for the tangential accelerations of the connecting rod, and also the accelerations of the slider when the crank rotates at 200 and 300 rpm respectively and the gudgeon-pin bearing is 0.127 mm.

Upon viewing Figures 6-9 it is clear that the pin and journal loose contact, or separate, twice during each revolution of the crank shaft as evidenced by the major excursions from the smooth curves of the zero-clearance mechanism. The first separation generally occurred at approximately 80 degrees of crank rotation and the second separation occurred at approximately 280 degrees of crank rotation. Upon reviewing the acceleration profiles of the analytical predictions presented, Figures 10-13, it is evident that there is excellent correlation between the theoretical and experimental results. These two sets of results could have been simultaneously plotted on the same diagram, however it is extremely difficult to differentiate between the two sets of results. Figures 10 and 11, indicate that the most serious impact occurred at 95 degrees and 298 degrees of crank rotation, while the experimental results, presented in Figures 6 and 7, indicate that the first impact occurs between 90 and 98 degrees of the crank rotation, and the second impact occurs between 290 and 298 degrees of crank rotation.

Figures 14 presents the longitudinal acceleration of the connecting rod at 300 rpm, in which the solid line is the experimental curve and the dotted line is the theoretical curve with zero clearance. Figure 15 shows the numerical predictions for the longitudinal acceleration of the connecting rod at 300 rpm with 0.127 mm clearance. Upon examining these two curves it is evident that the bearing clearance has very little affection in the longitudinal dynamic behavior of the connecting rod.

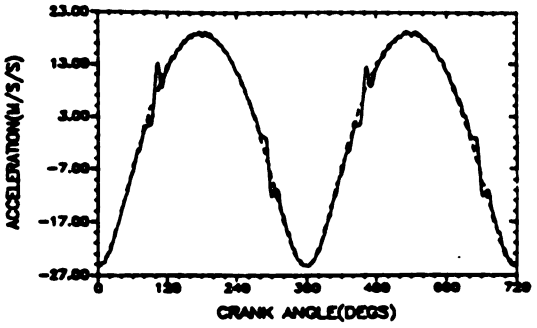

Fig. 8 Experimental slider acceleration. Mechanism operating speed 200 rpm, radial bearing clearance 0.000127 m.

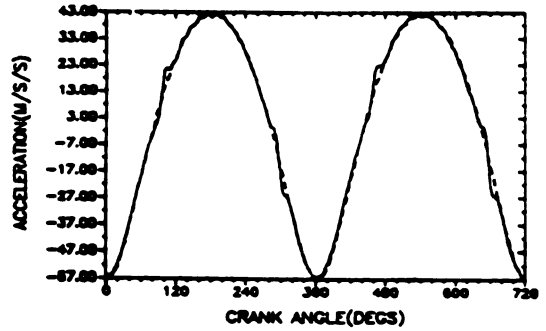

Fig. 9 Experimental slider acceleration. Mechanism operating speed 300 rpm, radial bearing clearance 0.000127 m.

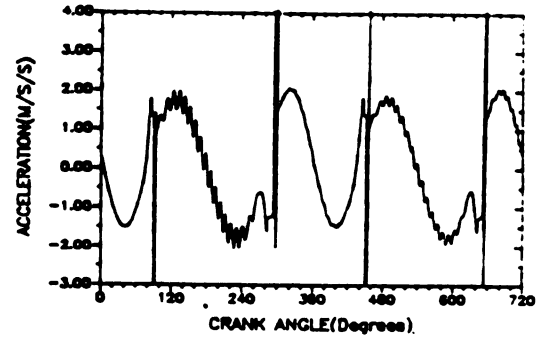

Fig. 10 Theoretical tangential acceleration of the connecting rod. Mechanism operating speed 200 rpm, radial bearing clearance 0.000127 m.

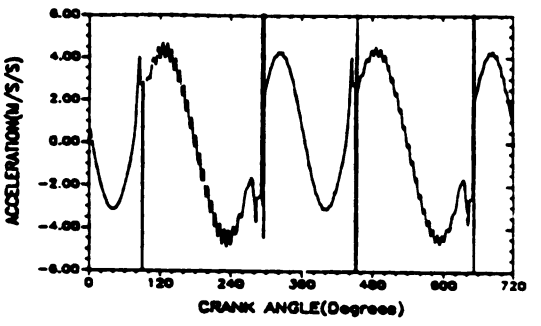

Fig. 11 Theoretical tangential acceleration of the connecting rod. Mechanism operating speed 300 rpm, radial bearing clearance 0.000127 m.

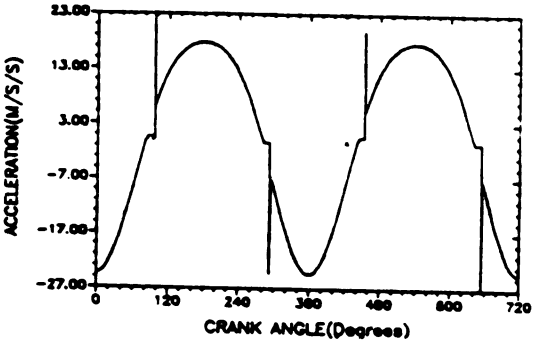

Fig. 12 Theoretical slider acceleration. Mechanism operating speed 200 rpm, radial bearing clearance 0.000127 m.

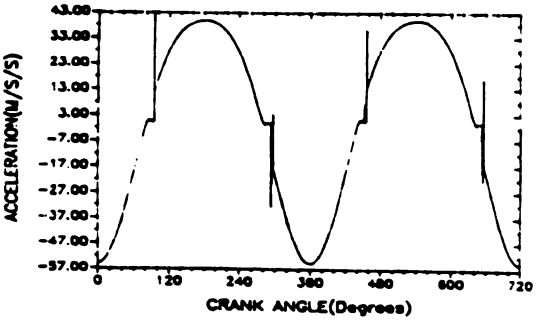

Fig. 13 Theoretical slider acceleration. Mechanism operating speed 300 rpm, radial bearing clearance 0.000127 m.

Figures 6 and 7 indicate that the first impact, at approximately 95 degrees crank rotation, creats a more severe vibrational response than the second impact at approximately 300 degrees of crank rotation which present the tangential acceleration profile of the connecting rod. The predictions in Figures 10 and 11 show the same results.

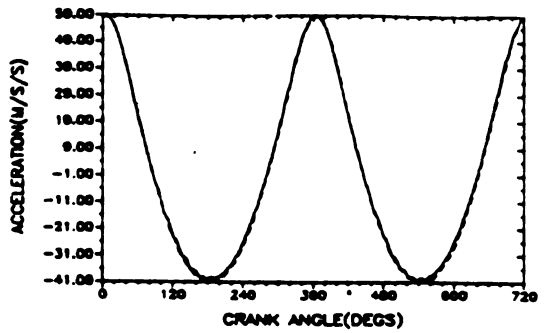

Fig. 14 Longitudial acceleration of connecting rod. Mechanism operating speed 300 rpm. Solid line presents the experimental result with 0.000127 m radial bearing clearance. The distinuous line presents the theoretical result without clearance.

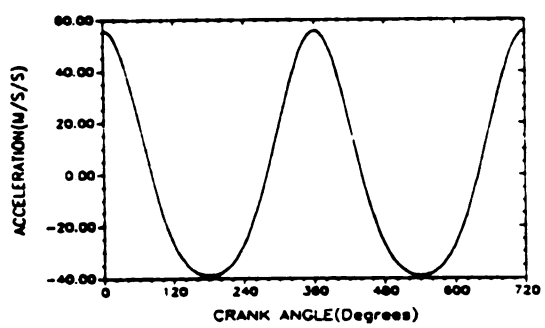

Fig. 15 Theoretical longitudial acceleration of connecting rod. Mechanism operating speed 300 rpm, radial bearing clearance 0.000127 m.

Since the coefficient of restitution was employed in modeling the dynamic response of this class of mechanism system and the impact duration was assumed to be arbitrary small in the numerical simulation, the impact force tends to infinity. The spikes in Figure 10 and 11 were truncated in order to facilitate comparision with the experimental curves. In fact the impact duration is finite, in the order of 10^{-5} second, and the frequencies above 60 hz were filtered while recording the experimental response data.

CONCLUSION

The mathematic model and intermittent behavior of a gudgeon pin of a slider-crank mechanism joint with radial clearance have been studied. The numerical results are in qualitative agreement with the experimental results. Two loss-of-contact situations occur during each mechanism cycle and the loss of contact have been accurately predicted along with the associated dynamic response behavior.

ACKNOWLEDGMENT

The first author wishes to gratefully acknowledge the financial support of the Chung-Cheng Institute of Technology, Taiwan, which has enabled him to undertake this research.

REFERENCES

1. Kobrinskii, A.E., Dynamics of Mechanisms with Elastic Connections and Impact Systems, Fliffe Book Ltd., London, 1969.

2. Wittenberg, J., Dynamics of Systems of Rigid Bodies, B.G. Teubner, Stuttgart, 1977.

3. Kane, T.R. and Levinson, D.A., "Multibody Dynamics," ASME Journal of Applied Mechanics, Vol. 50, 1978, pp. 1071-1078.

4. Haines, R.S., "Survey: 2-Dimensional Motion and Impact at Revolute Joints." Mechanism and Machine Theory, Vol. 15, 1980, pp. 361-370.

5. Kalker, J.J. "A Survey of the Mechanics of Contact Between Solid Bodies,"Zeitschrift fur Angewandte Mathematik und Mechanik, ZAMM 57, T3 - T17 (1977)

6. Khulief, Y.A. and Shabana, A.A., "Impact Responses of Multibody Systems with Consistent and Lumped Masses," Journal of Sound and Vibration, Vol. 104, 1986, pp. 187-207.

7. Bengisu, M.T., Hidayetoglu, T., and Akay, A., "A Theoretical and Experimental Investigation of Contact Loss in the Clearances of a Four-Bar Linkage," ASME Journal of Mechanism, Transmission and Automation in Design, Vol. 108, 1986, pp. 237-244.

8. Dubowsky, S., Deck, J.F., Costello, H., "The Dynamic Modeling of Flexible Spatial Machine System with Clearance Connections," ASME Paper No. 86-DET-62, and ASME Journal of Mechanisms, Transmissions and Automation in Design, (in press).

9. Haines, R.S., "An Experimental Investigation into the Dynamic Behavior of Revolute Joints with Varying Degrees of Clearance," Mechanism and Machine Theory, Vol. 20, 1985, pp. 221-231.

10. Dubowsky, S., and Moening, M.F., "An Experimental and Analytical Study of Impact Forces in Elastic Systems with Clearances," Mechanism and Machine Theory, Vol. 13, 1978, pp. 451-465.

11. Grant, S.J. and Fawcett, J.N., "Effects of Clearance at Coupler-Rocker Bearing of a Four-Bar Linkage," Mechanism and Machine Theory, Vol. 14, 1974, pp. 99-110.

12. Shimojima, H., Ogawa, K., and Matsumoto, K., "Dynamic Characteristics of Planar Mechanism with Clearances," Bulletin of Japanese Society of Mechanical Engineers, Vol. 21, 1978, pp. 303-308.

13. Wilson, R., and Fawcett, J.N., "Dynamics of the Slider-Crank Mechanism with Clearance in the sliding Bearing," Mechanism and Machine Theory, 1974, Vol. 9, pp. 61-80.

14. Miedema, B. and Mansour, W.M., "Mechanical Joints with Clearance: A Three-Mode Model," ASME Journal of Engineering for Industry, Vol. 98, 1976, pp. 1319-1323.

15. Osman, M.O.M., Behgat, B.M., and Sankar, T.S., "On the Prediction of Journal-Bearing Separation in High-Speed Mechanisms with Clearances," ASME paper 80-WA/DSC-36, 1980.

16. Mansour, W.M., and Townsend, M.A., "Impact Spectra and Intensities for High-Speed Mechanisms," ASME Journal of Engineering for Industry, Vol. 97, 1975, pp. 347-353.

17. Hunt, K.H., and Crossley, F.R.E., "Coefficient of Restitution Interpreted as Damping in Vibroimpact," ASME Journal of Applied Mechanics, Vol. 97, 1975, pp. 440-445.

18. Tatara, Y., "Effects of External Force on Contacting Times and Coefficients of Restitution in a Periodic Collision," ASME Journal of Applied Mechanics, Vol. 44, 1977, pp. 773-774.

19. Goldsmith, W., Impact: The Theory and Physical Behavior of Colliding Solids, Edward Arnold, London, 1960.

20. Soong, K., and Thompson B.S., "An Experimental Investigation of the Dynamic Response of a Mechanical System with Bearing Clearance," ASME Design Technology Conference, 1987. DE-Vol.10-2, Advances in Design Automation -1987, Volume Two, Robotics, Mechanisms, and Machine System, pp. 411-419.

EFFECTS OF INTERMITTENT CONTACT IN MECHANISMS OF THE PERFORMANCE OF NUMERICAL INTEGRATION METHODS

EFFECTS OF INTERMITTENT CONTACT IN MECHANISMS ON THE PERFORMANCE OF NUMERICAL INTEGRATION METHODS

by

J.M.B. Brown*, K. Soong+, W.K.D. Borthwick×,
M.V. Gandhi+ and B.S. Thompson+

* University of Dundee, Scotland, U.K.; Visiting Professor, Michigan State University
\+ Machinery Elastodynamics Laboratory, Mechanical Engineering Department, Michigan State University, USA
× Heriot-Watt University, Edinburgh, Scotland, U.K.

SUMMARY

High-speed mechanisms cannot be accurately stimulated, and hence designed, without incorporating link elasticity and joint-clearance effects in the mathematical models. Numerical simulations based on these mathematical models often incorporate algorithms of the Runge-Kutta type. The performance of this classical method applied to a simple oscillator is reviewed herein, and the error-performance is shown to collapse to first-order when the algorithm is applied to a spring/mass system with a stiffness discontinuity. Discrete energy changes are found to occur at discontinuity traversals with gains for hardening spring-systems and losses for softening spring-systems. These energy changes will occur each time contact is gained or lost when simulating the behavior of a flexible mechanism with intermittent contacts.

INTRODUCTION

In the last two decades commercial pressures have stimulated the development of mechanisms capable of higher operating speeds while requiring improvements in output characteristics and reductions in power consumption and acoustic pollution. Consequently, it has been necessary to develop more detailed theoretical models of mechanisms by incorporating elasticity and damping of links and mountings, and by also including the effects of clearances in the joints. Some of these theoretical developments are reviewed in references [1] and [2].

Even in the simplest of mechanisms the equations of motion obtained when the rigid-link/perfect-joint model is abandoned are of such complexity that the associated initial/boundary value problems cannot be solved analytically in closed-form. Progress in the study of these effects can thus only be made by the application of various numerical simulation techniques available with digital computers, in conjunction with experimental and/or analog investigations.

Numerical simulation requires the modelling of the distribution of mass and elastic stiffness, and the tracing of the temporal evolution from some initial conditions. While lumped-parameter models of mass and stiffness have been utilized [3] it is now generally accepted that the finite element approach [2] is more suitable for this spatial problem. Recent developments have included non-linear effects [4] and the use of composite materials [5]. There are two basic approaches to the simulation of the temporal evolution of the mechanism from a prescribed initial state; these are modal superposition, and direct numerical integration in time.

Modal superposition uses a linear combination of the vibrational mode shapes. In nonlinear systems the approach may require frequent redetermination. Furthermore, in mechanisms which have intermittent contacts whether by design or due to clearances, it is likely that many of the higher modes of vibration will be excited. Under such conditions modal superposition is likely to be more expensive than direct numerical integration [2].

Direct numerical integration procedures utilize a step-by-step approach in which, starting from known initial conditions, the equations of motion are effectively solved only at a series of discrete time points. The classical methods fall into two main groups [6,7], the Runge-Kutta algorithms, and multi-step algorithms. Both are widely used in mechanism simulations; the former, for example, as the classic fourth-order Runge-Kutta, [8], or Runge-Kutta-Merson [9]; the latter, in various types of predictor-corrector methods [10]. These methods are formulated for systems of first-order ordinary differential equations. Some methods applicable directly to equations of motion have been developed by structural dynamicists [11], and a form of one of these, the Newmark method, has been used to analyse mechanisms [5].

A common characteristic of intermittent contact mechanisms [12] and mechanisms with bearing clearances [13], is the occurrence of discontinuities of the system parameters, in time. Loss of contact is followed by a phase of independent response by two or more parts of the mechanism. This phase is terminated by a resumption of contact usually involving impact. Because of these repeated changes in connectivity there are corresponding changes in parameters and restraint conditions leading to, for example, repeated changes in the underlying natural modes of vibration. Recent research [14,15] indicates that special difficulties may be presented by the application of numerical integration algorithms to systems which experience repeated, sudden, changes of system parameters.

The purpose of this paper is to describe the application of the classical Runge-Kutta method to a test problem exhibiting sudden changes in system parameters. This widely used and usually very accurate method is shown to behave very badly when applied to a system of this type.

THE RUNGE-KUTTA ALGORITHM

The classical fourth-order scheme, often referred to as 'the Runge-Kutta method', is formulated for a system of first-order ordinary differential equations. Therefore the equation of motion of a single oscillator

$$m\ddot{z} + c\dot{z} + kz = F(t) \qquad (1)$$

must be re-expressed as the system

$$\dot{{}^1x} = {}^2x \qquad (2a,b)$$

$$\dot{{}^2x} = (F(t) - c\,{}^2x - k\,{}^1x)/m$$

In equations (1) and (2) k and c are stiffness and damping coefficients; F(t) is the applied forcing function; $z = {}^1x$ is the displacement, and $\dot{z} = {}^2x$ is the velocity, of the mass m.

The Runge-Kutta method applied to a single equation

$$\dot{y} = f(y,t) \qquad (3)$$

generates a sequence of approximations y_n where n = 0,1,2,... to the exact values $y(t_n)$ where $t_n = nh$ and h is the time-step. The algorithm has the form, for a single equation,

$$y_{n+1} = y_n + (k_0 + 2k_1 + 2k_2 + k_3)h/6 \qquad (4a)$$

where

$$k_0 = f(y_n, t_n) \qquad (4b)$$

$$k_1 = f(y_n + \tfrac{1}{2}hk_0,\ t_n + h/2) \qquad (4c)$$

$$k_2 = f(y_n + \tfrac{1}{2}hk_1,\ t_n + h/2) \qquad (4d)$$

$$k_3 = f(y_n + hk_2,\ t_n + h) \qquad (4e)$$

The errors generated by such a method are of order h^4 [6,7], provided that the function of equation (3) meets certain continuity conditions. This theoretical error-performance can be confirmed by the application of equations (4) to the undamped free vibration problem

$$m\ddot{z} + kz = 0 \qquad (5a)$$

$$z = z_0;\ \dot{z} = 0 \quad \text{at } t = 0 \qquad (5b,c)$$

$$k/m = 4\pi^2 \qquad (5c)$$

The displacements obtained for the first few oscillations using a time-step h = 0.05 (equal to 1/20th of the true period of the oscillator (5)) are shown in Figure 1. The numerical results are close to the form of the true solution $z = z_0 \cos 2\pi t$.

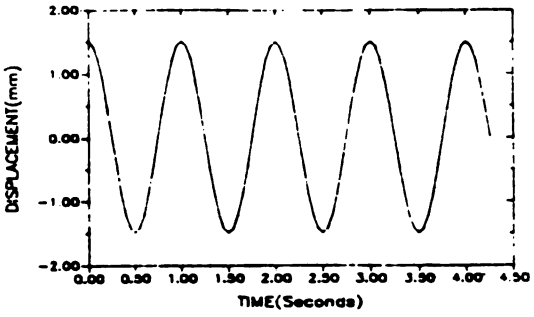

Figure 1 Spring/mass system displacement with constant stiffness; $\omega^2 = 4\pi^2 \left[\frac{1}{sec^2}\right]$; x_o = 1.5 mm; x_d = 1 mm; $\dot{x}_o$ = 0 mm/sec; cubic spline on displacements by 4th-order Runge-Kutta; exact solution points indistinguishable on scale of figure.

TABLE 1

Displacement error norm (equation 6) for the oscillator (equation 5) using Runge-Kutta method with time steps $h = 2^{-k}$

h	Error	Error/h^4
2^{-2}	0.27048307	69.2
2^{-3}	1.71146738E-2	70.1
2^{-4}	1.00850978E-3	66.1
2^{-5}	6.23348779E-5	65.6
2^{-6}	6.76618441E-6	79.9

Repetition of the analysis using uniform time-steps $h = 2^{-k}$ where k = 2,3,...6 resulted in error performance as shown in Table 1. The error shown in column 2 is

$$||z_n - z(t_n)||_\infty = \max_{n=1,2,\ldots N} |z_n - z(t_n)| \qquad (6)$$

where N = T/h is the number of time-steps in one exact period of oscillation. In column 3 the error divided by the fourth power of h is seen to be approximately constant for k = 2,...6. The data were obtained using only single precision arithmetic and so the agreement could be improved using double precision.

Thus the error-order h^4 for the Runge-Kutta method (4) has been verified for the simple oscillator (5). The actual errors are very small. For example, using h = 0.05 T as in Figure 1. $||\ ||_\infty$ as defined by equation (6) is 6·105788E-4.

corresponding to a maximum error in displacement during the first cycle of oscillation equal to 0.06%.

Similarly, the error in the energy of the oscillator i.e.,

$$E_n = \frac{1}{2} k z_n^2 + \frac{1}{2} m \dot{z}_n^2 \qquad (7)$$

is found to be 0.026% after one cycle of oscillation using the time step h = T/20, and to increase proportionately for the first few cycles.

Since the exact solution of equation (5) is $z = z_o \cos \omega t$, it corresponds to a pair of exponentials with the complex conjugate, purely imaginary, exponents $\pm i \omega t$. Thus by reference to published stability diagrams [6,7] the oscillation will be stable provided $\omega h < \sqrt{8}$ where $\omega^2 = k/m$.

The Runge-Kutta method applied to problems such as defined by equations (1) and (5), having well-behaved functional forms is thus highly accurate; though, of course, it is only conditionally stable. It has the further advantage of explicit formulation.

A TEST PROBLEM FOR INTERMITTENT CONTACT

The spring-mass arrangement shown in Figure 2 has been introduced in [15] as a test problem for mechanical systems experiencing sudden changes in parameters. The mass m is attached to ground through the spring of stiffness k_1. For small excursions the mass may oscillate within the range $-z_d \le z \le z_d$ where $z_d > 0$. For displacements $|z| > z_d$ the mass is assumed to contact (without loss of energy) the springs of stiffness k_2 which are precompressed such that the force/displacement characteristic is as shown in Figure 3. There is thus a sudden change of stiffness at $|z| = z_d$, and in addition, a sudden change of force.

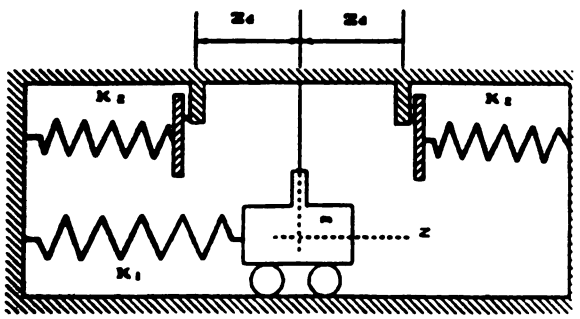

Figure 2 Spring/mass systems with clearance z_d and pre-loaded springs to obtain stiffness discontinuity.

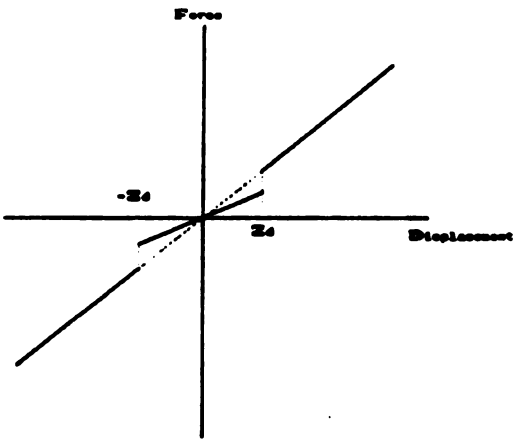

Figure 3 Force/displacement characteristics obtained from the arrangement of Figure 2.

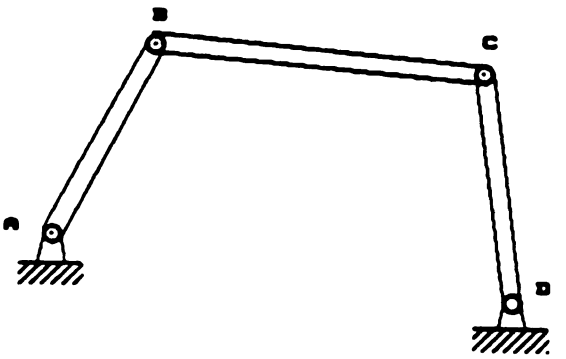

Figure 4 Four bar linkage mechanism.

The arrangement described above contains essential features of mechanisms with intermittent contact. For example, consider a 4-bar chain with clearance at the coupler/follower bearing as sketched in Figure 4. When contact exists at C the stiffness matrices of the two subsystems ABC and CD are linked. When contact is lost at C these two subsystems become independent; there is then a sudden change of elastic stiffness as seen by each subsystem. Contact-loss is analogous to passage from $|z| > z_d$ to $|z| < z_d$; when contact is re-established, this is equivalent to crossing from the inner zone to the outer zone of Figure 3.

Thus the application of a numerical integration algorithm to this test system should indicate the error performance which can be expected when the algorithm is applied to a whole mechanism. For a complete assessment of error the exact response in free vibration is required for the system. As is shown in reference [15] the exact solution consists of a chain of linear initial-value-problems with

change points each time the displacement $|z|$ crosses from one side of z_d to the other. In the case of initial conditions $z = z_o$ and $\dot{z} = 0$ at the first of the chained solution analyses the period of oscillation is shown in reference [15] to be

$$T = 4(\cos^{-1}(z_d/z_o)/\omega_o + \tan^{-1}(-z_d\omega_I/\dot{z}_c)/\omega_I) \quad (8a)$$

where

$$\dot{z}_c = -z_o\omega_o \sin(\cos^{-1}(z_d/z_o)) \quad (8b)$$

and (see Figure 3)

$$\omega_o^2 = (k_1 + k_2)/m; \qquad \omega_I^2 = k_1/m \quad (8c,d)$$

From equations (8) it is seen that the period depends on the relative incursion into the outer stiffness zone i.e., on z_o/z_d, and on the ratio of the stiffness k_o and k_I of the outer and inner zones respectively, i.e., on

$$r = k_o/k_I \quad (9)$$

For example, taking $k_I = 4\pi^2$ the period is 1.0 for $r = 1$, the ordinary linear oscillator; however, if $z_o/z_d = 1.5$ the period is 0.737631, for $r = 2$ and 0.535441 for $r = 4$. When the initial incursion is reduced to $z_o/z_d = 1.1$ the period for a stiffness ratio $r = 4$ is 0.664492 which is less than that for $r = 2$ with $z_o/z_d = 1.5$. Thus at larger stiffness ratios the period is sensitive to even small incursions into the outer zone. This property is advantageous in testing algorithm performance at intermittent contacts. Should the outer zone be less stiff than the inner (the 'softening' system) the period is greater than for the 'hardening' spring system. Thus for $z_o/z_d = 1.5$ and $r = 0.5$ the period is 1.331352.

APPLICATION OF RKA ALGORITHM TO THE TEST PROBLEM

The classical Runge-Kutta method of equations (4) was applied to the initial value problem

$$m\ddot{z} + kz = 0 \quad (10a)$$

$$k = k_I = 4\pi^2 \qquad (|z| \le z_d) \quad (10b)$$

$$k = k_o = 4\pi^2 r \qquad (|z| > z_d) \quad (10c)$$

$$z = z_o,\ \dot{z} = 0 \text{ when } t = 0 \quad (10d)$$

described in the previous section. In particular choosing $r = 2$, $z_o/z_d = 1.5$, $z_d = 1$ the result obtained using a time step $h = 0.05$ is the connected line shown in Figure 5. The amplitude of the numerically obtained oscillation is seen to grow rapidly. The exact solution to the problem (10) obtained as described in reference [15] is plotted at significant time points and of course maintains constant amplitude in the absence of any physical damping.

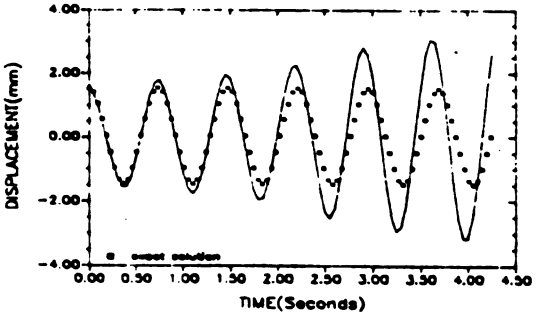

Figure 5 Spring/mass system displacement as in Figure 2 with $(k_1 + k_2)/k_1 = 2$; $k_1/m = 4\pi^2\left[\frac{1}{sec^2}\right]$; $x_o = 1.5$ mm; $x_d = 1$ mm; $\dot{x}_o = 0$ mm/sec; displacements by 4th order Runge-Kutta connected by cubic splines; exact solution unconnected squares.

A possible explanation for this behavior might lie in the stability condition

$$h \le \sqrt{8}/\omega \quad (11)$$

mentioned earlier for this algorithm. However, even in the stiff zone $\omega = \sqrt{(k_o/m)} = \pi\sqrt{8}$. Hence, condition (9) requires $h < 1/\pi$ which is certainly satisfied. Thus although the Runge-Kutta method is being applied correctly (according to the definition for continuous functions) it is unable to perform to its design order when applied to a system with a functional discontinuity (equation 10).

When $r < 1$ in equation (10c) the stiffness of the outer zone is less than that of the inner zone. Figure 6 illustrates the numerical oscillation obtained when $z_o/z_d = 1.5$, $z_d = 1$ (as in Figure 5) but $r = 0.5$ (compared to $r = 2$ for Figure 5). The oscillation now decreases steadily in amplitude and after about 3 complete oscillations is completely contained within the inner stiffness zone. Since no further discontinuity traversals occur the subsequent behavior is that expected from the method; namely, a very gradual loss of amplitude.

Returning to systems of the 'hardening' type, Figures 5 and 7 show the effects of increasing the stiffness ratio from 2 to 4 for the same initial conditions. The frequency of the oscillation is larger in Figure 7 because of the greater stiffness in the outer zone than in the system of Figure 5. The growth of amplitude/cycle is more rapid in Figure 7, attaining 3.5 in 4 cycles compared with 6 cycles in Figure 5. It may also be noted that after an amplitude of 4 is attained in Figure 7 the oscillation appears to become steady. This occurs because the energy of the oscillator is now so great

that the mass passes from the outer zone ($z > z_d > 0$) to the outer zone ($z < -z_d < 0$) in one time-step (and vice versa). Thus at each time point the function evaluations of equations (4) are all made in the same stiffness zone. The inner zone is effectively hidden from the numerical process, no discontinuities are traversed, and the usual performance of the algorithm is recovered.

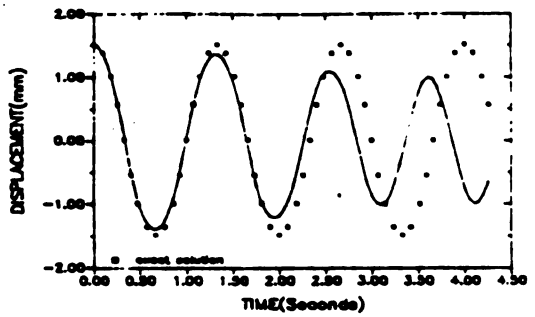

Figure 6 Spring/mass system displacement with outer zone stiffness half the inner zone stiffness (which is $4\pi^2$); m = 1 kg; other data as for Figure 5.

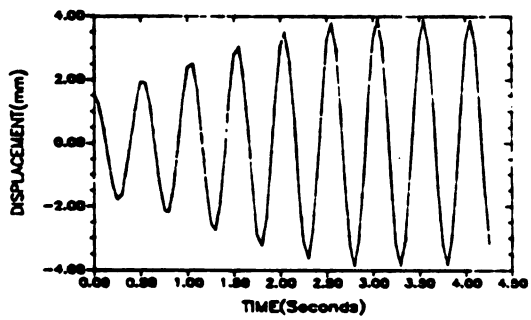

Figure 7 Spring/mass system displacement as for Figure 5, but $(k_1 + k_2)/k_1 = 4$; other information as in Figure 5.

Comparison of Figures 7 and 8 shows, for the same stiffness and initial conditions, the effect of halving the time-step. The amplitude of oscillation grows more slowly in Figure 8 requiring about 8 cycles to reach 3.5 compared with 4 cycles in the case of Figure 7. Thus the improvement in performance due to halving the time step is roughly proportional to the change of the step. This contrasts with the expectation of h^4 dependence which was confirmed for a simple oscillator in Table 1. Thus the effect of the discontinuity traversals has been to degrade the error performance of the classical Runge-Kutta method from order h^4 to order h. These findings are consistent with a result proved in a slightly different context by Feldstein and Goodman [16].

The effect of the initial incursion into the outer (stiff) zone is shown by Figures 7 and 9 which were obtained for the same stiffness ratio (r = 4), time step (h = 0.05) and discontinuity position z_d = 1. In both cases 6 cycles are required for amplitude growth to magnitude 4 at which the inner zone becomes 'hidden' from the numerical method. Thus the phenomenon depends on the discontinuity traversal itself, not on the extent of incursion into the outer zone.

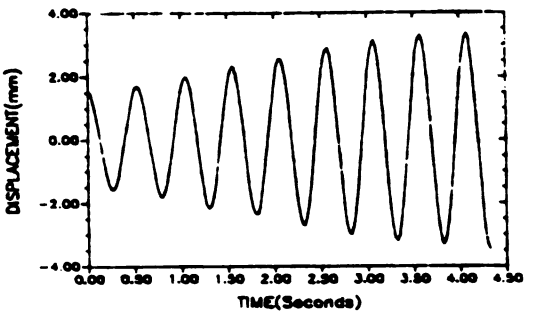

Figure 8 Spring/mass system displacement as for Figure 7, but h = 0.025.

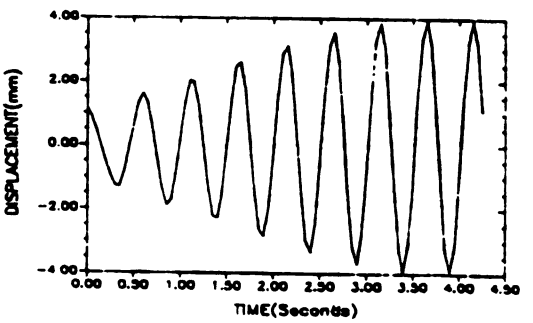

Figure 9 Spring/mass system displacement as for Figure 7, but with x_o = 1.1 mm.

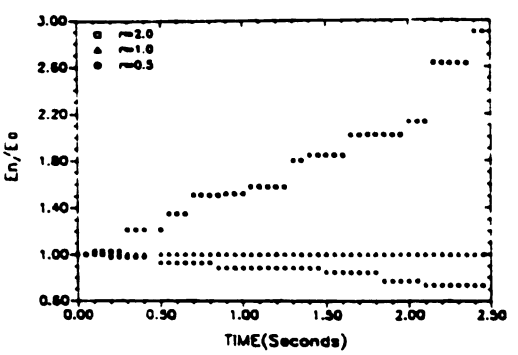

Figure 10 Relative energy of the spring mass systems of Figures 1,5,6 corresponding to stiffness ratios r = 1, r = 2, r = 0.5; x_o = 1.5 mm; x_d = 1 mm; $\dot{x}_o$ = 0 mm/sec; h = 0.05.

5.

The changes of the energy of the oscillator are illustrated in Figure 10 obtained using a time-step $h = 0.05$, and $z_o/z_d = 1.5$, $\dot{z}_d = 1$, $\dot{z}_o = 0$. The points for $r = 1$ correspond to a simple linear oscillator and show constant energy within the scale of this figure (actual loss, 0.065% at time 2.5). The energy in the 'hardening' case ($r = 2$) is seen to jump upwards each time a discontinuity traversal occurs. The period is about 0.74, and the 4 traversals of each cam be followed; namely, outer + to inner +, inner - to outer - , outer - to inner -, inner + to outer +. Thus energy increases at each traversal regardless of whether the crossing is from the inner to the outer zone or from the outer to the inner zone. The actual size of the jumps appears to vary substaintially and without obvious pattern. An explanation of these phenomena may be found in reference [15].

Although not visible at the scale of Figure 10 the energy decreases slightly during the time-steps between discontinuity traversals in accordance with the expectation of the Runge-Kutta method applied to an oscillator with constant stiffness. This is the case for both $r = 2$ and $r = 0.5$. In the latter case the energy jumps at discontinuity traversals are always seen to be to lower levels, as anticipated from Figure 6. The energy ultimately became approximately that for an initial displacement $z_o = z_d$ in agreement with the discussion of Figure 6.

CONCLUSIONS

The performance of Runge-Kutta methods which are widely used in mechanism simulation has been confirmed to be order h^4 when applied to a system of constant stiffness. There is a small decay of energy at a steady progression resulting in a slow decrease of amplitude.

However, when the Runge-Kutta method is applied to an oscillator with a discontinuous stiffness characteristic the error performance degrades to order h. For 'hardening' systems the energy jumps to a higher level at each traversal of the discontinuity regardless of the direction of crossing. Conversely with 'softening' systems the energy jumps to lower levels at each discontinuity traversal. These energy jumps might be order 20 percent, are of widely varying magnitude, without obvious pattern, and are generally enormous compared to the natural loss (< 0.1 percent per cycle typically). The energy jumps were not affected by the extent of the initial incursion into the outer zone.

Thus it is clearly evident that the application of this type of numerical integration method to flexible systems in which intermittent contacts occur could give rise to large spurious energy jumps. In a large mechanism simulation these jumps would be disguised somewhat, losses being attributed to impact for example, and gains to resonances. Further investigations are being carried out to establish methods of reducing or eliminating the energy jumps at discontinuities for Runge-Kutta methods, and other commonly used methods such as the Newmark family of integration algorithms.

REFERENCES

1. R.S. Haines, "Survey: 2-dimensional motion and impact at revolute joints," Mechanism and Machine Theory, 15, 361-370, 1980.

2. B.S. Thompson and C.K. Sung, "A survey of finite element techniques for mechanism design," Mechanism and Machine Theory, 21, 351-359, 1986.

3. J.P. Sadler and G.N. Sandor, "A lumped parameter approach to vibration and stress analysis of elastic linkages," ASME Journal of Engineering for Industry, B95, 549-557, 1973.

4. B.S. Thompson and C.K. Sung, "A variational formulation for the nonlinear finite element analysis of flexible linkages: theory, implementation, and experimental results, Journal of Mechanisms, Transmissions, and Automation in Design, 106, 482-488, 1984.

5 B.S. Thompson and C.K. Sung, "An analytical and experimental investigation of high-speed mechanisms fabricated with composite laminates," Journal of Sound and Vibration, 111, 399-428, 1986.

6. J.D. Lambert, Computational methods in ordinary differential equations, Wiley, Chichester, 1973.

7. C.W. Gear, Numerical initial value problems for ordinary differential equations, Prentice-Hall, Englewood Cliffs, NJ, 1971.

8. G.N. Sandor and A.G. Erdman, Advanced mechanism design: volume 2 analysis and synthesis, Prentice-Hall, Englewood Cliffs, NJ, 1984.

9. R. Wilson and J.N. Fawcett, "Dynamics of the slider-crank mechanism with clearance in the sliding bearing," Mechanism and Machine Theory, 9, 61-80, 1974.

10. S. Dubowsky and S.C. Young, "An experimental and analytical study of connection forces in high-speed mechanisms," ASME Journal of Engineering for Industry, 97B, 1160-1174, 1975.

11. K.-J. Bathe, Finite element procedures in engineering analysis, Prentice-Hall, Englewood Cliffs, NJ, 1982.

12. T.W. Lee and A.C. Wang, "On the dynamics of intermittent-motion mechanisms: Part I. Dynamic model and response," ASME Paper 82-DET-64 presented at the Design and Production Engineering Technical Conference, Washington, D.C., Sept. 12-15, 1982.

13. S. Dubowsky, J.F. Deck and H. Costello, "The dynamic modelling of spatial machine systems with clearance connections," ASME Paper 86-DET-62, presented at the Design Engineering Technical Conference, Columbus, Ohio, October 5-8, 1986.

14. W.K.D. Borthwick, "The numerical solution of discontinuous structural systems," Proc. 2nd Intl. Conf. on Recent Advances in Structural Dynamics, eds. M. Petyt and H.F. Wolfe, University of Southampton, England, 307-316, 1984.

15. J.M.B. Brown and W.K.D. Borthwick, "A test problem for structural systems with discontinuties," (to appear) Earthquake Engineering and Structural Dynamics.

16. A. Feldstein and R. Goodman, "Numerical solution of ordinary and retarded differential equations with discontinuous derivatives," Numerische Mathematik, 21, 1-13, 1973.

BIBLIOGRAPHY

BIBLIOGRAPHY

1. Alexander, R.M. and Lawrence, K.L., "An Experimental Investigation of the Dynamic Response of an Elastic Mechanism," ASME Journal of Engineering for Industry, 1974, Vol.96B, pp. 268-274.

2. Bakr, E. M. and Shabana A. A., "Effect of Geometric Elastic Non-Linearities on the Impact Response of Flexible Multi-Body Systems," Journal of Sound and Vibration, 1987, Vol. 112, No. 3, pp. 415-432.

3. Bengisu, M.T., Hidayetoglu, T. and Akay, A., "A Theoretical and Experimental Investigation of Contact Loss in the Clearances of a Four-Bar Mechanism,"ASME Journal of Mechanisms, Transmissions, and Automation in Design, Vol. 108, 1986, pp. 237-244.

4. Bolotin, V.V., The Dynamic Stability of Elastic System, Holden-Dsy, San Francisco, 1964.

5. Brown, J.M.B., Soong, K., Borthwick, W.K.D., Gandhi, M.V. and Thompson, B.S., "Effects of Intermittent Contact in Mechanisms of the Performance of Numerical Integration Methods," 10th Applied Mechanisms Conference, Dec. 1987, New Orleans, Louisiana.

6. Chace, M.A., "Analysis of the Time-Dependence of Multi-Freedom Mechanical Systems in Relative Coordinates,"ASME Journal of Engineering for Industry, Feb. 1967, Vol.89B, pp. 119-125.

7. Chace, M.A. and Bayazitoglu, Y.O., "Development and Application of a Generalized D'Alembert Force for Multifreedom Mechanical system, "ASME Journal of Engineering for Industry, Vol.93B,Feb. 1971, pp.317-327.

8. Chace, M.A. and Donald, A.S., "DAMN - Digital Computer program for the Dynamic Analysis of Generalized Mechanical Systems,"SAE Transactions, Vol. 80, pp. 969-983, 1971.

9. Chu, S.C. and Pan K.C., "Dynamic Response of a High-Speed Slider-Crank Mechanism With an Elastic Connecting Rod," ASME Journal of Engineering for Industry, 1975, Vol. 97B, pp. 542-550.

10. Cleghorn, W. L., Fenton, R. G. and Tabarrok, B., "Finite Element Analysis of High-Speed Flexible Mechanisms," Mechanism and Machine Theory, 1981, Vol. 16, No.4, pp. 407-424.

11. DRAM - Users Guide to Dram, Mechanical Dynamics, Inc., Ann Arbor, Michigan 48104, Dec. 1979.

12. Dubowsky, S. and Freudenstein, F., "Dynamic Analysis of Mechanical Systems with Clearances, Part 1: Formulation of Dynamic Model,"ASME Journal of Engineering for Industry, 1971, Vol. 93B, pp. 305-309.

13. Dubowsky, S. and Freudenstein, F., "Dynamic Analysis of Mechanical Systems with Clearances, Part 2: Dynamic Response,"ASME Journal of Engineering for Industry, 1971, Vol. 93B, pp. 310-316.

14. Dubowsky, S., "On Predicting the Dynamic Effects of Clearances in Planar Mechanisms,"ASME Journal of Engineering for Industry, 1974, Vol. 96B, pp. 317-323.

15. Dubowsky, S., "On Predicting the Dynamic Effects of Clearances in One-dimensional Closed Loop Systems,"ASME Journal of Engineering for Industry, 1974, Vol.96B, pp. 324-329.

16. Dubowsky, S., Young, S.C., "An Experimental and Analytical Study of Connection Forces in High-Speed Mechanisms,"ASME Journal of Engineering for Industry, 1975, Vol. 97B, pp. 1166-1174.

17. Dubowsky, S. and Gardner T. N., "Dynamic Interactions of Link Elasticity and Clearance Connections in Planar Mechanical Systems," ASME Journal of Engineering for Industry, 1975, Vol. 97B, PP.652-661.

18. Dubowsky, S. and Gardner T.N., "Design and Analysis of Multilink Flexible Mechanisms With Multiple Clearance Connections," ASME Journal of Engineering for Industry, 1977, Vol. 99B, PP. 88-96.

19. Dubowsky, S. and Moening M.F., "An Experimental and Analysis Study of Impact Forces In Elastic Mechanical Systems with Clearances," Mechanism and Machine Theory, 1978, Vol.13, PP. 451-465.

20. Dubowsky, S. and Morris, T.L., "An Analytical and Experimental Study of the Acoustical Noise Produced by Machine Links," ASME Journal of Vibration, Acoustics, Stress, and Reliability in Design, 1983, Vol. 105, pp.393-401.

21. Dubowsky, S., Norris, M., Aloni, E., Tamir, A., "An Analytical and Experimental Study of the Prediction of Impact in Planar Mechanical Systems with Clearances,"ASME Journal of Mechanisms, Transmissions, and Automation in Design, Vol. 106, 1984, pp. 444-451.

22. Dubowsky, S., Deck, J.F. and Costello H., "The Dynamic Modeling of Flexible Spatial Machine Systems With Clearance Connections", ASME Journal of Mechanisms, Transmissions, and Automation in Design, 1987, Vol. 109, pp. 87-94.

23. Earles, S.W.E. and Wu, C.L.S., "Motion Analysis of a Rigid-link Mechanism with Clearance at a Bearing, Using Lagrangian Mechanics and Digital Computation,"Mechanisms, Institute of Mechanical Engineers, London, England(1973), pp.83-89.

24. Earles, S.W.E., "Predicting the Occurrence of Contact Loss and Impact at a Bearing from a Zero-clearance Analysis,"Proc. of the IFToMM Fourth World Congress on the Theory of Machines and Mechanisms, Newcastle upon Tyne, England, 1975, pp. 1013-1018.

25. Earles, S.W.E. and Kilicay, O., "Predicting Impact Conditions due to Bearing Clearances in Linkage Mechanisms,"Proceedings of the Fifth World Congress on Theory of Machines and Mechanisms, 1979, Montreal, Canada, pp. 1078-1081.

26. Erdman, A.G., Sandor, G.N. and Oakberg, R.G., "A General Method for Kineto-Elastodynamic Analysis and Synthesis fo Mechanism," ASME Journal of Engineering for Industry, 1972, Vol. 94B, pp. 1193-1205.

27. Erdman A.G. and Sandor G.N., "Kineto-elastodynamics - a review of state of art and trends," Mechanism and Machine Theory, 1972, vol 7, pp. 19-33.

28. Funabashi H., Ogawa K., and Horie M., "A Dynamic Analysis of Mechanisms with Clearances", Bulletin of the JSME, Vol. 21, No. 161, Nov. 1978, Paper No. 161-14

29. Gandhi, M.V. and Thompson, B.S., "The Finite Element Analysis of Flexible Components of Mechanical Systems Using a Mixed Variational Principle," ASME Paper No. 80-DET-64.

30. Garrett, R.E. and Hall, A.S., "Effect of Tolerance and Clearance in Linkage Design,"ASME Journal of Engineering for Industry, 1969, Vol.91B , pp. 198-202.

31. Gear, C.W., Numerical Initial Value Problems in Ordinary Differential Equations, Prentice-Hall, Englewood Cliffs.

32. Gear, C.W., "Simultaneous Numerical Solution of Differential-Algebraic Equations,"IEEE Transactions on Circuit Theory, Vol. Ct-18, No. 1, Jan. 1971, pp.89-95.

33. Gibson, J.E., Introduction to Engineering Design, 1968, Holt, Rinehart and Winston, Inc., New York.

34. Goldsmith, W., Impact, the Theory and Physical Behavior of Colliding solids, London, E. Arnold, 1960.

35. Grant, S.J. and Fawcett, J.N., "Control of Clearance Effects in Mechanisms,"ASME Journal of Mechanical Design, Oct. 1978, Vol. 100, pp. 728-731.

36. Grant, S.J. and Fawcett, J.N., "Effects of Clearance at the Coupler-Rocker Bearing of a 4-Bar Linkage,"Mechanism and Machine Theory, 1979, Vol. 14, pp. 99-110.

37. Haines, R.S., "Survey: 2-Dimensional Motion and Impact at Revolute Joints,"Mechanism and Machine Theory, 1980, Vol. 15, pp. 361-370.

38. Haines, R.S. "A Theory of Contact Loss at Revolute Joints with Clearance,"Journal of Mechanical Engineering Science, Vol. 22, No. 3, 1980, pp. 129-136.

39. Haines, R.S., "Contact Loss at Revolute Kinematic Joints: a 'Ludodynamic' Theory Tested,"Institution of Mechanical Engineers, Vol. 199, No. C3, pp. 173-180.

40. Haines, R.S., "An Experimental Investigation Into The Dynamic Behaviour of Revolute Joints With Varying Degrees of Clearance,"Mechanism and Machine Theory, Vol. 20, 1985. No. 3, pp. 221-231.

41. Haug, E.J., Wu, S.C. and Yang, S.M., "Dynamics of Mechanical Systems With Coulomb Friction, Stiction, Impact and Constraint Addition-Deletion - I," Mechanism and machine Theory, 1986, Vol. 21, No. 5, pp. 401-406.

42. Hildebrand, F.B., Methods of Applied Mathematics, second edition, 1962 Prentice-Hall, Inc., Englewood Cliffs.

43. IMSL Library Reference Manual, 1982, published by IMSL, Houston, Texas.

44. Kane, T.R. and Levinson, D.A., "Multibody Dynamics," Journal of Applied Mechanics, 1983, Vol. 50, pp.1071-1078.

45. Keller, J.B., "Impact with Friction," Journal of Applied Mechanics, 1986, Vol. 53, pp. 1-4.

46. Khulief Y. A. and Shabana A. A., "Impact Responses of Multi-Body Systems With Consistent and Lumped Masses," Journal of Sound and Vibration, 1986, Vol. 104, No. 2, pp. 187-207.

47. Khulief Y. A. and Shabana A.A., "Dynamic Analysis of Constrained System of Rigid and Flexible Bodies with Intermittent Motion," ASME Journal of Mechanisms, Transmissions, and Automation in Design, 1986, Vol. 108, pp.38-45.

48. Kim, S.S., Shabana, A.A. and Haug, E.J., "Automated Vehicle Dynamic Analysis with Flexible Components," ASME Journal of Mechanisms, Transmissions, and Automation in Design, 1984, Vol. 106, pp. 127-132.

49. Kobrinskii, Dynamics of Mechanisms with Elastic Connections and Impact System, English translation by R. Lennox-napier, London, ILIFFE Books LTD., 1969.

50. Kolhatkar, S.A. and Yajnik, K.S., "The Effects of Play in the Joints of a Function - Generating Mechanism,"Journal of Mechanisms, Vol. 5, pp. 521-532, 1969.

51. Lanczos, C., The Variational Principles of Mechanics, third edition, University of Toronto Press, Toronto, 1966.

52. Lowen, G.G. and Jandrasits, W.G., "Survey of Investigations into the Dynamic Behavior of Mechanisms Containing Links with Distributed Mass and Elasticity," Mechanism and Machine Theory, 1972, Vol. 7, No. 1, pp. 3-17.

53. Lowen, G.G. and Chassapis, C., "The Elastic Behavior of Linkages: An Update," Mechanism and Machine Theory, 1986, Vol. 21, No. 1, pp. 33-42.

54. Mansour, W.M. and Townsend, M.A., "Impact Spectra and Intensities for High-speed Mechanisms,"ASME Journal of Engineering for Industry ,1975, Vol. 97B, pp. 347-353.

55. Martin, G.H., Kinematics and Dynamics of Machines, McGraw-Hill Book Company, New York, 1969.

56. Midha A., Erdman A.G. and Frohrib, D.A., "Finite Element Approach to Mathematical Modeling of High-Speed Elastic Linkages," Mechanism and Machine Theory, 1978, Vol. 13, pp. 603-618.

57. Midha A., Erdman A.G. and Frohrib D.A., "An Approximate Method for the Dynamic Analysis of Elastic Linkages," ASME Journal of Engineering for Industry, 1977, Vol. 97B, pp. 449-455.

58. Miedema, B. and Mansour, W.M., "Mechanical Joints with Clearance: a Three-Mode Model,"ASME Journal of Engineering for Industry, 1976, Vol. 98B, pp. 1319-1323.

59. Nath P.K. and Ghosh A., "Kineto-Elastodynamic Analysis of Mechanisms by Finite Element Method," Mechanism and Machine Theory, 1980, Vol. 15, pp. 179-197.

60. Nath P.K. and Ghosh A., "Steady State Response of Mechanisms with Elastic Links by Finite Element Method," Mechanism and Machine Theory, 1980, Vol. 15, pp. 199-211.

61. Nayfeh, A.H. and Mook, D.T., Nonlinear Oscillations, 1979

62. Neubauer, A.H., Jr., Cohen, R. and Hall, A.S.,Jr., "An Analytical Study of the Dynamics of an Elastic Linkage," ASME Journal of Engineering for Industry, 1966, Vol. 88B, pp.311-317.

63. Nikravesh, P.E., Computer-Aided Analysis of Mechanical Systems, Prentice Hall, Englewood Cliffs, NJ, 1988.

64. Paul, B., "Analytical Dynamics of Mechanisms - a Computer Oriented Overview,"Mechanism and Machine Theory, 1975, Vol. 10, pp. 481-507.

65. Reddy, J.N., Energy and Variational Methods in Applied Mechanics with an introduction to the finite element method, John Wiley & Sons, New York, 1984.

66. Reuleaux, F., "Theoretische Kinematik: Grundzüge einer Theorie des maschinenwesens. Vieweg, Brunswick, Deutschland (1875). English translation by A. B. W. Kennedy, Kinematics of Machinery, Macmillan, London(1876). Reprinted by Dover Publications, New York (1963).

67. Reid, K.N., Cohen, R., Garrett, R.E., Rabins, M.J., Richardson, H.H., Winer, W.O., Research Needs in Mechanical Systems, prepared by the Select Panel on Research Goals and Priorities in Mechanical Systems, for the National Science Foundation, ASME book I00178, 1984

68. Sadler J. P. and Sandor G. N., "A Lumped Parameter Approach to Vibration and Stress Analysis of Elastic Linkages," ASME Journal of Engineering for Industry, 1973, Vol. 95B, pp. 549-557.

69. Sadler, J.P. and Sandor G.N., "Nonlinear Vibration Analysis of Elastic Four-Bar Linkages," ASME Journal of Engineering for Industry , 1974, Vol. 96B, pp. 411-419.

70. Shabana A.A. and Wehage R.A., "Variable Degree-of-Freedom Component Mode Analysis of Inertia Variant Flexible Mechanical Systems," ASME Journal of Mechanisms, Transmissions, and Automation in Design, 1983 , Vol. 105, pp.371-378.

71. Shabana, A.A. and Wehage, R.A., "A Coordinate REduction Technique for Dynamic Analysis of Spatial Substructures with Large Angular Rotations," Journal of Struct Mechanics, 1983, Vol. 11, No.3, pp.401-431.

72. Shabana, A. A. and Wehage R. A., "Spatial Transient Analysis of inertia-Variant Flexble Mechanical Systems," Asme Journal of Mechanismsm, Transmissions, and Automation in Design, 1984, Vol.106, pp. 172-178.

73. Sheth, P.N. and Uicker, J.A. Jr., "IMP : A Computer-aided Design Analysis System for Mechanisms and Linkages," ASME Journal of Engineering for Industry, 1972, Vol. 94B, pp. 454-464.

74. Shigley, J. E. and Uicker J. J., Jr., Theory of Machines and Mechanisms, 1980, McGraw-Hill Book Company, N.Y.

75. Shimojma H., Ogawa K., and Matsumoto K., "Dynamic Characteristics of Planar Mechanisms with Clearances", Bulletin of th JSME, Vol. 21, No. 152, Feb. 1978, Paper No. 152-18

76. Simon, H.A., A Student's Introduction to Engineering Design, 1975, Pergamon Press Inc., New York.

77. Smith, M.R. and Maunder L., "Inertia forces in a four-bar linkage," Journal of Mechanical Engineering Science, 1967, Vol. 9, No. 3, pp. 218-225.

78. Song, J.O. and Haug, E.J., "Dynamic Analysis of Planar Flexible Mechanisms," Computer Methods in Applied Mechanics and Engineering, 1980, Vol. 24, pp. 359-381.

79. Soni, A.H., Huston, B., Paul, B., Haug, E., Waldron, K. and Bejczy, T., Draft: Strategic Research in Dynamic Systems and Control, Research Needs and Opportunities in Machine Dynamics, prepared by the Select Panel on Research Goals and Priorities in Machine Dynamics, for the National Science Foundation, Mechanical Engineering and Applied Mechanics Division.

80. Soong, K. and Thompson, B. S., "An Experimental and Analytical Investigation of the Dynamic Response of a Slider-crank Mechanism with Controlled Radial Clearance at the Gudgeon-pin Joint," 10th Applied Mechanisms Conference, Dec. 1987, New Orleans, Louisiana.

81. Stoer, J. and Bulirsch, R., Introduction to Numerical Analysis, Springer-Verlag, New York Inc., 1980.

82. Sung, C. K., Thompson, B. S., Crowley, P. and Cuccio, J., "An Experimental Study to Demonstrate the Superior Response Charaterictics of Mechanisms Constructed with Composite Laminates," Mechanism and Machine Theory, 1986, Vol. 21, No. 2, pp. 103-119.

83. Thompson, B.S. and Ashworth, R.P., "Resonance in Planar Mechanisms Mounted on Vibrating Foundations," Journal of Sound and Vibration, 1976, Vol. 49, No. 3, pp. 403-414.

84. Thompson, B.S. and Barr, A.D.S., "A Variational Principle for the Elastodynamic Motion of Planar Linkages," ASME Journal of Engineering for Industry, Vol. 98, Nov. 1976, PP.1306-1312.

85. Thompson, B.S., "The Analysis of an elastic Four-Bar Linkage on a Vibrating foundation using a Variational Method," ASME Journal of Mechanical Design, 1980, Vol. 102, No. 2, pp. 320-328.

86. Thompson, B.S., Zuccaro, D., Gamache, D. and Gandhi, M.V., "An Experimental and Analytical Study of the Dynamic Response of a Linkage Fabricated From a Unidirectional Fiber-Reinforced Composite Laminate," Journal of Mechanical Design, Paper No. 82-DET-67.

87. Thompson, B.S., "A Variational Formulation for the Finite Element Analysis of the Vibrating and Acoustical Response of High-Speed Machinery,"Journal of Sound and Vibration, Vol. 89, No. 1, 1983, pp. 7-15.

88. Thompson, B.S. and Sung, C.K., "A Variational Formulation for the Nonlinear Finite Element Analysis of Flexible Linkages: Theory, Implementation, and Experimental Results,"ASME Journal of Mechanisms, Transmissions, and Automation in Design, Vol. 106, No. 4, Dec. 1984, pp.482-488.

89. Thompson, B.S. and Sung, C.K., "A Survey of Finite Element Technique in Mechanism Design," Mechanism and Machine Theory, 1986, Vol. 21, No. 4, pp.351-359.

90. Thompson, B.S. and Sung, C.K., "A Theoretical and Experimental Study of the Response of Linkage Mechanisms Fabricated with Composite Laminates," Journal of Sound and Vibration, 1986, Vol. 111, No. 2, pp. 399-428.

91. Thompson, B. S., "Composite Laminate Components for Robotic and Machine Systems: Research issues in Design," Applied Mechanics Review, 1987, Vol. 40, No. 11, pp. 1545-1552.

92. Townsend, M. A. and Mansour, W. M., "A Pendulating Model for Mechanisms with Clearances in the Revolutes,"ASME Journal of Engineering for Industry, 1975, Vol. 97B, pp. 354-358.

93. Turcic, D.A. and Midha A., "Generalized Equations of Motion for the Dynamic Analysis of Elastic Mechanism Systems," Journal of Dynamic Systems,Measurement, and Control, 1984, Vol. 106, pp. 243-248.

94. Turcic, D.A. and Midha A., "Dynamic Analysis of Elastic Mechanism Systems. Part I: Applications," Journal of Dynamic Systems, Measurement, and Control, 1984, Vol. 106, pp. 249-254.

95. Turcic, D. A. and Midha A., "Dynamic Analysis of Elastic Mechanism Systems. Part II: Experimental Results," Journal of Dynamic Systems, Measurement, and Control, 1984, Vol. 106, pp. 255-260.

96. VaxLab/LabStar Programmer's Guide, AA-HX04B-TE, Digital Software, Digital Equipment Corporation, Maynard, Massachusetts.

97. Viscomi, B.V. and Ayre R.S., "Nonlinear Dynamic Response of Elastic Slider-Crank Mechanism," ASME Journal of Engineering for Industry, 1971, Vol. 93B, pp. 251-262.

98. Wehage, R.A. and Haug, E.J., "Generalized Coordinate Partitioning for Dimension Reduction in Analysis of Constrained Dynamic Systems," Journal of Mechanical Design, 1982, Vol. 104, pp. 247-255.

99. Wehage, R.A. and Haug, E.J., "Dynamic Analysis of Mechanical Systems with Intermittent Motion," ASME Journal of Mechanical Design, 1982, Vol. 104, pp. 778-784.

100. Wilson, C.E. Jr. and Michels, W.J., Mechanism, Design-Oriented Kinematics, American Technical Society, Chicago, Illinois. 1969.

101. Wilson, E. L. and Penzien, J., "Evaluation of Orthogonal Damping Matrices," International Journal for Numerical Methods in Engineering, 1972, Vol. 4, pp. 5-10.

102. Wilson, R. and Fawcett, J.N., "Dynamics of the Slider-Crank Mechanism with Clearance in the Sliding Bearing,"Mechanism and Machine Theory, 1974, Vol. 9, pp. 61-80.

103. Winfrey, R.C., "Elastic Link Mechanism Dynamics," ASME Journal of Engineering for Industry, 1971, Vol. 93B, pp. 268-272.

104. Winfrey, R.C., Anderson R.V. and Gnilka C.W., "Analysis of Elastic Machinery With Clearances," ASME Journal of Engineering for Industry 1973, Vol. 95B, pp. 695-703.

105. Wu, C.L.S. and Earles, S.W.E., "A Determination of Contact-loss at a Bearing of a Linkage Mechanism,"ASME Journal of Engineering for Industry, Vol.99B, May 1977, pp. 375-380.

106. Wu, S.C. and Yang, S.M.,Haug, E.J., "Dynamics of Mechanical Systems With Coulomb Friction, Stiction, Impact and Constraint Addition-Deletion - II," Mechanism and machine Theory, 1986, Vol. 21, No. 5, pp. 407-416.

107. Wu, S.C. and Yang, S.M.,Haug, E.J., "Dynamics of Mechanical Systems With Coulomb Friction, Stiction, Impact and Constraint Addition-Deletion - III," Mechanism and machine Theory, 1986, Vol. 21, No. 5, pp. 417-425.